

City Research Online

City St George's, University of London

Citation: Babawale, Z. A. (1988). Theoretical study of an absorption refrigeration system powered by CPC solar collectors for applications at near equatorial latitudes. (Unpublished Doctoral thesis, The City University)

This is the accepted version of the paper.

This version of the publication may differ from the final published version. To cite this item please consult the publisher's version.

Permanent repository link: https://openaccess.city.ac.uk/id/eprint/34083/

Copyright and Reuse: Copyright and Moral Rights remain with the author(s) and/or copyright holders. Copies of full items can be used for personal research or study, educational, or not-for-profit purposes without prior permission or charge, unless otherwise indicated, provided that the authors, title and full bibliographic details are credited, a hyperlink and/or URL is given for the original metadata page and the content is not changed in any way. For full details of reuse please refer to City Research Online policy.

City Research Online: http://openaccess.city.ac.uk/ publications@citystgeorges.ac.uk

THEORETICAL STUDY OF AN ABSORPTION REFRIGERATION SYSTEM POWERED BY CPC SOLAR COLLECTORS FOR APPLICATIONS AT NEAR EQUATORIAL LATITUDES .

by

ZACHEUS ADERANTI BABAWALE, MSc(Eng)

Ph.D. Thesis

THE CITY UNIVERSITY

LONDON

DEPARTMENT OF MECHANICAL ENGINEERING

July 1988 .

BRITISH LIBRARY

IMAGING SERVICES NORTH

Boston Spa, Wetherby
West Yorkshire, LS23 7BQ
www.bl.uk

BEST COPY AVAILABLE.

VARIABLE PRINT QUALITY

[redacted]

CONTENTS

	Page
List of Contents	i
List of Tables	vii
List of Figures	x
Acknowledgements	xiv
Abstract	xv
Nomenclature	xvi
1. INTRODUCTION	1
1.1 Introduction	1
1.2 Description of The System Models	4
1.3 Organization of Work Undertaken	5
2. REVIEW OF EXISTING SYSTEMS AND LITERATURE	8
2.1 Introduction	8
2.2 Absorption Cycles and Solar Energy	8
2.3 Concentrating Solar Energy Collectors	15
2.4 Conclusion	21
3. SOLAR RADIATION AND COLLECTION PERIOD	23
3.1 Introduction	23
3.2 Solar Radiation Availability	23
3.2.1 Introduction	23
3.2.2 Direct and diffuse components of solar radiation	24
3.2.3 Estimation of hourly radiation	29
3.2.4 Estimation of hourly radiation on tilted surfaces	31

3.3 Solar Energy Collection for CPC collectors 35

3.3.1 Transmission of direct and diffuse radiation through CPC collector glazing 35

3.3.2 Collection times and incident energy for CPC Collectors 38

3.4 Dust and Shading Effects on Collectors 43

4. DESIGN ANALYSIS OF A CPC SOLAR COLLECTOR 54

4.1 Introduction 54

4.2 The CPC Geometric Design Parameters 56

4.2.1 Reflector height and arc length 56

4.2.2 The CPC transmission factor 59

4.2.3 Optical loss due to gap between receiver and reflector 62

4.3 Thermal Analysis of The CPC Collector 69

4.3.1 Introduction 69

4.3.2 Radiation heat transfer in the CPC collector 72

4.3.3 Convective heat transfer in the CPC collector 76

4.3.4 Conductive heat transfer in the CPC collector 81

4.3.5 The CPC loss coefficient and useful energy gain 82

4.3.6 Thermal and optical efficiency of the collector 86

4.4 Parametric Study 86

4.4.1 Solution sequence 86

4.4.2 Performance analysis and results 89

4.4.3 Top loss coefficient correlation 92

4.5 Conclusion, Figures and Tables 94

5. AQUA-AMMONIA ABSORPTION REFRIGERATION SYSTEM 124

5.1 Introduction 124

5.1.1 The absorption cycles 125

5.1.2 The Rankine Cycle 125

5.1.3 The adsorption cycle 126

5.2 The Absorption Refrigeration Process 130

5.3 The absorption cycle working fluid 134

5.3.1 Requirements of the combination 134

5.3.2 Requirements of a refrigerant 135

5.3.3 Requirements of an absorbent 135

5.4 Types of Absorption Cycles 136

5.4.1 Water-ammonia system 136

5.4.2 Lithium bromide-water system 138

5.5 Property Data Equations for NH_3-H_2O Mixtures 142

5.5.1 The property data equations 144

5.5.2 Accuracy of the regression equations 145

5.6 Aqua-ammonia Cycles Analysis 146

5.6.1 The ideal absorption cycle 146

5.6.2 The practical NH_3-H_2O cycle 148

5.6.3 The basic aqua-ammonia cycle 152

5.6.4 Refined aqua-ammonia cycles 154

5.7 Low and High Sides Pressure Iteration Technique 158
5.8 Parametric Analysis 159
5.8.1 The ideal cycle 159
5.8.2 The basic cycle 161
5.8.3 The basic cycle with a reflux condenser 169
5.8.4 Addition of a solution heat exchanger 170
5.8.5 The addition of a refrigerant precooler 171
5.9 Conclusion 179
5.10 Discussion 181

6. COOLING LOAD
6.1 Introduction 183
6.1.1 Cooling load calculation method 183
6.1.2 Space heat gain by transfer function method 184
6.1.3 Space cooling load by transfer function method 186
6.2 The Heat Gain Components 187
6.2.1 Heat gain through exterior walls and roof 187
6.2.2 Heat gain through partition, ceiling and floor 191
6.2.3 Heat gain through the glass windows 191

6.2.4 Heat gain through doors 195
6.2.5 Heat gain from within the conditioned space 195
6.2.6 Heat gain from ventilation air 197
6.3 The Space Cooling Load 198
6.3.1 Instantaneous cooling load components 198
6.3.2 Transformed cooling load components 199
6.3.4 Adjustment of the room transfer coefficients 200
6.4 Refrigeration Load 200

7. COMBINED SYSTEM SIMULATION AND ECONOMIC COMPARISON 205
7.1 Introduction 205
7.2 System Description and Simulation 205
7.2.1 Description and database 205
7.2.1 The simulation 207
7.3 Refrigerant and Solution Storage 214
7.4 System Performance 215
7.5 Economic Comparison 228
7.6 Conclusion 230

8. CONCLUSION 233
8.1 General Remarks 233
8.2 Future Development 238

APPENDIX A TABLES 239

APPENDIX B COMPUTER PROGRAMS 270

RADCOR 270

RADLAGOS 272

LACPC 274

CPHEAT 276

REFRIG 285

REFSIM 297

Subroutine solarp 301

Subroutine htgain 303

Subroutine cload 304

APPENDIX C FLOW CHARTS 305

FLACCP 305

FLPROP 307

FLHEAT 310

APPENDIX D 312

Property data equations for water 312

Top loss coefficent regression analysis,

$45 \leq T_s \leq 215^{o}C$ 313

Top loss coefficient regression analysis,

$215 \leq T_s \leq 300^{o}C$ 315

NH_3-H_2O Absorption Cycle Sample Calculation 317

REFERENCES 327

LIST OF TABLES

Table No.	Title	Page
3.1	Correlation of Liu & Jordan, Page, and Collares-Pereira & Rabl correlations for Lagos (6.45°N) radiation data	30
3.2	Adjustments of CPC collector tilt, θ_a= 7°	45
3.3	Adjustments of CPC collector tilt, θ_a= 10°	48
3.4	Adjustments of CPC collector tilt, θ_a= 15°	51
3.5	Adjustments of CPC collector tilt, θ_a= 20°	52
3.6	Adjustments of CPC collector tilt, θ_a= 30°	53
4.1	Results for CPC collector, θ_a = 30°, ϵ_s = 0.9, α_s = 0.9	108
4.2	Results for CPC collector, θ_a = 20°, ϵ_s = 0.9, α_s = 0.9	110
4.3	Results for CPC collector, θ_a = 15°, ϵ_s = 0.9, α_s = 0.9	112
4.4	Results for CPC collector, θ_a = 10°, ϵ_s =0.9, α_s = 0.9	114
4.5	Results for CPC collector, θ_a = 30°, ϵ_s = 0.17, α_s = 0.89	116
4.6	Results for CPC collector, θ_a = 20° ϵ_s = 0.17, α_s = 0.89	118
4.7	Results for CPC collector, θ_a = 15°, ϵ_s = 0.17, α_s = 0.89	120
4.8	Results for CPC collector, θ_a = 10°, ϵ_s = 0.17, α_s = 0.89	122

6.1	Percentage of the daily range of the outside temperature	194
6.2	Coefficients a_j and t_j for regular sheet glass	194
6.3	Rates of heat gain per hour from Occupants of a conditioned space	202
6.4	Rate of heat gain from equipments	202
6.5	Ventilation air requirement	203
6.6	Heat equivalent of Occupancy	204
6.7	Average air changes for storage rooms	204
6.8	Rate of heat gain from inflitration air	204
7.1	Transfer Function Coefficients	212
7.2	Coefficients of Room Transfer Function	213
7.3	Monthly Cooling load for the Office building	232
A1.	Collection dates for CPC collector, $\theta_a = 7^{o}$, $\phi = 4^{o}N$	239
A2.	Collection dates for CPC collector, $\theta_a = 7^{o}$, $\phi = 6.25^{o}N$	242
A3.	Collection dates for CPC collector, $\theta_a = 7^{o}$, $\phi = 14^{o}N$	245
A4.	Collection dates for CPC collector, $\theta_a = 10^{o}$, $\phi = 4^{o}N$	248
A5.	Collection dates for CPC collector, $\theta_a = 10^{o}$, $\phi = 6.25^{o}N$	250
A6.	Collection dates for CPC collector, $\theta_a = 10^{o}$, $\phi = 14^{o}N$	252

A7. Collection dates for CPC collector, $\theta_a = 15^o$, $\phi = 4^oN$ 254

A8. Collection dates for CPC collector, $\theta_a = 15^o$, $\phi = 6.25^oN$ 256

A9. Collection dates for CPC collector, $\theta_a = 15^o$, $\phi = 14^oN$ 258

A10. Collection dates for CPC collector, $\theta_a = 20^o$, $\phi = 4^oN$ 260

A11. Collection dates for CPC collector, $\theta_a = 20^o$, $\phi = 6.25^oN$ 262

A12. Collection dates for CPC collector, $\theta_a = 20^o$, $\phi = 14^oN$ 264

A13. Collection dates for CPC collector, $\theta_a = 30^o$, $\phi = 4^oN$ 266

A14. Collection dates for CPC collector, $\theta_a = 30^o$, $\phi = 6.25^oN$ 267

A15. Collection dates for CPC collector, $\theta_a = 30^o$, $\phi = 14^oN$ 268

A16. The CPC collector simulation input data 269

LIST OF FIGURES

Fig. No.	Title	Page
1	Solar-powered NH_3-H_2O absorption System	7
3.0	Location of Nigeria in West Africa	25
3.1	Monthly average daily radiation on horizontal surfaces for two locations in West Africa	26
3.2	Monthly average daily ambient temperature for two locations in West Africa	27
3.3	Incident beam radiation on horizontal and inclined surfaces	33
3.4	Fully developed CPC collector	39
3.5	Coordinate system and elements used in description of Sun's direction vector	40
3.6	Sun's projection angle on X-Z plane	41
3.7	Projection on a north-south plane of the CPC acceptance angle and slope	42
4.1	Graphical truncation of CPC collector	63
4.2	Elements and coordinates system used in developing the curves of the reflector	64
4.3	Relector height/aperture width for CPC collector with tubular receiver	65
4.4	Reflector arc length/aperture width for CPC collector with tubular receiver	66
4.5	Average number of reflections (within acceptance angle) for CPC with tubular receiver	67

4.6	Gap between the tubular receiver and reflector	68
4.7	Energy exchange for CPC collector with nonevacuated tubular receiver	70
4.8	Body force in Nusselt number expression acting on the film on an inclined surface	78
4.9	U_t for CPC with nonevacuated tubular receiver, $\epsilon_s = 0.9$, $S = 30^o$, $h_w = 30$ W/m^{2}K	96
4.10	U_t for CPC with nonevcuated tubular receiver, $\epsilon_s = 0.9$, $S = 5^o$, $h_w = 30$ W/m^2 K	97
4.11	U_t for CPC with nonevacuated tubular receiver, $\epsilon_s = 0.1$, $S = 30^o$, $h_w = 30$ W/m^{2}K	98
4.12	U_t for CPC with nonevacuated tubular receiver, $\epsilon_s = 0.1$, $S = 5^o$, $h_w = 30$ W/m^{2}K	99
4.13	U_t for CPC with nonevacuated tubular receuver, $\epsilon_s = 0.9$, $S = 30^o$, $h_w = 5$ W/m^2 K	100
4.14	U_t for CPC with nonevacuated tubular receiver, $\epsilon_s = 0.9$, $S = 5^o$, $h_w = 5$ W/m^2 K	101
4.15	U_t for CPC with nonevacuated tubular receiver, $\epsilon_s = 0.1$, $S = 30^o$, $h_w = 5$ W/m^2 K	102
4.16	U_t for CPC with nonevacuated tubular receiver, $\epsilon_s = 0.1$, $S = 5^o$, $h_w = 5$ W/m^2 K	103
4.17	U_t for CPC with nonevacuated tubular receiver, $\epsilon_s = 0.9$, $T_b = 10^o$C, $h_w = 30$ W/m^{2}K	104
4.18	U_t for CPC with nonevacuated tubular receiver, $\epsilon_s = 0.9$, $T_b = 40^o$C, $h_w = 30$ W/m^{2}K	105

4.19	U_t for CPC with nonevacuated tubular receiver, ϵ_s = 0.9, S = 30°, T_b = 40°C	106
4.20	U_t for CPC with nonevacuated tubular receiver, ϵ_s = 0.1, S = 30°, T_b = 40°C	107
5.1	A basic absorption cycle	127
5.2	Schematic diagram of a Rankine cycle	128
5.3	Schematic diagram of the adsorption cycle	129
5.4	A simple intermittent absorption cycle	133
5.5	A single-stage NH_3-H_2O absorption cycle	137
5.6	A NH_3-H_2O cycle for domestic application	140
5.7	System schematic for a lithium bromide-water absorption cycle	141
5.8	A basic aqua-ammonia absorption cycle	150
5.9a	A carnot refrigeration cycle	151
5.9b	A reversible Carnot cycle	151
5.10	A complete aqua-ammonia absorption cycle	156
5.11	A basic NH_3-H_2O cycle refined with a reflux condenser	157
5.12	Variation of COP for an ideal absorption cycle	160
5.13	Basic NH_3-H_2O cycle COP, T_c= T_a= 27°C	163
5.14	Basic NH_3-H_2O cycle COP, T_c= T_a= 35°C	164
5.15	Basic NH_3-H_2O cycle COP, T_c= T_a= 50°C	165
5.16	Variation of basic cycle M_{ws}/M_r, T_c=T_a=27°C	166
5.17	Variation of basic cycle M_{ws}/M_r, T_c=T_a=35°C	167
5.18	Variation of basic cycle M_{ws}/M_r, T_c=T_a=50°C	168

5.19	Variation of COP for basic cycle refined with a reflux condenser, $T_c = T_a = 27^oC$	172
5.20	Variation of COP for basic cycle refined with a reflux condenser, $T_c = T_a = 35^oC$	173
5.21	Variation of COP for basic cycle refined with a reflux condenser, $T_c = T_a = 50^oC$	174
5.22	Variation of M_{ws}/M_r for refined cycle, $T_c = T_a = 27^oC$	175
5.23	Variation of M_{ws}/M_r for refined cycle, $T_c = T_a = 35^oC$	176
5.24	Variation of M_{ws}/M_r for refined cycle, $T_c = T_a = 50^oC$	177
5.25	Comparison of COP for five different cycles, $T_c = T_a = 43^oC$, $T_r = 70^oC$	178
7.1	Solar-powered NH_3-H_2O absorption sysyem	210
7.2	Plan of One-Story office building	211
7.3	heat transfer rates for the office building	218
7.4	Refrigerant store for the office building	219
7.5	Solution store for the office building	220
7.6	System performance for the office building	221
7.7	Heat transfer rates for beef cold storage	222
7.8	Refrigerant store for beef cold storage	223
7.9	Solution store for beef cold storage	224
7.10	System performance for beef cold storage	225
7.11	Solar radiation incident on the collector surface	226
7.12	Collector and generator temperature	227

ACKNOWLEDGEMENTS

I would like to thank my Supervisor, Dr J R Simonson for the support and encouragement given throughout this research work.

My appreciation also goes to Professor G T S Done, the Department of Mechanical Engineering, and The City University for the award of Robert Kitchin (Saddlers) Scholarship to cover part of the course fees.

Finally, I would like to thank my wife for her patience and support throughout this course of study.

ABSTRACT

The operation of an air-cooled aqua-ammonia absorption refrigeration system through the use of solar energy has been investigated using Computer modelling techniques. The study conducted has revealed a potential for the system to be powered by a nontracking CPC solar collector with nonevacuated tubular receiver, for applications at near equatorial latitudes.

A conditional equation has been developed to determine the collection times and tilt adjustment requirements for the collector. Also, in the absence of any empirical equation for calculating the collector top loss coefficient, U_t, correlation equations have been developed. The performance analysis indicated an outlet water temperature up to 150^{o}C is obtainable with concentration ratio between 2.5 and 4.7, with 2 to 6 seasonal tilt adjustments.

Polynomia property data equations for NH_3-H_2O mixtures have been developed in a form readily adaptable to a Computer program. Extensive thermodynamic cycle analysis of the aqua-ammonia cycles revealed an average generator temperature of 105^{o}C is required for water-cooled system, and about 120^{o}C for air-cooled cycles. The results also indicated a minimum generator temperature requirement depending on a given set of operating temperatures.

Simulation of the combined system of the CPC collector and aqua-ammonia cycle indicated that application of the system is possible for cooling of office buildings and refrigerated products. The results also showed the storage of refrigerant and solution to be thermodynamically feasible.

An economic comparison with a conventional vapour compression system revealed the estimated cost of the solar system to be three times higher. Suggestions have been made for further investigation, as it is hoped that further research work will be inspired from the present work.

NOMENCLATURE

A	Area (m^2)
C	Concentration ratio
Cp	Specific heat (kJ/kg^oC)
COP	Coefficient of performance
CPC	Compound Parabolic Concentrator
D	Diameter (m)
E	Heat exchanger effectiveness
EXP	Exponential
Fr	Heat removal factor
FC	Fully developed CPC concentration ratio
FW	Fully developed CPC width (m)
FH	Fully developed CPC height (m)
G	Global solar radiation (W/m^2)
Gr	Grashof number
g	gravitational acceleration (m/s^2)
g	gap between absorber tube and reflector back (m)
H	Total enthalpy (kJ)
H	Daily solar radiation (W/m^2)
H	Height (m)
HSP	High side pressure (bar)
h	Convective heat transfer coefficient ($W/m^2\ ^oC$)
h	Enthalpy (kJ/kg)
hL	Enthalpy of liquid (kJ/kg)
hV	Enthalpy of vapour (kJ/kg)
I	Hourly solar radiation (W/m^2)
K	Extinction coefficient

K_t	Clearness index
k	Conductivity (W/m K)
L	Length (m)
L	Optical loss
LSP	Low side pressure (bar)
M	Massflow rate (kg/s)
MFL	Mass fraction in liquid (kg)
N	Day of year
<n>	Average number of reflections
Nu	Nusselt number
P	Pressure (bar)
Pr	Prandtl number
Q	Heat transfer (W)
q	Heat transfer (W/m^2)
R	Radius (m)
Re	Reynold number
S	Tilt angle (^{o})
T	Temperature (^oC)
TC	Truncated CPC concentration ratio
TW	Truncated CPC width (m)
TH	Truncated CPC height (m)
T_r	Reflux condenser (^oC)
t	time (hours, 1.00 = 1 a.m)
U	Loss coefficient ($W/m^2\ ^oC$)
v	Specific volume (m^3/kg)
W	Width (m)
W_p	Pump work (W)
X	Thickness (m)

X	Concentration of ammonia in solution
XL	Concentration of ammonia in liquid
XV	Concentration of ammonia in vapour

α	absorptance
δ	declination angle (^{o})
ϵ	Emissivity
ϵ_{eff}	Effective emissivity
$\varnothing$	Latitude (^{o})
γ	Azimuth angle (^{o})
θ_a	Acceptance angle (^{o})
θ_d	Edge ray angle (^{o})
θ_i	Incident angle (^{o})
τ	Transmittance
τ_C	CPC transmission factor
ρ	Reflectivity
ρ	Density (kg/m^3)
σ	Stefan Boltzman constant = 5.67×10^{8} W/m^2 K^4
ω	Hour angle (^{o})
ω_s	Sunset angle (^{o})
υ	Kinematic viscosity (m^2/s)
μ	Dynamic viscisity (kg/m s)
η	Efficiency

Subscripts:

a	Absorber
b	Beam radiation
b	Ambient

C	CPC collector
c	Condenser
c	Glass cover
d	Diffuse radiation
e	Evaporator
e	Effective
g	Generator
h	horizontal
i	Inlet
i	Incident
o	Outlet
o	Outside
r	Reflector
s	Tubular receiver
v	Vertical
rm	Room

CHAPTER 1

INTRODUCTION

1.1 INTRODUCTION

The energy content and continuous availability of solar radiation at near equatorial latitudes makes solar energy an attractive energy source for producing refrigeration. The daily variations of cooling demand and solar incidence are considerably in phase, and a solar powered refrigeration system can be installed in this region for various applications, with or without a need for storage of thermal energy.

In many of the developing countries located in this tropical region, electricity supply is minimal, with constant supply failures in towns, and no supply at all in rural communities. Availability of a solar refrigeration system which requires little or no conventional energy to operate would, therefore, raise quality of life and health standards, and promote economic growth in these countries.

Solar energy can be used to operate refrigeration equipment either by direct conversion to electricity to drive vapour compression systems, or by using the heat collected to energize heat activated cycles. However, of all possible solar refrigeration schemes, the absorption cycle has been found to be most viable for use in these countries. The technology required for the operation and

maintenance of such system is relatively simple.

Although the absorption refrigeration system has been in use for many years, it is recently that interest has rapidly increased in its application through the use of solar energy. The lithium bromide-water absorption cycle is the only solar refrigeration system that is in commercial production at the present, and only use for air-conditioning of buildings. The requirements of this system for relatively high evaporating temperatures and, water-cooled condenser and absorber with the probable need for a cooling tower, have made it unsuitable for use in many developing countries where there is inadequate supply of water and electricity. A system that requires minimum or no conventional energy, that can be air-cooled and, used for both high and low temperature applications would be ideal. The ammonia-water absorption cycle meets most of these requirements.

Unfortunately, whereas the energizing temperature for lithium bromide-water cycle ranges below 100°C, an air-cooled ammonia-water cycle requires about 120°C to function. Since the solar energy collector must be able to supply energy at temperatures greater than the energizing temperature, the use of ordinary flat plate collectors as in the lithium bromide-water system is not possible with an air-cooled ammonia-water cycle. The evacuated glass tube flat plate collector or a concentrating collector must be used to obtain energy at

such high temperature. However, the cost of installation, operation and maintenance of these collectors, except a non-tracking concentrator may be too high in many developing countries. The present investigation is intended to demonstrate that, operation of the aqua-ammonia absorption refrigeration cycle is possible with the use of a non-tracking concentrating collector at near equatorial latitudes.

The investigation involved a detailed thermodynamic cycle analysis of the NH_3-H_2O absorption systems, and design analysis of a two-dimensional troughlike non-tracking concentrating collector. This thesis describes the mathematical modelling of the aqua-ammonia absorption cycle and the two-dimensional Compound Parabolic Concentrator (CPC) collector.

Furthermore, it has been recognised that the solar refrigeration system cannot meet 100% of the refrigeration demand at all the time without a form of storage, despite the fact that, the solar radiation availability and refrigeration demand are considerably in phase. The storage of refrigerant and solution have been considered and modelled. The combined solar collector - absorption refrigeration system has been simulated for various applications.

1.2 DESCRIPTION OF THE SYSTEM MODELS

The simulation model for the solar absorption refrigeration system provides a means of estimating and analysing the system dynamic performance. A detailed knowledge of the processes in both the absorption cycle and the CPC collector is therefore necessary to develop an accurate simulation model. The development of the simulation program involves interconnecting the mathematical models of each of the aqua-ammonia cycle and the CPC collector components.

Mathematical model of the absorption cycle is based on energy and mass balances around each component of the cycle. It includes the assumption that there is equilibrium between the liquid and vapour phases where they coexist. With a given set of operating temperatures, property data equations are solved by numerical method, the high and low sides pressure are obtained by iteration technique, and concentration of ammonia-water solution and, mass and energy flow rates are determined per unit mass of strong solution. For the solar refrigeration simulation model, the evaporator energy flow rate is determined for a given collector energy output, rather than per unit massflow of the strong solution.

For the thermal performance of the collector, the mathematical model is developed to provide the hourly energy gain of the collector. The known input parameters

of the CPC collector are: the acceptance half-angle, desired concentration ratio after truncation, and the hourly solar radiation data. The collector simulation model provides numerical solutions for the various equations that descibe the CPC parameters, including the heat loss coefficicents.

Refrigerant and solution storage have been proposed for the present investigation. Their mathematical models consist of first order differential equations which are solved using first order approximation. The final simulation model for the solar powered absorption refrigeration system shown in figure 1, page 7, is the combination of models for the collector, the absorption cycle and the storage system.

1.3 ORGANIZATION OF WORK UNDERTAKEN

Estimation of the hourly solar energy availability and the collection times for the CPC collector located at latitudes between 4 and 14^{o}N have been undertaken in chapter three. Design analyses of the CPC collector have been carried out in chapter four. These include the geometrical characteristics and thermal performance of the collector. Correlation equations for the collector's top loss coefficient have also been developed in this chapter.

In chapter five, regression analysis of the property data of ammonia-water mixtures has been carried out to

provide property data equations . These equations are used in the comprehensive computer analysis of thermodynamics of ammonia-water absorption cycles also undertaken in this chapter.

An office building air-conditioning cooling load and a cold store refrigeration load, based on ASHRAE methods were estimated in chapter six. The refrigerant and solution store mathematical models were developed in chapter seven. Also, the solar powered refrigeration system has been simulated for applications at latitude $6.45^{o}N$ to access its instantaneous efficiency and dynamic performance. Economic analysis of the system has also been undertaken in this chapter . Finally, conclusion have been drawn in chapter eight.

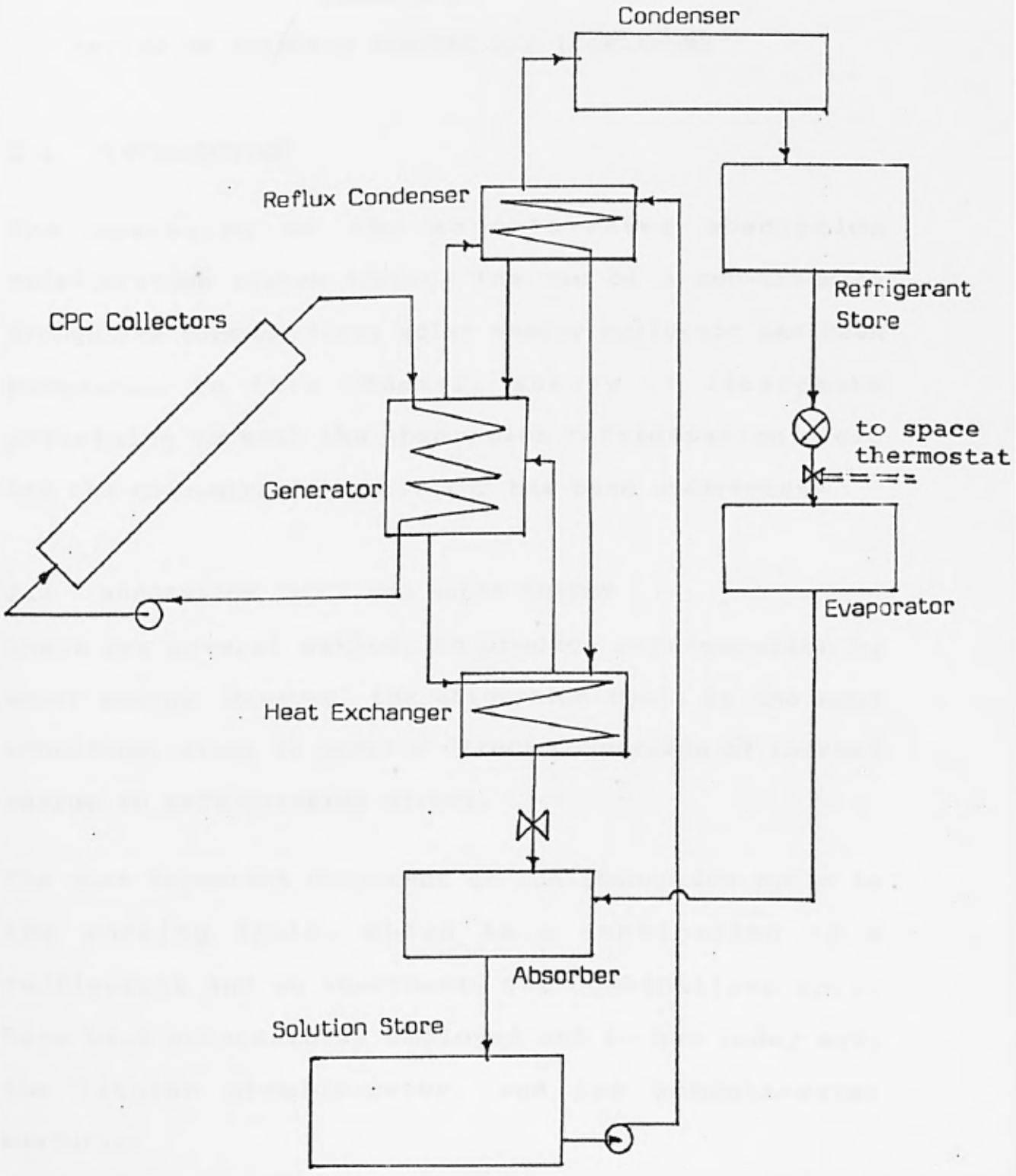


Fig. 1 Solar powered NH_3-H_2O absorption system

CHAPTER 2

REVIEW OF EXISTING SYSTEMS AND LITERATURE

2.1 INTRODUCTION

The operation of the ammonia-water absorption refrigeration system through the use of a non-tracking troughlike concentrating solar energy collector has been proposed. In this chapter, survey of literature pertaining to both the absorption refrigeration cycle and the concentrating collector has been undertaken.

2.2 ABSORPTION CYCLE AND SOLAR ENERGY

There are several methods to produce refrigeration by solar energy. However, the absorption cycle is the most promising, since it permits direct conversion of thermal energy to refrigerating effect.

The most important component of the absorption cycle is the working fluid, which is a combination of a refrigerant and an absorbent. The combinations which have been successfully employed and in use today are, the lithium bromide-water, and the ammonia-water mixtures.

In judging the suitability of a refrigerant-absorbent combination a number of properties have to be considered. One which has been generally considered the

most important is a large negative deviation from Raoults law, Dodge (1944). For ideal solutions whose components, the solute and the solvent, have no special molecular attraction or repulsion for each other, Raoults law states that: at a given temperature, the vapour pressure (p) of the solute over the solution equals its vapour pressure (p_o) in the pure state mulptiplied by its mole fraction (n) in the solution; ($p/p_o = n$). Thus in an ideal combination, the vapour pressure of the absorbent should be negligible compared to that of the refrigerant, and the total pressure over the solution would entirely be due to that of the refrigerant. In practice, however, for the same partial pressure to be provided by a solution at a given temperature, Buffington (1949) has found that the mole fraction of the solute have to be greater than the ideal, and for this condition the solution exhibits a negative deviation fron the Raoults law. The most crucial among the requirements he has proposed for successful combinations is that, the equilibrium solubility of a refrigerant in an absorbent should be very high at the absorber temperature and a pressure corresponding to the low-side pressure of the absorption system. High concentration strong solution would avoid the circulation of excessive amount of solution and prevent the resulting large internal heat losses and the requirement for huge equipment. His recommendation was based on the need for low pumping cost and the ability

to achieve favourable temperature levels.

Jacob, Albright and Tucker (1969) have tested several combinations to determine the effect of absorbent on the coefficient of performance (C.O.P) of the absorption cycle . Two refrigerants, ammomia and sulphur dioxide were separately tested with various absorbents. They concluded that the strong solution concentration should not be too high if a high C.O.P value is desirable. Unfortunately, a highly negative deviation from Raoults law gives a high strong solution concentration necessary to reduce pumping, heating and equipment costs. Through the application of the laws of thermodynamics, Mansoori and Patel (1979) have also shown that the coefficient of performance is dependent on the properties of the refrigerant, absorbent and their combination.

Review of all possible combinations have shown that the ammonia-water combination is the most suitable for air-cooled and low temperature applications. It has been chosen for the present study and the review that follows is on ammonia-water cycle only.

The engineering design of the ammonia-water absorption cycle requires accurate data on the physical and thermodynamic properties of the mixtures over a wide range of conditions. Several works have been reported on the combination, however the range covered by each of the investigators varies widely, and correlation of results is difficult. For instance; vapour pressures of

ammonia-water solution at temperatures between 0^{o} and $61.3^{o}C$, and at a limited range of ammonia concentration were presented by Perman (1901,1903). Scatchard, Epstein, Warburton and Cody (1947) presented tables for the saturation pressure, fraction of water in the mixture in vapour phase, and the relative volatility. They also derived the enthalpy of the mixtures based on empirical equations and formulae for the free energy of the vapour. Macriss, Eakin, Ellington and Hubler (1964) have measured the dew points and enthalpies of the mixture in liquid phase, and incorporated their measurements with the work of Scatchard,Epstein, Warburton and Cody (1947), to calculate the enthalpies of the solution in vapour phase. Their results which covered a wider range of concentration and pressures were presented in tabular form and as a chart.

The fact that solar energy is an intermittent heat source has led the majority of earlier investigators to use the intermittent absorption cycle, which produces less refrigeration than the continuous cycle, Chinnappa (1962) and, Vankatesh, Sriramulu and Gupta (1979). Since refrigeration is generally needed in a continuous manner, it is more advantageous to develop a continuous system. The present investigation is only concerned with the continuous aqua-ammonia cycle.

The performance of the continuous aqua-ammonia absorption refrigeration cycles has been predicted from theoretical analyses by many workers. The analysis by Whitlow (1966) was based on a three ton capacity air-cooled system. He identified the major sources of loss in the system as : the reflux condenser loss, absorbent in the vapour flowing to the condenser, throttling valve loss and heat exchange with the surroundings. However, the effects of system parameters on C.O.P were not considered. The effect of components operating temperatures on the C.O.P was presented by Stoecker and Reed (1971). They have shown that the refinement of the basic absorption cycle tremendously increased the C.O.P of the system. The effect of concentration and other system parameters were not mentioned.

Briggs (1971) has presented mathematical model for the concurrent, crosscurrent and countercurrent absorbers for use in the ammonia-water systems. He concluded that the concurrent absorption type is the most suitable for air-cooled application, since the absorption can be carried out in small horizontal tubes.

The analysis by Wilbur and Mitchell (1975) have shown that the strong solution concentration is dependent on the evaporator and condenser temperatures. They concluded that there is a minimum generator temperature requirement at a specific condenser temperature for normal operation of the system. The cycle analysed did

not include a reflux condenser. A limited range of operating temperatures was considered and significance of other system variables were not mentioned.

Huag and Chang (1978) have suggested five system parameters as the independent system design variables and presented a feasible design region. The effect of the reflux ratio was considered in their analysis, however, instead of using a reflux condenser to obtain the reflux, ammonia liquid from the total condenser was used. Moreover, their calculation was based on a single concentration value at the condenser exit, and a condenser temperature. The implications of these system parameters at other operating conditions were not presented.

The influence of operating temperatures, weak solution concentration and the relative circulation on system performance was presented by Whitlow (1976) for a solar operated cycle. The system analysed did not include a reflux condenser, and a limited range of operating temperatures was considered.

Krochta and Rumsey (1977) have analysed a system operated by solar energy for cooling and freezing of food. The effects of operating temperatures, and the ratio of strong solution pumped to the generator to ammonia vapour produced in the generator, on system performance were presented. The system was a water-cooled basic absorption cycle, the addition of

refinement components to improve the system performance, and the influence of concentrations were not presented. Shiran, Shitzer and Degari (1982) have analysed the operating and economic parameters of a solar air-conditioning system using aqua-ammonia cycle. They concluded that for a solar powered absorption refrigeration system to work, the collector outlet water temperature must be higher than the cut in/cut off temperature of the cycle, and that there is an optimal value for this temperature depending on other operating temperatures.

The first purposely built aqua-ammonia absorption refrigeration system powered by hot water from a flat plate collector for air-conditioning application, was reported by Faber, Flanigan, Lopez and Polifka (1966). The concentration of strong solution at the absorber was reported to be between 0.5 and 0.6, with the heating water temperature ranging from 60 to 100^{o}C. At steady state operation, 2.4 tons of refrigeration capacity and corresponding C.O.P of 0.57 were obtained, with heating water inlet temperature of 79.4^{o}C. Further increase in the strong solution concentration was reported to cause the pressure in the absorber to rise and cooling capacity to drop. Further explanation of experimental findings about the effect of other system parameters on the performance were not reported. The condenser and absorber were water-cooled.

Other experimental works that have been reported so far involved modification of existing gas-fired aqua-ammonia units to solar powered systems, Simmons and Whalig (1975). Dao, Simmons, Wolgast and Whalig (1976) reported the modification of a 17.6kW refrigeration capacity, gas-fired unit to operate at a capacity of 6kW, with 77^{o}C generator temperature and, condenser and absorber temperature of 35^{o}C, 6^{o}C evaporator temperature with corresponding C.O.P of 0.65.

2.3 CONCENTRATING SOLAR ENERGY COLLECTORS

For many solar thermal processes, it is desirable to deliver energy at higher temperatures than those obtainable with the ordinary flat plate collectors. By concentrating the solar radiation by at least an order of magnitude, higher delivery energy temperature can be achieved. Concentration also becomes necessary in the case of high performance evacuated glass tube flat plate collectors, when the cost of the evacuated receiver per unit area is higher than the cost of reflectors per unit area. However, the principal advantage of the flat plate collectors is the utilization of both direct and diffuse radiation without diurnal tracking.

Many designs have been set forth for the concentrating collectors, with each type best suited for a particular application. The single-axis tracking, line-focus

concentrators are employed when higher temperatures are required, for example, as in solar electric systems. These collectors are capable of concentrating only the direct and near-direct components of solar radiation, and concentration ratio as high as 50 is achievable, Nelson, Evans and Bansal (1975).

The two-axis tracking, point-focus concentrating collectors, such as the paraboloidal dishes (solar furnace), are capable of higher concentration ratios than single-axis tracking concentrators, with values well over 1000, Laszlo (1965). They are more expensive and only capable of concentrating the direct component of the solar radiation.

The use of heliostat with central absorbing power tower can provide concentration ratios of several thousands, with system operating temperatures over 1700^{o}C. However, each heliostat must be individually controlled and a central computer system is needed to achieve the tracking requirements, Gervais and Box (1975). The systems utilize only the direct component of the solar flux.

The last category of the concentrating collectors are the nontracking line-axis concentrators. They operate at temperatures intermediate between the ordinary flat plate collectors and the single-axis tracking concentrators. A line-axis concentrator which has been recently proposed for solar energy applications, that

achieves the highest concentration ratio for a given acceptance half-angle is the Compound Parabolic Concentrator (CPC) by Winston (1974). Concentration ratios up to 10 or more can be achieved depending on the acceptance half-angle θ_a, and if seasonal or daily tilt adjustments are acceptable. For the nontracking concentrators, the acceptance angle $2\theta_a$ is the angular excursion of the Sun during a specified period of time, Rabl (1976a). Tabor (1958) have shown that due to the cosine effect, non-tracking concentrating collectors gain little energy at hours far from solar noon, and not much is lost if the operating time is restricted to six or seven hours daily. The relationship between concentration ratio and cut-off time for the CPC collector has been presented by Rabl (1976a). Since the CPC collector is the other major subject of the present investigation, the remainder of this review is on the CPC collector only.

Subsequent to the discovery of the basic CPC for solar energy collection by Winston (1974), several variations of the concentrator have been described which are relevant to special applications. The use of the CPC for concentrating radiation onto a receiver of different cross-sections was proposed by Winston and Hinterberger (1975). Rabl (1976b) has presented differential equations that describe the reflector of a two-dimensional CPC with arbitary receiver shapes. Mills

and Guitronich (1978) have presented parametric expressions for calculating the height and reflector arc length of the concentrator. Alternative equations obtained from numerical analysis of the CPC trough with arbitrary degree of truncation were presented by McIntire (1979). Baum and Gordon have also derived analytical expressions for the same CPC parameters.

Winston (1970) and, Rabl and Winston (1976) have shown that solar radiation incident on the CPC aperture within the acceptance angle, that is, with $\theta_i < \theta_a$ will be accepted and reach the receiver; whereas all the radiation with $\theta_i > \theta_a$ will bounce back and forth between the reflector sides and eventually reemerge through the aperture as rejected radiation. Using the second law of thermodynamics, Rabl (1976a) has also shown that the CPC has the maximum possible concentration ratio for a given acceptance half-angle.

Radiation heat exchange in enclosures with specular surfaces, such as the CPC, has been treated by Sarofim and Hottel (1966). The use of Exchange factor in the analysis of radiation heat transfer between such surfaces have been covered in great detail by Sparrow and Cess (1970). The evaluation of the exchange factor, however, involves summation of a large or infinite number of reflections of radiation in a ray tracing procedure. An alternative approach for evaluating the CPC exchange factor based on the concept of the average

number of reflections has been developed by Rabl (1976c,1977). He presented analytical expressions for estimating the average number of reflections for full and truncated CPC trough with flat and fin receivers. Carvalho, Collares-Pereira, Gordon and Rabl(1985) have derived parametric equations for calculating the average number of reflections for arbitrarily truncated CPC with tubular receiver.

Another important consideration in the design of the CPC collector is the gap between the reflector and the receiver. The design principle of the concentrator by Welford and Winston (1978) requires the receiver to touch the bottom of the concentrator. However, a gap has to be introduced when evacuated glass envelope is used, or in order to reduce conductive heat losses since a reflector made of aluminum sheet and in direct contact with a receiver is an efficient cooling fin. Rabl, Goodman and Winston (1979) have suggested various approaches to incorporating the gap, and expressions for estimating the optical loss due to a gap were presented.

The evaluation of the CPC collector thermal performance requires a knowledge of the loss coefficients and their dependence on the various geometrical and operational parameters. The heat transfer modes for a CPC collector with flat receiver have been analysed by Rabl (1976b). Abdel-Khalik, Li and Randall (1978) have used finite element techniques to evaluate natural convection heat

transfer in a vertically oriented CPC collector with flat receiver. They presented charts for estimating the Nusselt numbers as a function of the Rayleigh number and concentration ratio. The thermal process in a CPC cusp fitted with an evacuated double pipe was analysed by Hsieh (1981) using mathematical formulations based on the CPC parameters. Based on the same CPC configuration, Hsieh and Mei (1983) have presented empirical equations for calculating the loss coefficient between the concentrator and the ambient.

To reduce convective heat losses from the receiver to the environment, and protect the receiver and reflector surfaces from dust and other contaminants in the environment, the CPC trough can be covered by glazing. The effect of the glazing in attenuating beam radiation expressed in terms of the cover transmittance has been presented by Duffie and Beckman (1980). For the transmittance of the glazing for diffuse radiation, Brandemuehl and Beckman (1980) have presented the effective beam incidence angle that can be used to obtain the transmittance for diffuse radiation incident on the CPC glazing.

The use of the CPC collector for various solar thermal applications have been reported by many investigators. The feasibility of low concentration ratio CPC collector for low temperature applications, and comparison of its performance with ordinary flat plate collectors have

been assessed by Gordon (1986). He concluded that the CPC collector with low concentration ratio between 1 and 2, can deliver comparable or more yearly energy relative to corresponding flat plate collectors. Collares-Pereira (1985) have tested a 1.5 concentration ratio non-evacuated CPC collector, and compared its performance with a selectively coated ordinary flat plate and an evacuated tube flate plate collectors. His results have shown that the CPC collector performs better than the other two types for operating temperatures between 35 and 100^{o}C.

Carvalho, Collares-Pereira and Gordon (1987) have used a wide range of design configurations to carry out economic optimization of stationary non-evacuated low concentration ratio CPC collectors. They suggested concentration ratio of 1.3 to 1.4, and a acceptance half-angle of 30^{o} for an optimal collector.

Many of the above references have been used by the author to build the CPC collector simulation model as presented in chapters three and four.

2.4 CONCLUSION

The heat-powered NH_3-H_2O absorption cycle has been found to be the most promising refrigeration system that can be used for airconditioning, food freezing and cooling applications, with air-cooled condenser and absorber.

Although the system has been used for these applications for many years through the use of LPG, natural gas or kerosine as the heat source; it has been found that the design principle for the cycle operating at both lower and higher temperature ranges still has not been well developed, and the system operation is maintained only by the high temperature energy source. Therefore to use the cycle through solar energy would require a detailed and accurate thermodynamic analysis of the cycle.

It is the author's contention that the delivery energy temperature required to drive the air-cooled aqua-ammonia absorption refrigeration systems, located at near equatorial latitudes can be met successfully through the use of a nontracking, nonevacuated CPC collector with tubular receiver.

CHAPTER 3

SOLAR RADIATION AND COLLECTION PERIOD

3.1 INTRODUCTION

In this chapter, the hourly irradiation incident on the collector surface has been obtained from the available measured total radiation data on the horizontal surface. Equations to test if incident beam radiation is accepted by the CPC at any particular time, and to obtain the collection period and tilt adjustments requirements have been developed.

3.2 SOLAR RADIATION AVAILABILITY

3.2.1 INTRODUCTION

A knowledge of the available solar radiation, it's direct and diffuse components, and the beam incidence angle on the collecting surface, is a prerequisite for the detailed and accurate prediction of performance of any solar thermal system.

In the tropics where many developing countries are located, there are limited measured solar radiation data due to lack of facilities. Where this is available, the most common is a measure of daily totals of radiation on a horizontal surface. Therefore to estimate solar radiation available to solar systems, one has to use either theoretical models to predict the incident energy

or use any of the available techniques that have been developed for estimating desired parameters from the available measured data.

Figure 3.0 shows Nigeria which has been specifically chosen for the present investigation because of its geographical location and size. The country is climatically a microcosm of West Africa. It is situated in the southeastern section of West Africa between latitudes 4 and 14^{o}N, and covers an area in excess of 900,000km^{2}. The solar radiation data used in this study are based on the work of Davis (1966) and Ojo (1972). The data have been collected over a period of six years from different locations in Nigeria. Figures 3.1 and 3.2 show respectively, the plot of monthly mean daily global radiation and temperature for two locations in Nigeria.

3.2.2 DIRECT AND DIFFUSE COMPONENTS OF SOLAR RADIATION

Outside the earth's atmosphere, the incident solar radiation is entirely direct. When it enters the earth's atmosphere, it undergoes complex interaction with various atmospheric components, such as, scattering by water droplets and dust particles, absorption by gases within the atmosphere, and refraction. The scattered radiation from various parts of the sky dome is the diffuse component of the solar radiation incident on earth's surface.

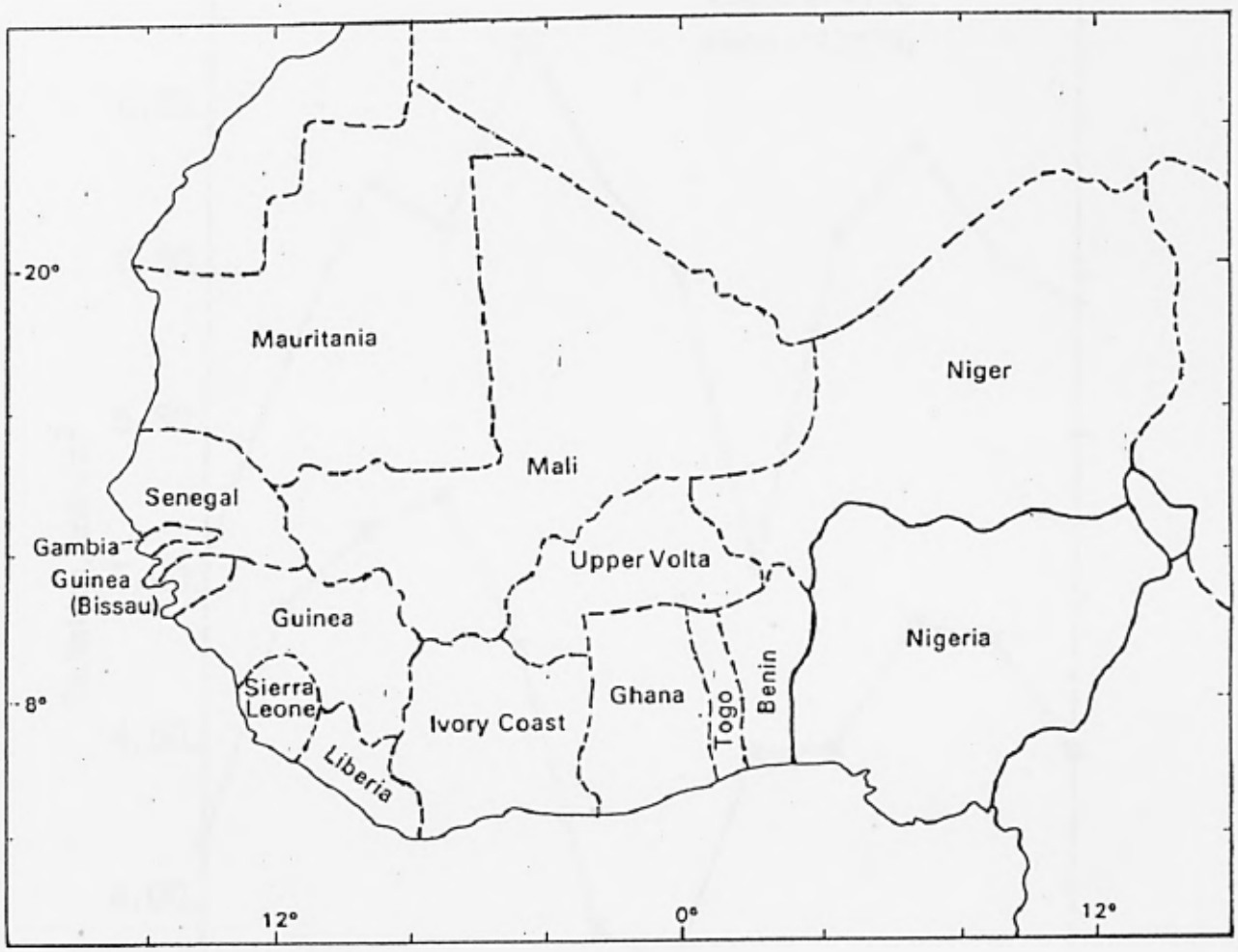


Fig. 3.0 Location of Nigeria in West Africa

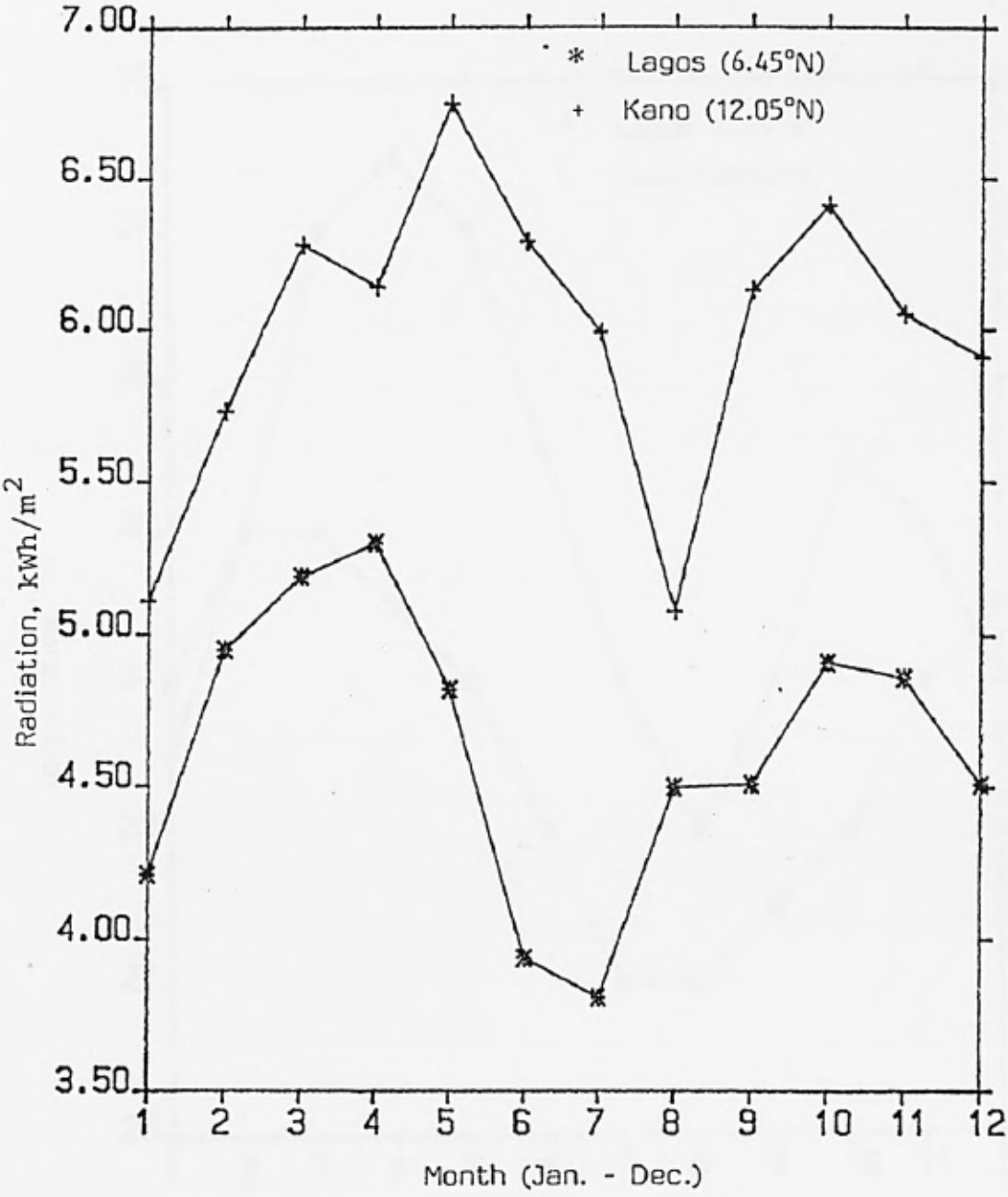


Fig. 3.1 Monthly average daily radiation on horizontal surfaces for two locations in West Africa.

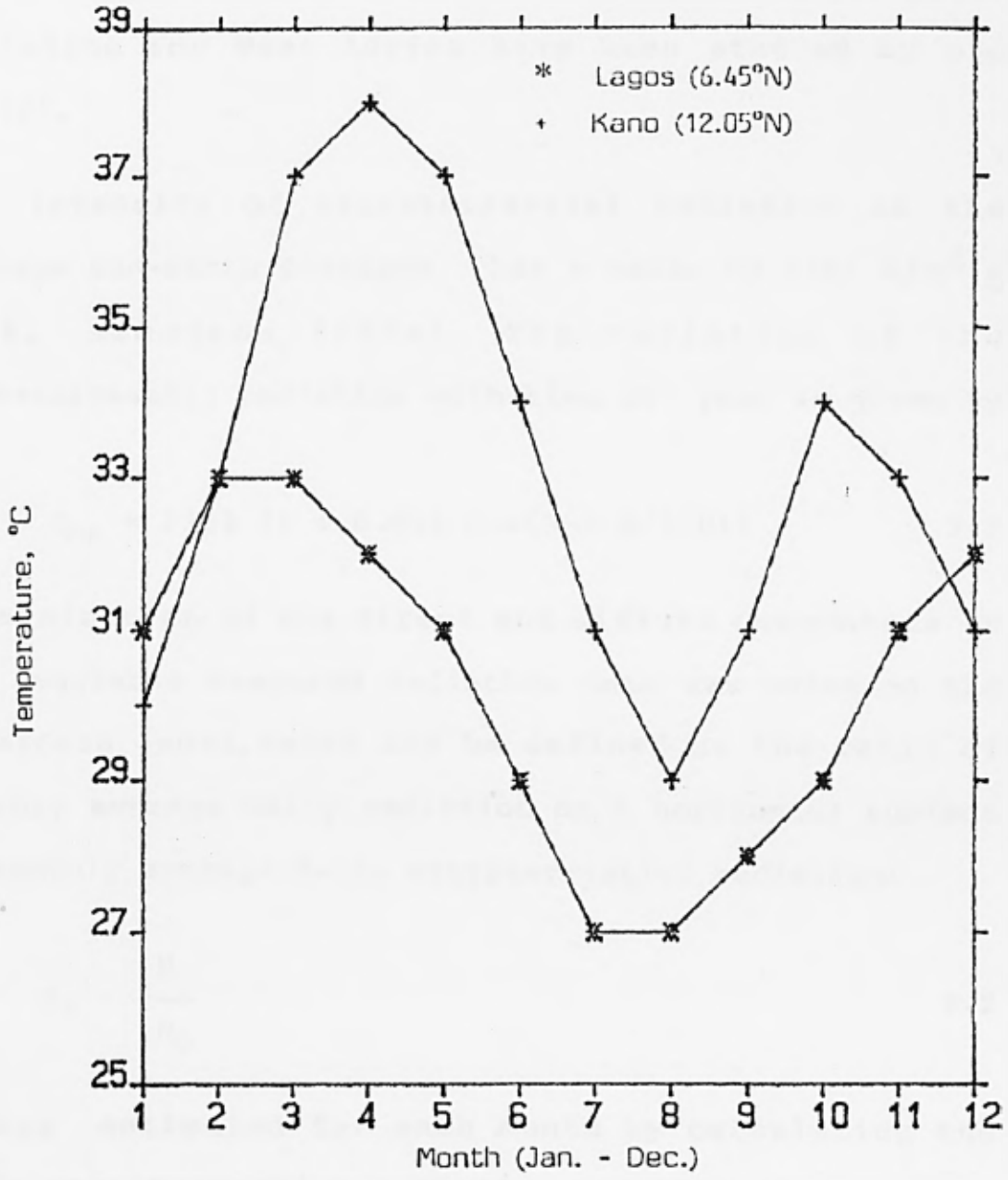


Fig. 3.2 Monthly average daily ambient temperature for two locations in West Africa.

The daily variation of solar incidence is greatly dependent on the cloud. The presence of clouds in the sky blocks the direct radiation and increases the diffuse component of the incoming radiation. Different types of clouds and their effects on the total solar radiation for West Africa have been studied by Ojo (1972).

The intensity of extraterrestial radiation at the average Sun-earth distance has a value of 1353 W/m^2 $\pm$ 1.5%, Simonson (1984). The variation of the extraterrestial radiation with time of year is given by

$$G_{on} = 1353\ (1 + 0.033\ \mathrm{Cos}(360\ N/370)) \qquad 3.1$$

Determination of the direct and diffuse components of the available measured radiation data was based on the clearness index,which can be defined as the ratio of monthly average daily radiation on a horizontal surface to monthly average daily extraterrestial radiation:

$$K_t = \frac{H}{H_o} \qquad 3.2$$

H_o was estimated for each month by calculating the daily extraterrestial radiation on horizontal surface for each day of the month, summing the results, and dividing by the number of days in the month. The calculation is shown in program radcor.f in appendix B.

The daily extraterrestial radiation is given by:

$$H_o(N) = 1353\ (24/\Pi)\ (1 + 0.033\ \text{Cos}(360\ N/370)(\ \text{Cos}\ \emptyset\ \text{Cos}\,\delta\ \ \text{Cos}\ \omega_s + \omega_s(2\Pi/360)\ \text{Sin}\ \emptyset\ \text{Sin}\ \delta) \quad 3.3$$

Where:

$$\omega_s = \text{Cos}^{-1}(-(\text{Tan}\ \emptyset\ \text{Tan}\ \delta) \quad 3.4$$

$$\delta = 23.45\ \text{Sin}((N-80)360/370) \quad 3.5$$

Using the clearness index, the fraction of the measured total radiation for Lagos(6.45^{o}N) that is diffuse was obtained with the correlation of Collares-Pereira and Rabl(1979). Table 3.1 shows the comparison of this correlation with that of Liu and Jordan(1962), and Page(1966). The Collares-Pereira and Rabl correlation is given by:

$$\frac{H_d}{H} = 0.775 + 0.00653(\omega_s - 90) - (0.505 + 0.00455(\omega_s - 90))\ \text{Cos}(115K_t - 103) \quad 3.6$$

The beam component of the total radiation is given by:

$$H_b = H - H_d \quad 3.7$$

3.2.3 ESTIMATION OF HOURLY RADIATION

In the absence of measured hourly radiation data, predicted hourly irradiation from the daily total has been used to carry out the prediction of hourly performance of the solar thermal system.

Table 3.1 Comparison of Liu & Jordan, Page, and Collares-Pereira & Rabl correlations for Lagos(6.45°N) radiation data.

MONTH	H kW/m^2	EXT kW/m^2	KT	L&J H_d/H	Pg H_d/H	C&R H_d/H
1	4.21	9.27	0.4543	0.4107	0.4866	0.4554
2	4.95	9.83	0.5038	0.3676	0.4307	0.4182
3	5.19	10.28	0.5049	0.3667	0.4295	0.4175
4	5.30	10.34	0.5124	0.3606	0.4210	0.4123
5	4.82	10.08	0.4780	0.3894	0.4598	0.4374
6	3.94	9.86	0.3997	0.4656	0.5484	0.5005
7	3.81	9.91	0.3843	0.4829	0.5657	0.5136
8	4.50	10.15	0.4434	0.4209	0.4990	0.4643
9	4.51	10.22	0.4414	0.4228	0.5012	0.4657
10	4.91	9.90	0.4962	0.3739	0.4393	0.4237
11	4.86	9.35	0.5195	0.3549	0.4129	0.4071
12	4.51	9.02	0.4999	0.3708	0.4351	0.4210

Collares-Pereira and Rabl(1979) have produced correlation equation which gives the ratio of hourly total to daily total radiation, as a function of day length and the hour in question as :

$$r_t = \frac{I}{H} = \Pi/24\ (a + b\ \text{Cos}\ \omega)\ \frac{\text{Cos}\ \omega - \text{Cos}\ \omega_s}{\text{Sin}\ \omega_s - (2\Pi\omega_s/360)\ \text{Cos}\ \omega_s} \qquad 3.8$$

The ratio of hourly diffuse to daily diffuse radiation is given by:

$$r_d = \frac{I_d}{H_d} = \Pi/24\ \frac{(\text{Cos}\ \omega - \text{Cos}\ \omega_s)}{\text{Sin}\ \omega_s - (2\Pi\omega_s/360)\ \text{Cos}\ \omega_s} \qquad 3.9$$

Where:

$$a = 0.409 + 0.5016\ \text{Sin}(\omega_s - 60) \qquad 3.10$$

$$b = 0.6609 - 0.4767\ \text{Sin}(\omega_s - 60) \qquad 3.11$$

The hourly beam component is given by:

$$I_b = I - I_d \qquad 3.12$$

3.2.4 ESTIMATION OF HOURLY RADIATION ON TILTED SURFACE

The amount of radiation on the tilted collector surface was obtained from the horizontal radiation data, by using the beam incidence angle on both the horizontal and inclined surfaces.

The angle of incidence is a function of geographical angles of location on the earth surface, day of year and time of day. The equation for calculating this angle

has been adopted from Simonson (1984), and Sayigh(1977). Equation relating the beam incidence angle on an inclined surface with other angles is given by:

$$\begin{aligned}\cos\theta = {} & \sin\delta \sin\phi \cos S - \sin\delta \cos\phi \sin S \cos\gamma \\ & + \cos\delta \cos\phi \cos S \cos\omega \\ & + \cos\delta \sin\phi \sin S \cos\gamma \cos\omega \\ & + \cos\delta \sin S \sin\gamma \sin\omega \end{aligned} \qquad 3.13$$

For horizontal surface, $S = 0^{o}$, and the angle of incidence is the Zenith angle of the Sun, θ_z, and is given by:

$$\cos\theta_z = \cos\delta \cos\phi \cos\omega + \sin\delta \sin\phi \qquad 3.14$$

If the surface is sloped towards the equator $\gamma = 0^{o}$, and the angle of incidence is given by:

$$\begin{aligned}\cos\theta = {} & \sin\delta \sin\phi \cos S - \sin\delta \cos\phi \sin S \\ & + \cos\delta \cos\phi \cos S \cos\omega \\ & + \cos\delta \sin\phi \sin S \cos\omega \\ = {} & \sin(\phi - S) \sin\delta + \cos(\phi - S) \cos\delta \cos\omega \end{aligned} \qquad 3.15$$

The hourly incidence angle on the collector surface was calculated with the declination angle (δ) taken as constant for any particular day, the hour angle (ω) was estimated at the midpoint of an hour (at 8 for the hour between 7.30 and 8.30) and assumed constant for that hour. The beam incidence angle is therefore taken as constant for the one hour time step.

Once the incidence angles on both the horizontal and

tilted surfaces are known, the angular correction for the beam radiation on the incline surface is obtained using the geometric factor, R_b. The factor can be defined as the ratio of beam radiation on the tilted surface to that on a horizontal surface. It can be expressed in terms of the components shown in fig. 3.3.

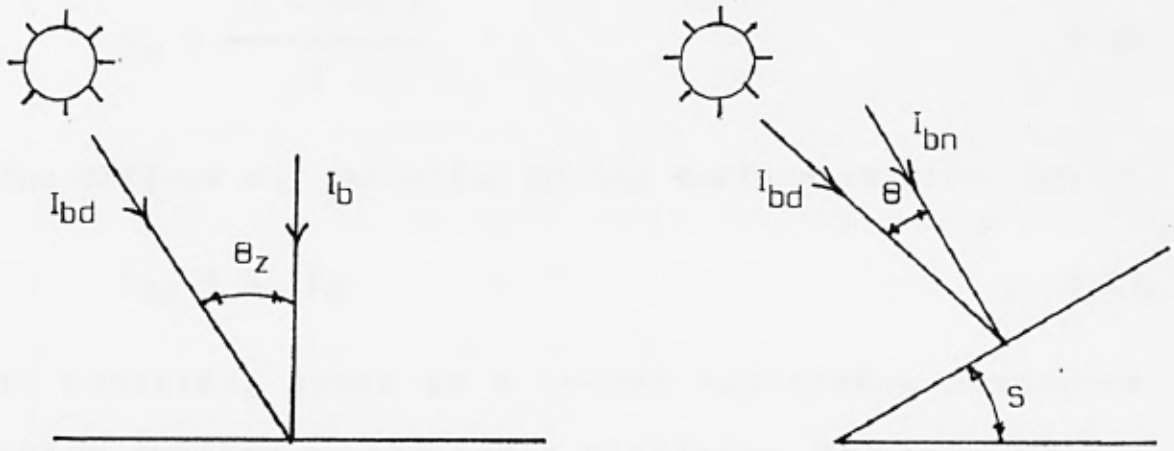


Fig. 3.3 Incident beam radiation on horizontal and inclined surfaces.

From the geometry of fig. 3.3 :

$$I_b = I_{bd} \cos \theta_z \qquad 3.16$$

$$I_{bn} = I_{bd} \cos \theta \qquad 3.17$$

$$R_b = \frac{I_{bn}}{I_b} = \frac{I_{bd} \cos \theta}{I_{bd} \cos \theta_z}$$

$$= \frac{\cos(\phi - S) \cos \delta \cos \omega + \sin(\phi - S) \sin \delta}{\cos \phi \cos \delta \cos \omega + \sin \phi \sin \delta} \qquad 3.18$$

$$I_{bn} = R_b I_b \qquad 3.19$$

The angular correction for the diffuse component on the incline surface depends on the distribution of diffuse radiation over the sky, which generally is not well known. If isotropic diffuse sky radiation is assumed, the diffuse angular correction factor is equal to the view factor of the tilted surface to the sky, and it is given by:

$$R_d = \frac{1 + \text{Cos } S}{2} \qquad 3.20$$

The diffuse sky radiation on the surface is given by:

$$I_{dn} = R_d \, I_d \qquad 3.21$$

In addition, there is a ground reflection component which applies to the total radiation. The view factor for reflection from the ground is given by:

$$R_g = \frac{1 - \text{Cos } S}{2} \qquad 3.22$$

The diffuse ground radiation on the surface is given by:

$$I_g = (I_b + I_d) \, \rho \, (1 - \text{Cos } S)/2 \qquad 3.23$$

All the above equations have been incorporated into the program radlagos shown in appendix B to obtain the hourly radiation data.

3.3 SOLAR ENERGY COLLECTION FOR THE CPC COLLECTOR

3.3.1 TRANSMISSION OF DIRECT AND DIFFUSE RADIATION THROUGH THE CPC COLLECTOR GLAZING

In order to reduce convective heat losses from the receiver to the environment, and to protect the receiver and the reflector surfaces from dust and other contaminants in the atmosphere, the collector is covered with glass. For detailed and accurate analysis of the collector performance, a knowledge of the transmission, reflection and absorption of solar radiation by the glass cover is necessary. The optical properties of the glass cover are functions of the incoming radiation, and the glazing material thickness, refractive index and extinction coefficient. The refractive index and extinction coefficient are assumed constant in the solar energy spectrum for the clear glass considered in this study.

The optical properties of the glass cover for beam radiation can be obtained by using the beam incidence angle. For the single glazing considered, there are two glass/air interfaces which cause reflection losses. The reflection from the interface has two components of polarisation resolved parallel and perpendicular to the plane of incidence. Excluding any absorption by the glass, these components are given respectively by:

$$r_{11} = \frac{\mathrm{Tan}^2(\theta_r - \theta_i)}{\mathrm{Tan}^2(\theta_r - \theta_i)} \qquad 3.24$$

$$r_I = \frac{\mathrm{Sin}^2(\theta_r - \theta_i)}{\mathrm{Sin}^2(\theta_r - \theta_i)} \qquad 3.25$$

The angle of refraction ,θ_r, can be obtained from Snell's law:

$$\frac{\mathrm{Sin}\ \theta_i}{\mathrm{Sin}\ \theta_r} = \frac{n_r}{n_i} \qquad 3.26$$

The refractive index n_i and n_r have been taken as 1 and 1.526 for air and the glass cover respectively.

The transmissivity of the cover with absorption of radiation taken into consideration is obtained from Bouguer's law, Duffie and Beckman (1980):

$$\tau_a = e^{-KX/\mathrm{Cos}\ \theta_r} \qquad 3.27$$

Using the ray-tracing technique, with inclusion of reflection and absorption losses, and taking the transmission of the incident unpolarized radiation as the average of the two polarized components, the cover optical properties are given by Simonson(1984) as:
Transmittance :

$$\tau = \frac{1}{2}\left[\frac{\tau_a\ (1 - r_{11})^2}{1 - (r_{11}\ \tau_a)^2} + \frac{\tau_a\ (1-r_I)^2}{1 - (r_I\ \tau_a)^2}\right] \qquad 3.28$$

Reflectance :

$$\rho = \frac{1}{2}\{[\, r_{11} + \frac{(1 - r_{11})^2\, \tau_a^{\,2}\, r_{11}}{1 - (r_{11}\, \tau_a)^2}\,] + [\, r_I + \frac{(1 - r_I)^2\, \tau_a^{\,2}\, r_I}{1 - (r_I\, \tau_a)^2}\,]\} \qquad 3.29$$

The absorptance is given by:

$$\alpha = 1 - \tau - \rho \qquad 3.30$$

The transmittance of the CPC glazing system for diffuse radiation has been studied by Brandemuehl and Beckman(1980). They proposed the effective beam radiation incidence angle which can be used to obtain the diffuse transimittance for CPC of any acceptance angle. The effective beam angle can be obtained from:

$$\theta_e = 44.86 - 0.0716\, \theta_a + 0.00512\, \theta_a^{\,2} - 0.00002798\, \theta_a^{\,3} \qquad 3.31$$

Transmittance for diffuse radiation is given by:

$$\tau_d = \tau_b(\theta_e) \qquad 3.32$$

It is calculated by replacing θ_i with θ_e in equations 3.24 to 3.30.

The above equations have been programmed and are shown in appendix B as subroutines BEAM, DIFFUS, and OPTPRO.

3.3.2 COLLECTION TIMES AND INCIDENT ENERGY FOR THE THE CPC COLLECTOR

Orientation of the CPC collector is related to the fixed lateral acceptance angle, $2\theta_a$, shown in figure 3.4. Therefore, a CPC cusp located in the northern latitude should be oriented with its longitudunal axis aligned in the east-west direction, and sloped towards the equator. With this arrangement the projection of the angle of incidence of the beam radiation in the north-south vertical plane lies within the limits $\pm \theta_a$ during the collection time without the need for diurnal tracking.

In determining the daily collection times, the geometric aspects that influence the energy incident on the collecting surface have been considered. The geometric relationships between a collecting plane of a particular orientation relative to the earth at any time, and the position of the sun relative to that plane can be described by equations 3.13 to 3.15 in section 3.1.4. Relationships for other orientations in addition to equations 3.13 to 3.15 are as follows:

For a vertical surface facing south, $S = 90^{o}$, $\gamma = 0^{o}$:

$$\cos \theta_v = - \sin \delta \cos \phi + \cos \delta \sin \phi \cos \omega \qquad 3.34$$

For vertical surface facing west, $S = 90^{o}$, $\gamma = -90^{o}$:

$$\cos \theta_{v,90} = - \cos \delta \sin \omega \qquad 3.35$$

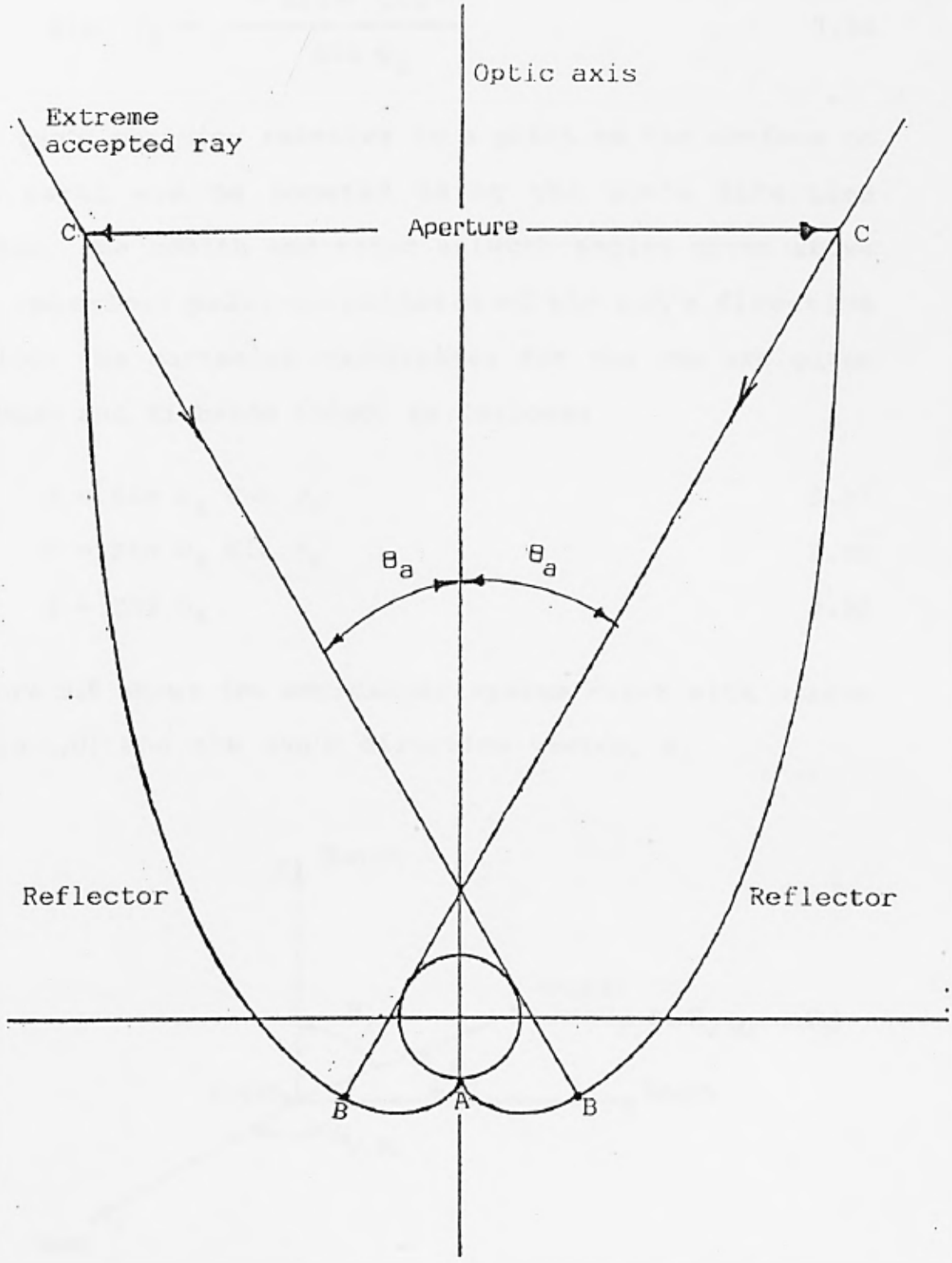


Fig. 3.4 Fully developed two-dimensional CPC collector with tubular receiver, showing acceptance half-angle θ_a, and extreme accepted rays.

The solar azimuth angle, γ_s, is given by:

$$\text{Sin } \gamma_s = \frac{-\text{Sin}\,\omega\ \text{Cos}\,\delta}{\text{Sin}\ \theta_z} \qquad 3.36$$

The sun's position relative to a point on the surface of the earth can be located using the sun's direction vector. The zenith and solar azimuth angles given above are spherical polar coordinates of the sun's direction vector. The cartesian coordinates for the sun are given by Bush and Richards (1980) as follows:

$$X = \text{Sin } \theta_z \text{ Cos } \gamma_s \qquad 3.37$$

$$Y = \text{Sin } \theta_z \text{ Sin } \gamma_s \qquad 3.38$$

$$Z = \text{Cos } \theta_z \qquad 3.39$$

Figure 3.5 shows the coordinate system X-Y-Z with origin at (0,0,0) and the sun's direction vector, S.

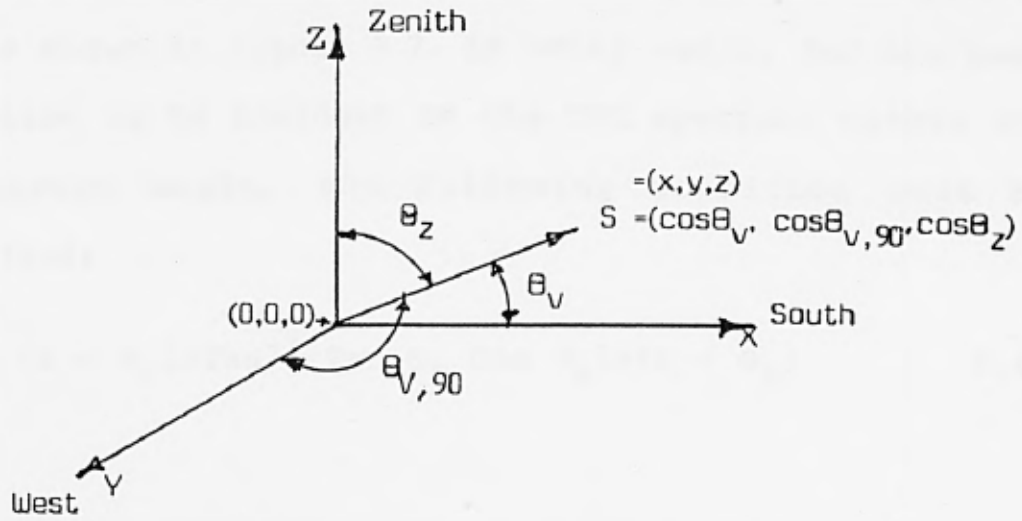


Fig. 3.5 Coordinate system and elements used in description of sun's direction vector.

When the sun vector is projected onto the X-Z plane as shown in figure 3.6, the projection is located by the angle Ψ, given by:

$$\text{Tan } \Psi = \frac{\text{Sin } \theta_z \text{ Cos } \gamma_s}{\text{Cos } \theta_z}$$

$$= \text{Tan } \theta_z \text{ Cos } \gamma_s \qquad 3.40$$

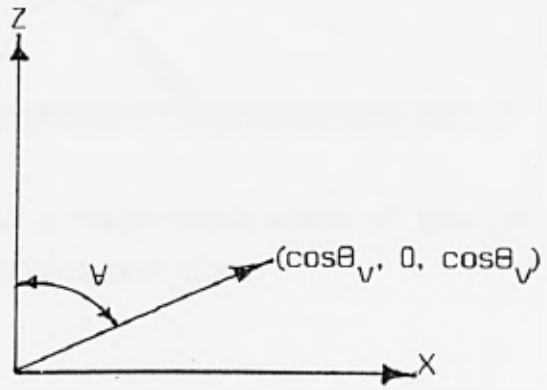


Fig. 3.6 Sun's projection angle on X-Z plane.

In order to collect energy at any particular time, the projection angle Ψ, must lie within the acceptance planes shown in figure 3.7. In other words, for the beam radiation to be incident on the CPC aperture within the acceptance angle, the following condition must be satisfied:

$$(S - \theta_a) \leq \text{Tan}^{-1}(\text{Tan } \theta_z \text{ Cos } \gamma_s) \leq (S + \theta_a) \qquad 3.41$$

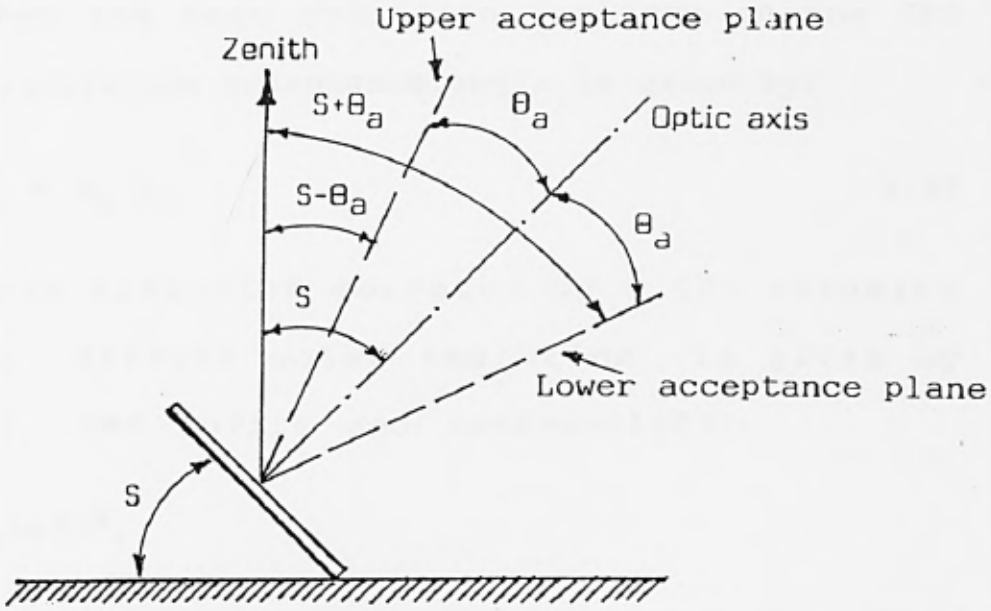


Fig. 3.7 Projection on a north-south plane of the CPC acceptance angles and slope.

Equation 3.41 and those for calculating the solar angles have been incorporated into the program LACPC in appendix B, and flowchart FLACCP in appendix C shows the solution procedure. The CPC daily collection times for minimum 7 hour per day collection time without diurnal tracking have been determined. Results for various acceptance half-angles and slopes, for locations between 4 and 14°N latitude were obtained. However, because of the huge data generated from this simulation, it has only been possible to present few result data shown in tables A1 to A15 in appendix A. The collector tilt adjustment requirements derived from the results data are presented in tables 3.2 to 3.6.

If the condition of equation 3.41 is satisfied at any particular time for a given acceptance half-angle and

tilt, then the beam radiation incident on the CPC aperture within the acceptance angle is given by:

$$I_{b,C} = R_b I_b \qquad 3.42$$

The diffuse radiation accepted by a CPC assuming isotropic diffuse solar radiation is given by Rabl(1980), and Duffie and Beckman(1980):

If $(S + \theta_a) \leq 90^o$,

$$I_{d,C} = I_{d,h}/C \qquad 3.43$$

If $(S + \theta_a) > 90^o$,

$$I_{d,C} = I_{d,h} \frac{(1/C + \text{Cos } S)}{2} + I_t \rho \frac{(1/C - \text{Cos } S)}{2} \qquad 3.44$$

3.4 DUST AND SHADING EFFECTS ON THE CPC COLLECTOR

The severity of dust problem depends on the location, reflector material and ease of maintenance. The effect of the dust, however, depends on whether the collector's reflector is exposed to the environment. When the collector is glazed as considered in the present investigation, then the scattering and absorption caused by the dust on the reflector are eliminated. On the other hand, dust on the glazing reduces the glass transmittance and increases its absorptance. Therefore, adequate provision must be made

for routine washing of the glazing, especially, since the slope of a collector located near equatorial latitudes (0 - 15^{o}N), may not be large enough to provide relative self-cleaning.

Duffie and Beckman(1980) have recommended for design purposes, a 2% loss due to dirt on a glass cover, and the radiation absorbed by the receiver can be multiplied accordingly by a loss factor of 0.98. The effect of shading on the collector can also be significant when adjacent structures intercept solar radiation. A shading correction factor of 0.97 can be used for design purposes.

Table 3.2 Adjustments of CPC collector tilt to obtain minimum 7hr/day collection time without diurnal tracking ; $\theta_a = 7^o$, $\phi = 4^oN$

Number of tilt adjustments per year = 10

No.	TILT (S^o)	COLLECTION PERIOD WITHOUT ADJUSTMENT	TOTAL DAYS
1	29	1/Jan - 28/Jan	28
2	23	25/Jan - 18/Feb	25
3	13	19/Feb - 16/Mar	26
4	7	3/Mar - 24/Apr	53
5	16	24/Apr - 19/May	26
6	22	16/May - 28/Jul	74
7	15	29/Jul - 22/Aug	25
8	7	19/Aug - 10/Oct	53
9	18	10/Oct - 2/Nov	24
10	22	20/Oct - 13/Nov	25
11	29	13/Nov - 31/Dec	49

Table 3.2 cont.

Adjustments of CPC collector tilt to obtain minimum 7hr/day collection time without diurnal tracking ; $\theta_a = 7^{\circ}$, $\phi = 6.25^{\circ}N$

Number of tilt adjustments per year = 10

No.	TILT (S°)	COLLECTION PERIOD WITHOUT ADJUSTMENT	TOTAL DAYS
1	31	1/Jan - 29/Jan	29
2	24	29/Jan - 21/Feb	24
3	14	22/Feb - 19/Mar	26
4	7	8/Mar - 29/Apr	53
5	15	27/Apr - 24/May	28
6	21	22/May - 22/Jul	62
7	15	20/Jul - 16/Aug	28
8	7	14/Aug - 5/Oct	53
9	19	5/Oct - 30/Oct	25
10	24	20/Oct - 12/Nov	24
11	31	12/Nov - 31/Dec	50

Table 3.2 cont.

Adjustments of CPC collector tilt to obtain minimum 7hr/day collection time without diurnal tracking ; $\theta_a = 7^{\circ}$, $\phi = 14^{\circ}N$

Number of tilt adjustments per year = 10

No.	TILT (S°)	COLLECTION PERIOD WITHOUT ADJUSTMENT	TOTAL DAYS
1	39	1/Jan - 28/Jan	28
2	32	28/Jan - 21/Feb	25
3	22	22/Feb - 18/Mar	25
4	11	14/Mar - 8/Apr	26
5	7	22/Mar - 23/May	63
6	11	12/May - 1/Aug	82
7	7	21/Jul - 21/Sep	63
8	20	21/Sep - 15/Oct	25
9	30	15/Oct - 31/Oct	17
10	32	20/Oct - 13/Nov	25
11	39	13/Nov - 31/Dec	45

Table 3.3 Adjustments of CPC collector tilt to obtain minimum 7hr/day collection time without diurnal tracking ; $\theta_a = 10^o$, $\phi = 4^oN$

Number of tilt adjustments per year = 6

No.	TILT (S^o)	COLLECTION PERIOD WITHOUT ADJUSTMENT	TOTAL DAYS
1	30	1/Jan - 6/Feb	37
2	20	25/Jan - 7/Mar	42
3	10	19/Feb - 9/May	80
4	20	27/Apr - 16/Aug	112
5	10	4/Aug - 22/Oct	80
6	25	20/Oct - 12/Dec	54
7	30	4/Nov - 31/Dec	58

Table 3.3 cont.

Adjustments of CPC collector tilt to obtain minimum 7hr/day collection time without diurnal tracking ; $\theta_a = 10^{\circ}$, $\phi = 6.25^{\circ}N$

Number of tilt adjustments per year = 6

No.	TILT (S°)	COLLECTION PERIOD WITHOUT ADJUSTMENT	TOTAL DAYS
1	30	1/Jan - 13/Feb	44
2	15	13/Feb - 23/Mar	39
3	10	24/Feb - 16/May	82
4	20	4/May - 9/Aug	98
5	10	28/Jul - 17/Oct	82
6	20	1/Oct - 9/Nov	40
7	30	28/Oct - 31/Dec	65

Table 3.3 cont.

Adjustments of CPC collector tilt to obtain minimum 7hr/day collection time without diurnal tracking ; $\theta_a = 10^{\circ}$, $\phi = 14^{\circ}N$

Number of tilt adjustments per year = 5

No.	TILT (S°)	COLLECTION PERIOD WITHOUT ADJUSTMENT	TOTAL DAYS
1	36	1/Jan - 18/Feb	49
2	30	25/Jan - 7/Mar	42
3	15	1/Mar - 6/Apr	37
4	10	11/Mar - 2/Oct	206
5	25	25/Sep - 2/Nov	39
6	36	23/Oct - 31/Dec	70

Table 3.4 Adjustments of CPC collector tilt to obtain minimum 7hr/day collection time without diurnal tracking ; $\theta_a = 15^o$, $\phi = 4^oN$

Number of tilt adjustments per year = 2

No.	TILT (S^o)	COLLECTION PERIOD WITHOUT ADJUSTMENT	TOTAL DAYS
1	30	1/Jan - 24/Feb	55
2	15	25/Jan - 16/Nov	296
3	30	17/Oct - 31/Dec	76

Table 3.4 cont.

Adjustment of CPC collector tilt to obtain minimum 7hr/day collection time without diurnal tracking : $\theta_a = 15^o$, $O = 6.25^oN$

Number of tilt adjustments per year = 2

No.	TILT (S^o)	COLLECTION PERIOD WITHOUT ADJUSTMENT	TOTAL DAYS
1	30	1/Jan - 1/Mar	60
2	15	1/Feb - 9/Nov	282
3	30	12/Oct - 31/Dec	81

Table 3.4 cont.

Adjustments of CPC collector tilt to obtain minimum 7hr/day collection time without diurnal tracking ; $\theta_a = 15^o$, $\phi = 14^oN$

Number of tilt adjustments per year = 2

No.	TILT (S^o)	COLLECTION PERIOD WITHOUT ADJUSTMENT	TOTAL DAYS
1	31	1/Jan - 16/Mar	75
2	15	19/Feb - 22/Oct	246
3	31	27/Sep - 31/Dec	96

Table 3.5 Adjustment of CPC collector tilt to obtain minimum 7hr/day collection time without diurnal tracking : $\theta_a = 20^o$, $4 \leq \phi < 9^oN$

Number of tilt adjustments per year = 0

No.	TILT (S^o)	COLLECTION PERIOD WITHOUT ADJUSTMENT	TOTAL DAYS
1	20	1/Jan - 31/Dec	365

Table 3.5 cont.

Adjustments of CPC collector tilt to obtain minimum 7hr/day collection time without diurnal tracking : $\theta_a = 20^o$, $10 \leq \phi \leq 14^oN$

Number of tilt adjustments per year = 2

No.	TILT (S^o)	COLLECTION PERIOD WITHOUT ADJUSTMENT	TOTAL DAYS
1	30	1/Jan - 28/Mar	87
2	15	8/Feb - 2/Nov	268
3	30	15/Sep - 31/Dec	108

Table 3.6 Adjustments of CPC collector tilt to obtain minimum 7hr/day collection time without diurnal tracking ; $\theta_a = 30^o$.

Number of tilt adjustments per year = 0			
Collection period = 1/Jan - 31/Dec (365 days)			
Latitude (ϕ^o)	4	6.25	14
Tilt (S^o)	$6 \leq S < 30$	$8 \leq S \leq 30$	$20 < S \leq 30$

CHAPTER 4

DESIGN ANALYSIS OF A CPC SOLAR COLLECTOR

4.1 INTRODUNCTION

Geometrical parameters for the CPC collector with tubular receiver are presented in this chapter. Thermal analysis of the collector has been undertaken, and correlation equations for the top loss coefficient were developed. Predictions of the collector performance using the radiation data for Lagos ($6.45^{o}N$) have been made.

The conventional flat plate solar energy collectors can supply heat up to a maximum of about $65^{o}C$ above ambient temperature. However, when a higher delivery temperature is required, concentration of solar radiation becomes necessary. The concentrating collectors optically concentrate the incident radiant energy onto a small area (the receiver) where it is transformed into heat.

The heat loss from a solar energy collector is proportional to the receiver area, and inversely proportional to the concentration ratio in the case of the concentrating collectors. Consequently, the concentration ratio is an important parameter that is considered in the design of a solar concentrator. It can be defined on a geometric basis as :

$$C = \frac{\text{aperture area}}{\text{receiver area}} \qquad 4.1$$

The concentration ratio is intimately related to the acceptance angle, which is the angular range over which the radiation is accepted without moving all or part of the collector. The two-dimensional CPC collector shown in figure 4.1, page 63 is characterized by the acceptance half-angle, θ_a, which determines the maximum possible concentration ratio given by Winston(1974) as :

$$C_{max} = \frac{1}{\text{Sin } \theta_a} \qquad 4.2$$

This ideal concentration ratio can be attained only by a fully developed CPC for any given angular acceptance; and when the CPC is aligned in the east-west direction it can achieve a concentration ratio of about 10 without diurnal tracking. This is due to the change in solar elevation (vertical solar swing) during the central 7 hour of the day which is at most $\pm$ 6°, Rabl(1976a).

The major advantages of the CPC collector are that minimal or no tracking is required, and both the direct and diffuse components of the solar radiation are utilised. Delivery temperatures up to 200°C can be achieved even with a non-evacuated receiver, Hsieh(1979).

The bad feature of the CPC collector is the large reflector area relative to the aperture area required to achieve the ideal concentration ratio. Fortunately, this

disadvantage can be alleviated by truncation of the full- height CPC to reduce the reflector material, with little loss in concentration ratio. The top portion of a fully developed CPC does not intercept much radiation and can therefore be discarded.

In the remaining sections of this chapter, the design and thermal analyses of the CPC collector with nonevacuated tubular receiver have been undertaken.

4.2 THE CPC GEOMETRIC DESIGN PARAMETERS

4.2.1 THE REFLECTOR HEIGHT AND ARC LENGTH

The reflector at each side of the CPC collector as shown in figure 4.1 page 63, is made up of two distinct segments. The first segment is the involute section curve AB, and the second is the upper reflector section curve BC. The development of the full CPC is based on the cartesian coordinates system shown in figure 4.2, page 64. For a given acceptance half-angle θ_a, and a tubular receiver of radius R, the distance ρ , along a tangent line from the receiver is related to the angle θ between the negative y-axis and the radius to the point of tangency T by the following analytical expressions by Rabl(1976b):

For the involute section, curve AB, with $|\theta| \leq (\theta_a + \pi/2)$:

$$\rho(\theta) = R\,\theta \qquad 4.3$$

and the coordinates X and Y are given by:

$$X = R\ (\text{Sin}\ \theta - \theta\ \text{Cos}\ \theta) \qquad 4.4$$

$$Y = R\ (-\ \text{Cos}\ \theta - \theta\ \text{Sin}\ \theta) \qquad 4.5$$

For the upper reflector section , curve BC, with $(\theta_a + \pi/2) \leq |\theta| \leq (3\pi/2 - \theta_a)$:

$$\rho(\theta) = R\ [\ \frac{\theta + \theta_a + \pi/2 - \text{Cos}(\theta - \theta_a)}{1 + \text{Sin}(\theta - \theta_a)}\ ] \qquad 4.6$$

and the coordinates X and Y are given by :

$$X = R\ \text{Sin}\ \theta - \rho(\theta)\ \text{Cos}\ \theta \qquad 4.7$$

$$Y = -R\ \text{Cos}\ \theta - \rho(\theta)\ \text{Sin}\ \theta \qquad 4.8$$

The top portion of the reflector, where the curve becomes almost parallel to the y-axis, is ineffective and contributes little to the concentration. In practical design, the full CPC has to be truncated to reduce reflector material cost and depth of the collector box. The concentration ratio of a truncated CPC is therefore lower than that given by equation 4.2 . Based on the definition of equation 4.1, the concentration ratio is given by:

$$C = \frac{W}{2\ \Pi\ R} \qquad 4.9$$

The truncation can be carried out graphically by drawing a horizontal line parallel to the X-axis across the cusp

at a predetermined height, and discarding the part of the curve above this line as shown in figure 4.1 page 63 . The shape of the curve below the cut off line, TT, is unaffected by the truncation, and the acceptance angle is still the same as the full CPC from which it was truncated.

The truncation can also be performed analytically by defining the curve to a maximum θ value less than $(3\pi/2 - \theta_a)$ in equations 4.6 to 4.8 .

The height of a fully developed CPC collector with tubular receiver is given by Rabl, Goodman, and Winston(1979) as:

$$H_f = \pi R \, (1/(\sin \theta_a \tan \theta_a) + 0.5 + 1/(\pi \sin \theta_a) \qquad 4.10$$

Based on the above equation, the corresponding expression for the height of a truncated CPC has been defined by the author as :

$$H_t = \pi R \, (C/\tan \theta_d + 0.5 + 1/(\pi \sin \theta_d) \qquad 4.11$$

Equation 4.11 has been used to calculate the height of a truncated CPC and has been found to agree with the graphical solution. The edge ray angle, θ_d, was obtained from numerical solution of the equation given by Baum and Gordon(1984):

$$C = [(1/\pi)\text{Sin}\ \theta_d\ (\frac{2\pi + \theta_a - \theta_d + \text{Sin}(\theta_a + \theta_d)}{1 - \text{Cos}(\theta_a + \theta_d)})]$$

$$- (1/\pi)\ \text{Cos}\ \theta_d \qquad 4.12$$

The reflector arc length can be obtained from the analytical expressions given by Baum and Gordon (1984) :

$$L_r = R(\theta_a + \pi/2)^2 + 2R(-1 + 1/\text{Sin}\ \theta_m)$$
$$+ R(2\pi + \theta_a - \theta_d)((\text{Cos}\ \theta_m/\text{Sin}^2\theta_m) - \ln(\text{Tan}\ \theta_m/2))$$
$$- 4R(Gc - sc) \qquad 4.13$$

Where,

$$\theta_m = (\theta_a + \theta_d)/2 \qquad 4.14$$

$$Gc = 0.915965594 \text{ (catalan's constant)}$$

$$sc = \sum_{k=1}^{\infty} \frac{\text{Sin}[0.5(2k - 1)(\theta_a + \theta_d)]}{(2k - 1)^2} \qquad 4.15$$

Equations 4.3 to 4.15 have been programmed and are shown in both subprograms CPCDESG and CPCPRO in appendix B. The flowchart FLPROP in appendix C shows the method of solution of these equations. Variation of the collector height and reflector arc length are shown in figures 4.3 and 4.4, pages 65 and 66 respectively .

4.2.2 THE CPC TRANSMISSION FACTOR

In the analysis of radiation heat transfer between surfaces, a knowledge of the fraction of radiant energy leaving one surface that arrives at the other is necessary. For diffusely emiting and diffusely

reflecting surfaces, the view factor provides information on this fraction. However, when specularly reflecting surfaces are involved, as in the CPC, then the analysis is facilitated by the use of exchange factor (or the transmission factor).

The exchange factor can be defined as the fraction of the diffuse radiation leaving one surface which reaches another surface either directly or via any intervening specular reflections. Its evaluation involves the ray-tracing technique, requiring a summation of large or infinite number of reflections. In enclosures consisting of curved specular surfaces such as the CPC, the task of evaluating the exchange factor using the numerical method is even more difficult than for flat surfaces, Sparrow and Cess(1970). Fortunately, a simple expression based on the concept of the average number of reflections, which can be used to obtain approximate value for the CPC transmission factor has been presented by Rabl(1977) :

$$\tau_C = \rho_r^{\langle n \rangle_i} \qquad 4.16$$

Rabl(1976c) has also shown that the average number of reflections for a CPC can be expressed as :

$$\langle n \rangle_i = E_{r-s}(A_r/A_s) \qquad 4.17$$

E_{r-s} is the fraction of the radiation emitted by the reflector that would reach the receiver in the limit of

ideal reflectivity. Analytical expression for calculating the average number of reflections for a CPC with flat receiver was presented by Rabl(1976c,1977). For the CPC with tubular receiver, the average number of reflections is given by Carvalho, Collares-Pereira, Gordon and Rabl(1985) :

$$\langle n \rangle_i = \{ \frac{\sqrt{2}}{2\pi} \int_{\theta_a + \pi/2}^{3\pi/2 - \theta_a} d\theta \frac{(\theta_a + \pi/2 + \theta - \text{Cos}(\theta - \theta_a))(1 - \text{Sin}\,\theta_p)}{[1 + \text{Sin}(\theta - \theta_a)]^{1.5}} \} + (1/4\pi)(\theta_a + \pi/2)^2 \qquad 4.18$$

Where, $\theta_p = (\theta - \theta_a - \pi/2)/2$

The value given by equation 4.18 is the averaged value over all rays within the field of view, that is, all the radiation which hits the aperture within the acceptance angle of the CPC ($\theta_i < \theta_a$).

All the radiation incident on the aperture outside the acceptance angle ($\theta_i > \theta_a$) bounces back and forth between the reflector walls until it re-emerges through the aperture. The average number of reflections for all the radiation incident on the aperture outside the accepatance angle is given by Rabl(1976c) :

$$\langle n \rangle_o = \frac{1}{1 - \text{Sin}\,\theta_a} [\frac{A_r}{A_c}(1 - E_{r-s}) - \frac{A_r}{A_s} E_{r-s}] + [(A_r/A_s)E_{r-s}] \qquad 4.19$$

The integration in equation 4.18 was evaluated numerically using Simpson's technique. The flowchart

FLPROP in appendix C shows the procedure, and the program is presented by subprogram CPCPRO in appendix B. Variation of the average number of reflections is shown in figure 4.5 page 67.

4.2.3 OPTICAL LOSS DUE TO GAP BETWEEN RECEIVER AND CPC

The design principles of the CPC collectors require that the receiver touchs the reflector as shown in figure 4.2 page 64 . However, a gap between the receiver and the reflector is necessary to reduce conductive heat losses since a reflector made of aluminium sheet in direct contact with the receiver is an effective cooling fin. The gap is also needed in the case of a CPC with evacuated receiver to incorporate the evacuated glass envelope.

Introduction of the gap causes optical losses, and a compromise between optical and thermal performance must be made. Rabl, Goodman and Winston(1979) have presented several approaches to incorporating the gap, and analytical expressions for evaluating the optical losses for the various methods.

The solution adopted in the present investigation is truncation of the reflector edge near the receiver as shown in figure 4.6 page 68 . The optical loss due to the gap g, created is given by:

$$L = (1/\pi)\{[\frac{2g}{R} + (\frac{g}{R})^2]^{1/2} - \cos^{-1}(\frac{R}{g+R})\} \qquad 4.20$$

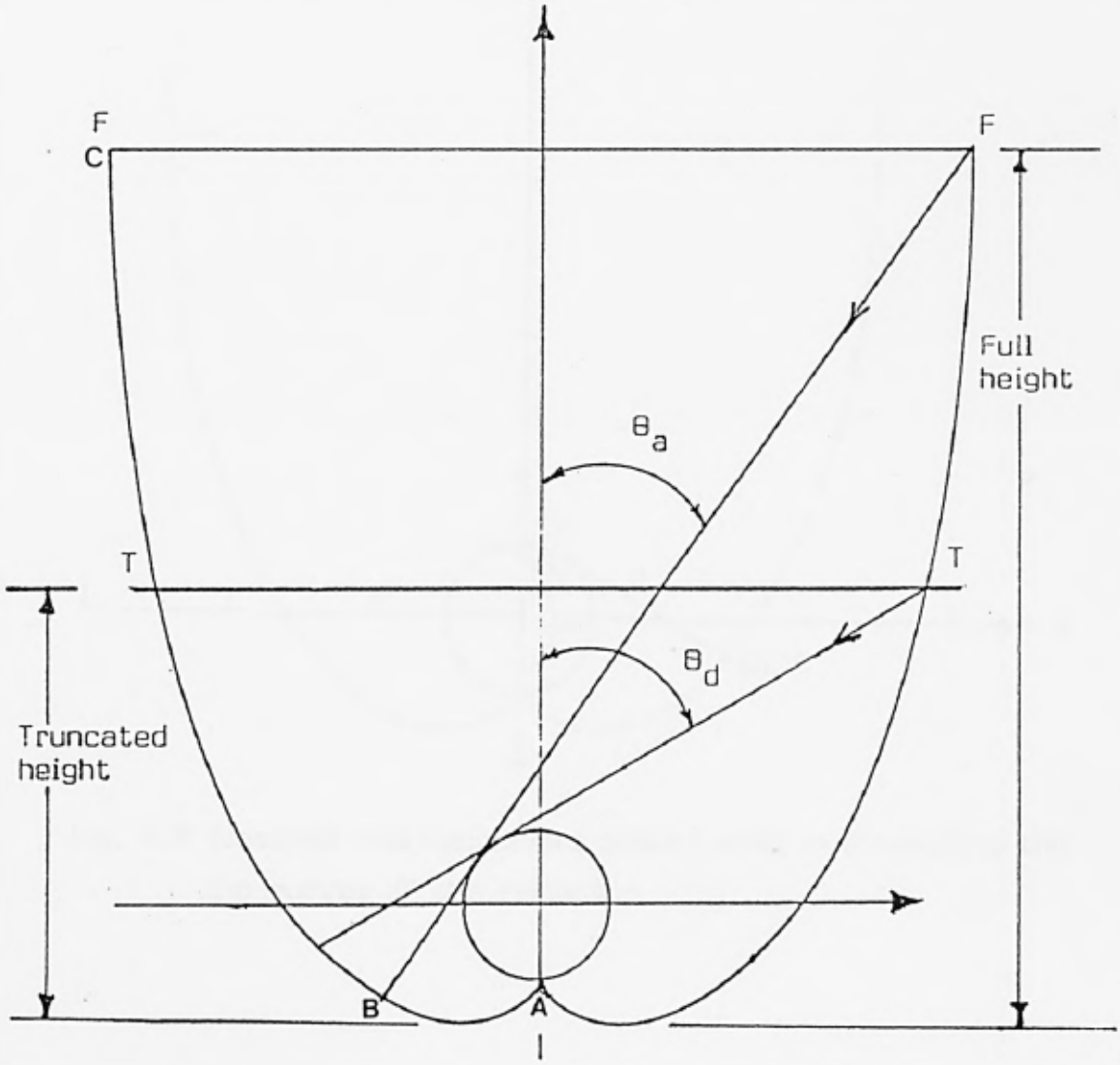


Fig. 4.1 Graphical truncation of the CPC collector. Fully developed CPC aperture is FF; when truncated at point T, the aperture is TT with corresponding extreme edge ray angle θ_d.

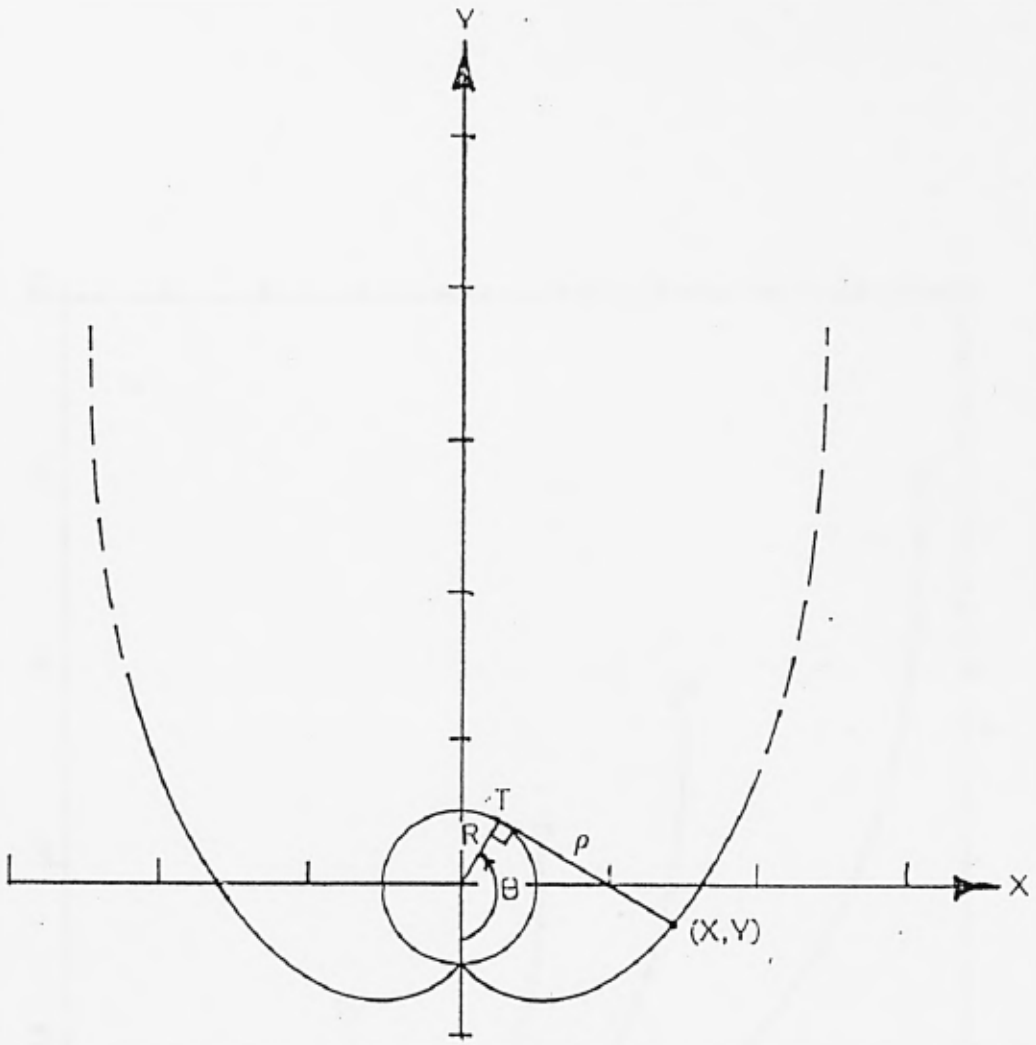


Fig. 4.2 Elements and coordinate system used in developing the the curves of the reflector.

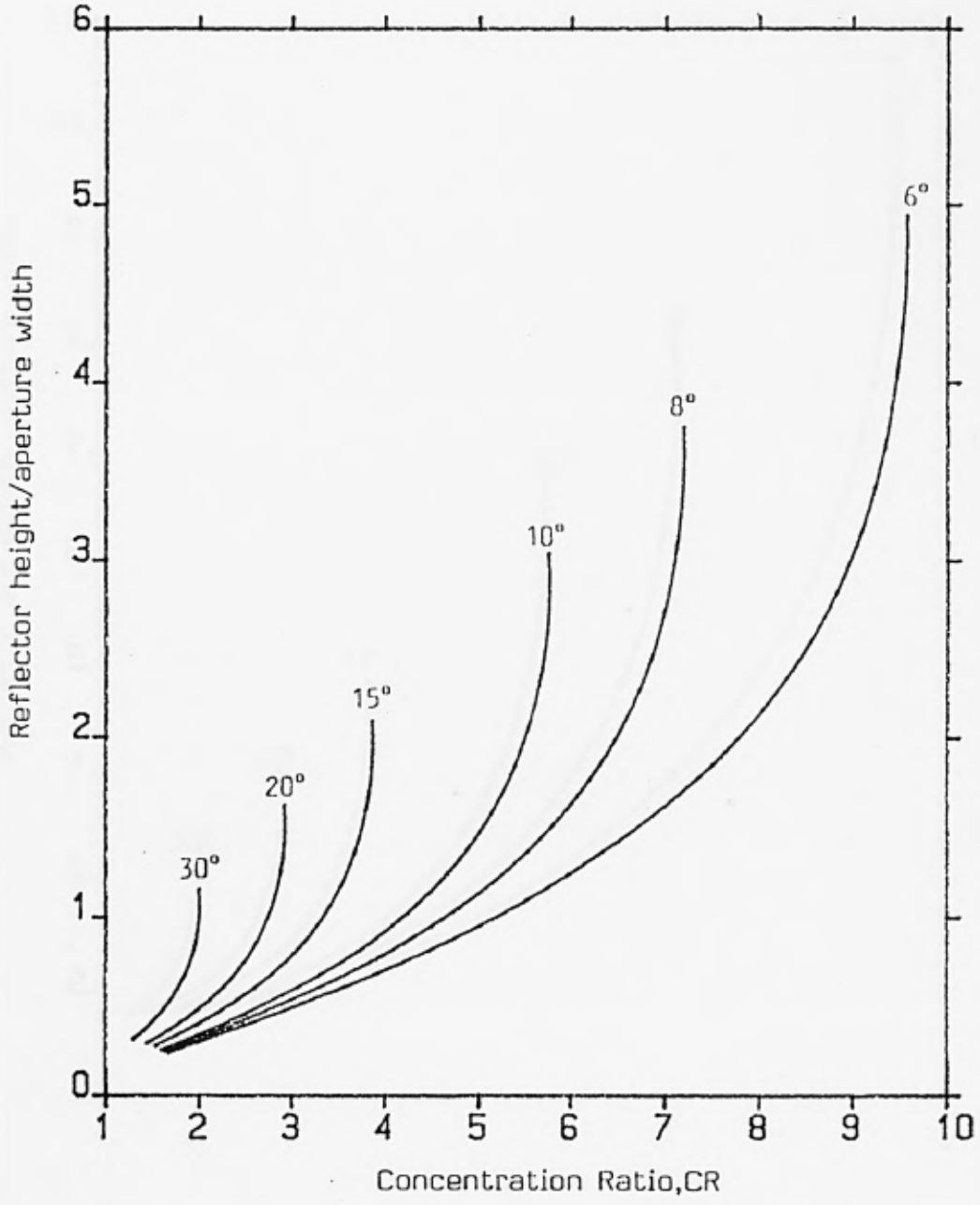


Fig. 4.3 Reflector height/aperture width for CPC with tubular receiver vs CR, for different acceptance half-angles.

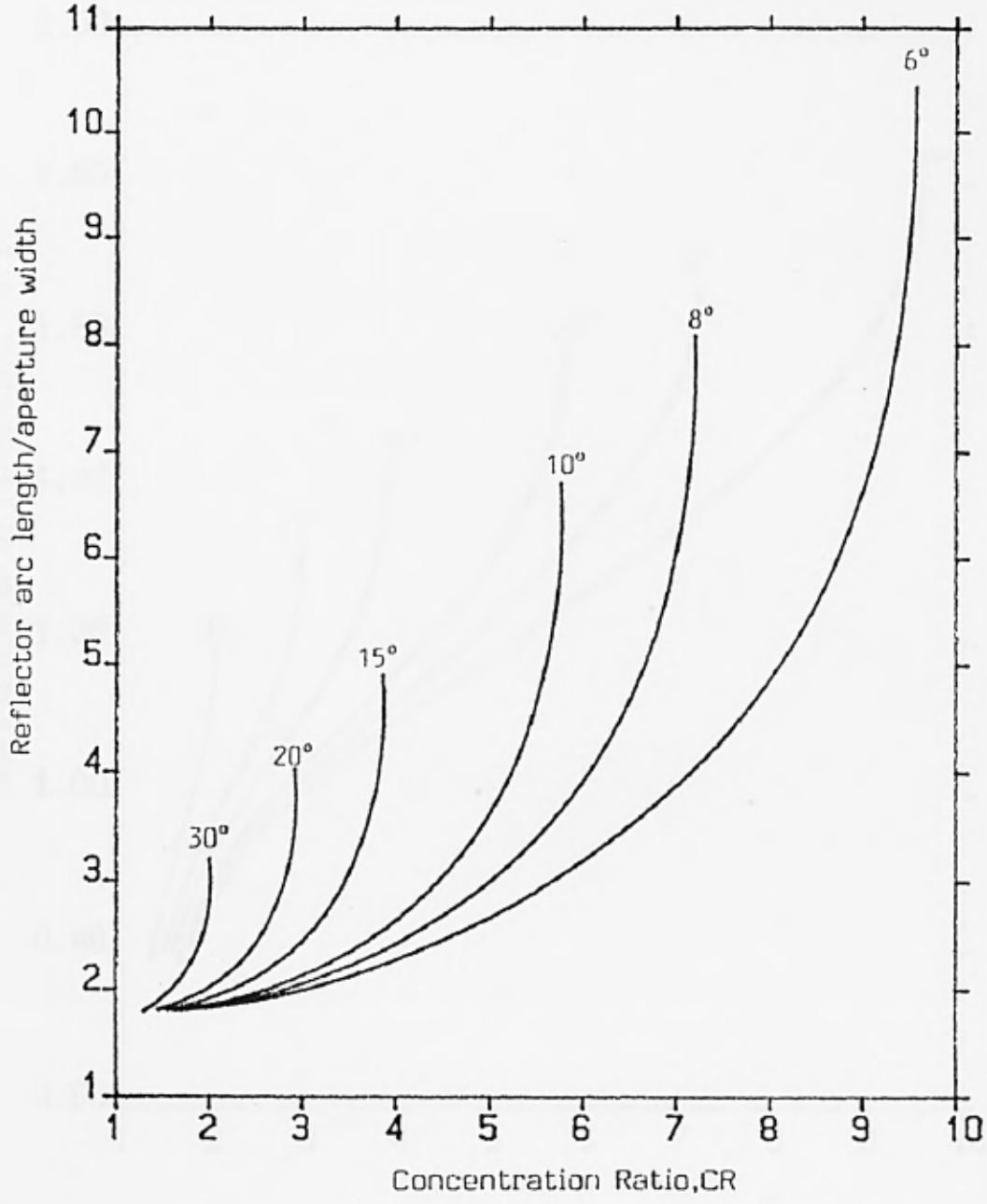


Fig. 4.4 Reflector arc length/aperture width for CPC with tubular receiver vs CR, for different acceptance half-angles.

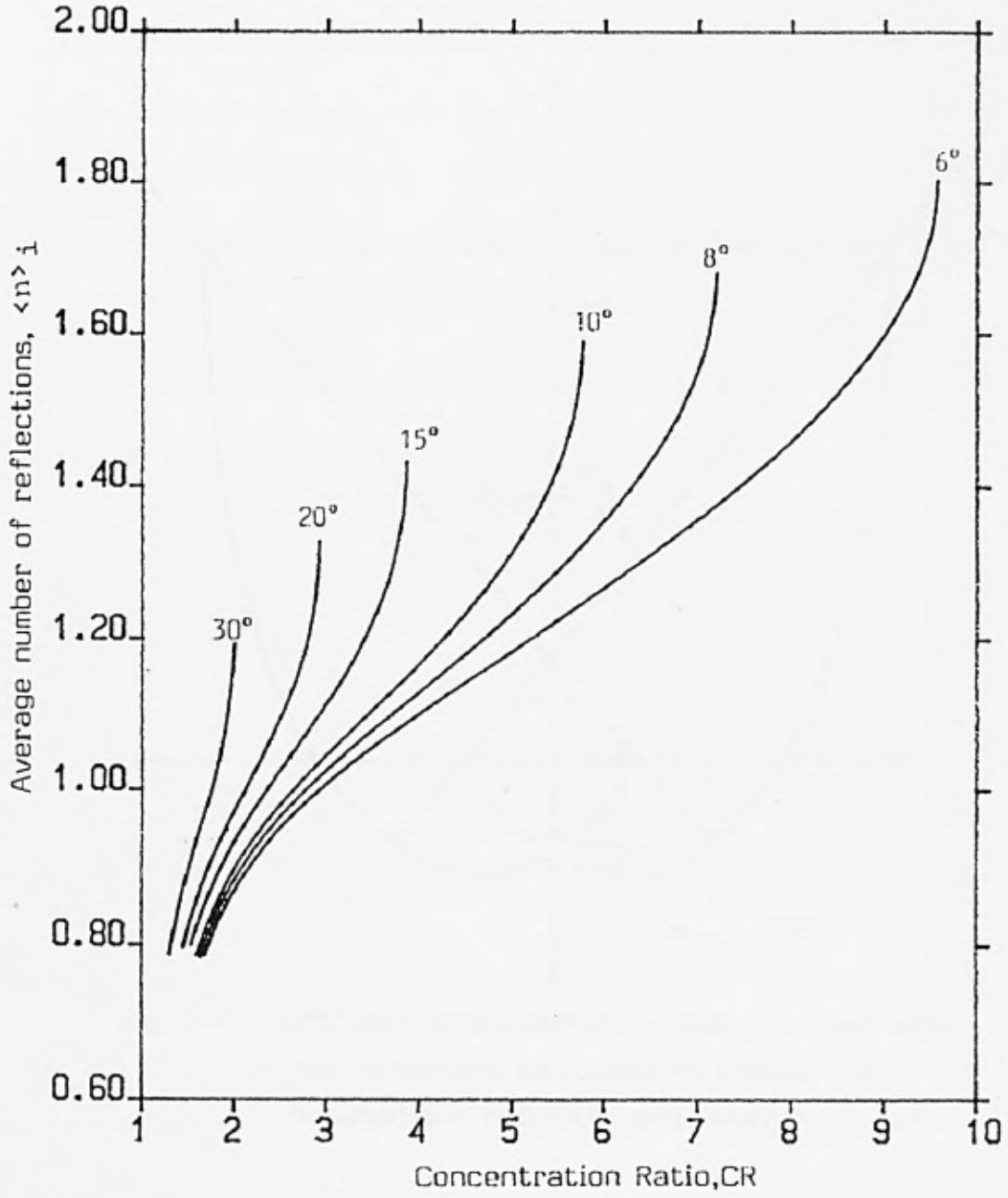


Fig. 4.5 Average number of reflections (within acceptance angle) for CPC with tubular receiver vs CR, for different acceptance half-angles.

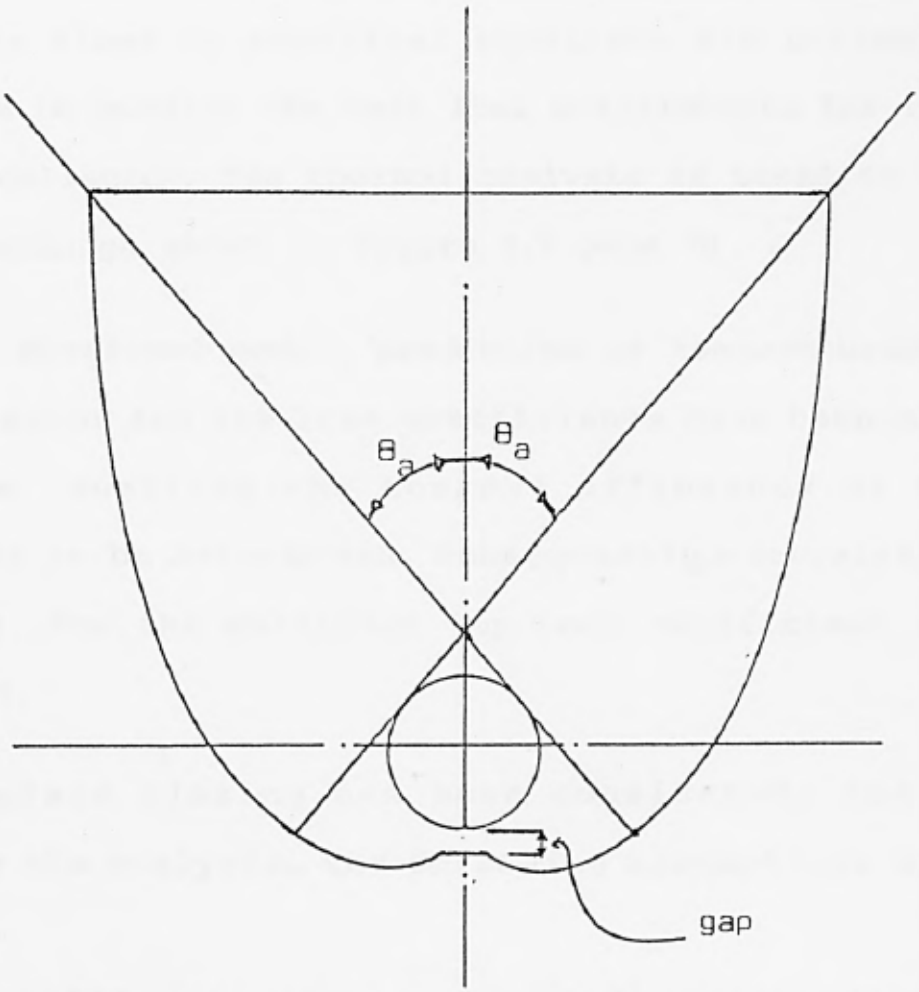


Fig. 4.6 CPC with nonevacuated tubular receiver with the reflectors truncated to create gap between the reflector and receiver.

4.3 THERMAL ANALYSIS OF THE CPC COLLECTOR

4.3.1 INTRODUCTION

In this section, the thermal processes in the CPC collector with nonevacuated tubular receiver have been formulated using heat transfer analysis. This becomes necessary since no empirical equations are currently available to predict the heat loss coefficients for this type of collector. The thermal analysis is based on the energy exchange shown in figure 4.7 page 70 .

With the developed model, prediction of temperatures in the collector and the loss coefficients have been made possible, enabling the thermal efficiency of the collector to be determined. Subsequently, a correlation equation for the collector top loss coefficient was developed.

Single glass glazing has been considered, and to simplify the analysis, the following assumptions were made:

1. The CPC cusp is assumed to be ideal with no fabrication errors. The maximum possible concentration ratio consistent with the acceptance half-angle is given by equation 4.2 .

2. All rays incident on the aperture within the acceptance angle can reach the receiver. The radiation that can be accepted by the CPC is given by equations 3.42 to 3.44

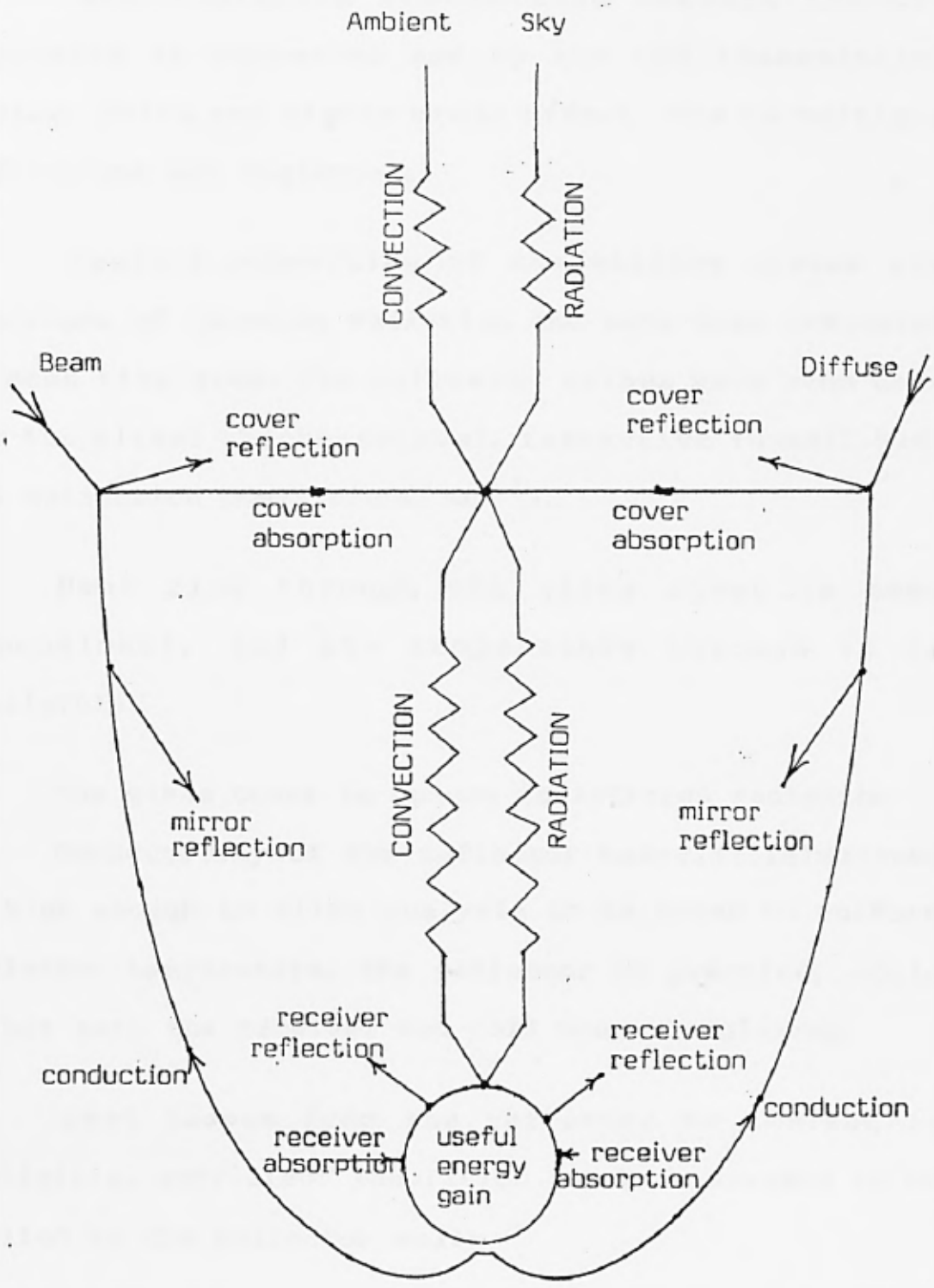


Fig. 4.7 Energy exchange for CPC collector with non-evacuated tubular receiver based on accepted beam and diffuse components of incident radiation

3. The radiation transmitted through the CPC enclosure is accounted for by the CPC transmission factor. Third and higher order effect due to multiple reflections are neglected.

4. Optical properties of the glazing system are functions of incoming radiation and have been evaluated at each time step. The following values have been used for the glass: thickness(3mm), refractive index(1.526) and extinction coefficient($3mm^{-1}$).

5. Heat flow through the glass cover is one-dimensional, and the temperature through it is negligible.

6. The glass cover is opaque to infrared radiation

7. Conductivity of the reflector material (aluminum) is high enough to allow analysis to be based on uniform reflector temperature. The reflector in practice, would be hot near the receiver and cold near the glazing.

8. Heat losses from the reflector to ambient is negligible, sufficient insulation has been assumed to be applied to the reflector walls.

9. The receiver surface properties are assumed to take mean values, irrespective of incidence angle of the incoming radiation, and have been taken as constant.

10. For the bouyancy driven convective heat transfer in the tilted CPC enclosure, the Nusselt number is taken as the average of the sum of the resolved vertical and horizontal Nusselt number components.

11. Steady-state performance is assumed.

12. The glazing and the receiver have uniform temperature distributions.

13. Collector components properties are independent of temperatures.

4.3.2 RADIATION HEAT TRANSFER IN THE CPC COLLECTOR

The optical properties of the glass cover as function of the incoming radiation are estimated by the subprograms BEAM, DIFFUS and OPTPRO. These properties are in turn used to estimate the fraction of the accepted radiation absorbed by the various components of the collector.

The fraction of the accepted beam and diffuse radiation absorbed by the glass cover are given respectively by:

$$Q_{b,c} = I_{b,C}(\alpha_{b,c} + \alpha_{d,c}\ \tau_{b,c}\ \rho_s\ \tau_C^2\ )A_c \qquad 4.21$$

$$Q_{d,c} = I_{d,C}\ \alpha_{d,c}(1 + \tau_{d,c}\ \rho_s\ \tau_C^2\ )A_c \qquad 4.22$$

The second term inside the brackets of equations 4.21 and 4.22 acounts for the portion of respective component of radiation that is transmitted through the glass cover, reflected by the receiver, and absorbed by the lower surface of the cover. It is a second order effect,

higher orders effect have been neglected since their contribution to overall collector performance is negligible Rabl(1976c). This effect results from the round trips (reflections, rereflections and attenuation) of the radiation in the CPC.

The beam and diffuse radiation components absorbed by the receiver are respectively given by:

$$q_{b,s} = I_{b,C}\ \tau_{b,c}\ \tau_C\ \alpha_s\ L_o \qquad 4.23$$

$$q_{d,s} = I_{d,C}\ \tau_{d,c}\ \tau_C\ \alpha_s\ L_o \qquad 4.24$$

The total radiation absorbed by the receiver is given by:

$$q_s = q_{b,s} + q_{d,s} \qquad 4.25$$

or,

$$Q_s = q_s\ A_s$$

The term L_o, accounts for the optical loss discussed in section 4.2.3 and is given by:

$$L_o = 1 - L$$

and L is given by equation 4.20

The amount of solar radiation absorbed by the reflector, taken into consideration all the radiation incident on the CPC inside and outside the acceptance angle, is given by:

$$Q_r = A_c\ I_C\ \tau_c\ \alpha_r \left\{\frac{I_C}{I_t}(1 - \tau_C) + \left[\left(1 - \frac{I_C}{I_t}\right)\right.\right.$$

$$\left.\left.(1 - \rho_r^{\langle n\rangle_o}\right] \right\} \qquad 4.26$$

The radiative heat transfer in the CPC comprises of the net radiation transfer between the receiver and the aperture, the net transfer from the receiver to the reflector, and from the reflector to the aperture. Formulations of these net transfers, taken into consideration radiation inside and outside the acceptance angle are given by Rabl(1976c) :

The net transfer between the receiver, s, and the aperture,c, is given by:

$$Q_{sc} = \epsilon_{e,sc} A_s \sigma (T_s^4 - T_c^4) \qquad 4.27$$

Where,

$$\epsilon_{e,sc} = \frac{\tau_c \epsilon_c \epsilon_s}{1 - \tau_c^2 \rho_c \rho_s} \qquad 4.28$$

The net transfer between the receiver,s, and the reflector walls,r, is given by:

$$Q_{sr} = \epsilon_{e,sr} A_s \sigma (T_s^4 - T_r^4) \qquad 4.29$$

Where,

$$\epsilon_{e,sr} = \left(\frac{1 + \tau_c \rho_c}{1 - \tau_c^2 \rho_c \rho_s}\right)(1 - \tau_c) \epsilon_s \qquad 4.30$$

The net transfer between the reflector and the aperture is given by:

$$Q_{rc} = \epsilon_{e,rc} A_s \sigma (T_r^4 - T_c^4) \qquad 4.31$$

Where,

$$\epsilon_{e,rc} = \left[\left(\frac{1 + \tau_c \rho_s}{1 - \tau_c^2 \rho_c \rho_s}\right)(1 - \tau_c) + \left(\frac{1 - \rho_r \langle n \rangle_o}{1 - \rho_r \langle n \rangle_o \rho_c}\right)\left(\frac{A_c - A_s}{A_s}\right)\right] \epsilon_c \qquad 4.32$$

The assumption of uniform reflector temperature implies that the reflector experiences only thermal radiation from the receiver and the aperture, and the temperature can be obtained by combination of equations 4.29 to 4.32 :

$$T_r^4 = \frac{\epsilon_{e,sr} T_s^4 + \epsilon_{e,rc} T_c^4}{\epsilon_{e,sr} + \epsilon_{e,rc}} \qquad 4.33$$

The total radiative heat loss from the receiver to the cover in terms of A_s, T_s, and T_c, is given by:

$$Q_{rad,s \to r+c} = \epsilon_{eff} A_s \sigma (T_s^4 - T_c^4) \qquad 4.34$$

Where,

$$\epsilon_{eff} = \epsilon_{e,sc} + \left(\frac{\epsilon_{e,sr} \epsilon_{e,rc}}{\epsilon_{e,sr} + \epsilon_{e,rc}}\right) \qquad 4.35$$

The radiative heat exchange between the cover and the sky is given by:

$$Q_{rad,c-sky} = \epsilon_c A_c \sigma (T_c^4 - T_{sky}^4) \qquad 4.36$$

The sky temperature can be obtained from the equation given by Swinbank(1963) relating the sky temperature to local ambient temperature :

$$T_{sky} = 0.0552\ T_b^{1.5} \qquad 4.37$$

All the above formulations have been incorporated into the program CPHEAT in appendix B.

4.3.3 CONVECTIVE HEAT TRANSFER IN THE CPC COLLECTOR

A knowledge of the convective heat loss coefficients for the CPC collector and their dependence on various geometrical and operational parameters is necessary for accurate evaluation of the collector performance. Experimental and analytical studies have been performed to obtain natural convective heat transfer coefficients for simple rectangular enclosures by, Arnold, Catton and Edward(1976). However, in the absence of any detailed experimental information for the complicated geometry of the CPC, the approach below has been adopted to estimate its convective heat transfer.

By the assumption that the reflector material is of high conductivity, with insulated walls and uniform temperature, all interactions with the reflector walls can be neglected. Hence, the surface film coefficients for heat transfer from both the receiver to the air inside the CPC enclosure, and from the air to the glass cover can be used to evaluate the convective heat transfer.

Surface heat transfer coefficient can be expressed as:

$$h = \frac{k}{X} Nu$$

For the tubular receiver, X = D (diameter)

For the cover glass, X = W (aperture width)

The following empirical equations given by McAdams(1954) have been used :

For horizontal tube,

$$Nu_{s,h} = 0.53[Gr_D Pr]^{0.25} \qquad 4.38$$

for $10^3 < Gr_D Pr < 10^9$

or, $$h_{s,h} = 0.18\ T^{1/3} \qquad 4.39$$

for $10^9 < Gr_D Pr < 10^{12}$

For vertical tube,

$$Nu_{s,v} = 0.59[Gr_D Pr]^{0.25} \qquad 4.40$$

for $10^4 < Gr_D Pr < 10^9$

or, $$Nu_{s,v} = 0.13[Gr_D Pr]^{1/3} \qquad 4.41$$

for $10^9 < Gr_D Pr < 10^{12}$

The empirical equations given by Kreith(1973) for flat plates have been used for the glass cover :

For horizontal plate,

$$Nu_{c,h} = 0.54[Gr_W Pr]^{0.25} \qquad 4.42$$

for $10^5 < Gr_W Pr < 2 \times 10^7$

or, $$Nu_{c,h} = 0.14[Gr_W Pr]^{1/3} \qquad 4.43$$

for $2x10^7 < Gr_W Pr < 3x10^{10}$

For vertical plate,

$$Nu_{c,v} = 0.59[Gr_W Pr]^{0.25} \qquad 4.44$$

for $10^4 < Gr_W Pr < 10^9$

or, $$Nu_{c,v} = 0.13[Gr_W Pr]^{1/3} \qquad 4.45$$

for $10^9 < Gr_W Pr < 10^{12}$

The Nusselt number for the sloped collector has been evaluated as the average of the sum of the resolved horizontal and vertical components of the above Nusselt numbers. The principle is shown on figure 4.8 .

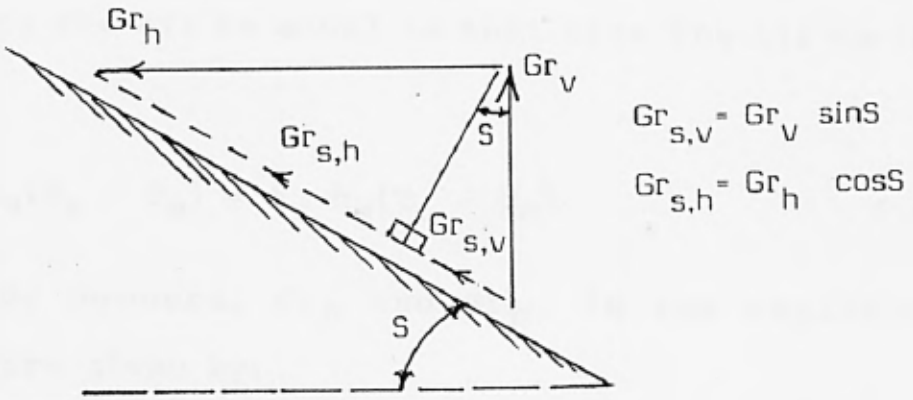


Fig. 4.8 Body force in Nusselt's expression acting on the film on an inclined surface.

For the east-west mounted CPC collector in this study the tubular receiver is always horizontal, and the Nusselt number is given by equation 4.38 or 4.39 :

$$Nu_S = Nu_{S,h} \qquad 4.46$$

and for the glass cover:

$$Nu_c = 0.5[Nu_{c,h}Cos\ S + Nu_{c,v}Sin\ S] \qquad 4.47$$

Since the surface resistances at the receiver and at the lower surface of the glazing are in series, the overall convective heat transfer in the CPC enclosure is given by:

$$Q_{conv,s-c} = \frac{T_s - T_c}{(1/A_s\ h_s) + (1/A_c\ h_c)} \qquad 4.48$$

Iteration technique has been used to determine the mean air temperature inside the CPC enclosure, by the requirement that the convective heat transfer from the receiver to the air be equal to that from the air to the glazing:

$$A_s\ h_s(T_s - T_a) = A_c\ h_c(T_a - T_c) \qquad 4.49$$

The Grashof numbers, Gr_D and Gr_W, in the empirical equations are given by:

$$Gr_D = \frac{g\ \beta_s D^3\ \Delta T_s}{\nu^2} \qquad 4.50$$

$$Gr_W = \frac{g\ \beta_c W^3\ \Delta T_c}{\nu^2} \qquad 4.51$$

Where,

$\beta_s = 1/T_{sm}$; $\quad T_{sm} = (T_s + T_a)/2$; $\quad \Delta T_s = T_s - T_a$

$\beta_c = 1/T_{cm}$; $\quad T_{cm} = (T_a + T_c)/2$; $\quad \Delta T_c = T_a - T_c$

The conductivity k, and kinematic viscosity , have been obtained from the parameterised expressions :

$$\nu = \nu_o T^{1.7}; \quad \nu_o = 9.76*10^{-10} \ m^2 s^{-1} (^oK)^{-1.7}$$

$$k = k_o T^{0.7}; \quad k_o = 4.86*10^{-4} \ Wm^{-1} (^oK)^{-0.7}$$

From above, the surface heat transfer coefficients are given by;

For the tubular receiver,

$$h_s = \frac{k}{D} Nu_s$$

$$= \frac{k_o T_{sm}^{0.7}}{D} Nu_{s,h}$$

$$= \frac{k_o}{\sqrt{\nu_o}} (gPr)^{0.25} \ (\Delta T_s/D)^{0.25} \ T_{sm}^{-0.4} \qquad 4.52$$

Similarly, for the glass cover:

$$h_c = 0.5 \frac{k_o}{\sqrt{\nu_o}} (gPr)^{0.25} \ (\Delta T_c/W)^{0.25} \ T_{cm}^{-0.4}$$

$$(0.54 \ Cos \ S + 0.59 \ Sin \ S) \qquad 4.53$$

The convection heat loss from the glass cover to ambient is given by :

$$Q_{conv,c-b} = A_c \ h_b (T_c - T_b) \qquad 4.54$$

The cover/ambient convection heat transfer coefficient is given by McAdams(1954) :

$$h_b = 5.7 + 3.8\ V \qquad 4.55$$

4.3.4 CONDUCTIVE HEAT TRANSFER IN THE CPC COLLECTOR

The conductive heat losses in the CPC collector occur through the back, sides and pipe fittings. With the introduction of a gap beween the tubular receiver and the reflector as shown in figure 4.6 page 69, the loss through the back has been alleviated. The conductive losses through the reflector walls to the glazing depend on the reflector temperature distribution. These losses have been assumed negligible in the present study because of the assumption of uniform reflector temperature. However, simple approximation can be provided by assuming a linear temperature gradient along the reflector wall to the glazing, and the conductive heat loss can be evaluated from :

$$Q_{cond,r-c} = k_r\ x_r\ L_C\ (T_{rm} - T_c)/L_r \qquad 4.56$$

The mean reflector temperature T_{rm} can be obtained from equation 4.33 .

For a CPC collector with flat receiver and reasonable amount of insulation, a single effective conductance, U_{cond}, that lumped all the conductive losses through the back, sides, and pipe fittings was given by Rabl(1976c)

to be in the range :

$$U_{cond} = 0.3 \text{ to } 0.6 \text{ Wm}^{-2} (^{o}C)^{-1}$$

4.3.5 THE CPC LOSS COEFFICIENTS AND USEFUL ENERGY GAIN

The analyses of heat transfer modes carried out in the preceeding sections have been employed to obtain the various components loss coefficients. The glass cover temperature is determined by an iteration technique, with the requirement that the heat flow from the receiver to the glass cover equals the heat flow from the cover to the ambient :

$$Q_{s-c} = Q_{c-b}$$

From preceding sections, these heat transfer are given by :

$$\begin{aligned} Q_{s-c} &= Q_{rad,s-r+c} + Q_{conv,s-c} + Q_s + Q_r \\ &= \epsilon_{eff} A_s \sigma (T_s^4 - T_c^4) \\ &\quad + A_c h_c h_s (T_s - T_c)/(h_s + h_c C) \\ &\quad + [(I_{b,C} (\alpha_{b,c} + \alpha_{d,c} \tau_{b,c} \rho_s \tau_C^2)) \\ &\quad + (I_{d,c} \alpha_{d,c} (1 + \tau_{d,c} \rho_s \tau_C^2))]A_c \end{aligned} \qquad 4.57$$

and,

$$\begin{aligned} Q_{c-b} &= Q_{rad,c-sky} + Q_{conv,c-b} \\ &= \epsilon_c A_c \sigma (T_c^4 - T_{sky}^4) \\ &\quad + A_c h_b (T_c - T_b) \end{aligned} \qquad 4.58$$

The overall heat loss between the receiver and the

ambient is given by :

$$Q_l = \frac{(T_s - T_b)}{(1/A_s\ U_{sc} + 1/A_c\ U_{cb} + 1/A_c\ U_{cond})} \qquad 4.59$$

The loss coefficient occuring between the receiver and the cover based on the aperture area is given by :

$$U_{sc} = \frac{Q_{c-b}}{A_c\ (T_s - T_c)} \qquad 4.60$$

The loss coefficient occuring between the cover and the ambient is given by :

$$U_{cb} = \frac{Q_{c-b}}{A_c\ (T_c - T_b)} \qquad 4.61$$

The CPC loss coefficient is given by:

$$U_l = \frac{1}{(1/U_{sc} + 1/U_{cb} + 1/U_{cond})} \qquad 4.62$$

By neglecting U_{cond}, the loss (or top loss) coefficient is given by:

$$U_{top} = \frac{1}{(1/U_{sc} + 1/U_{cb})} \qquad 4.63$$

The useful energy gain in the collector is extracted in the form of heat by water flowing inside the tubular receiver, and is expressed as :

$$Q_u = M\ C_p\ (T_o - T_i) \qquad 4.64$$

or

$$Q_u = A_s\ U_{sw}\ (T_s - (T_i + T_o)/2) \qquad 4.65$$

From equations 4.64 and 4.65 :

$$T_o = (M\ C_p\ T_i - A_s\ U_{sw}\ (0.5\ T_i - T_s))/(M\ C_p + 0.5\ A_s\ U_{sw}) \qquad 4.66$$

The heat transfer coefficient, U_{sw}, accounts for both conduction across the tube wall and convection of fluid inside the tube, contact resistance has been neglected in the present study. Based on the tubular receiver area, the coefficient is given by:

$$U_{sw} = \left[\frac{D_o}{D_i\ h_w} + \frac{D_o\ \ln(D_o/D_i)}{2\ k_s} \right]^{-1} \qquad 4.67$$

The total heat transfer for the CPC collector can be expressed as :

$$Q_t = Q_u + Q_l \qquad 4.68$$

The convective heat transfer coefficient, h_w, inside the tube can be calculated with the assumption that the flow is laminar and fully developed, and can be obtained from the empirical equation given by Kreith (1973) :

$$Nu_D = 1.86\ (Re_D\ Pr\ D_i/L)^{0.33}\ (\mu_w/\mu_s)^{0.14} \qquad 4.69$$

$$h_w = Nu_D\ k_w/D_i$$

The Reynold number is given by:

$$Re_D = V_w\ D_i\ \rho_w/\mu_w$$

The useful energy gain can also be expressed in terms of the receiver temperature and absorbed energy as :

$$Q_u = A_c\, q_s - A_s\, U_l\, (T_s - T_b) \qquad 4.70$$

By eliminating T_s from equations 4.65 and 4.70, the useful energy gain is also given by :

$$Q_u = A_c \frac{U_{sw}}{U_{sw} + U_l} \left[q_s - \frac{1}{C} U_l\, (T_f - T_b) \right] \qquad 4.71$$

Where,

$$T_f = (T_o + T_i)/2$$

The term, $U_{sw}/(U_{sw} + U_l)$ is the collector flow efficiency factor, F', and can also be expressed as:

$$F' = U_o/U_l$$

Where,

$$U_o = [1/U_l + 1/U_{sw}]^{-1}$$

The useful energy gain has also been expressed in terms of the heat removal factor, Fr, as :

$$Q_u = A_c\, Fr\, [q_s - (U_l/C)(T_i - T_b)] \qquad 4.72$$

Where,

$$Fr = \frac{C\, M\, C_p}{A_c\, U_l} \left[1 - EXP\left(- \frac{A_s\, U_l\, F'}{M\, C_p}\right)\right] \qquad 4.73$$

To derive expression for the mean receiver temperature T_s, equation 4.70 was equated to equation 4.72 :

$$T_s = T_i + ((Q_u\, C)/(A_c\, U_l))((1 - Fr)/Fr) \qquad 4.74$$

Thermophysical properties of water used in the analysis are obtained from the property data equations presented in appendix D. The parameterised equations were obtained from the regression of the property data by Mayhew and Rogers(1974). The Minitab statistical package in the City University Computer software library has been used.

4.3.6 THERMAL AND OPTICAL EFFICIENCY OF THE COLLECTOR

Having determined the useful energy gain and the heat losses, translation of the losses into efficiency is undertaken. The collector thermal efficiency is given by :

$$\eta = Q_u / I_t \, A_c \qquad 4.75$$

The optical efficiency of the collector gives the fraction of the total insolation that is absorbed by the collector and it is given by :

$$\eta_o = (I_C / I_t) \, \tau_{b,c} \, \tau_C \, \alpha_s \, L_o \qquad 4.76$$

4.4 PARAMETRIC STUDY

4.4.1 SOLUTION SEQUENCE

Detailed modelling of the thermal processes in the collector was based on the formulations that have been developed in sections 4.2 and 4.3 . The relevant data which have been used as the computer program input are listed in table A16 in appendix A.

For a given acceptance half-angle θ_a, and concentration ratio C, the CPC geometric parameters were calculated using the equations in section 4.2 . With θ_a and C, equation 4.12 was solved iteratively to determine the edge ray angle θ_d. The iteration was done until the solution converges to $\pm$1.E−6 . The edge ray angle and the acceptance half-angle were then used to calculate the collector height and reflector arc length from equations 4.11 and 4.13 respectively. Next, the average number of reflections $\langle n \rangle_i$, was estimated using Simpson's numerical integration technique to solve equation 4.18 .

The transmission factor τ_C, and the average number of reflections for radiation incident on the aperture outside the acceptance angle $\langle n \rangle_o$, were estimated using $\langle n \rangle_i$ in equations 4.16 and 4.19 respectively. Next, τ_C and $\langle n \rangle_o$ were used to calculate the effective emissivities from equations 4.28, 4.30, 4.32 and 4.35 . The above design parameters were obtained from the subroutines CPCPRO, CPCDESG, and CPCPROP shown in appendix B.

The collector performance prediction was done on hourly basis, and the hourly solar angles were estimated from equations 3.14, 3.15, and 3.33 to 3.36 in chapter three. These angles, in turn, were used in equation 3.41 also in chapter three to test if the incident radiation falls within the acceptance angle, and thus accepted by the

CPC. Subsequently, the optical properties of the glass cover for beam radiation were calculated using the beam incidence angle in equations 3.24 to 3.30. For the diffuse radiation, the effective beam incidence angle obtained from equation 3.31 was used in equations 3.24 to 3.30 to estimate the diffuse optical properties. These properties have been calculated in subroutines BEAM, DIFFUS and OPTPRO in appendix B.

The heat transfer analysis was carried out by solving the equations in section 4.3 iteratively. The iteration process is shown on the flowchart FLHEAT in appendix C. For each hour and a given inlet water temperature, the iteration began by initialization of the receiver temperature T_s, temperature of air in the CPC enclosure T_a, and the glass cover temperature T_c.

Firstly, the convective heat transfer coefficients h_c and h_s were estimated from equations 4.52 and 4.53 . Then, the left and right sides of equation 4.49 were evaluated iteratively until their difference converges to less than $\pm$ 0.001 . In turn, Equations 4.57 and 4.58 were solved iteratively until their difference converges to less than $\pm$ 0.001. The collector top loss coefficient U_t was then calculated from equations 4.60, 4.61 and 4.63 .

Next, the thermophysical properties of water were evaluated at the inlet water temperature, except the kinematic viscosity which was evaluated at both inlet

water temperature and the receiver temperature. The convective heat transfer coefficient inside the tube h_w was then estimated from equation 4.69, and the total heat transfer coefficient U_{sw}, by equation 4.67 .

With U_t and U_{sw}, F' was evaluated and used in equation 4.73 to obtain the heat removal factor Fr. The useful energy gain Q_u was then calculated with equation 4.72 . The total heat transfer in the CPC, Q_t, was obtained from equation 4.68. The mean receiver temperature, T_s was estimated from equation 4.74, and the outlet water temperature from equation 4.66 .

Next, the difference between Q_t equation 4.68 and Q_s equation 4.25 is determined . If this value is greater than $\pm$ 0.01, the calculated mean receiver temperature becomes the new intial value and the above process is repeated until the difference is less than $\pm$ 0.01 .

Finally, having determined T_c, T_a, T_s, U_t, T_o and Q_u, the overall heat transfer coefficient U_o, was calculated. The thermal and optical efficiencies were evaluated from equations 4.75 and 4.76 respectively.

4.4.2 PERFORMANCE ANALYSIS AND RESULTS

Variation of the collector height, reflector arc length, and the average number of reflections within the acceptance angle, for various acceptance half-angles are shown in figures 4.3 to 4.5, pages 65 to 67 .

The influences of other design variables on the collector top loss coefficient, U_t, have been investigated. Some of these results have been plotted and are shown in figures 4.9 to 4.20, pages 96 to 107 . Absorption of radiation by the glass cover has been neglected in the above figures, since the slight increase in the cover temperature due to the absorption creates an insulating effect which is beneficiary to the receiver. Furthermore, the conductive and back losses are practically negligible because of the use of highly reflective aluminium reflector which acts like a radiation shield, the addition of insulation to the reflector further suppresses the heat flow from the collector.

In general, the loss coefficient increases nonlinearly with receiver temperature, and decreases as the concentration ratio increases. Figures 4.9, 4.10, 4.13 and 4.14 show the result for using nonselective receiver surface coating, whereas figures 4.11, 4.12, 4.15 and 4.16 show the effect of a selective coating on the receiver surface .

The effect of the collector tilt on the loss coefficient is shown in figures 4.17 and 4.18. The loss coefficient increases as the collector is tilted further from the horizontal. Figures 4.19 and 4.20 show the effect of the convection heat transfer coefficient (h_b) for wind blowing over the collector cover, for non-selective and

selective receiver surfaces respectively.The effect is greater for low concentration ratio collectors.

The collector hourly performance for different inlet water temperatures was obtained in terms of the operating temperatures (T_o, T_c, T_s), loss coefficients (U_l, U_o), $(T_s - T_i)/I_t$, heat removal factor Fr, and collector thermal efficiency. Absorption of radiation by the glass cover was included in the estimation of the top loss coefficient. Results for collectors having acceptance half-angles of 30^o, 20^o, 15^o, 10^o, are presented in tables 4.1 to 4.4, pages 108 to 115 for nonselective receiver surface, and tables 4.5 to 4.8, pages 116 to 123 for selective surface. The tables show that the operating temperatures and loss coefficients increase with the inlet water temperature. The maximum outlet water temperature and collector efficiency occur at the time of highest irradiation. All the above parameters vary in phase with the irradiation except Fr, which shows little or no variation for the different operating conditions that have been investigated. The tables also show that the optical efficiency decreases as the concentration ratio increases. This is due to the fraction of diffuse radiation accepted by a CPC, and in the total insolation . High concentration ratio CPC collectors utilise only a small proportion of the diffuse radiation and should not be employed at a location where the diffuse component of the incident

radiation is high.

4.4.3 TOP LOSS COEFFICIENT CORRELATION

The exact calculation of the top loss coefficient using the formulations in sections 4.2 through 4.3 has consumed much computer time, because of the number of iterations involved. Although, figures 4.9 to 4.20 prepared from the analysis are useful for hand calculations, when computer simulations of the collector performance are required they are inadequate for use. Therefore, correlation equations for the top loss coefficient have been developed from the analysis results data, using least square curve fits.

To obtain the greatest accuracy and best fit, the data have to be divided into two receiver temperature ranges. The correlation equations and their accuracy are given below. Details of the regression analysis are presented in appendix D .

For $45 \leq T_s \leq 215^{\circ}C$:

$$U_t = 10^{-4} \{ \epsilon_s[T_s(8.55 - 0.1113 T_b + 0.3209 T_s) + T_b(50.406 T_b - 2411.2) + 1682.14 \theta_a - 29.06 S + 242.25 h_b + 1019 C] + T_s [25.67 + 0.5141 T_b + 1.1244 h_b - C(3.397 + 0.035 T_b) + 0.0406 T_s] + T_b(20.46 C + 0.05 h_b - 96.4) - C[0.0271 T_s^2 + 0.39 T_b^2 + 41.131 h_b + 11.235 S] + 155.57 S + 26.07 h_b \} + 1.0535 \quad 4.79$$

Standard deviation of equation 4.79 = 0.2662

Correlation coefficient = 98.9 %

For $215 < T_s \leq 300^{\circ}$ C :

$$U_t = 10^{-4}\{ \epsilon_s [T_s(0.231 T_b + 0.4733 T_s - 92.11) + 38.6 T_b + 1827.5 \theta_a - 40.88 S + 381.88 h_b - 1295.4 C] + T_s [68.95 + 0.019 T_b + C(26.509 + 0.0128 T_b - 0.0836 T_s)] + T_b(28.9 - 11.78 C) + h_b [201.5 - 69.126 C + 0.6021 (T_s - T_b)] + S(166.57 - 11.126 C) + 518.5 \theta_a \} - 1.9848 \qquad 4.80$$

Standard deviation of equation 4.80 = 0.2988

Correlation coefficient = 99.4%

The acceptance half-angle θ_a, and the collector slope S, are both in degree ($^{\circ}$), and T_s and T_b are in Celcius ($^{\circ}$C).

The above equations, and the respective standard deviation and correlation accuracy, are valid for the following conditions:

$$0.1 \leq \epsilon_s \leq 0.9$$

$$5 \leq h_b \leq 30 \text{ W/m}^2 {}^{\circ}\text{C}$$

$$5 \leq S \leq 30^{\circ}$$

$$10 \leq T_b \leq 40^{\circ}\text{C}$$

$$6 \leq \theta_a \leq 30^{\circ}$$

$$1.5 \leq C \leq 8$$

When equations 4.79 and 4.80 were used for the ranges

shown below, the error was between 4 and 7% from the exact solutions :

ϵ_s = 0.05 and 0.95

S = 3 and 40°

T_b = 5 and 50°C

C = 1.3 and 10

θ_a = 5 and 35°

4.5 CONCLUSION, FIGURES AND TABLES

The CPC collector's height and reflector arc length shown in figures 4.3 and 4.4, agreed with those obtained from numerical method by McIntire (1979) within ± 2% . There is complete agreement between the average number of reflections $\langle n \rangle_i$, for θ_a = 20 and 30°, shown in figure 4.5, and those pesented by Carvalho, Collares-Pereira and Gordon(1985). In the absence of any reported data for $\langle n \rangle_i$, for θ_a less than 20° for a CPC with tubular receiver , comparison has been made with values for the CPC with fin receiver which Rabl(1980) has recommended to be used for a CPC with tubular receiver. For $6 \leq \theta_a \leq 20°$, the values by Rabl differ between ± 6.5% of the values obtained in this study for the CPC with tubular receiver .

From the above results, it was concluded that the mathematical models which have been developed for the CPC geometrical parameters are accurate enough for

subsequent use.

There is no reported previous work that treats the top loss coefficient for a nonevacuated CPC collector with tubular receiver, for the range of acceptance half-angles considered in the present investigation. Therefore a comparison with those for nonevacuated CPC collector with flat receiver by Rabl(1976c) was made. The values for the flat receiver were found to be higher by 17%, for the same concentration ratio and operating parameters. The general trend, however are the same.

The general trend of the collector thermal efficiency agreed with those of Hsieh(1981) and Rabl(1976c). The optical efficiency shows that the use of high concentration ratio CPC is not desirable at locations with large diffuse component of solar radiation.

The performance results have shown that, sufficiently high delivery energy temperature to drive air-cooled aqua-ammonia refrigeration systems can be achieved by the use of the nonevacuated CPC collector, with θ_a between 30 and 20^o (or $1.5<C<3$) if selective coating is used on the copper tube; And with θ_a from 15^o downwards (or $C>3$) if nonselective coating of black paint is used. This conclusion forms the basis for the simulation work on the solar powered NH_3-H_2O refrigeration system in chapter seven .

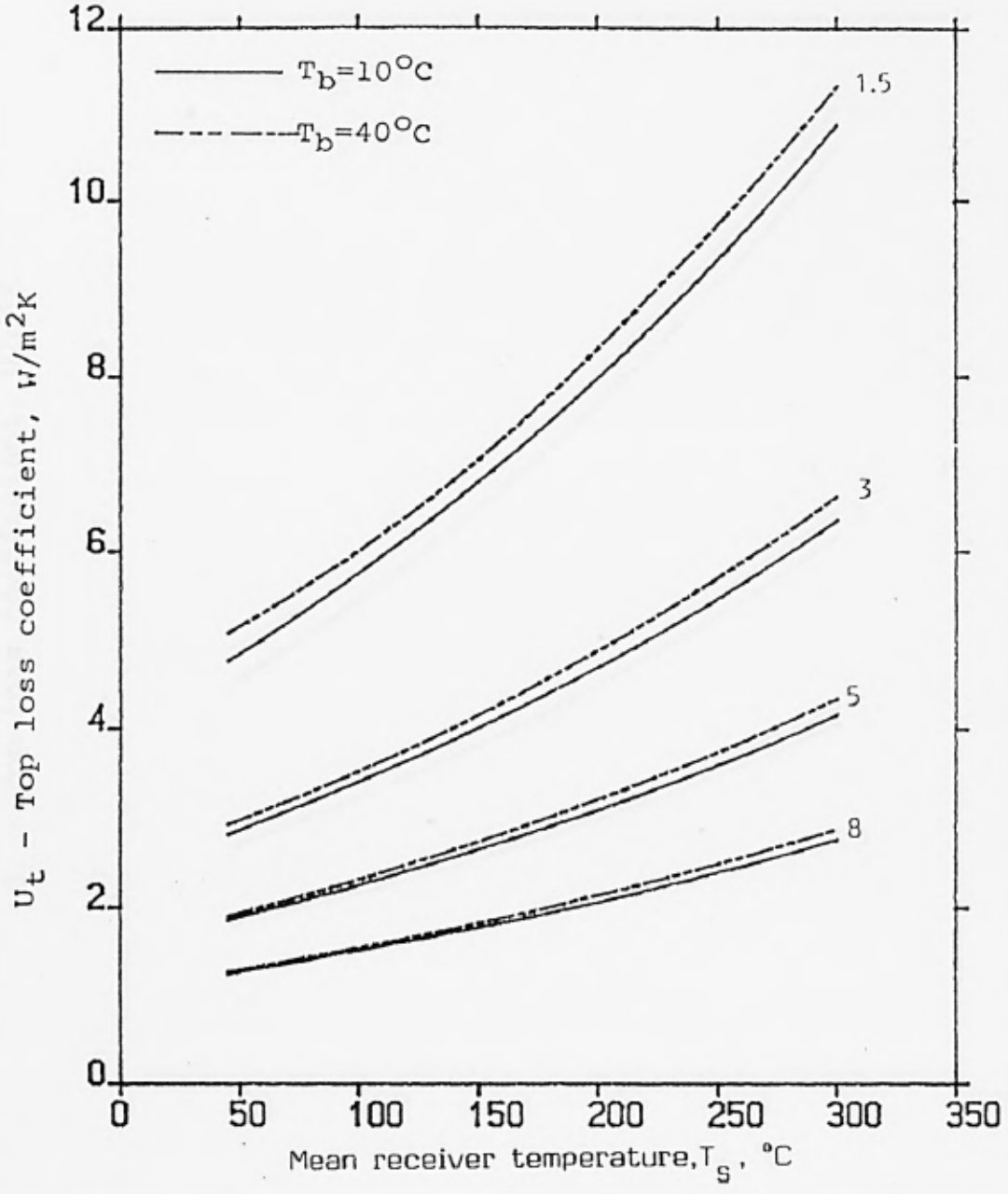


Fig. 4.9 U_t for CPC with non-evacuated tubular receiver vs T_s, for four different CR : ϵ_s = 0.9 ; S = 30° ; h_w = 30 W/m²K

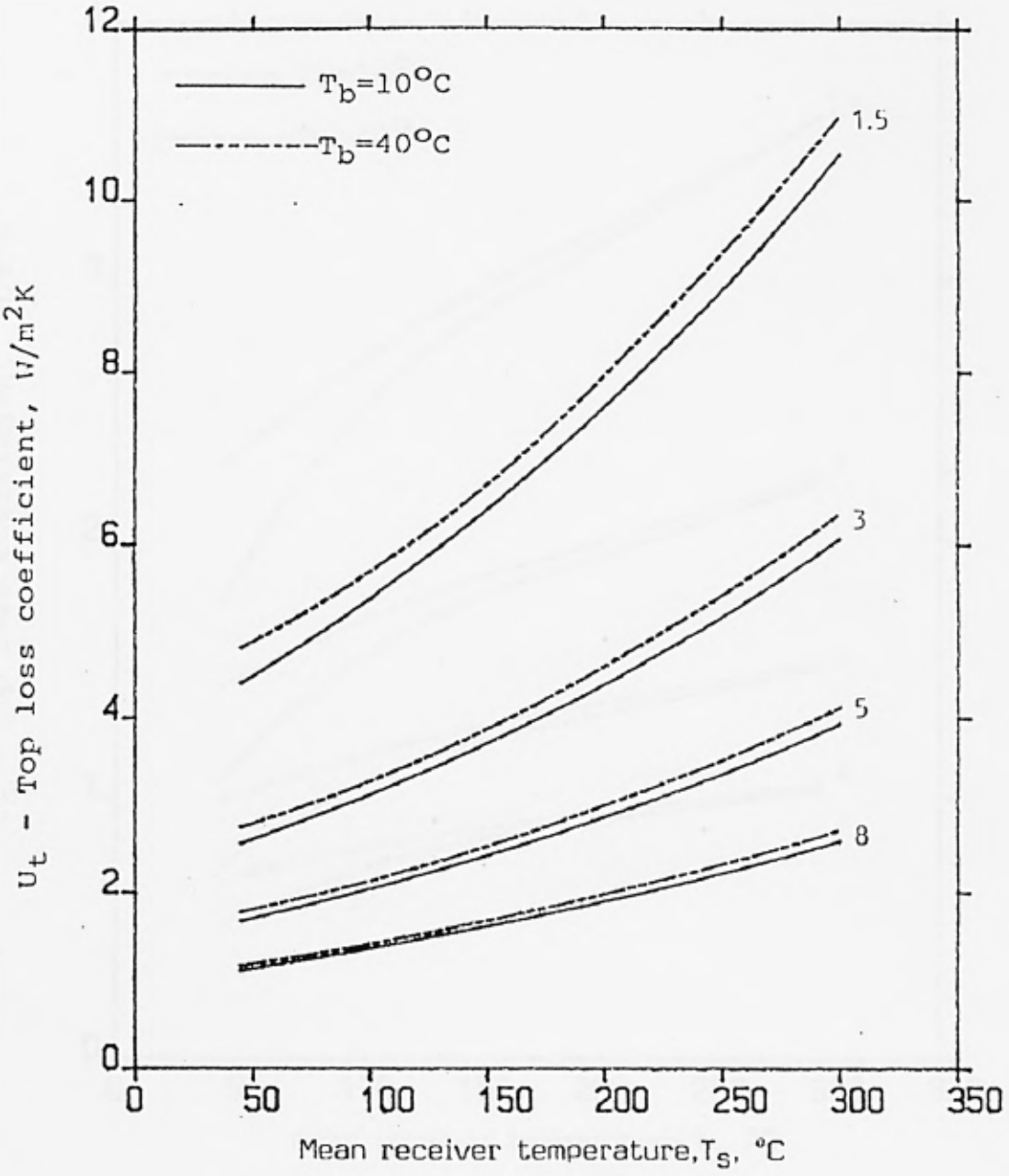


Fig. 4.10 U_t for CPC with non-evacuated tubular receiver vs T_s, for four different CR : ϵ_s = 0.9 ; S = 5° ; h_w = 30 W/m² K

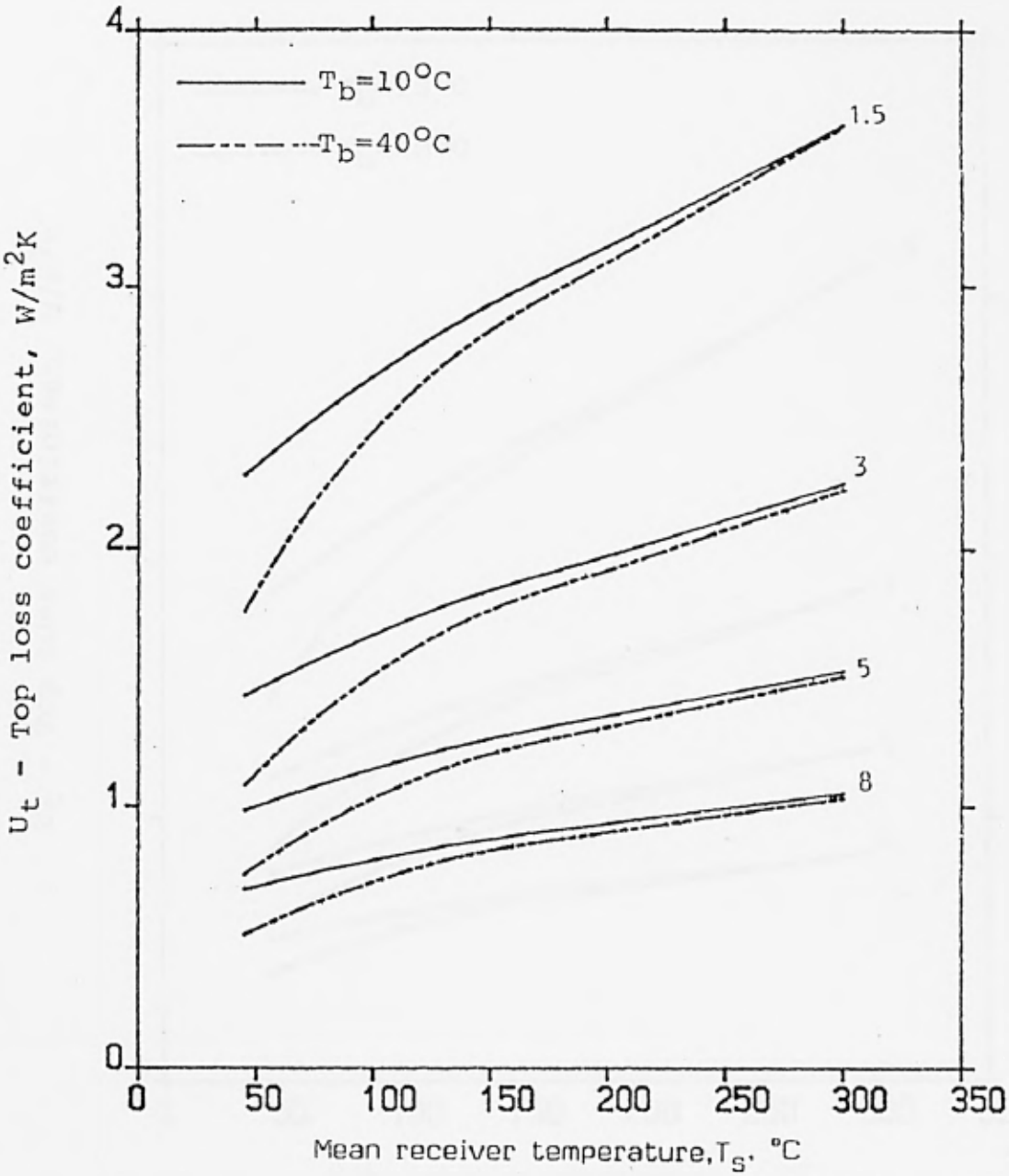


Fig. 4.11 U_t for CPC with non-evacuated tubular receiver vs T_s, for four different CR : ϵ_s = 0.1 ; S = 30° ; h_w = 30 W/m² K

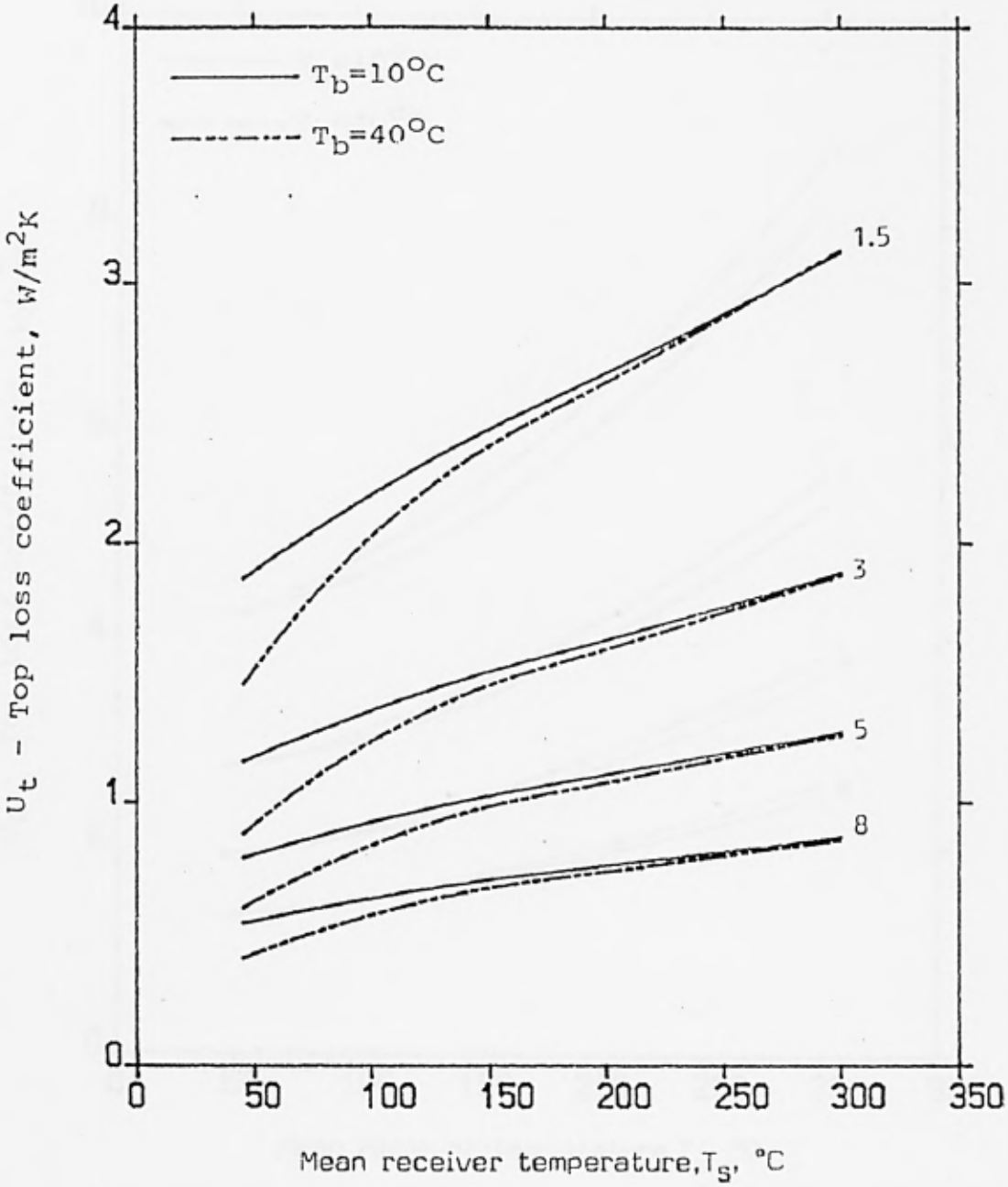


Fig. 4.12 U_t for CPC with non-evacuated tubular receiver vs T_s, for four different CR : ϵ_s = 0.1 ; S = 5° ; h_w = 30 W/m² K

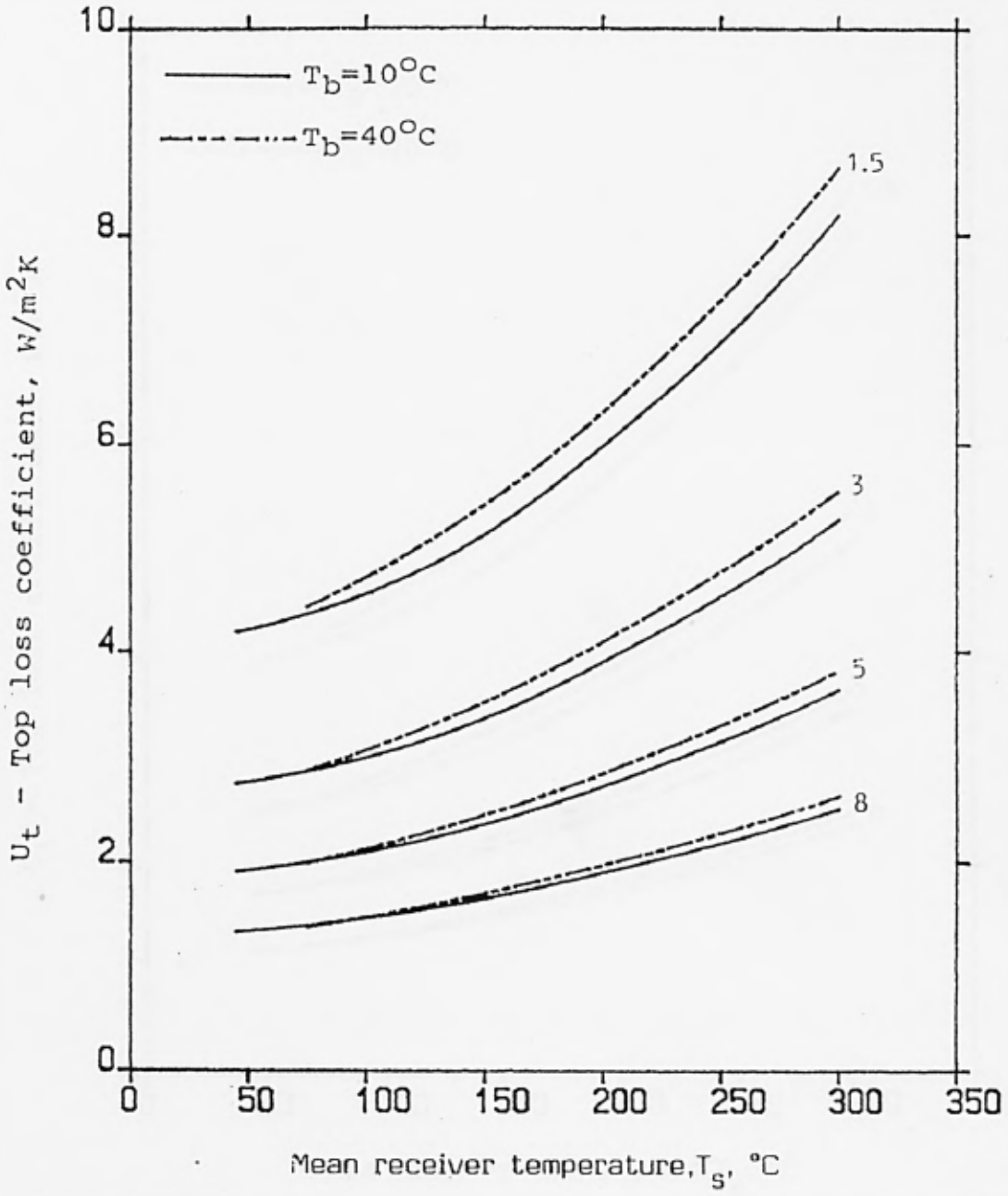


Fig. 4.13 U_t for CPC with non-evacuated tubular receiver vs T_s, for four different CR : ϵ_s = 0.9 ; S = 30° ; h_w = 5 W/m² K

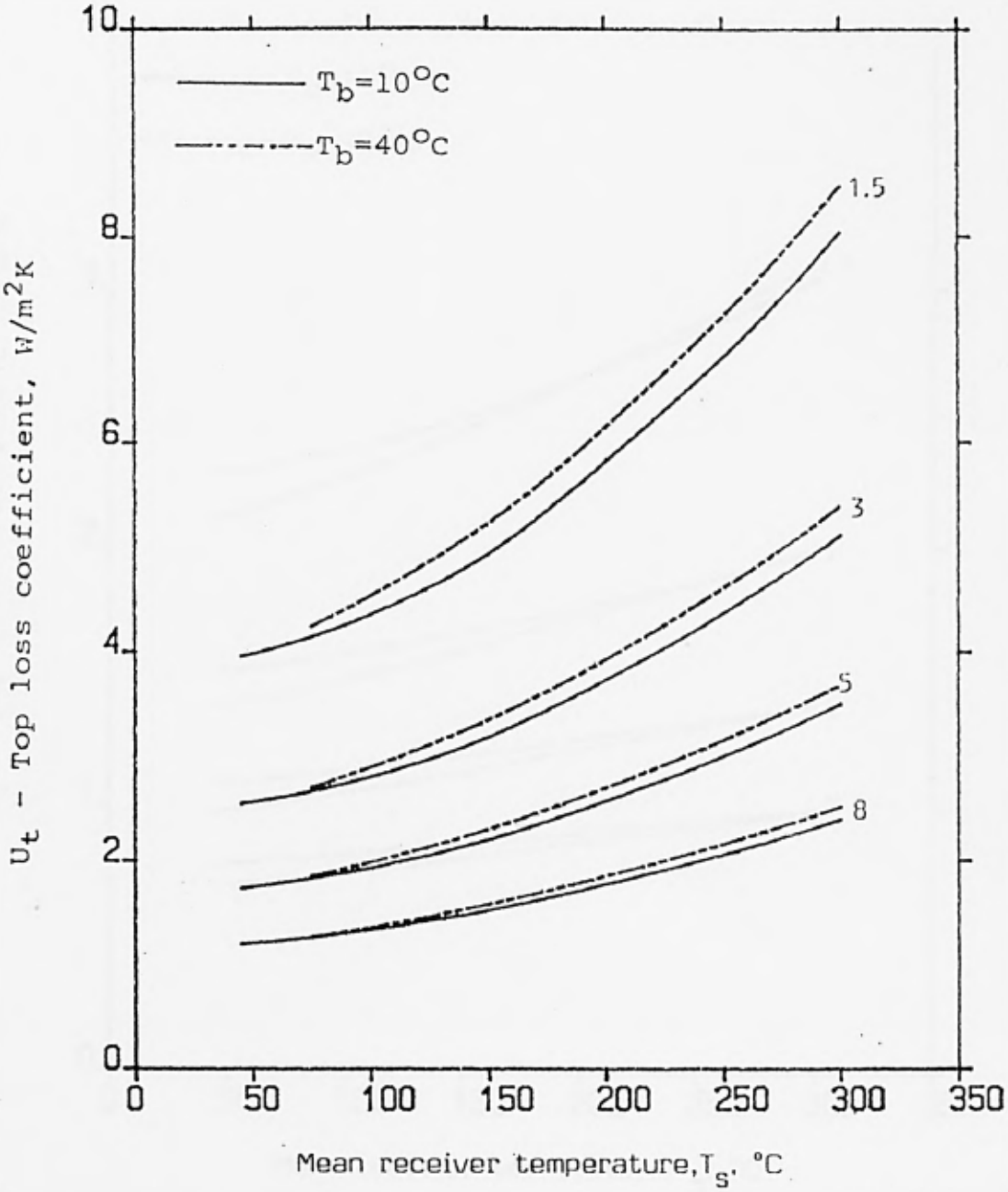


Fig. 4.14 U_t for CPC with non-evacuated tubular receiver vs T_s, for four different CR : ϵ_s = 0.9 ; S = 5° ; h_w = 5 W/m² K

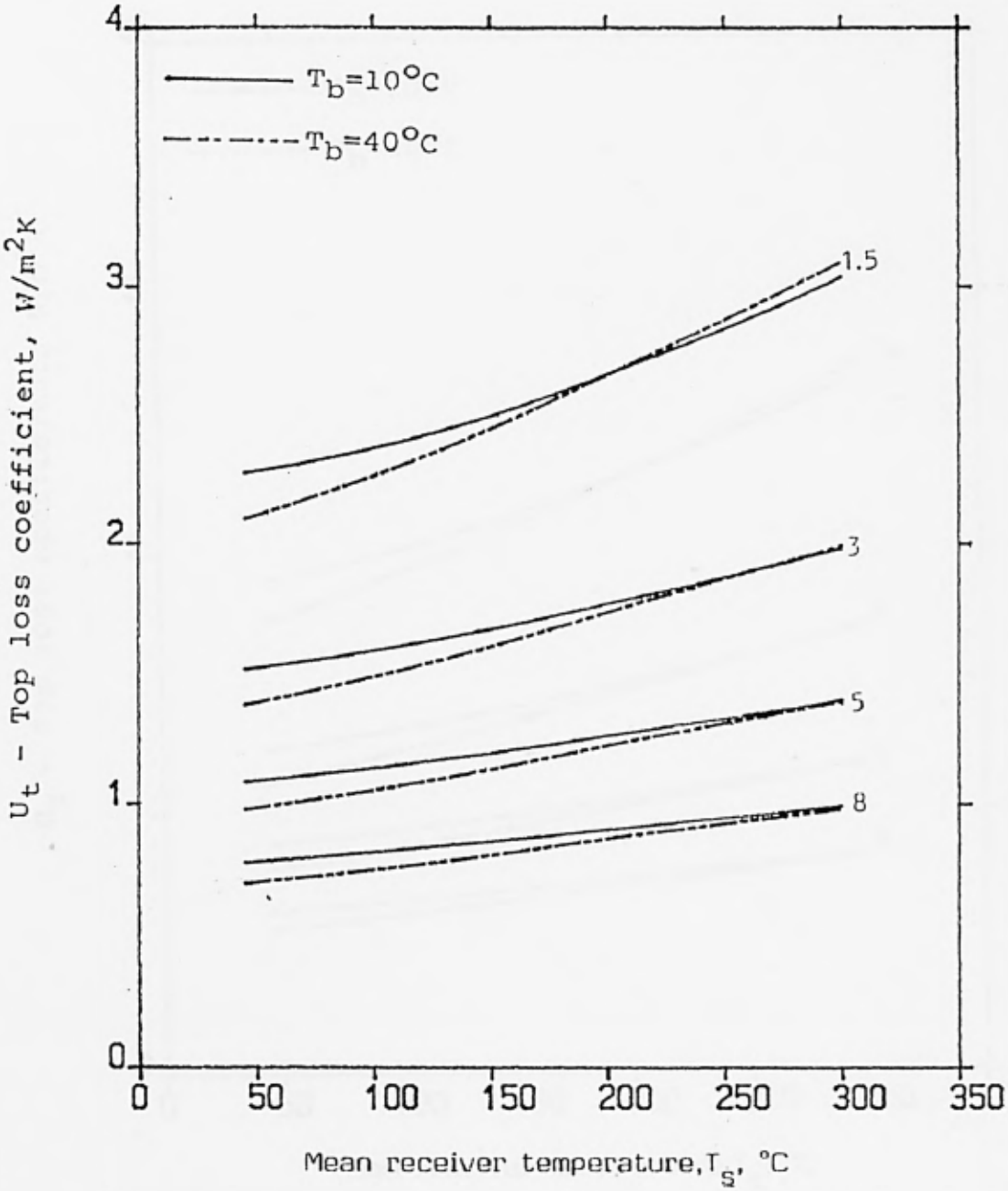


Fig. 4.15 U_t for CPC with non-evacuated tubular receiver vs T_s, for four different CR : ϵ_s=0.1 ; S = 30° ; h_w= 5 W/m² K

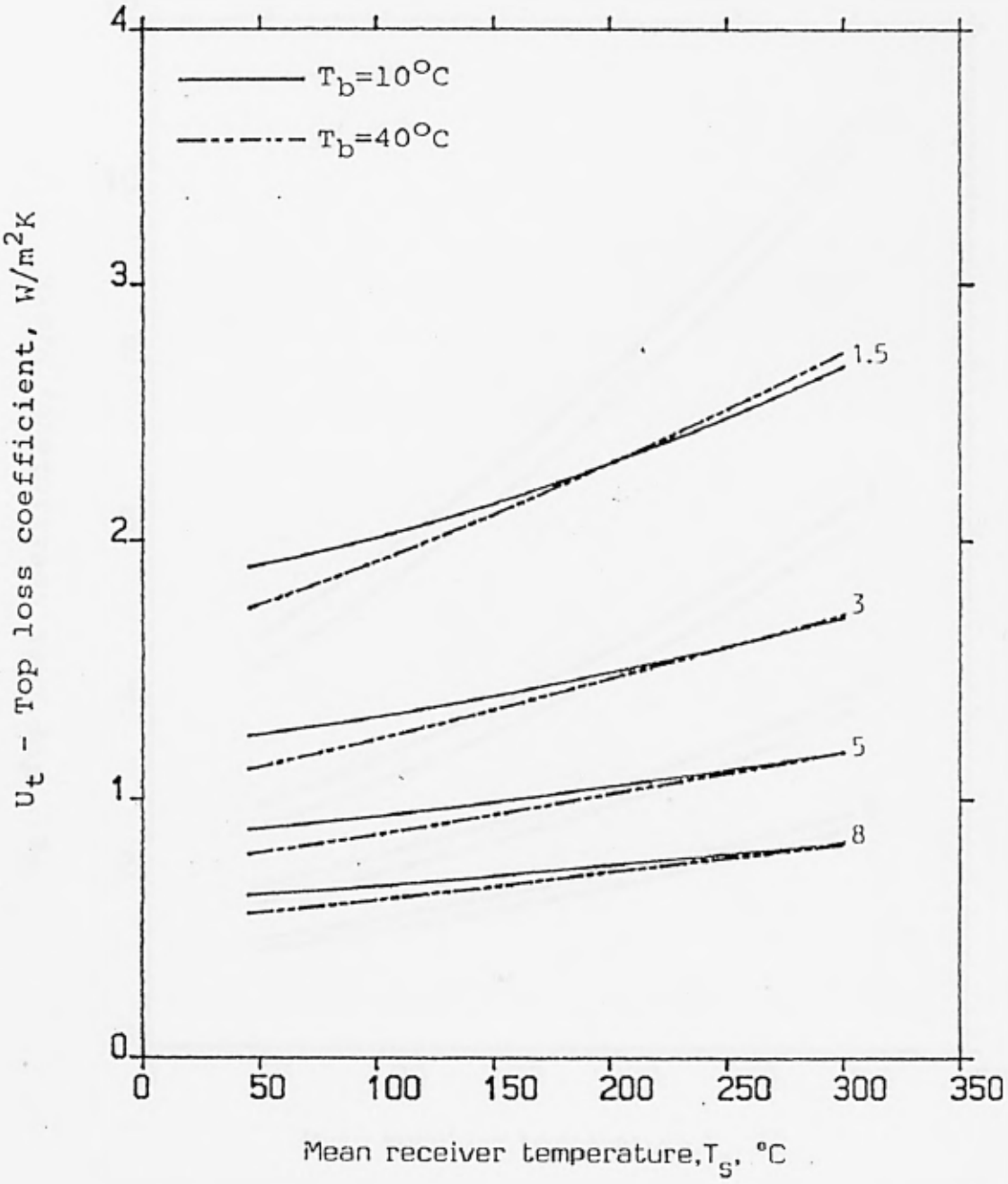


Fig. 4.16 U_t for CPC with non-evacuated tubular receiver vs T_s, for four different CR : ϵ_s = 0.1 ; S = 5° ; h_w = 5 W/m² K

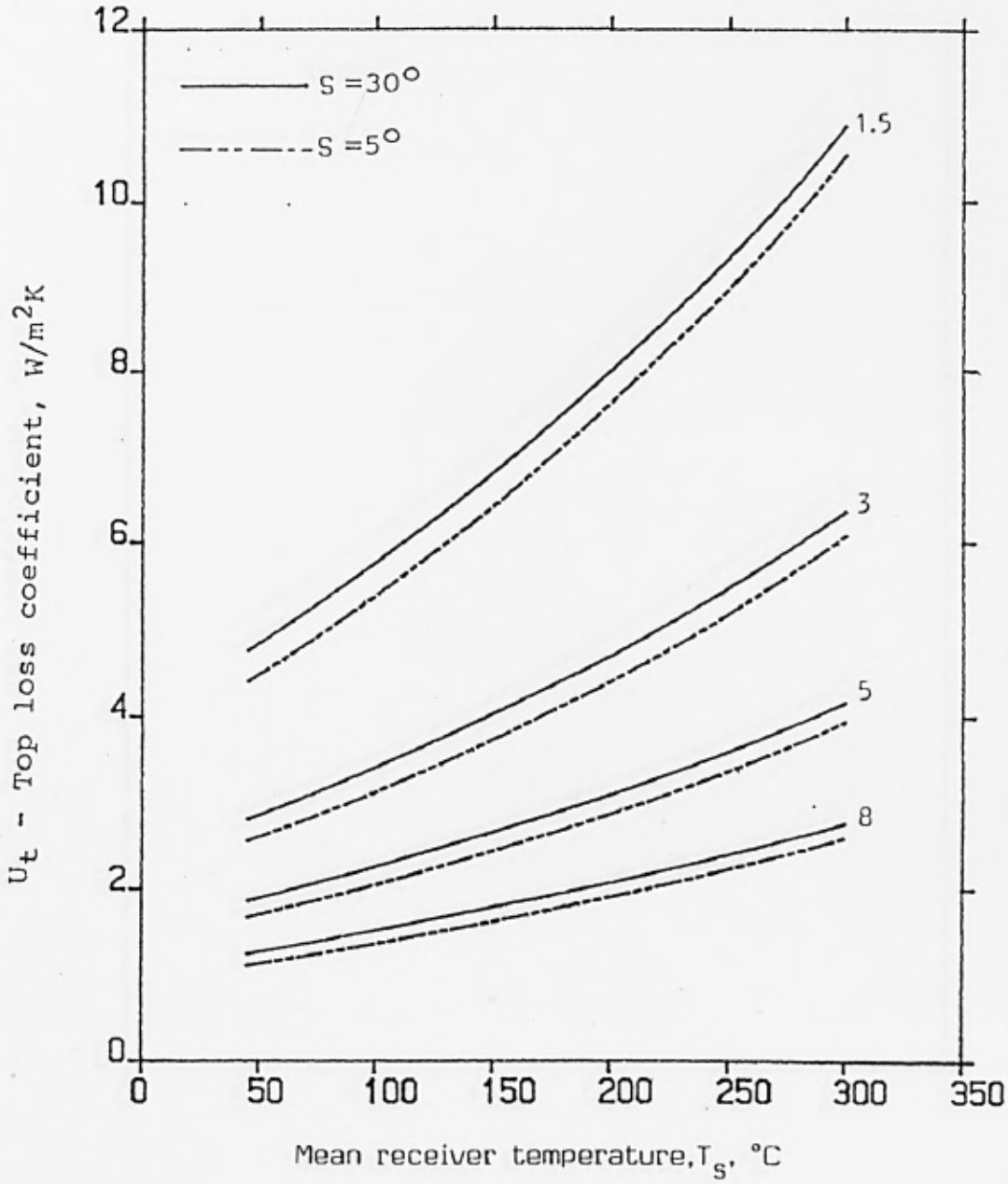


Fig. 4.17 U_t for CPC with non-evacuated tubular receiver vs T_s, for four different CR : ϵ_s = 0.9 ; T_b = 10°C ; h_w = 30 W/m² K

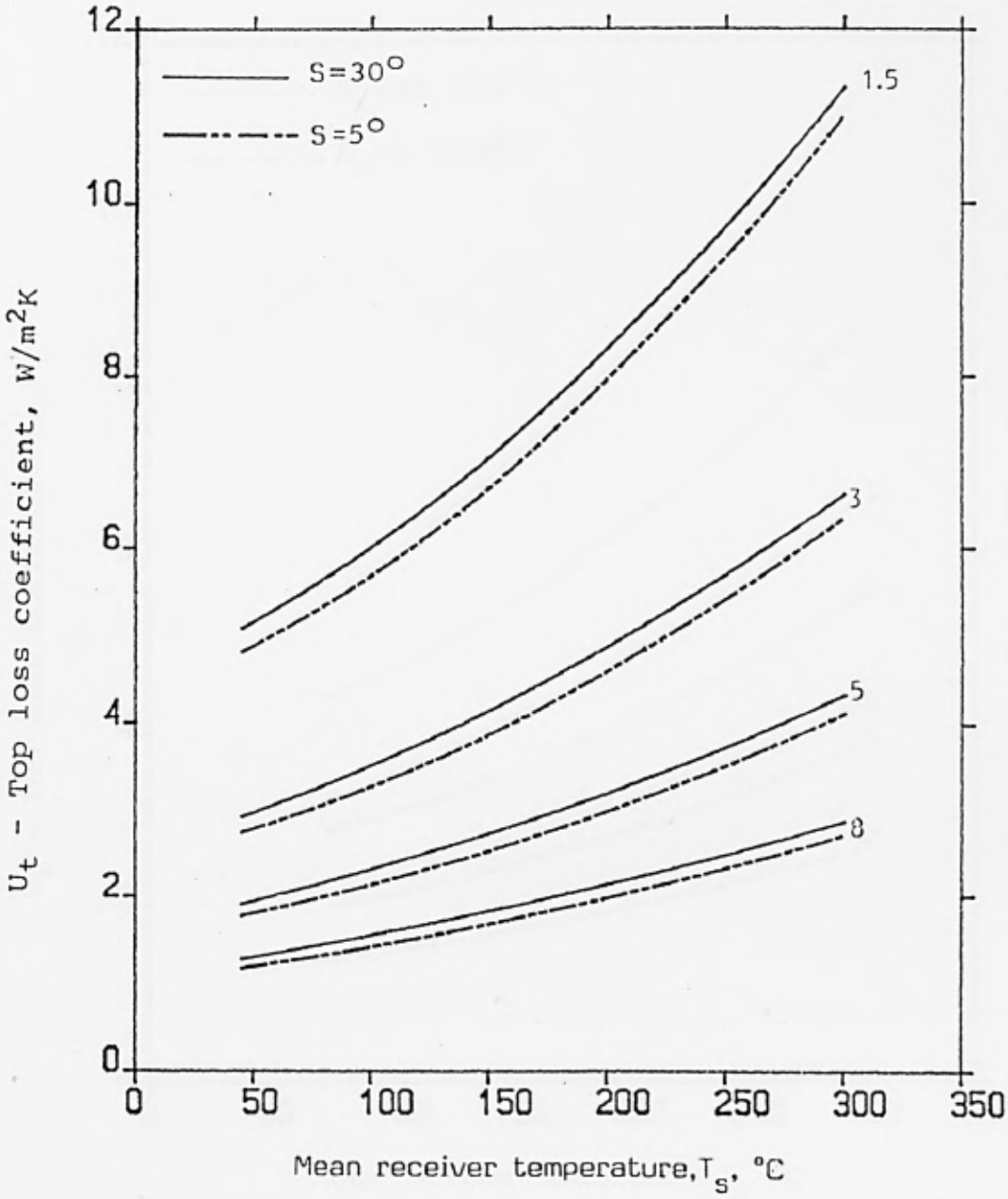


Fig. 4.18 U_t for CPC with non-evacuated tubular receiver vs T_s, for four different CR : ϵ_s = 0.9 ; T_b = 40°C ; h_w = 30 W/m² K

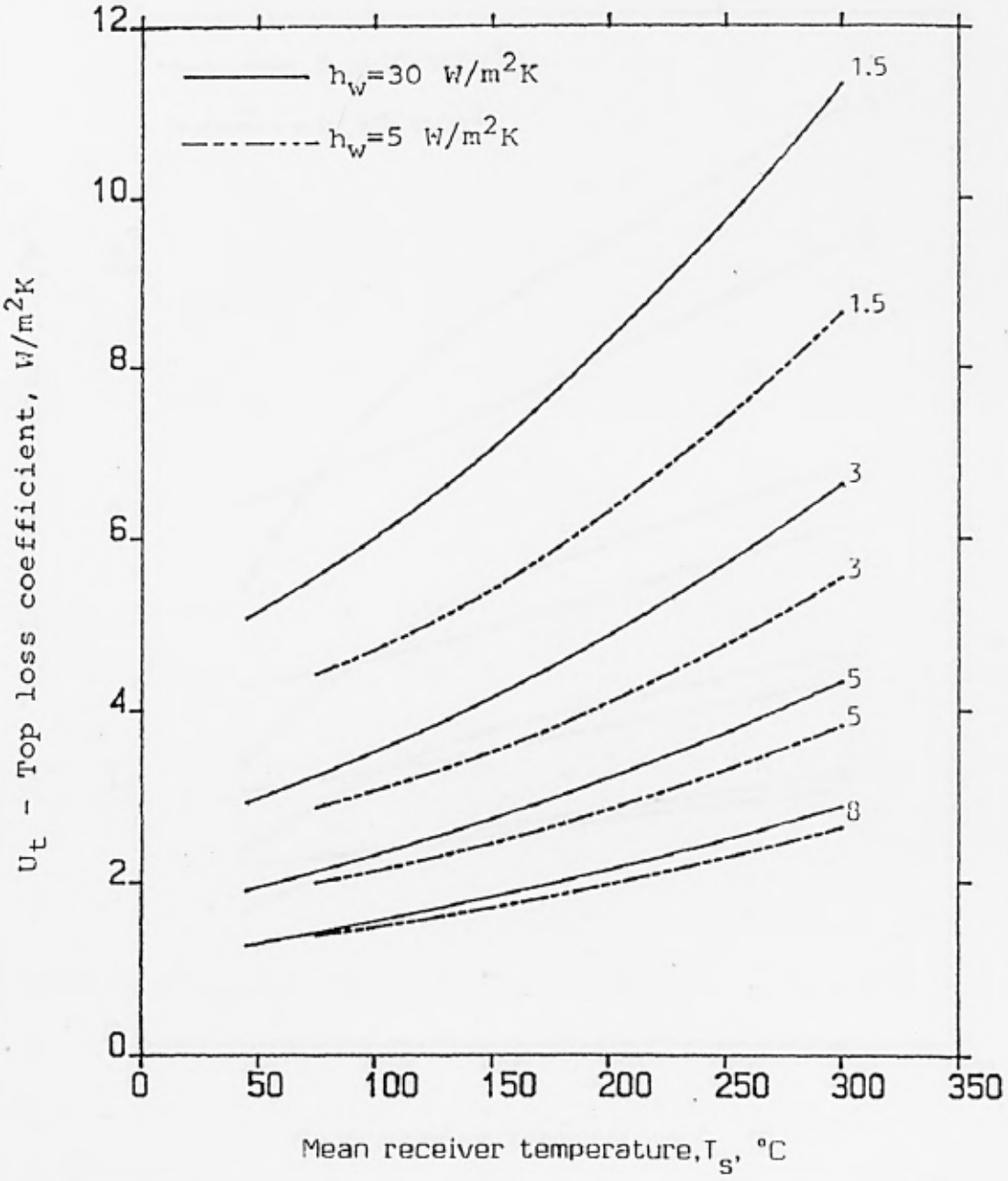


Fig. 4.19 U_t for CPC with non-evacuated tubular receiver vs T_s, for four different CR : ϵ_s= 0.9 ; S = 30° ; T_b= 40°C

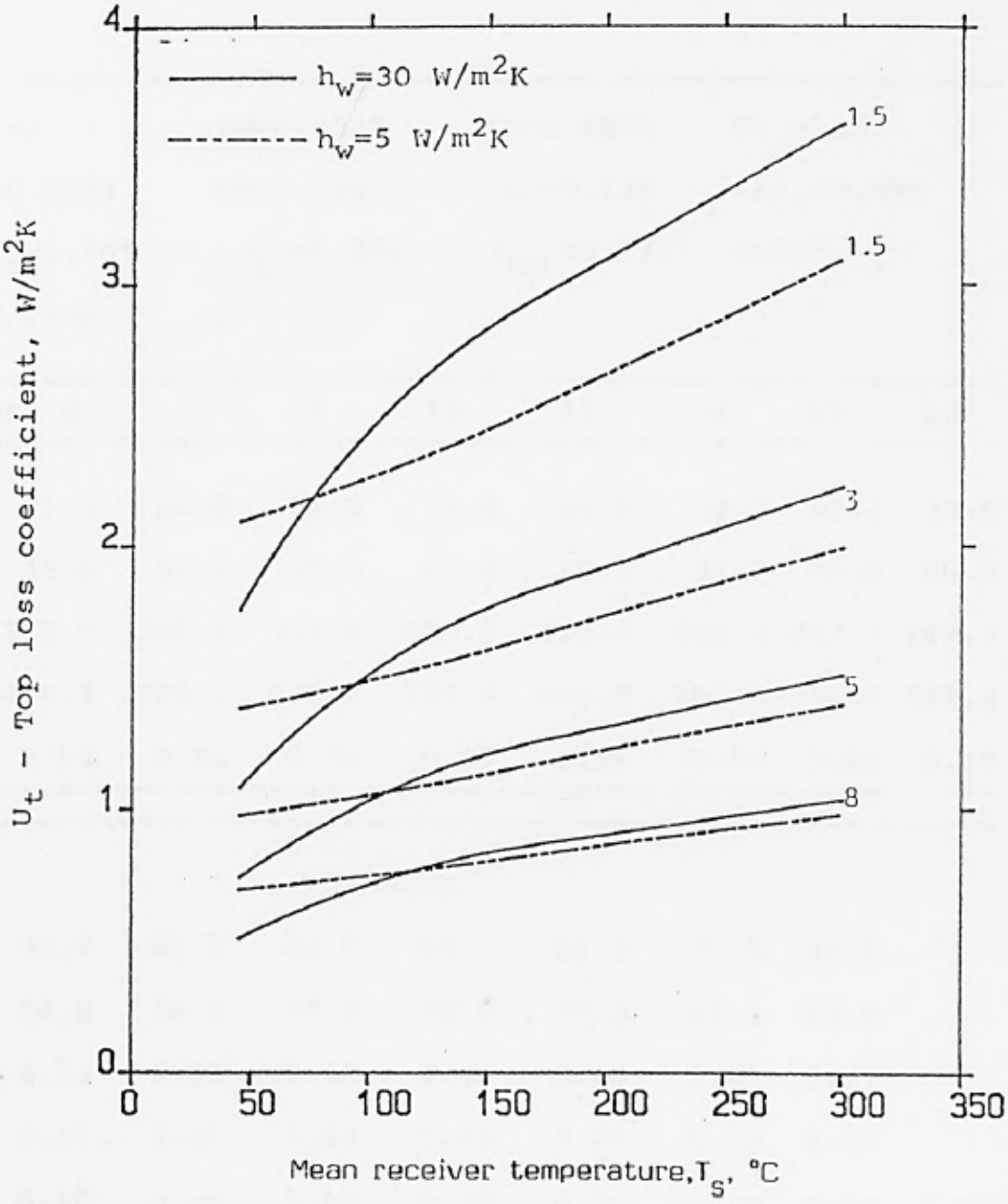


Fig. 4.20 U_t for CPC with non-evacuated tubular receiver vs T_s, for four different CR : ϵ_s = 0.1 ; S = 30° ; T_b = 40°C

Table 4.1 Results for CPC collector with $\theta_a=30^o$, $\epsilon_s=0.9$, $\alpha_s=0.9$

FC =2	FW=0.0942	FH=0.1084	TC =1.5	
TW=0.0707	TH=0.0292	L_r =0.136	$\langle n \rangle_i$=0.896	
$\langle n \rangle_o$=1.755	τ_c =0.864	ϵ_{eff} =0.7767	S=20^o	
Adj/yr=0				

TIME	9	10	11	12	13	14	15	16
T_b	27.9	28.8	29.8	30.8	31.6	32.0	32.2	32.0
θ_i	46.6	32.7	20.1	13.6	20.1	32.7	46.6	60.9
I_b	252.7	348.1	415.4	439.6	415.4	348.1	252.7	149.7
I_t	454.3	595.0	690.8	724.7	690.8	595.0	454.3	292.2
η_o	0.54	0.56	0.56	0.57	0.56	0.56	0.54	0.49

$T_i=80^oC$

T_o	80.7	81.9	82.8	83.1	82.9	82.1	80.9
T_c	34.8	36.1	37.2	38.0	38.8	39.1	38.9
U_l	5.33	5.39	5.42	5.43	5.44	5.41	5.37
U_o	5.16	5.21	5.24	5.25	5.26	5.23	5.19
η	0.10	0.20	0.25	0.27	0.26	0.22	0.13
DT	0.116	0.090	0.077	0.073	0.075	0.084	0.107
FR	0.941	0.941	0.940	0.940	0.940	0.940	0.941

Table 4.1 cont.

TIME	9	10	11	12	13	14	15	16
				T_i=95°C				
T_o		96.0	96.8	97.2	96.9	96.1		
T_c		39.1	40.2	41.0	41.7	42.0		
U_1		5.64	5.67	5.68	5.69	5.66		
U_o		5.44	5.47	5.48	5.49	5.47		
η		0.10	0.16	0.18	0.17	0.12		
DT		0.113	0.097	0.092	0.095	0.108		
FR		0.938	0.938	0.938	0.938	0.938		
				T_i=110°C				
T_o			110.8	111.1	110.8	110.1		
T_c			43.4	44.3	45.0	45.2		
U_1			5.93	5.94	5.95	5.92		
U_o			5.72	5.73	5.74	5.72		
η			0.07	0.09	0.07	0.01		
DT			0.117	0.111	0.115	0.131		
FR			0.935	0.935	0.935	0.935		

Table 4.2 Results for CPC collector with $\theta_a=20^o$, $\epsilon_s=0.9$, $\alpha_s=0.9$

FC =2.924 FW=0.1378 FH=0.2230 TC =2.4

TW=0.1131 TH=0.0783 L_r =0.262 $\langle n \rangle_i$=1.068

$\langle n \rangle_o$=2.285 τ_C =0.841 ϵ_{eff}=0.7931 S=20°

Adj/yr=0

TIME	9	10	11	12	13	14	15	16
T_b	27.9	28.8	29.8	30.8	31.6	32.0	32.2	32.0
θ_i	46.6	32.7	20.1	13.6	20.1	32.7	46.6	60.9
I_b	252.7	348.1	415.4	439.6	415.4	348.1	252.7	149.7
I_t	454.3	595.0	690.8	724.7	690.8	595.0	454.3	292.2
η_o	0.45	0.48	0.49	0.49	0.49	0.48	0.45	0.40
				T_i=95°C				
T_o	97.1	98.9	100.1	100.6	100.2	99.0	97.3	95.3
T_c	34.8	36.0	37.1	38.0	38.8	39.0	38.9	38.4
U_1	3.98	4.02	4.05	4.06	4.06	4.04	4.00	3.96
U_o	3.89	3.92	3.95	3.96	3.96	3.94	3.90	3.86
η	0.18	0.25	0.29	0.30	0.29	0.26	0.19	0.04
DT	0.153	0.118	0.102	0.097	0.100	0.113	0.144	0.216
FR	0.956	0.955	0.955	0.955	0.955	0.955	0.955	0.956

Table 4.2 cont.

TIME	9	10	11	12	13	14	15	16
				T_i=110°C				
T_o	111.3	113.1	114.4	114.8	114.4	113.2	111.5	
T_c	37.2	38.4	39.5	40.4	41.2	41.4	41.2	
U_l	4.17	4.21	4.24	4.25	4.26	4.23	4.20	
U_o	4.07	4.11	4.14	4.14	4.15	4.12	4.09	
η	0.11	0.20	0.24	0.25	0.24	0.21	0.13	
DT	0.184	0.142	0.123	0.116	0.120	0.137	0.175	
FR	0.954	0.953	0.953	0.953	0.953	0.953	0.954	
				T_i=125°C				
T_o	125.5	127.3	128.5	129.0	128.6	127.4	125.7	
T_c	39.6	40.9	42.1	43.0	43.7	43.9	43.7	
U_l	4.37	4.41	4.44	4.45	4.46	4.43	4.40	
U_o	4.26	4.30	4.33	4.33	4.34	4.32	4.29	
η	0.04	0.14	0.19	0.21	0.20	0.15	0.05	
DT	0.215	0.166	0.143	0.136	0.141	0.160	0.206	
FR	0.952	0.952	0.952	0.952	0.952	0.952	0.952	
				T_i=140°C				
T_o		141.3	142.6	143.1	142.5	141.5		
T_c		43.7	44.9	45.7	46.5	46.7		
U_l		4.62	4.65	4.66	4.67	4.64		
U_o		4.50	4.53	4.53	4.54	4.52		
η		0.09	0.14	0.16	0.14	0.09		
DT		0.189	0.163	0.155	0.161	0.184		
FR		0.950	0.950	0.950	0.950	0.950		

Table 4.3 Results for CPC collector with $\theta_a=15^o$, $\epsilon_s=0.9$, $\alpha_s=0.9$

FC =3.864	FW=0.1821	FH=0.3805	TC =3.3	
TW=0.1555	TH=0.1512	L_r =0.430	$\langle n \rangle_i$=1.174	
$\langle n \rangle_o$=2.835	τ_C =0.826	ϵ_{eff}=0.8037	S=15^o	
Adj/yr=2				

TIME	9	10	11	12	13	14	15	16
T_b	27.9	28.8	29.8	30.8	31.6	32.0	32.2	32.0
θ_i	45.6	31.1	17.2	8.6	17.2	31.1	45.6	60.4
I_b	257.1	354.1	422.5	447.1	422.5	354.1	257.1	152.8
I_t	458.7	601.0	697.9	732.2	697.9	601.0	458.7	294.8
η_o	0.42	0.44	0.45	0.45	0.45	0.44	0.42	0.37
			T_i=95^{o}C					
T_o	99.1	101.5	103.1	103.7	103.2	101.6	99.3	96.6
T_c	33.0	34.2	35.4	36.3	37.1	37.3	37.2	36.6
U_1	3.08	3.12	3.15	3.15	3.16	3.13	3.10	3.05
U_o	3.03	3.06	3.09	3.09	3.10	3.07	3.04	3.00
η	0.25	0.30	0.33	0.33	0.33	0.31	0.26	0.15
DT	0.156	0.122	0.106	0.100	0.103	0.116	0.147	0.220
FR	0.965	0.965	0.965	0.965	0.965	0.965	0.965	0.966

Table 4.3 cont.

TIME	9	10	11	12	13	14	15	16
				T_i=110°C				
T_o	113.5	115.9	117.5	118.1	117.6	116.0	113.7	111.0
T_c	34.9	36.1	37.3	38.2	39.0	39.2	39.0	38.5
U_1	3.23	3.27	3.30	3.30	3.31	3.28	3.25	3.21
U_o	3.17	3.21	3.24	3.24	3.25	3.22	3.19	3.15
η	0.21	0.27	0.30	0.31	0.30	0.28	0.22	0.10
DT	0.187	0.145	0.126	0.120	0.124	0.140	0.178	0.268
FR	0.964	0.964	0.963	0.963	0.963	0.963	0.964	0.964
				T_i=125°C				
T_o	127.9	130.2	131.9	132.5	131.9	130.3	128.0	125.4
T_c	36.9	38.1	39.4	40.3	41.0	41.2	41.0	40.4
U_1	3.39	3.43	3.46	3.46	3.47	3.44	3.41	3.37
U_o	3.32	3.36	3.39	3.39	3.40	3.37	3.34	3.30
η	0.17	0.24	0.27	0.28	0.27	0.25	0.18	0.03
DT	0.218	0.169	0.147	0.139	0.144	0.164	0.209	0.317
FR	0.963	0.962	0.962	0.962	0.962	0.962	0.962	0.963
				T_i=140°C				
T_o	142.2	144.5	146.2	146.8	146.2	144.6	142.3	
T_c	39.0	40.3	41.6	42.5	43.2	43.4	43.2	
U_1	3.55	3.59	3.62	3.62	3.63	3.61	3.57	
U_o	3.48	3.52	3.55	3.55	3.56	3.53	3.50	
η	0.13	0.21	0.24	0.25	0.24	0.21	0.14	
DT	0.249	0.193	0.167	0.159	0.164	0.187	0.240	
FR	0.962	0.961	0.961	0.961	0.961	0.961	0.961	

Table 4.4 Results for CPC collector with $\theta_a=10^o$, $\epsilon_s=0.9$, $\alpha_s=0.9$

FC =5.759	FW=0.2714	FH=0.8245	TC =4.70
TW=0.2215	TH=0.2782	L_r =0.715	$\langle n\rangle_i$=1.264
$\langle n\rangle_o$=3.329	τ_C =0.814	ϵ_{eff} =0.8128	S=10^o
Adj/yr=6			

TIME	9	10	11	12	13	14	15	16
T_b	27.9	28.8	29.8	30.8	31.6	32.0	32.2	32.0
θ_i	45.1	30.2	15.4	3.6	15.4	30.2	45.1	60.1
I_b	259.5	357.4	426.4	451.3	426.4	357.4	259.5	153.7
I_t	461.1	604.3	701.8	736.4	701.8	604.3	461.1	296.2
η_o	0.39	0.41	0.42	0.43	0.42	0.41	0.39	0.34
				T_i=95^{o}C				
T_o	101.9	105.1	107.3	108.1	107.4	105.2	102.0	98.3
T_c	31.3	32.6	33.8	34.8	35.6	35.8	35.6	35.1
U_l	2.29	2.33	2.35	2.36	2.36	2.33	2.30	2.26
U_o	2.26	2.29	2.32	2.32	2.33	2.30	2.27	2.23
η	0.29	0.33	0.35	0.35	0.35	0.33	0.30	0.22
DT	0.162	0.127	0.112	0.106	0.109	0.122	0.152	0.225
FR	0.974	0.974	0.974	0.974	0.973	0.974	0.974	0.974

Table 4.4 cont.

TIME	9	10	11	12	13	14	15	16
				T_i=110°C				
T_o	116.4	119.7	121.9	122.7	122.0	119.8	116.5	112.9
T_c	32.8	34.0	35.3	36.2	37.0	37.2	37.0	36.4
U_l	2.40	2.44	2.47	2.47	2.48	2.45	2.41	2.37
U_o	2.37	2.40	2.43	2.43	2.44	2.41	2.38	2.34
η	0.27	0.31	0.33	0.34	0.33	0.32	0.28	0.19
DT	0.193	0.151	0.132	0.126	0.130	0.146	0.184	0.274
FR	0.973	0.973	0.973	0.973	0.972	0.973	0.973	0.973
				T_i=125°C				
T_o	131.0	134.2	136.5	137.3	136.5	134.3	131.1	127.4
T_c	34.3	35.6	36.9	37.8	38.6	38.8	38.5	37.9
U_l	2.52	2.56	2.58	2.59	2.60	2.57	2.53	2.49
U_o	2.48	2.52	2.55	2.55	2.56	2.53	2.50	2.46
η	0.25	0.30	0.32	0.32	0.32	0.30	0.26	0.16
DT	0.224	0.175	0.152	0.145	0.150	0.170	0.215	0.322
FR	0.972	0.972	0.972	0.972	0.971	0.972	0.972	0.972
				T_i=140°C				
T_o	145.4	148.7	150.9	151.8	151.0	148.8	145.5	141.9
T_c	36.0	37.3	38.5	39.5	40.3	40.4	40.2	39.5
U_l	2.64	2.68	2.71	2.71	2.72	2.69	2.66	2.62
U_o	2.60	2.64	2.67	2.67	2.68	2.65	2.62	2.58
η	0.23	0.28	0.30	0.31	0.30	0.28	0.23	0.12
DT	0.255	0.199	0.173	0.164	0.170	0.193	0.246	0.371
FR	0.971	0.971	0.971	0.971	0.971	0.971	0.971	0.971

Table 4.5 Results for CPC collector with $\theta_a=30^o$, $\epsilon_s=0.17$, $\alpha_s=0.89$

FC =2		FW=0.0942		FH=0.1084		TC =1.5		
TW=0.0707		TH=0.0292		L_r =0.136		$\langle n \rangle_i$=0.896		
$\langle n \rangle_o$=1.755		τ_C =0.864		ϵ_{eff}=0.1532		S=20^o		
Adj/yr=0								
TIME	9	10	11	12	13	14	15	16
T_b	27.9	28.8	29.8	30.8	31.6	32.0	32.2	32.0
θ_i	46.6	32.7	20.1	13.6	20.1	32.7	46.6	60.9
I_b	252.7	348.1	415.4	439.6	415.4	348.1	252.7	149.7
I_t	454.3	595.0	690.8	724.7	690.8	595.0	454.3	292.2
η_o	0.53	0.55	0.56	0.56	0.56	0.55	0.53	0.48
				T_i=80^{o}C				
T_o	82.1	83.4	84.3	84.6	84.3	83.5	82.3	80.8
T_c	30.4	31.3	32.5	33.5	34.2	34.6	34.7	34.5
U_l	2.66	2.67	2.68	2.69	2.69	2.67	2.64	2.61
U_o	2.61	2.62	2.64	2.65	2.64	2.63	2.60	2.57
η	0.29	0.35	0.38	0.39	0.39	0.36	0.31	0.18
DT	0.120	0.092	0.079	0.075	0.077	0.087	0.111	0.167
FR	0.970	0.970	0.970	0.970	0.970	0.970	0.970	0.970

Table 4.5 cont.

TIME	9	10	11	12	13	14	15	16
				T_i=95°C				
T_o	96.7	97.9	98.8	99.1	98.8	98.0	96.8	95.4
T_c	31.9	32.8	34.0	35.0	35.7	36.1	36.2	36.0
U_l	2.76	2.77	2.78	2.79	2.78	2.77	2.75	2.72
U_o	2.71	2.72	2.73	2.74	2.74	2.72	2.70	2.68
η	0.23	0.30	0.34	0.35	0.34	0.31	0.24	0.08
DT	0.152	0.117	0.100	0.095	0.098	0.111	0.142	0.217
FR	0.969	0.969	0.969	0.969	0.969	0.969	0.969	0.969
				T_i=110°C				
T_o	111.2	112.4	113.3	113.6	113.3	112.5	111.3	
T_c	33.4	34.4	35.5	36.6	37.3	37.7	37.7	
U_l	2.85	2.86	2.88	2.88	2.88	2.87	2.85	
U_o	2.80	2.81	2.83	2.83	2.83	2.82	2.80	
η	0.16	0.25	0.29	0.31	0.30	0.26	0.17	
DT	0.183	0.141	0.121	0.115	0.119	0.136	0.174	
FR	0.968	0.968	0.968	0.968	0.968	0.968	0.968	
				T_i=125°C				
T_o	125.6	126.9	127.8	128.1	127.8	127.0	125.7	
T_c	35.1	36.0	37.2	38.2	38.9	39.3	39.4	
U_l	2.95	2.96	2.97	2.98	2.98	2.97	2.95	
U_o	2.90	2.91	2.92	2.93	2.92	2.91	2.90	
η	0.08	0.19	0.24	0.26	0.25	0.20	0.10	
DT	0.215	0.165	0.142	0.134	0.140	0.160	0.206	
FR	0.967	0.967	0.967	0.967	0.967	0.967	0.967	

Table 4.6 Results for CPC collector with $\theta_a=20^o$, $\epsilon_s=0.17$, $\alpha_s=0.89$

FC =2.924 FW=0.1378 FH=0.2230 TC =2.4

TW=0.1131 TH=0.0783 L_r =0.262 $\langle n\rangle_i$=1.068

$\langle n\rangle_o$=2.285 τ_C =0.841 ϵ_{eff}=0.1548 S=20°

Adj/yr=0

TIME	9	10	11	12	13	14	15	16
T_b	27.9	28.8	29.8	30.8	31.6	32.0	32.2	32.0
θ_i	46.6	32.7	20.1	13.6	20.1	32.7	46.6	60.9
I_b	252.7	348.1	415.4	439.6	415.4	348.1	252.7	149.7
I_t	454.3	595.0	690.8	724.7	690.8	595.0	454.3	292.2
η_o	0.45	0.47	0.48	0.48	0.48	0.47	0.45	0.40
				T_i=95°C				
T_o	98.5	100.3	101.5	102.0	101.6	100.4	98.6	96.6
T_c	30.4	31.3	32.5	33.5	34.3	34.7	34.8	34.3
U_l	2.01	2.01	2.03	2.03	2.03	2.02	2.00	1.97
U_o	1.98	1.99	2.00	2.01	2.00	1.99	1.98	1.94
η	0.30	0.34	0.36	0.37	0.37	0.35	0.30	0.21
DT	0.156	0.121	0.104	0.099	0.102	0.115	0.147	0.221
FR	0.977	0.977	0.977	0.977	0.977	0.977	0.977	0.978

Table 4.6 cont.

TIME	9	10	11	12	13	14	15	16
				T_i=110°C				
T_o	113.1	115.0	116.2	116.7	116.2	115.0	113.2	111.2
T_c	31.6	32.5	33.6	34.7	35.4	35.9	35.9	35.5
U_l	2.08	2.08	2.10	2.10	2.10	2.09	2.07	2.04
U_o	2.05	2.06	2.07	2.07	2.07	2.06	2.05	2.02
η	0.26	0.32	0.34	0.35	0.35	0.32	0.27	0.16
DT	0.188	0.145	0.126	0.119	0.123	0.140	0.179	0.271
FR	0.977	0.976	0.976	0.976	0.976	0.976	0.977	0.977
				T_i=125°C				
T_o	127.7	129.6	130.8	131.3	130.9	129.6	127.8	125.8
T_c	32.8	33.7	34.9	35.9	36.7	37.1	37.1	36.7
U_l	2.15	2.15	2.16	2.17	2.17	2.16	2.14	2.12
U_o	2.12	2.12	2.14	2.14	2.14	2.13	2.12	2.09
η	0.23	0.29	0.32	0.33	0.32	0.30	0.24	0.11
DT	0.220	0.170	0.147	0.139	0.144	0.164	0.211	0.321
FR	0.976	0.976	0.976	0.976	0.976	0.976	0.976	0.976
				T_i=140°C				
T_o	142.3	144.2	145.4	145.9	145.5	144.2	142.4	140.4
T_c	34.1	34.9	36.1	37.2	37.9	38.3	38.4	37.9
U_l	2.21	2.22	2.23	2.24	2.23	2.23	2.21	2.19
U_o	2.19	2.19	2.20	2.21	2.21	2.20	2.19	2.16
η	0.19	0.27	0.30	0.31	0.30	0.27	0.20	0.05
DT	0.252	0.194	0.167	0.159	0.165	0.189	0.243	0.371
FR	0.976	0.976	0.976	0.976	0.976	0.976	0.976	0.976

Table 4.7 Results for CPC collector with θ_a=15°, ϵ_s=0.17, α_s=0.89

FC =3.864 FW=0.1821 FH=0.3805 TC =3.3

TW=0.1555 TH=0.1512 L_r=0.430 $\langle n \rangle_i$=1.174

$\langle n \rangle_o$=2.835 τ_c=0.826 ϵ_{eff}=0.1556 S=15°

Adj/yr=2

TIME	9	10	11	12	13	14	15	16
T_b	27.9	28.8	29.8	30.8	31.6	32.0	32.2	32.0
θ_i	45.6	31.1	17.2	8.6	17.2	31.1	45.6	60.4
I_b	257.1	354.1	422.5	447.5	422.4	354.1	257.1	152.8
I_t	458.7	601.0	697.9	732.2	697.9	601.0	458.7	294.8
η_o	0.41	0.44	0.45	0.45	0.45	0.44	0.41	0.37

T_i=95°C

T_o	100.2	102.6	104.2	104.8	104.3	102.7	100.3	97.7
T_c	29.4	30.3	31.5	32.6	33.4	33.8	33.9	33.4
U_l	1.55	1.55	1.57	1.57	1.57	1.56	1.54	1.51
U_o	1.53	1.54	1.55	1.56	1.56	1.55	1.53	1.50
η	0.32	0.35	0.37	0.38	0.37	0.36	0.32	0.25
DT	0.159	0.124	0.108	0.102	0.105	0.118	0.149	0.223
FR	0.982	0.982	0.982	0.982	0.982	0.982	0.982	0.983

Table 4.7 cont.

TIME	9	10	11	12	13	14	15	16
				T_i=110°C				
T_o	115.0	117.4	119.0	119.6	119.0	117.4	115.0	112.4
T_c	30.3	31.2	32.4	33.5	34.3	34.7	34.8	34.3
U_1	1.60	1.61	1.62	1.62	1.62	1.62	1.60	1.57
U_o	1.59	1.59	1.60	1.61	1.61	1.60	1.59	1.56
η	0.30	0.34	0.36	0.36	0.36	0.34	0.31	0.22
DT	0.190	0.148	0.128	0.122	0.126	0.143	0.181	0.273
FR	0.982	0.982	0.982	0.982	0.982	0.982	0.982	0.982
				T_i=125°C				
T_o	129.7	132.1	133.7	134.3	133.7	132.1	129.8	127.1
T_c	31.3	32.2	33.4	34.5	35.2	35.7	35.7	35.2
U_1	1.65	1.66	1.67	1.68	1.68	1.67	1.65	1.63
U_o	1.64	1.64	1.65	1.66	1.66	1.65	1.64	1.61
η	0.28	0.33	0.35	0.35	0.35	0.33	0.29	0.19
DT	0.222	0.172	0.149	0.142	0.147	0.167	0.213	0.323
FR	0.981	0.981	0.981	0.981	0.981	0.981	0.982	0.982
				T_i=140°C				
T_o	144.4	146.8	148.4	149.0	148.4	146.8	144.4	141.8
T_c	32.3	33.2	34.4	35.5	36.2	36.6	36.7	36.2
U_1	1.71	1.71	1.72	1.73	1.73	1.72	1.71	1.68
U_o	1.69	1.69	1.70	1.71	1.71	1.70	1.69	1.67
η	0.26	0.31	0.33	0.34	0.33	0.31	0.27	0.16
DT	0.254	0.197	0.170	0.162	0.168	0.191	0.245	0.372
FR	0.981	0.981	0.981	0.981	0.981	0.981	0.981	0.981

Table 4.8 Results for CPC collector with $\theta_a=10^o$, $\epsilon_s=0.17$, $\alpha_s=0.89$

FC =5.759 FW=0.2714 FH=0.8245 TC =4.7

TW=0.2215 TH=0.2782 L_r =0.715 $\langle n\rangle_i$=1.264

$\langle n\rangle_o$=3.329 τ_c=0.814 ϵ_{eff} =0.1563 S=10^o

Adj/yr=6

TIME	9	10	11	12	13	14	15	16
T_b	27.9	28.8	29.8	30.8	31.6	32.0	32.2	32.0
θ_i	45.1	30.2	15.4	3.6	15.4	30.2	45.1	60.1
I_b	259.5	357.4	426.4	451.3	426.4	357.4	259.5	153.7
I_t	461.1	604.3	701.8	736.4	701.8	604.3	461.1	296.2
η_o	0.39	0.41	0.42	0.42	0.42	0.41	0.39	0.34
				T_i=95^{o}C				
T_o	102.7	105.9	108.2	109.0	108.2	106.0	102.7	99.1
T_c	28.5	29.5	30.7	31.8	32.6	33.0	33.1	32.6
U_l	1.14	1.15	1.16	1.17	1.17	1.16	1.14	1.11
U_o	1.13	1.14	1.15	1.16	1.16	1.15	1.13	1.10
η	0.33	0.36	0.37	0.37	0.37	0.36	0.33	0.27
DT	0.163	0.129	0.113	0.107	0.110	0.123	0.154	0.227
FR	0.987	0.987	0.987	0.987	0.987	0.987	0.987	0.987

Table 4.8 cont.

TIME	9	10	11	12	13	14	15	16
				T_i=110°C				
T_o	117.5	120.8	123.0	123.8	123.0	120.8	117.6	113.9
T_c	29.2	30.2	31.4	32.5	33.2	33.7	33.7	33.2
U_l	1.18	1.19	1.20	1.20	1.20	1.20	1.18	1.15
U_o	1.17	1.18	1.19	1.20	1.20	1.19	1.17	1.15
η	0.32	0.35	0.36	0.37	0.36	0.35	0.32	0.26
DT	0.195	0.153	0.134	0.127	0.131	0.148	0.186	0.227
FR	0.987	0.987	0.986	0.986	0.986	0.987	0.987	0.987
				T_i=125°C				
T_o	132.3	135.6	137.9	138.7	137.9	135.6	132.4	128.7
T_c	29.9	30.9	32.1	33.2	34.0	34.4	34.4	33.9
U_l	1.22	1.22	1.24	1.24	1.24	1.23	1.22	1.20
U_o	1.21	1.22	1.23	1.23	1.23	1.23	1.21	1.19
η	0.31	0.34	0.36	0.36	0.36	0.34	0.31	0.24
DT	0.227	0.177	0.155	0.147	0.152	0.172	0.218	0.327
FR	0.986	0.986	0.986	0.986	0.986	0.986	0.986	0.987
				T_i=140°C				
T_o	147.1	150.4	152.7	153.5	152.7	150.4	147.2	143.5
T_c	30.7	31.6	32.8	33.9	34.7	35.1	35.2	34.7
U_l	1.26	1.26	1.27	1.28	1.28	1.27	1.26	1.24
U_o	1.25	1.25	1.26	1.27	1.27	1.26	1.25	1.23
η	0.30	0.33	0.35	0.35	0.35	0.33	0.30	0.23
DT	0.259	0.201	0.175	0.167	0.173	0.196	0.249	0.376
FR	0.986	0.986	0.986	0.986	0.986	0.986	0.986	0.986

CHAPTER 5

AQUA-AMMONIA ABSORPTION REFRIGERATION SYSTEM

5.1 INTRODUCTION

Application of solar energy to produce lower temperatures required for cooling and freezing of foods has been suggested many times in the literature. However, little exits in the way of technical and feasibility studies for this purpose.

In this chapter, regression of the property data of ammonia-water mixtures has been undertaken to provide property data equations. A mathematical model of the aqua-ammonia absorption refrigeration system has been developed. The property data equations are used in a computer program to carry out a detailed and extensive thermodynamic cycle analysis of the system. Important system parameters and limitations that should be considered in the design of the system have been identified, and performance curves which can be used for quick system design are provided.

Solar energy may be used to operate refrigeration equipment either by direct conversion to electricity for power to drive a conventional vapour compression cycle, or by using the heat collected to energise a heat-activated cycle.

The types of system which can operate from the heat obtained from a solar collector include, the absorption

cycles, Rankine cycle, adsorption cycle, Stirling and Brayton cycles, and the use of photovoltaic cells to generate electricity to drive a vapour compression cycle. The most promising cycles are described below.

5.1.1 THE ABSORPTION CYCLES

In the absorption cycle shown in figure 5.1, page 127, the refrigerant is driven from a strong solution in the generator at high pressure P_2, then condensed in the condenser at the same pressure. It is then expanded to low pressure P_1 before it evaporates in the evaporator to provide the cooling effect. The vapour is then absorbed in the absorber at P_1 by the weak solution left from step one. Next, it is pumped in solution back to P_2 where the process is repeated.

5.1.2 THE RANKINE CYCLE

The schematic diagram in figure 5.2, page 128 shows a Rankine cycle. The heat from a solar collector system is added to a low boiling point organic liquid at pressure P_1 in the boiler to evaporate it. The vapour is then expanded in a turbine to pressure P_2 to produce mechanical work. Next, the vapour from the turbine is condensed at P_2 and the resulting liquid is pumped back to the boiler via a regenerator to repeat the process. The mechanical work produced is used to drive a conventional refrigeration compressor. The remaining system components for a cooling application are standard

items, Rigmore and Barber (1975).

The Rankine cycle has the advantage of being able to operate an electric generator whenever excess solar energy exists beyond that needed for driving the compressor.

5.1.3 THE ADSORPTION CYCLE

Figure 5.3, page 129, shows the schematic diagram of an adsorption cycle. A typical embodiment of air to be conditioned is adiabatically dried with a resultant increase in temperature as the latent heat of its moisture is converted to sensible heat. This air stream is then cooled nearly to ambient temperature in its dry condition to reduce its enthalpy. It is then passed through a humidifier which cools it by conversion of sensible to latent heat at reduced enthalpy. The system shown in figure 5.3 is equipped with a solar heating coil which provides the first heat of reactivation heating, after which further heating is provided by fuel burning.

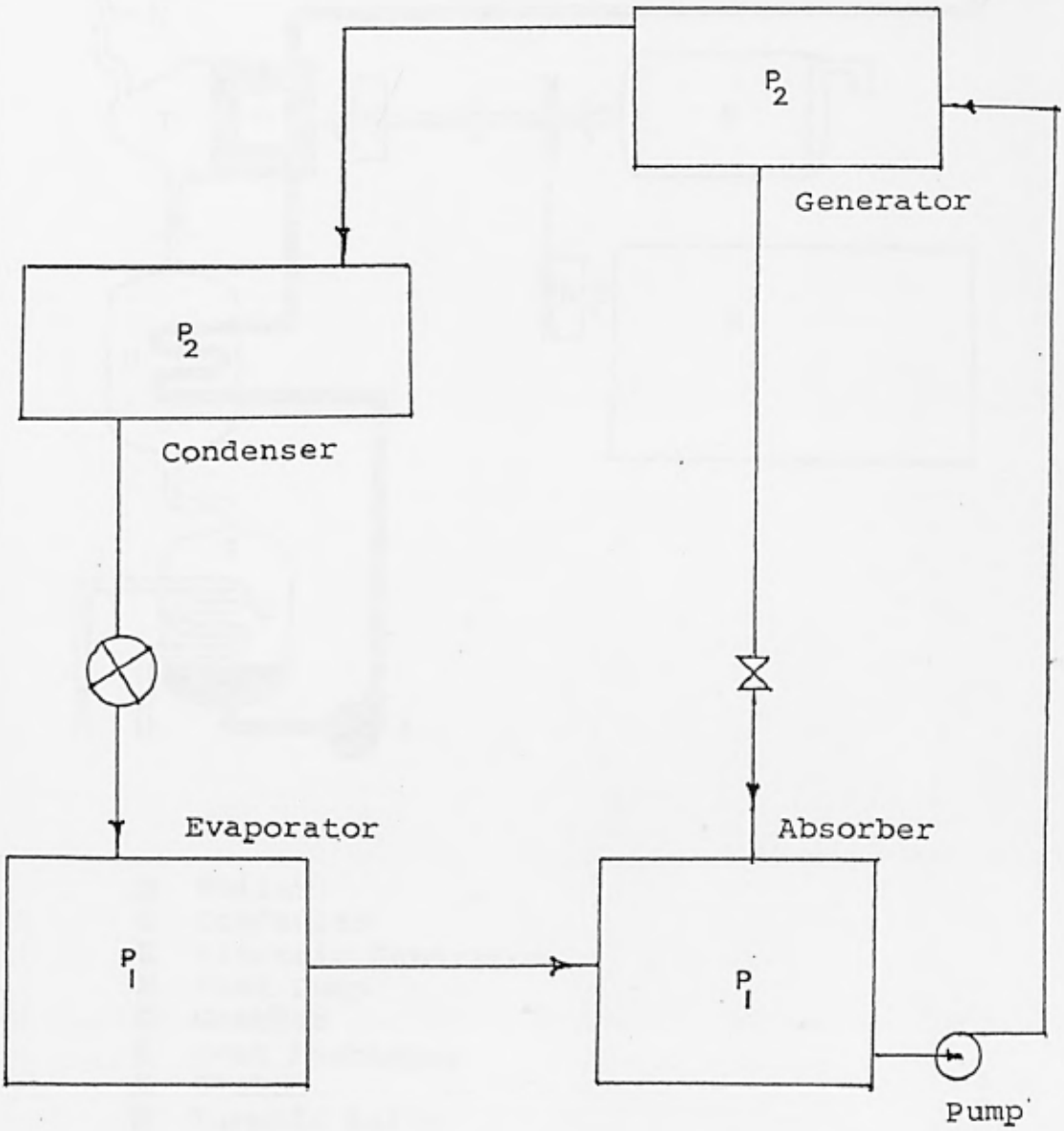
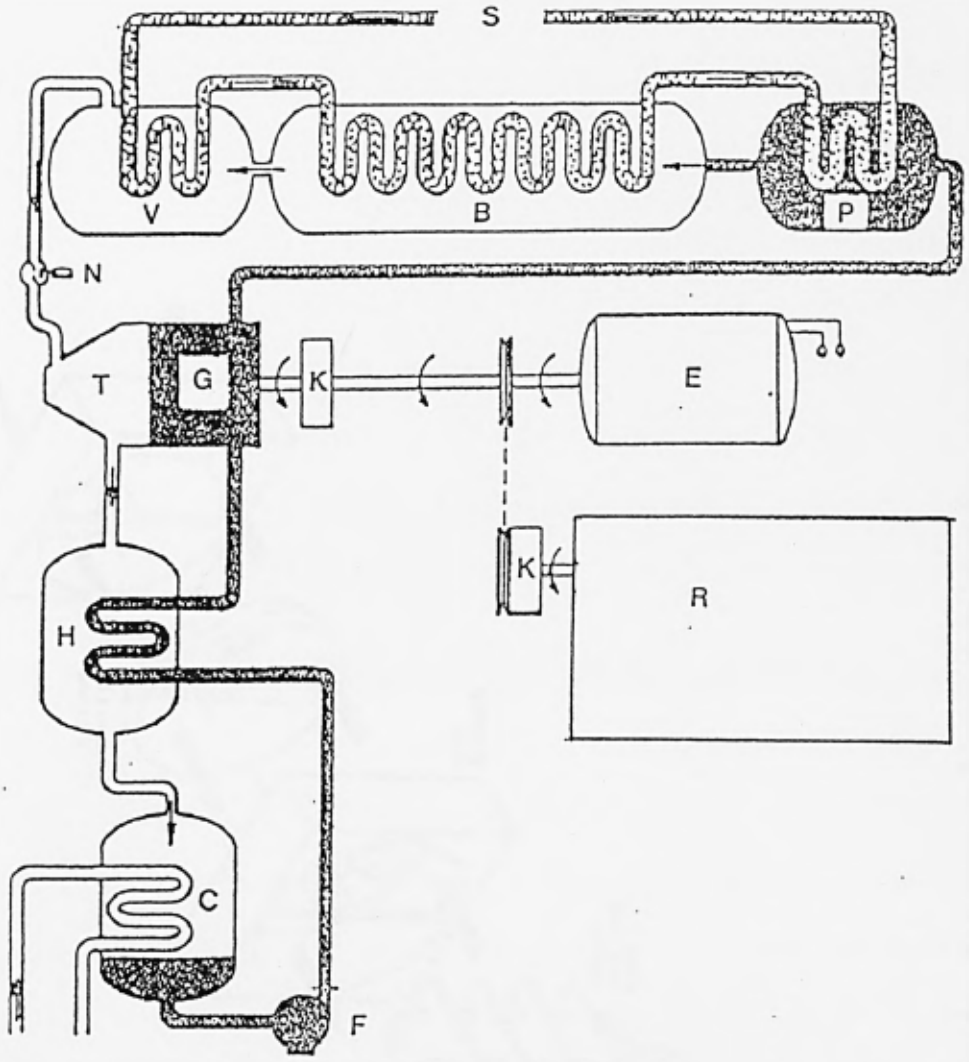


Fig. 5.1 A basic absorption cycle



B Boiler
C Condenser
E Electric Generator
F Feed Pump
G Gearbox
H Heat Exchanger
K Clutch
N Turnoff Valve
P Preheater
R A Vapour Compression Refrigeration System
S Solar Collector Water
T Turbine
V Vapour Seperator

Fig. 5.2 Schematic diagram of a Rankine cycle

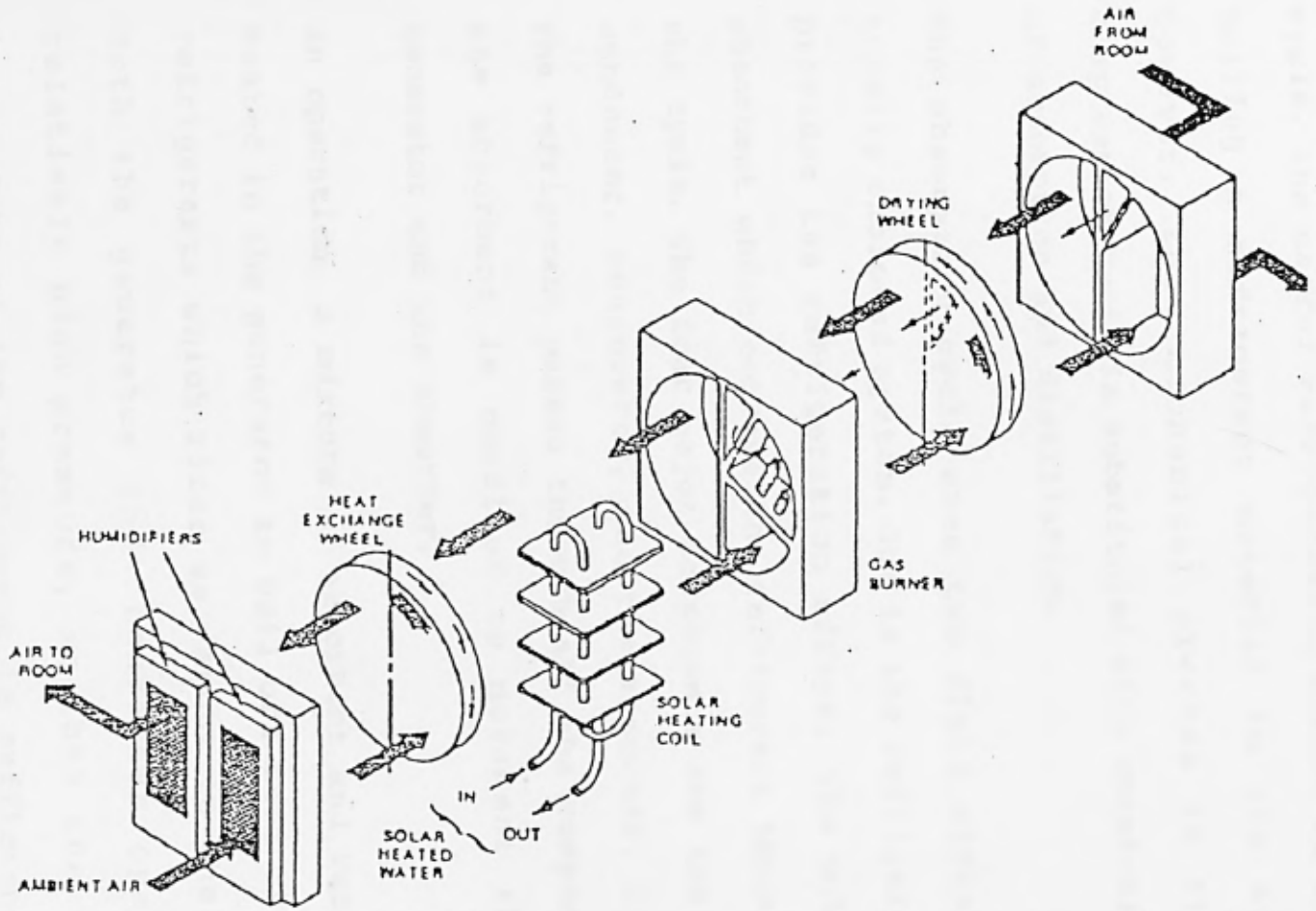


Fig. 5.3 Schematic diagram of the Adsorption cycle

5.2 THE ABSORPTION REFRIGERATION PROCESS

Of all the possible solar cooling schemes, the absorption cycle has been found to be the most promising. In similarity to the vapour compression cycle, the useful refrigeration effect is obtained by boiling a refrigerant material in the evaporator. However, the mechanical process in the vapour compression cycle is substituted with chemical processes of absorption and distillation.

The absorption cycle uses two fluid streams in the totally enclosed system. One is the refrigerant, which provides the refrigeration effect, the other is the absorbent which conveys the refrigerant through part of the cycle. The four major components are the generator, condenser, evaporator, and the absorber, figure 5.1 . The refrigerant passes through all the components while the absorbent is confined to movement through the generator and the absorber.

In operation, a mixture of absorbent and refrigerant is heated in the generator to boil off most or all of the refrigerant, which rises as vapour to the condenser. Both the generator and condenser operate at a relatively high pressure, so that the condensing temperature of the refrigerant is sufficiently high to permit rejection of the latent heat to ambient or cooling water. The liquid refrigerant is then throttled to lower pressure so that it can boil at a relatively

low temperature in the evaporator, and therefore absorb heat from the medium to be cooled. The vapourised refrigerant then passes to the absorber where it dissolves in the weak (absorbent) solution which has come to the absorber from the generator. The cool solution (strong) now rich in refrigerant is pumped back to the generator to repeat the process.

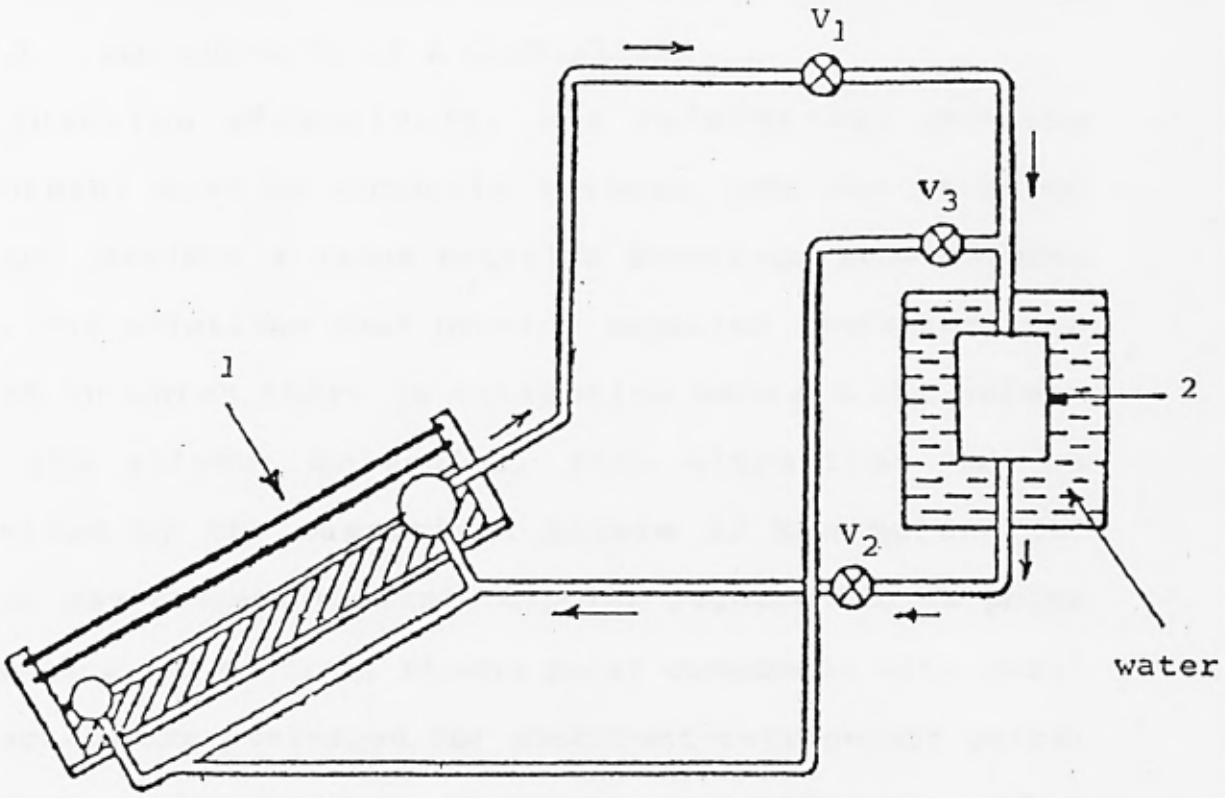
Furthermore, in the absorption system the refrigerant material is liquified and vapourised twice during a cycle, as compared with once in the vapour compression system. The additional vapourisation and condensation are necessary to substitute chemical processes for the mechanical compressor. The generator and the absorber perform the same function as the compressor by taking low-pressure refrigerant vapour from the evaporator and delivering high-pressure vapour to the condenser.

The absorption cycle can be used as an intermittent or a continuous system. In the intermittent type of system, the generator and the absorber are combined to form the regeneration process, while the condenser and the evaporator are combined to form the refrigeration process. It consists of two major operations involving regeneration and refrigeration. These two operations occur one after the other and the refrigeration effect is discontinously produced. During the regeneration process, heat is supplied to vapourise the solution in the generator and driven off to the condenser where it

is condensed and stored. At the end of the generation, the heat source is isolated and the refrigeration process begins. The liquid refrigerant then vapourises and produces the cooling effect in the evaporator and the vapour formed is reabsorbed in the absorber. Thus during the generation process the generator is in communication with the condenser, and during the refrigeration process the evaporator is in communication with the absorber. Valves are necessary to control the heat source during the generation and absorption phases of the cycle, and to close off the evaporator from the generator during heating.

The fact that solar energy is an intermittent heat source has led the majority of earlier investigators to use intermittent cycle which produces less effective cooling than the continuous system, Vankatesh, Sriramulu and Gupta(1979), and Chinnappa(1961,1962). Figure 5.4, page 133, shows the flow diagram of an intermittent closed cycle system.

In the continuous absorption cycle, refrigeration and generation processes occur simultaneously, and a continuous cooling effect is produced. Figure 5.1 shows a continuous closed cycle system, and the present investigation is concerned only with the closed cycle continuous aqua-ammonia system.



1 Collector = generator/absorber
2 Vessel immersed in water = condenser/evaporator
V_1 , V_2 , V_3 = Valves

Generation process :
Collector becomes generator
Vessel becomes condenser
V_1 is opened, V_2 and V_3 are closed

End of generation process :
V_1 is closed.
Collector is cooled until the solution left in it is at ambient temperature, then V_1 and V_3 are opened to equalize pressures.

Refrigeration process :
V_2 is opened.
Vessel becomes evaporator
Collector becomes absorber

Fig. 5.4 A simple intermittent absorption cycle

5.3 ABSORBENT - REFRIGERANT COMBINATIONS

5.3.1 REQUIREMENTS OF A COMBINATION

To function effectively, the refrigerant and the absorbent must be mutually soluble, and the solution should exhibit a large negative deviation from Raoults law. The solutions that provide negative deviations are those in which there is attraction between the solute and the solvent molecules. Such attraction may be provided by the electrical nature of the molecules, which may possess electric dipoles referred to as polar molecules. In general, strong polar compounds with small molecules are preferred for absorbent-refrigerant pairs; because polar compounds enter reversible complex formations easily and small molecules can be more polar and tend to have higher heats of vapourisation, Buffington(1949).

Other characteristics required of the combinations are, low specific heat, low viscosity, high equilibrium solubility at the required temperature and pressure in the absorber, and the freezing point of the liquid must be lower than the lowest temperature in the cycle.

If the vapour pressure of the absorbent is negligible, the partial pressure of the refrigerant in the absorber determines the operating temperature of the evaporator. The absorber vapour pressure is determined by the pressure-temperature-concentration (P-T-X) relation of

the combination. The condenser temperature likewise depends upon the partial pressure of refrigerant over the solution in the generator. Thus, fixing the operating temperatures and concentrations of the solution in the absorber and generator fixes the temperatures of the evaporator and condenser.

5.3.2 REQUIREMENTS OF A REFRIGERANT

The refrigerant must be thermally stable throughout the range of operation, and should not undergo irreversible reaction with any material in the system. To minimise the effect of leaks in the system, the vapour pressure should be close to atmospheric. Also, to minimise the circulation rate of refrigerant, the heat of vapourisation should be high. The specific heat of the refrigerant liquid and vapour should be as low as possible. The toxicity threshold limit should not be greater than the maximum to which a healthy person can be exposed to for eight hours a day and five days a week.

5.3.3 REQUIREMENTS OF AN ABSORBENT

The absorbent must be chemically stable and noncorrosive over the range of operating temperatures. The boiling point should be high so that its vapour pressure is low at the generator temperatures. The absorbent solution should have a low viscosity to reduce the energy required for circulation and to insure high heat

transfer coefficients. The heat capacity should be low so that heating and cooling requirements in the absorbent circulation loop are not excessive.

5.4 TYPES OF ABSORPTION CYCLES

5.4.1 WATER - AMMONIA SYSTEM

Schematic diagram of a single-stage aqua-ammonia absortion cycle with a rectifier, reflux condenser and a heat exchanger is shown in figure 5.5, page 137. Ammonia possesses very desirable properties as a refrigerant, it has a high latent heat of vapourisation of about 1454 kJ/kg at 10^{o}C. Water is a very good absorbent for ammonia, it reduces the partial pressure of the refrigerant to about one-third of that predicted by Raoults law, Buffington(1949). However, the partial vapour pressure of water at the temperature and concentration in the generator is sufficiently great that some water vapourises along with the refrigerant. A rectifying column and a reflux condenser are used for purification of the refrigerant vapour before it passes to the condenser, since the presence of water is undesirable in the evaporator.

Due to the elaborate auxilliary components needed to improve the performance of this cycle, the first cost is usually high. However, the maintenance cost is low since the only moving part is the solution pump.

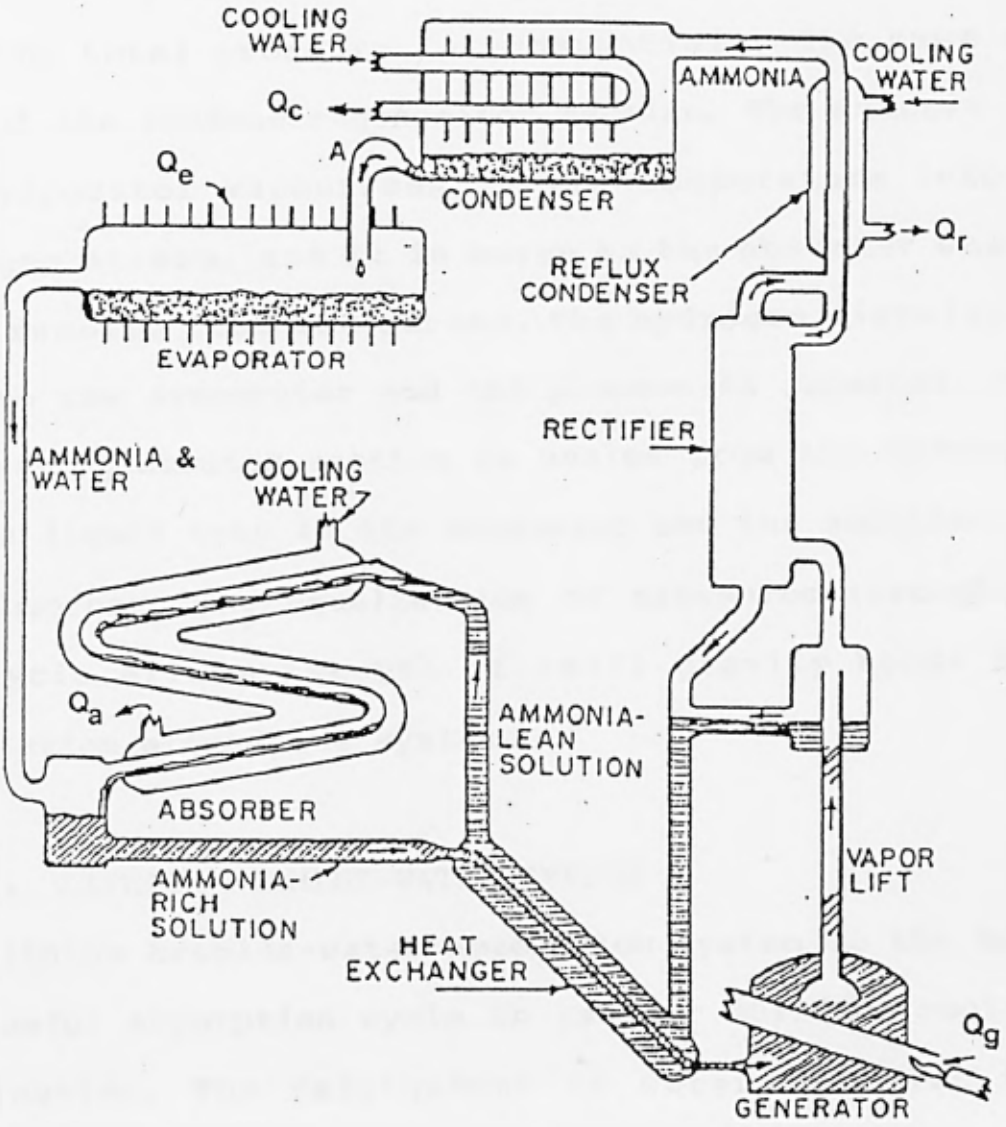


Fig. 5.5 A Single-stage NH_3-H_2O absorption system

Another version of the aqua-ammonia cycle that was adapted to household refrigeration is shown in figure 5.6, page 140. Three fluids, ammonia-water and hydrogen are circulated in the cycle. The hydrogen is introduced into the evaporator-absorber section of the system, so that the total pressure is substantially the same as that of the condenser-generator section. The ammonia in the evaporator vapourises at low temperature into a hydrogen stream, and it is borne to the absorber where it is removed from the stream. The hydrogen circulates back to the evaporator and the process is repeated. The condenser-generator section is sealed from the hydrogen by the liquid trap in the condenser and the solution in the absorber. The equalisation of pressures throughout the cycle allows the use of small gravity heads for circulation around the system.

5.4.2. LITHIUM BROMIDE-WATER SYSTEM

The lithium bromide-water absorption system is the most successful absorption cycle in use for building cooling application. The refrigerant is water, and lithium bromide is the absorbent. Water is an ideal refrigerant because of its very high heat of vapourisation. It is extremely stable, nontoxic and cheap, and has a boiling range covering air-conditioning temperatures at workable pressures. Lithium bromide-water solution also exhibits some of the widest known deviations from the Raoult`s law, and therefore gives favourable operating conditions

and coefficient of performance. However, the combination is extremely corrosive to the materials ordinarily used for construction.

Compared to the ammonia-water system, the lithium bromide-water system shown schematically in figure 5.7, page 141, can be simpler, since its outstanding feature is the nonvolatility of the absorbent. This eliminates the need for rectifying equipment, however, the main disadvantages of the system are its requirement for relatively high evaporating temperatures, and water-cooling of the condenser and absorber with a probable need for cooling tower.

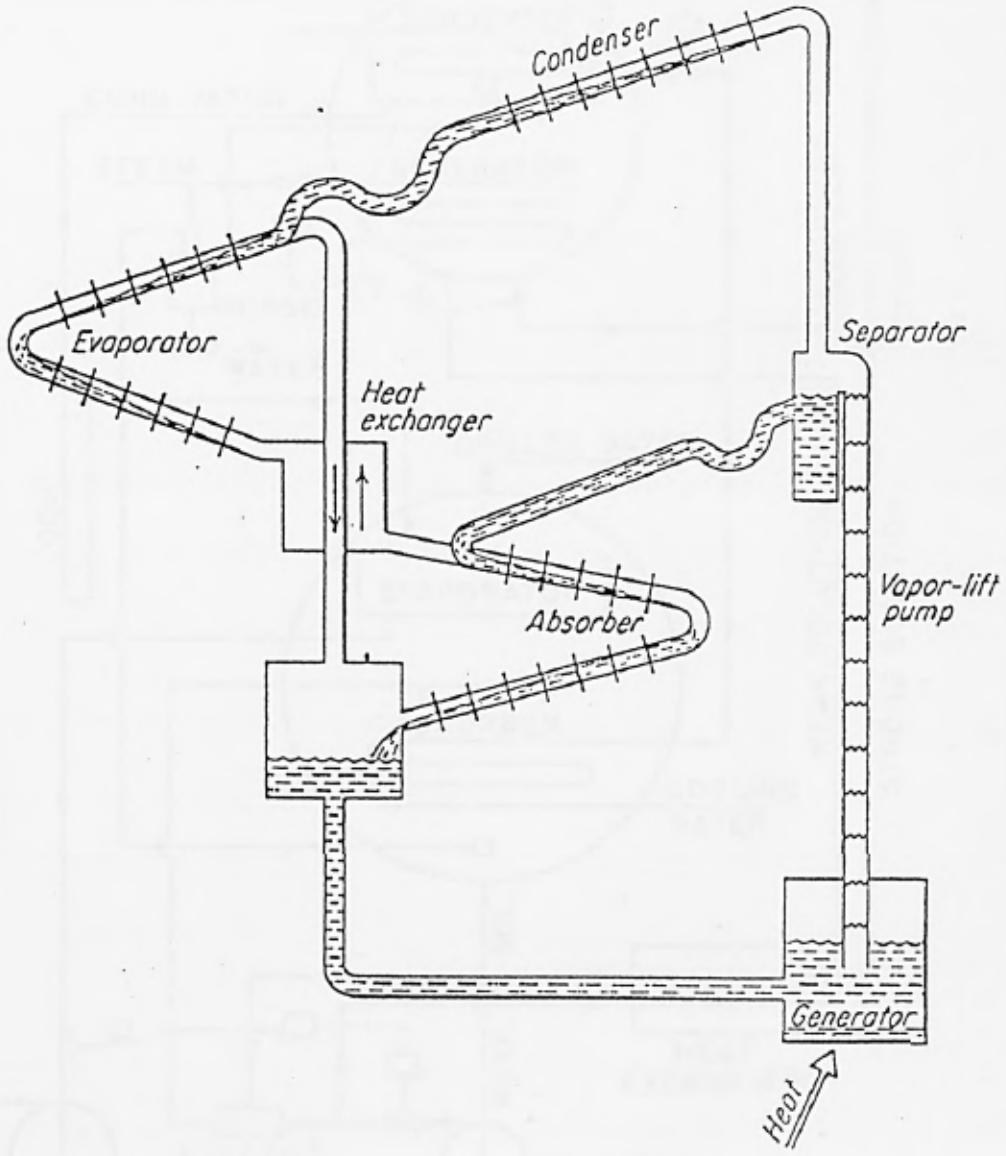


Fig. 5.6 A NH_3-H_2O cycle for domestic application

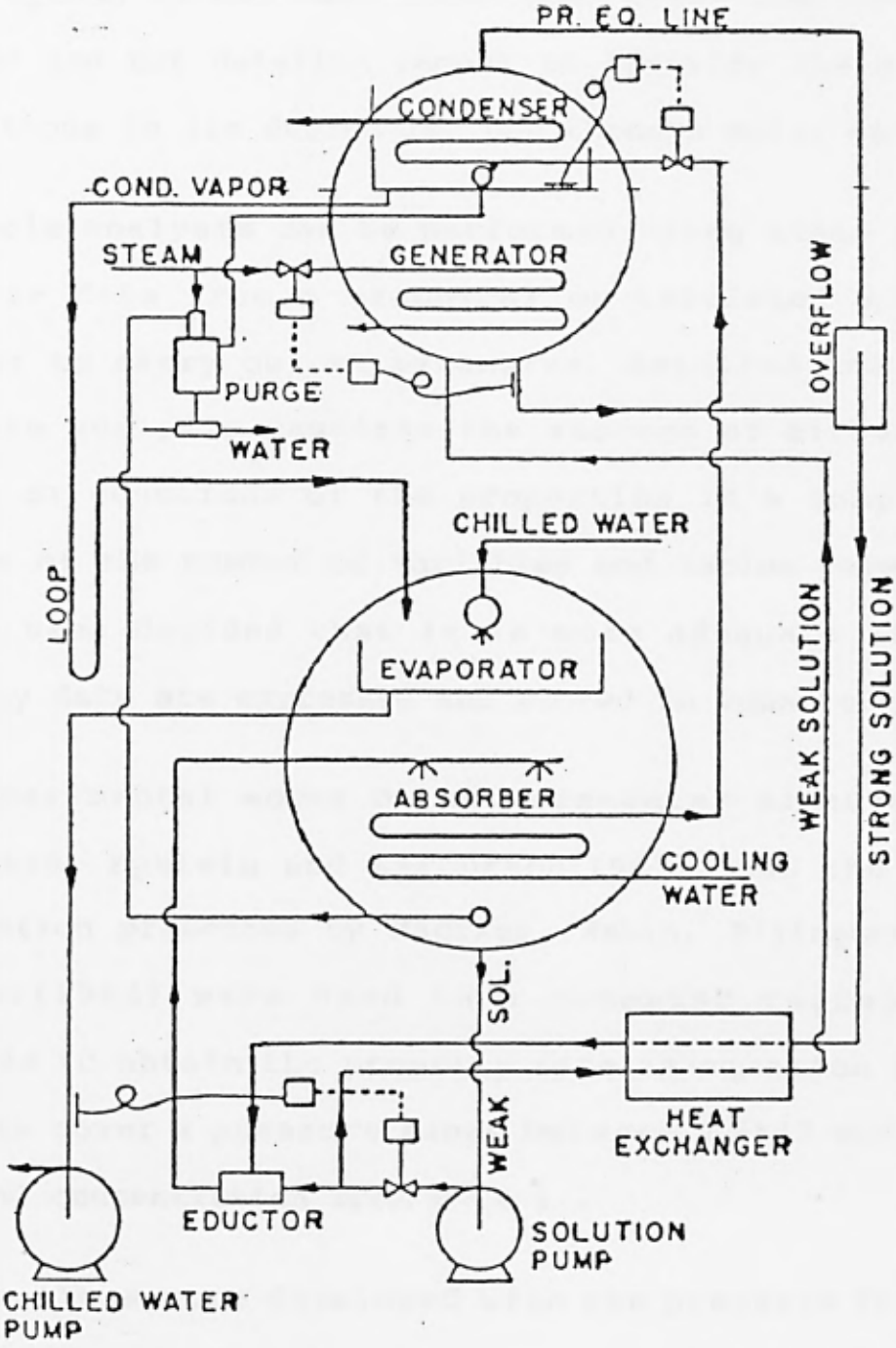


Fig. 5.7 System schematic for a Water-Lithium bromide absorption cycle

5.5 PROPERTY DATA EQUATIONS FOR NH_3-H_2O MIXTURES

Although many investigators have analysed the ammonia-water cycle, it has been found that their analysis are limited and not detailed enough to identify the system limitations in its design for use through solar energy.

The cycle analysis can be performed using state point property data from a graphical or tabulated source. However to carry out an extensive, detailed and more accurate analysis requires the storage of either the tables or equations of the properties in a computer. Because of the number of variables and tables involved, it has been decided that it is more adequate if the property data are expressed and stored in equation form.

The experimental works on ammonia-water mixtures by Scatchard, Epstein and Warburton(1947), and the data information presented by Macriss, Eakin, Ellington and Huebler(1964) were used in a computer regression analysis to obtain the property data in equation form. The data cover a pressure range between 0.5517 and 34.4 bar, and concentration from 0 to 1 .

The equations were developed with the pressure (P) and the concentration of the mixture in liquid state (XL) as the independent variables; and the temperature (T), enthalpy of liquid (HL), enthalpy of vapour (HV) and concentration of the mixture in vapour state (XV) as dependent variables :

$$T = f(XL,P)$$

$$XV = f(XL,P)$$

$$HL = f(XL,T)$$

$$HV = f(XV,T)$$

The multiple polynomia regression and the computer program were based on the Least Square method, Hald(1952), and Dorn and McCracken(1976) .

The supressor variables and the degree of polynomia that gave the best results were determined from several trials involving the variables and powers of the variables. It was not possible to obtain any accuracy when the regression was done at a single range for each of the dependent variable. Hence the data have to be divided into two pressure ranges; a low-pressure range of 0.5517 to 6.8996 bar, and a high-pressure range from 6.8996 to 34.4 bar.

Furthermore, the high-pressure range vapour enthalpy data have to be subdivided into two liquid concentration ranges to obtain the greatest accuracy. The ranges for the concentration were determined when the high-pressure range data were plotted with [$\log_e(1-XV)/\log_e(1-XL)$] versus [XL], and the curves showed breaks at XL between 0.3 and 0.6 . Hence, the regression was done over two ranges of XL : a low-concentration of 0 to 0.5, and high-concentration of 0.4 to 1 .

Still on the high-pressure range vapour enthalpy data; at the liquid concentration (XL) range of 0.4 to 1 and

at a vapour concentration (XV) approaching unity, the best fit was obtained at a limiting vapour concentration of 0.99997 and above this value, the vapour enthalpy equation changes. The property data equations and their accuracy are given below.

5.5.1 THE PROPERTY DATA EQUATIONS

For the low-pressure range of $0.5517 \leqslant P \leqslant 6.8996$ bar :

$$T = 74.381 + (((- 29.88\ XL + 31.83)XL^2 + 153.27)XL - 279.364)XL - (7.425 - 0.5247\ P)XL\ P + (24.5686 - 1.73506\ P)P \quad 5.1$$

$$XV = 1.0 - (1.0 - XL)^{RV} \quad 5.2$$

Where,

$$RV = 12.2277 + ((- 5.323\ XL + 3.669)XL^2 - 7.227 + 0.43728\ P)XL^2 - 0.69767\ P \quad 5.3$$

$$HL = (((- 230.54\ XL + 325.07)XL^2 + 40.338)XL - 130.678)XL + (0.02987\ XL + 0.819621)T - 4.5327 \quad 5.4$$

$$HV = 459.283 + (- 6.390\ XV^2 - 216.118)XV + (((- 4.283E\text{-}06 - 5.725E\text{-}06\ XV)T + 0.0004730)T + 0.346988)T \quad 5.5$$

For the high pressure range of $6.8996 \leqslant P \leqslant 34.4828$ bar:

$$T = 134.503 + (((- 117.681\ XL + 163.763)XL^2 + 90.534)XL - 279.449)XL - (1.37279 - 0.017558\ P)XL\ P + (5.03861 - 0.057194\ P)P \quad 5.6$$

$$XV = 1.0 - (1.0 - XL)^{RV} \qquad 5.7$$

Where,

$$RV = 7.93530 + ((13.196\ XL - 18.550)XL^2 + 0.0812 + 0.090074\ P)XL^2 - 0.100112\ P \qquad 5.8$$

$$HL = (((-\ 162.067\ XL + 226.51)XL^2 + 84.076)XL - 142.599)XL + (0.00084716\ T\ XL + 0.812789)T - 4.161 \qquad 5.9$$

If $0 \leqslant XL \leqslant 0.5$:

$$HV = 510.327 + ((85.128\ XV - 142.55)XV - 208.922)XV + ((2.8037E\text{-}09\ T - 3.162E\text{-}06\ XV)T^2 + 0.24238\ XV)T \qquad 5.10$$

If $0.4 \leqslant XL \leqslant 1.0$:

$$HV = 339.331 + ((-\ 0.0193901\ XWL - 0.32584)XWL^2 + 23.4633)XWL + ((3.7767E\text{-}08\ T^2 - 0.0018819\ XV)T + 0.17724\ XV)T \qquad 5.11$$

Where,

$XWL = \log_e(1.0 - XV)$, if $XV \leqslant 0.99997$

$XWL = \log_e(0.00003)$, for $XV > 0.99997$

5.5.2 ACCURACY OF THE REGRESSION EQUATIONS

The accuracy of the above property data equations has been determined over the entire data that have been regressed. In comparison with the property data information by Macriss, Eakin, Ellington and Huebler(1964), the maximum deviations of these equations are :

For the low pressure range $0.5517 \leq P \leq 6.8996$ bar :

VARIABLE	DEVIATION	%
Temperature T	$\pm$ 2.36°C	$\pm$ 3.5
Relative Volatility RV	$\pm$ 0.769	$\pm$ 6.2
Enthalpy of liquid HL	$\pm$ 2.55 kJ/kg	$\pm$ 2.4
Enthalpy of vapour HV	$\pm$ 2.509 kJ/kg	$\pm$ 5.3

For the high pressure range of $6.8996 \leq P \leq 34.4828$ bar:

VARIABLE	DEVIATION	%
Temperature T	$\pm$ 1.54°C	$\pm$ 2.5
Relative volatility RV	$\pm$ 0.534	$\pm$ 7.5
Enthalpy of liquid HL	$\pm$ 1.507 kJ/kg	$\pm$ 5.6
Enthalpy of vapour HV	$\pm$ 1.847 kJ/kg	$\pm$ 8.2

5.6 AQUA-AMMONIA CYCLES ANALYSES

5.1 THE IDEAL ABSORPTION CYCLE

The efficiency of an ideal absorption cycle is dependent only on the operating temperatures of the cycle components. In practical cycles, it is not possible to fix an arbitrary combination of these temperatures, because other factors influence the efficiency and successful operation of the system as shown in the next sections.

If the inlet and outlet temperatures of the evaporator in the basic absorption cycle shown in figure 5.8, page 150, are assumed equal, and the effects of the working fluid and processes are neglected, then the cycle can be

considered as ideal.

The thermal efficiency or coefficient of performance, which can be defined as the ratio of the cooling effect to the energy input to secure this effect is given by :

$$COP = Q_e/Q_g \qquad 5.12$$

For a conventional vapour compression refrigeration cycle operating reversibly between T_e and T_c, as shown in figure 5.9a, page 151, the coefficient of performance is given by :

$$COP = Q_e/(Q_c - Q_e) = T_e/(T_c - T_e) \qquad 5.13$$

If the processes in the absorption cycle are thermodynamically reversible, a heat balance gives :

$$Q_e + Q_g = Q_c + Q_a \qquad 5.14$$

And the net entropy change in the cycle is given by :

$$Q_e/T_e + Q_g/T_g = Q_c/T_c + Q_a/T_a \qquad 5.15$$

If the evaporator and the condenser are considered as components of a reversible Carnot cycle figure 5.9b, page 151, then :

$$Q_c/T_c = Q_e/T_e \qquad 5.16$$

and by the same reasoning for the generator and the absorber :

$$Q_g/T_g = Q_a/T_a \qquad 5.17$$

By combining and rearranging equations 5.14 to 5.17, the COP of an ideal absorption cycle is given by :

$$COP = Q_e/Q_g = [(T_g - T_a)/T_g][T_e/(T_c - T_e)] \qquad 5.18$$

Equation 5.18 has been incorporated into a computer program to determine the effects of these operating temperatures on the coefficient of performance of the absorption cycle. Some of the performance curves have been plotted and are shown in figure 5.12 page 160.

5.6.2 THE PRACTICAL NH_3 - H_2O CYCLE

In practical absorption cycles the properties of the working fluid, and the processes in the cycle in addition to the operating temperatures, influence the coefficient of performance of the absorption system.

In ammonia-water systems, the vapour that leaves the generator contains some fraction of water vapour, which also liquifies in the condenser and flows into the evaporator with the ammonia. During the throttling process in the expansion valve, some of the liquid flashes into vapour, leaving the remaining liquid after the expansion valve with a higher water content. As the mixture of liquid and flashed vapour flow through the evaporator, heat is absorbed and more liquid is vapourised. As more liquid vapourises, the remaining

liquid's water content increases and requires an increase in temperature to vapourise since the pressure in the evaporator remains constant. When all the ammonia liquid has vapourised, the water is left behind in the evaporator and would need to be removed.

To remove the water from the evaporator at the same rate as it enters, requires some of the ammonia liquid to leave the evaporator as purge liquid. For a detailed and accurate analysis, it is therefore necessary to specify a combination of any two of the following and the other two to be determined to account for the water in the evaporator :

1. Evaporator inlet temperature
2. Evaporator exit temperature
3. Low-side pressure
4. Mass of purge liquid

In any refrigeration application, the evaporator temperature which is the same as the evaporator inlet temperature is normally given, therefore in all the analysis that have been performed in this investigation, the evaporator inlet temperature is known and the exit temperature has been assumed to be $6^{o}C$ higher than the inlet. Thus, the inlet and exit evaporator temperatures are specified and the low-side pressure and the mass of purge liquid are found by iteration.

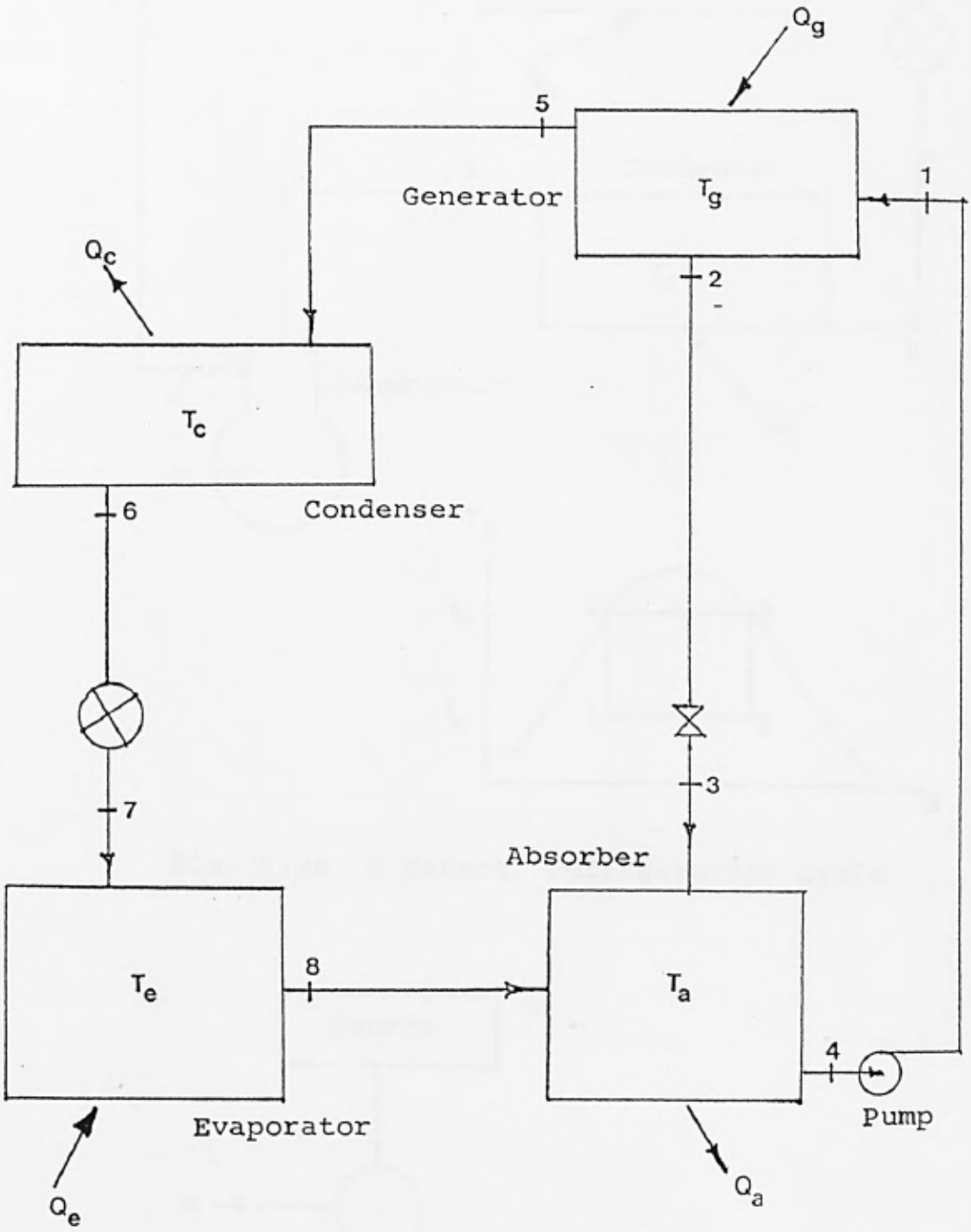


Fig. 5.8 A basic aqua-ammonia absorption cycle

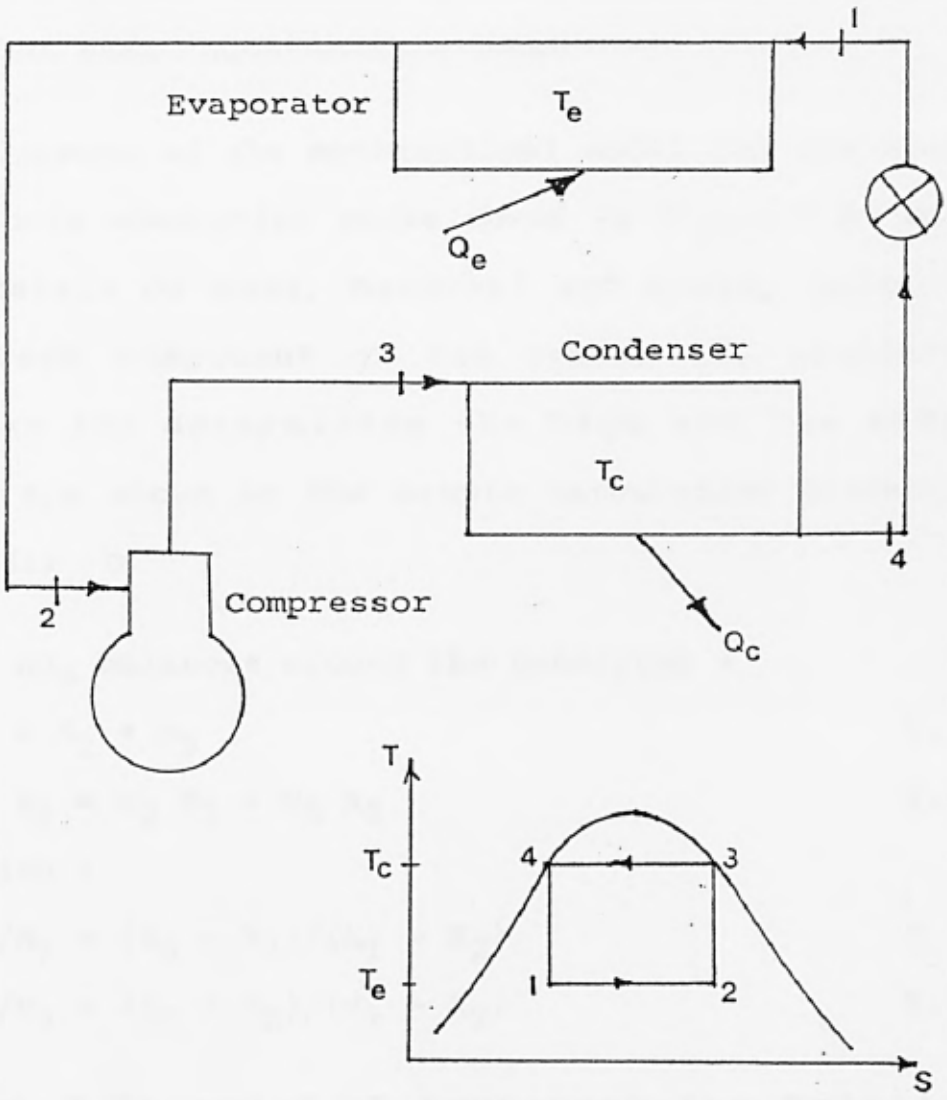


Fig. 5.9a A Carnot refrigeration cycle

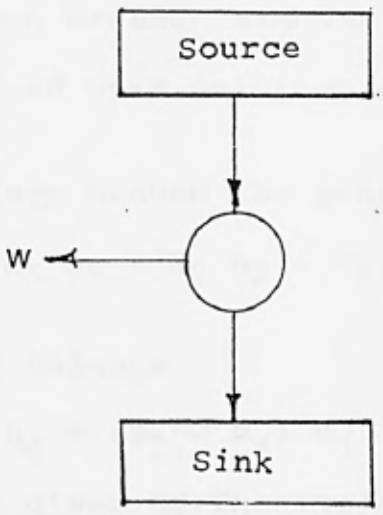


Fig. 5.9b A reversible Carnot cycle

5.6.3 THE BASIC AQUA-AMMONIA CYCLE

The development of the mathematical model for the basic aqua-ammonia absorption cycle shown in figure 5.8, page 150, consists of mass, material and energy balances around each component of the cycle. The iteration technique for determining the high and low sides pressure are shown in the sample calculation presented in appendix D.

Mass and NH_3 balances around the generator :

$$M_1 = M_2 + M_5 \qquad 5.19$$

$$M_1 X_1 = M_2 X_2 + M_5 X_5 \qquad 5.20$$

rearranging :

$$M_2/M_5 = (X_5 - X_1)/(X_1 - X_2) \qquad 5.21$$

$$M_1/M_5 = (X_5 - X_2)/(X_1 - X_2) \qquad 5.22$$

Equation 5.21 and 5.22 represent the Relative Circulation and the Specific Circulation respectively. The quotent $(X_1 - X_2)$ in both equations is the distillation breadth and it is the difference between the strong and weak solution concentrations.

Energy balance around the generator :

$$Q_g = M_5 h_5 + M_2 h_2 - M_1 h_1 \qquad 5.23$$

Pump energy balance :

$$h_1 - h_4 = (P_1 - P_4) v_4 \qquad 5.24$$

where v_4 is given by Threlkeld(1970) as :

$$v_4 = (1 - X_1) v_{H_2O} + 0.85 X_1 v_{NH_3} \qquad 5.25$$

or

$$Wp = M_1 (h_1 - h_4) \qquad 5.26$$

Mass and NH_3 balances around the absorber :

$$M_4 = M_3 + M_8 \qquad 5.27$$

$$M_4 X_4 = M_3 X_3 + M_8 X_8 \qquad 5.28$$

Energy balance around the absorber :

$$Q_a = M_3 h_3 + M_8 h_8 - M_4 h_4 \qquad 5.29$$

For the condenser :

$$M_5 = M_6$$

$$X_5 = X_6$$

$$Q_c = M_5(h_5 - h_6) \qquad 5.30$$

For the expansion valve :

$$M_6 = M_7$$

$$h_6 = h_7 \qquad 5.31$$

Calculation of the quatity of the flashed vapour is shown in the sample calculation in appendix D.

For the regulator valve :

$$M_2 = M_3$$

$$X_2 = X_3$$

$$h_2 = h_3 \qquad 5.32$$

For the evaporator :

$$M_8 = M_7 = M_6 = M_5$$

$$Q_e = M_5(h_8 - h_7) \qquad 5.33$$

Calculation of the mass of purge liquid is shown in the sample calculation in appendix D .

The coefficient of performance is given by :

$$COP = Q_e/Q_g$$

5.6.4 REFINED AQUA-AMMONIA CYCLES

The modelling of each component that has been added to the basic cycle to refine the system are presented below. The complete cycle shown in figure 5.10, page 156, has been used and the sample calculation in appendix D is based on this figure.

Mass and NH_3 balances around the generator :

$$M_3 = M_4 + M_6 - M_7 \qquad 5.34$$

$$M_3 X_3 = M_4 X_4 + M_6 X_4 - M_7 X_7 \qquad 5.35$$

Generator energy balance :

$$Q_g = M_6 h_6 + M_4 h_4 - M_3 h_3 - M_7 h_7 \qquad 5.36$$

Mass and NH_3 balance around the absorber :

$$M_1 = M_5 + M_{11} \qquad 5.37$$

$$M_1 X_1 = M_5 X_5 + M_8 X_{11} \qquad 5.38$$

$$M_1 = M_3 \; ; \quad M_5 = M_4 \; ; \quad M_{11} = M_8$$

$$X_1 = X_3 \; ; \quad X_5 = X_4 \; ; \quad X_{11} = X_8$$

Substituting for M_3 in above equations and rearranging :

$$M_4/M_8 = (X_8 - X_3)/(X_3 - X_4) \qquad 5.39$$

Substituting for M_4 and rearranging :

$$M_3/M_8 = (X_8 - X_4)/(X_3 - X_4) \qquad 5.40$$

Equation 5.39 and 5.40 represent the Relative circulation and the Specific solution circulation.

Absorber energy balance :

$$Q_a = M_4\ h_5 + M_8\ h_{13} - M_3\ h_{15} \qquad 5.41$$

Pump energy balance :

$$W_p = M_3(h_1 - h_{15}) \qquad 5.42$$

Mass and NH_3 balances around the reflux condenser :

$$M_6 = M_7 + M_8 \qquad 5.43$$

$$M_6\ X_6 = M_7\ X_7 + M_8\ X_8 \qquad 5.44$$

Substituting for M_6 and rearranging :

$$M_7/M_8 = (X_8 - X_6)/(X_6 - X_7) \qquad 5.45$$

Equation 5.45 is the reflux ratio.

Reflux condenser energy balance :

$$M_3\ h_3 = M_3\ h_2 + M_6\ h_6 - M_7\ h_7 - M_8\ h_8 \qquad 5.46$$

Condenser energy balance :

$$Q_c = M_8(h_8 - h_9) \qquad 5.47$$

Refrigerant precooler energy balance :

$$M_9\ h_9 = M_{10}\ h_{10} + M_{13}\ h_{13} - M_{12}\ h_{12} \qquad 5.48$$

Evaporator energy balance :

$$Q_e = M_8(h_{12} - h_{11}) \qquad 5.49$$

Solution heat exchanger energy balance :

$$M_3\ h_3 = M_4\ h_4 + M_3\ h_2 - M_4\ h_5 \qquad 5.50$$

The $COP = Q_e/Q_g$

The above equations and those developed in the sample calculation in appendix D have been incorporated into the computer program Refrig presented in appendix C. The results are discussed in section 5.7 below.

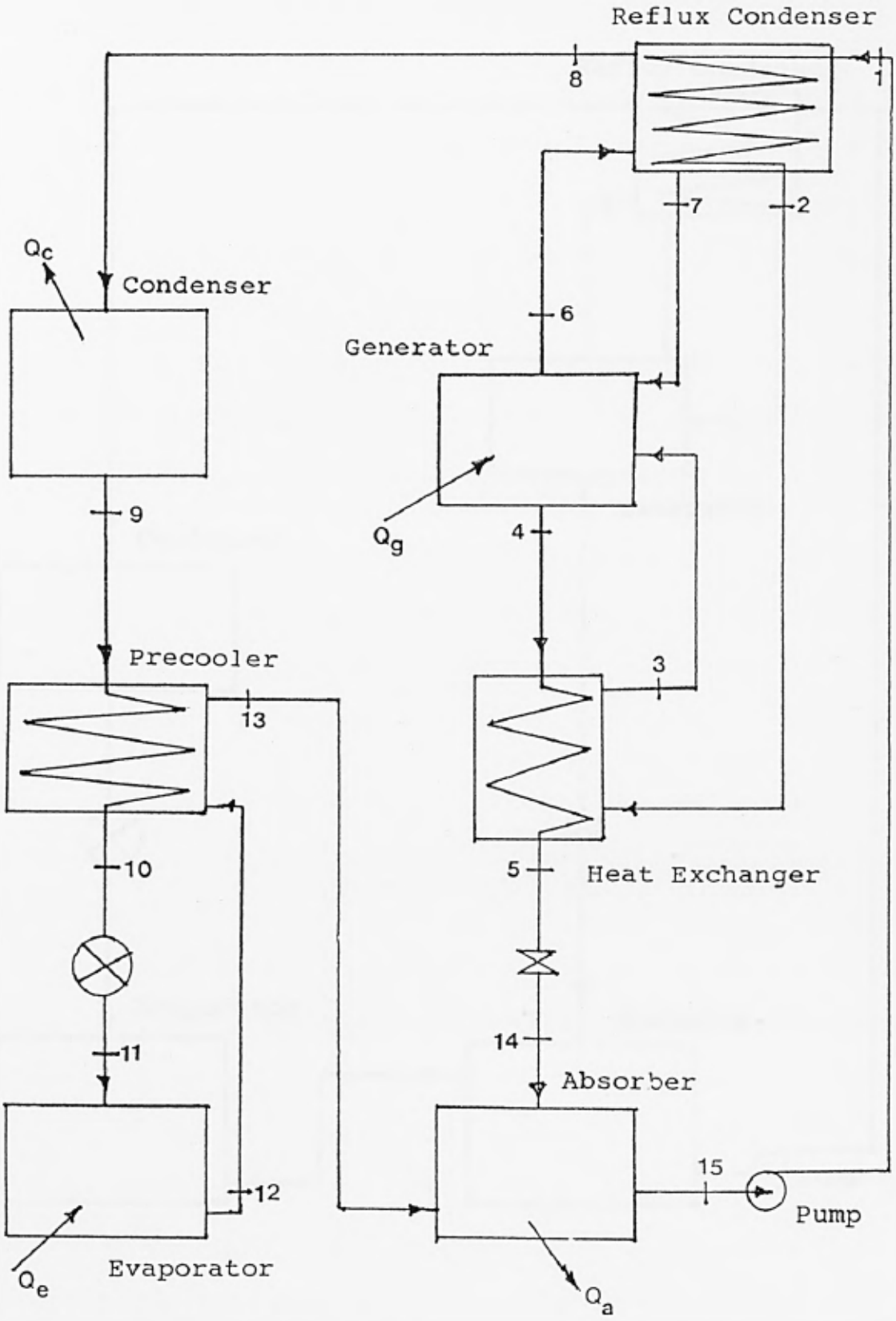


Fig. 5.10 A complete aqua-ammonia absorption cycle

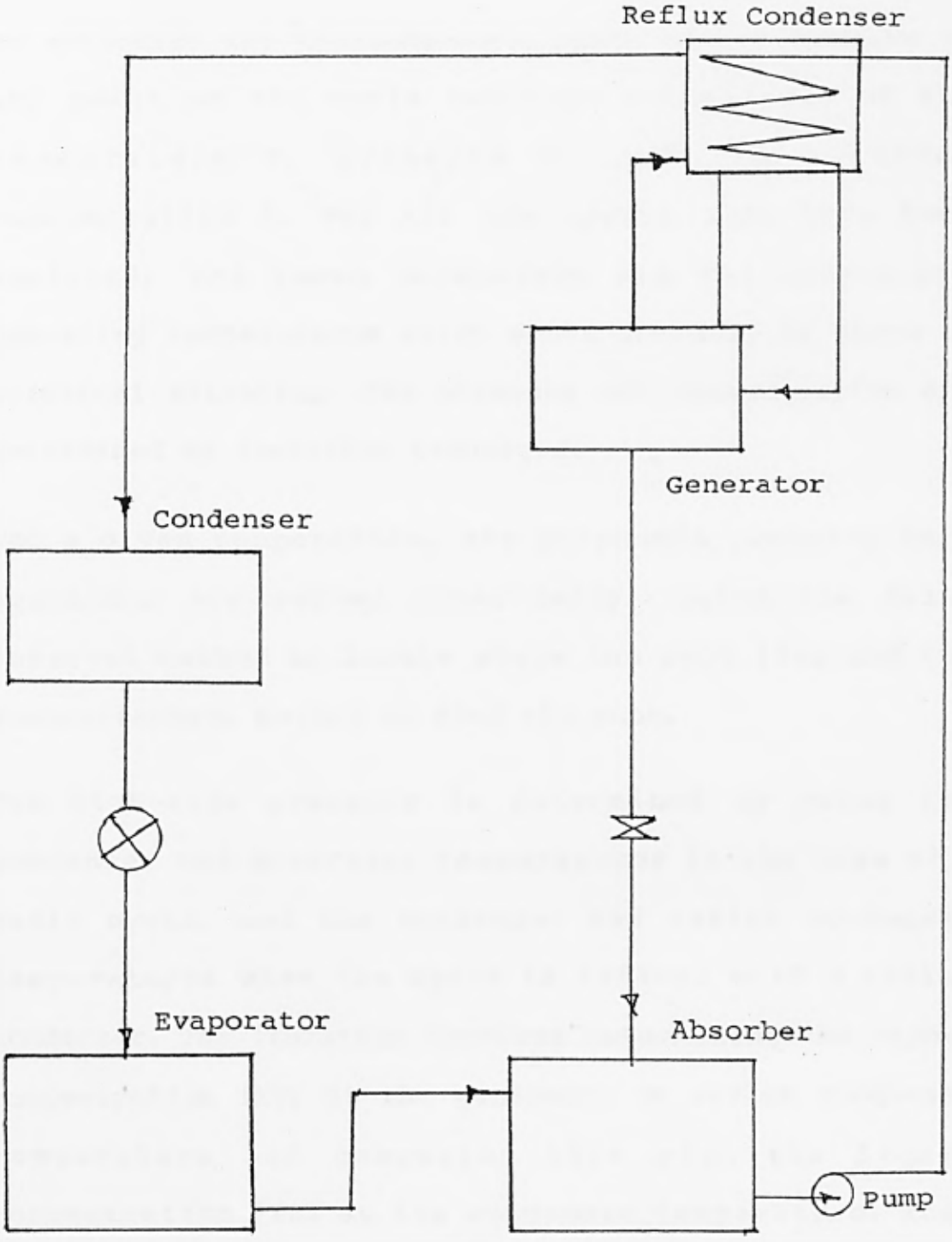


Fig. 5.11 A basic NH_3-H_2O cycle refined with a Reflux Condenser

5.7 LOW AND HIGH SIDES PRESSURE ITERATION TECHNIQUE

To establish the thermodynamic state of the mixture at any point on the cycle requires a knowledge of the temperature T, pressure P, and the solution concentration X. For all the cycles that have been analysed, the known parameters are the components operating temperatures which would normally be known in practical situation. The pressure and concentration are determined by iteration technique.

For a given temperature, the polynomia property data equations are solved numerically, using the false interval method to locate where the root lies and the Newton-Raphson method to find the root.

The high-side pressure is determined by using the condenser and generator temperatures in the case of a basic cycle, and the condenser and reflux condenser temperatures when the cycle is refined with a reflux condenser. The iteration involves determining the vapour concentration (XV) at the generator or reflux condenser temperature and comparing this with the liquid concentration (XL) at the condenser temperature. When these two concentrations are the same at the same value of pressure, then that pressure corresponds to the high-side pressure of the cycle. This procedure is clearly presented in the sample calculation in appendix D.

The iteration procedure for the low-side pressure is also well presented in the sample calculation in appendix D. It invoves initialisation of the pressure and the iteration continues until the pressure converges to a value. The above methods as demonstrated in the sample calculation are shown in the computer program Refrig in appendix C.

5.8 PARAMETRIC ANALYSIS

Vast quatity of results data have been gathered from the analysis and to present a reasonable proportion, graphical presentation has been employed. The most pertinent performance curves for each cycle analysed are presented.

5.8.1 THE IDEAL CYCLE

Figure 5.12, page 160, shows a plot of some of the perforance curves for an ideal absorption cycle. The COP is shown to increase with the generator and evaporator temperatures. The analysis showed that an increase in either or both the condenser and absorber temperatures causes the COP to fall.

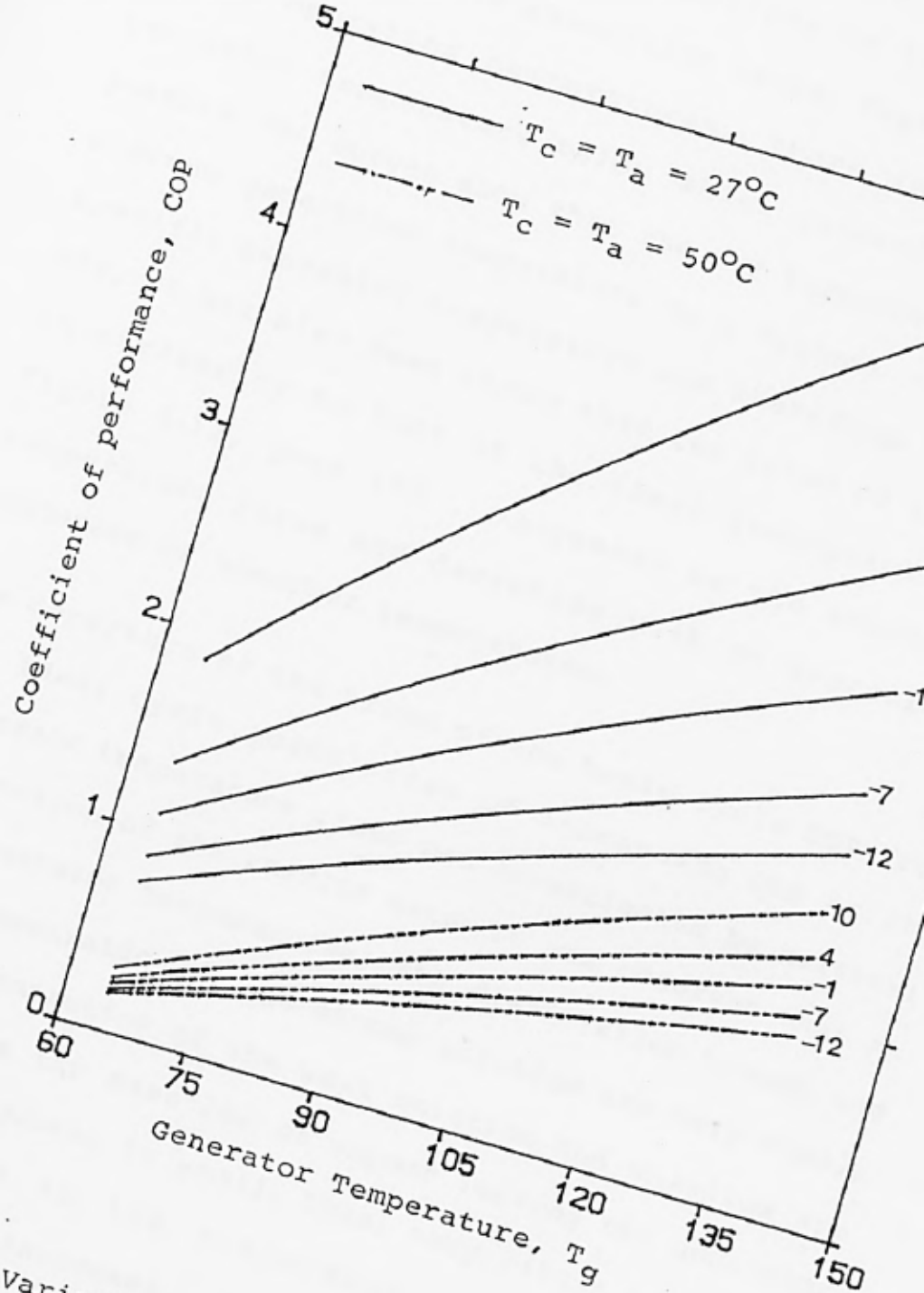


Fig. 5.12 Variation of COP for an ideal absorption cycle

5.8.2 THE BASIC CYCLE

Figures 5.13 to 5.15 on pages 163 to 165, show the influence of operating conditions on the COP of the basic aqua-ammonia absorption cycle. Depending on the set of operating temperatures, there is a minimum generator temperature below which generation is not possble. The curves show that the COP increases from the minimum generation temperature to a highest value at a specific generator temperature and therefrom it drops off. It has also been shown that the trend of the COP, in similarity to that of the ideal absorption cycle figure 5.12, page 160 , increases as the evaporator temperature rises and decreases with an increase in condenser or absorber temperatures.

The departure of the trend of the basic cycle COP from the ideal cycle postulation of increasing COP as the generator temperature rises was investigated by critical examination of the results data. It was observed that at low generator temperatures; the distillation breadth and the concentration of the strong solution are very small, the concentration of the weak solution and massflow are high while the massflow of vapour leaving the generator to the condenser is small. Thus, very little ammonia is being sent to the evaporator. As the generator temperature increases, the distillation breadth becomes larger and the COP increases. However, it starts to drop once it reaches a highest value at a specific generator temperature despite the continual increase of the

distillation breadth and generator temperature. The results revealed that; as the generator temperature goes higher the high-side pressure drops, the concentration of vapour leaving the generator to the condenser falls but the massflow increases, the mass of purge liquid from the evaporator increases, the generator heat load increases and the refrigerating effect in the evaporator drops. All these combined were considered to be responsible for the fall of the COP as the generator temperature increases above the point of maximum COP. The significance of other calculated system parameters are summarised in section 5.8 .

Variations of the basic cycle circulation ratio with operating temperatures are shown in figures 5.16 to 5.18, pages 166 to 168. The ratio depends on the strong and weak solutions concentrations. The relative circulation increases as the concentration of the strong solution decreases, while on the hand it decreases as the weak solution concentration falls. Since the relative circulation is a ratio of the massflow rates in the cycle, it affects the heating and cooling requirements in the generator and absorber respectively.

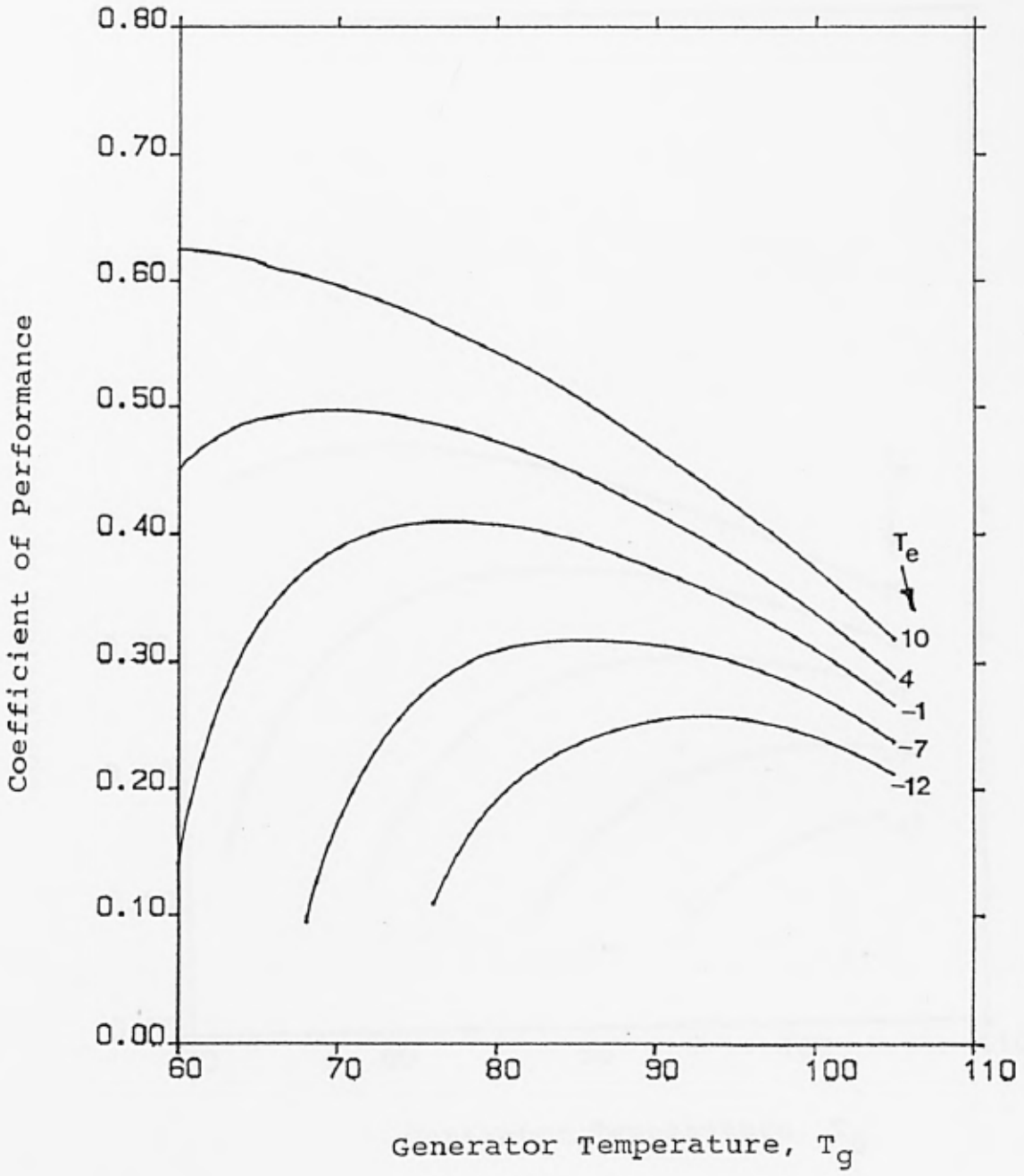


Fig. 5.13 Basic NH_3-H_2O cycle COP for, $T_c = T_a = 27$

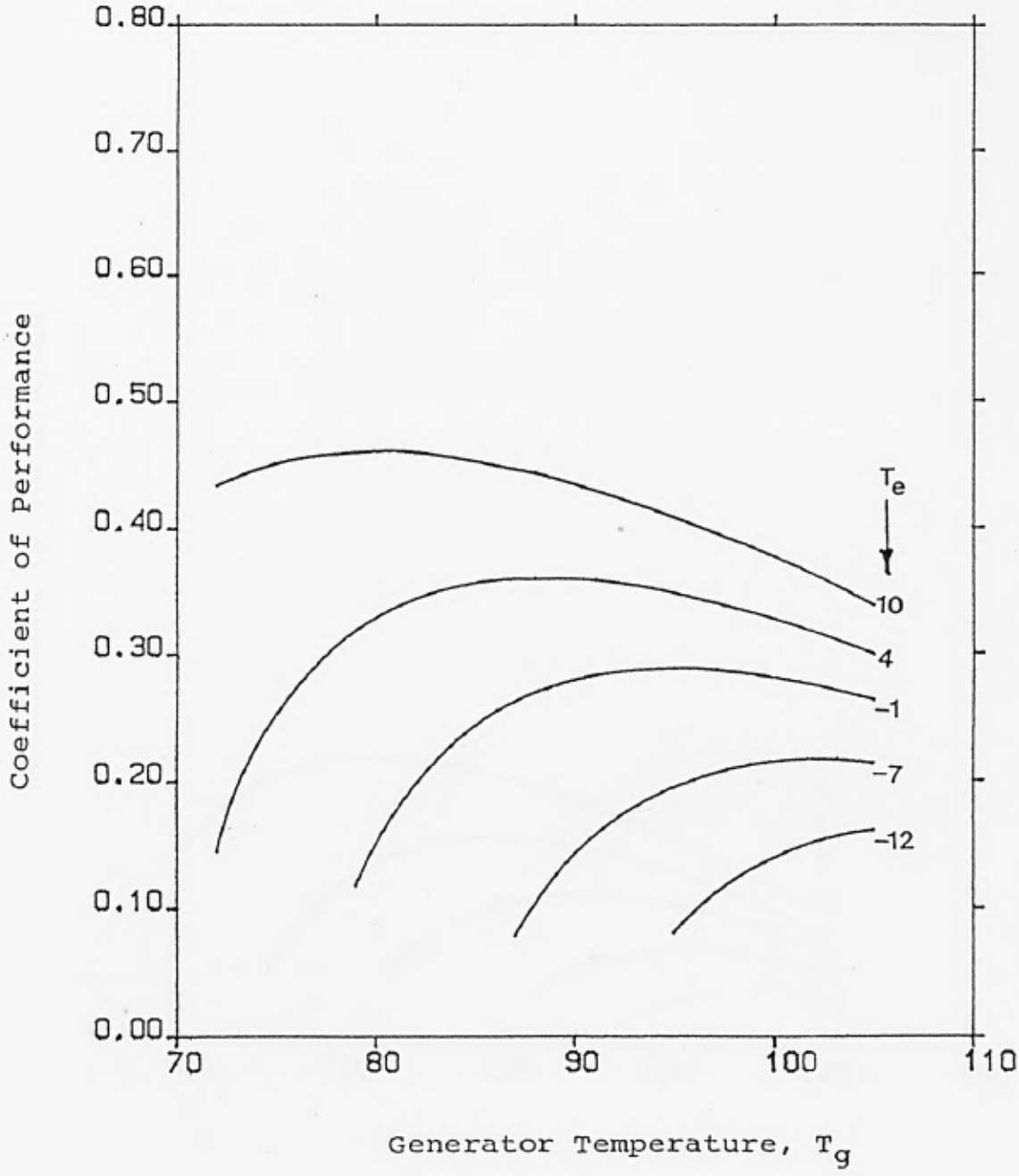


Fig. 5.14 Basic NH_3-H_2O cycle COP for, $T_c = T_a = 35$

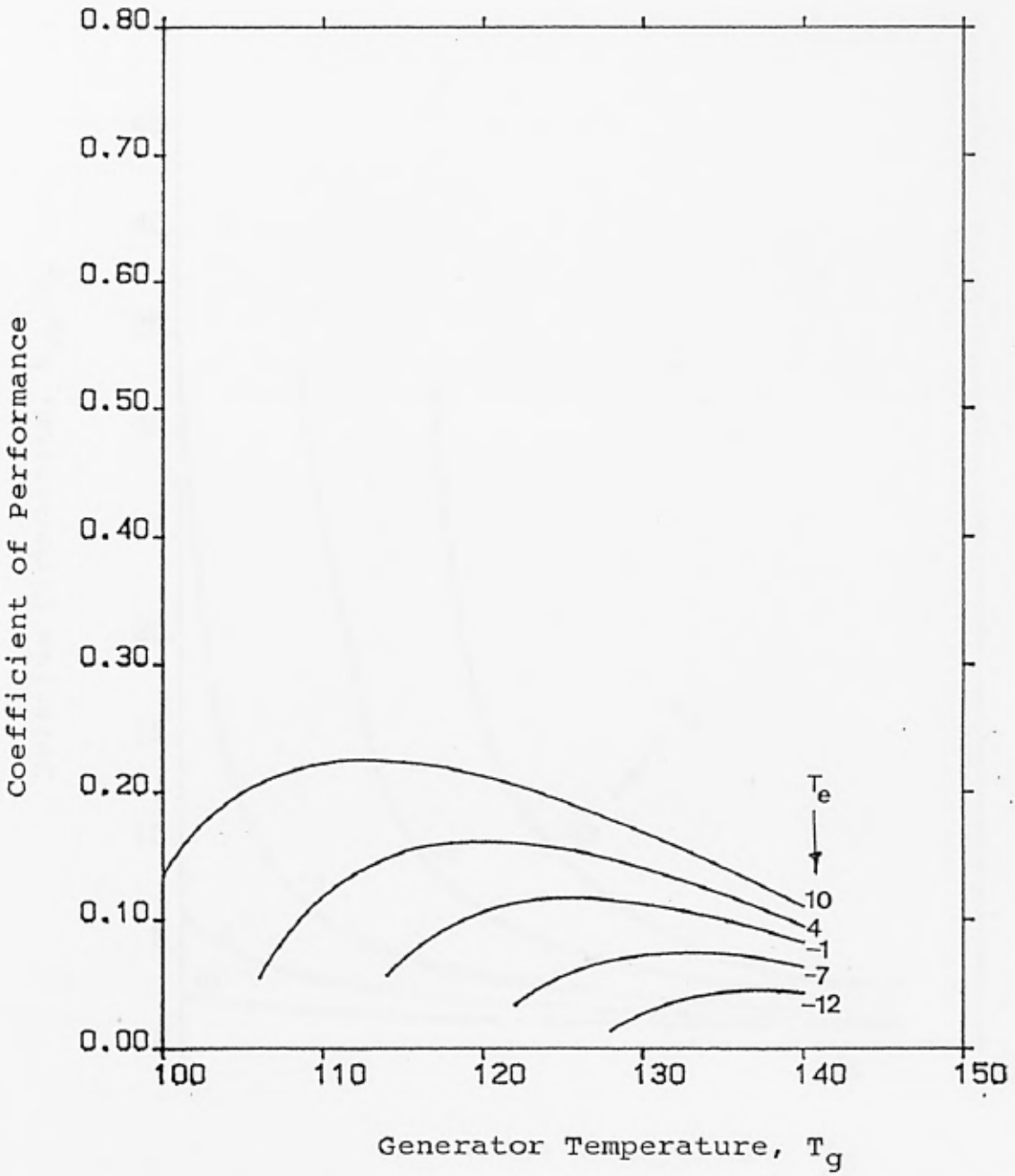


Fig. 5.15 Basic NH_3-H_2O cycle COP for, $T_c = T_a = 50$

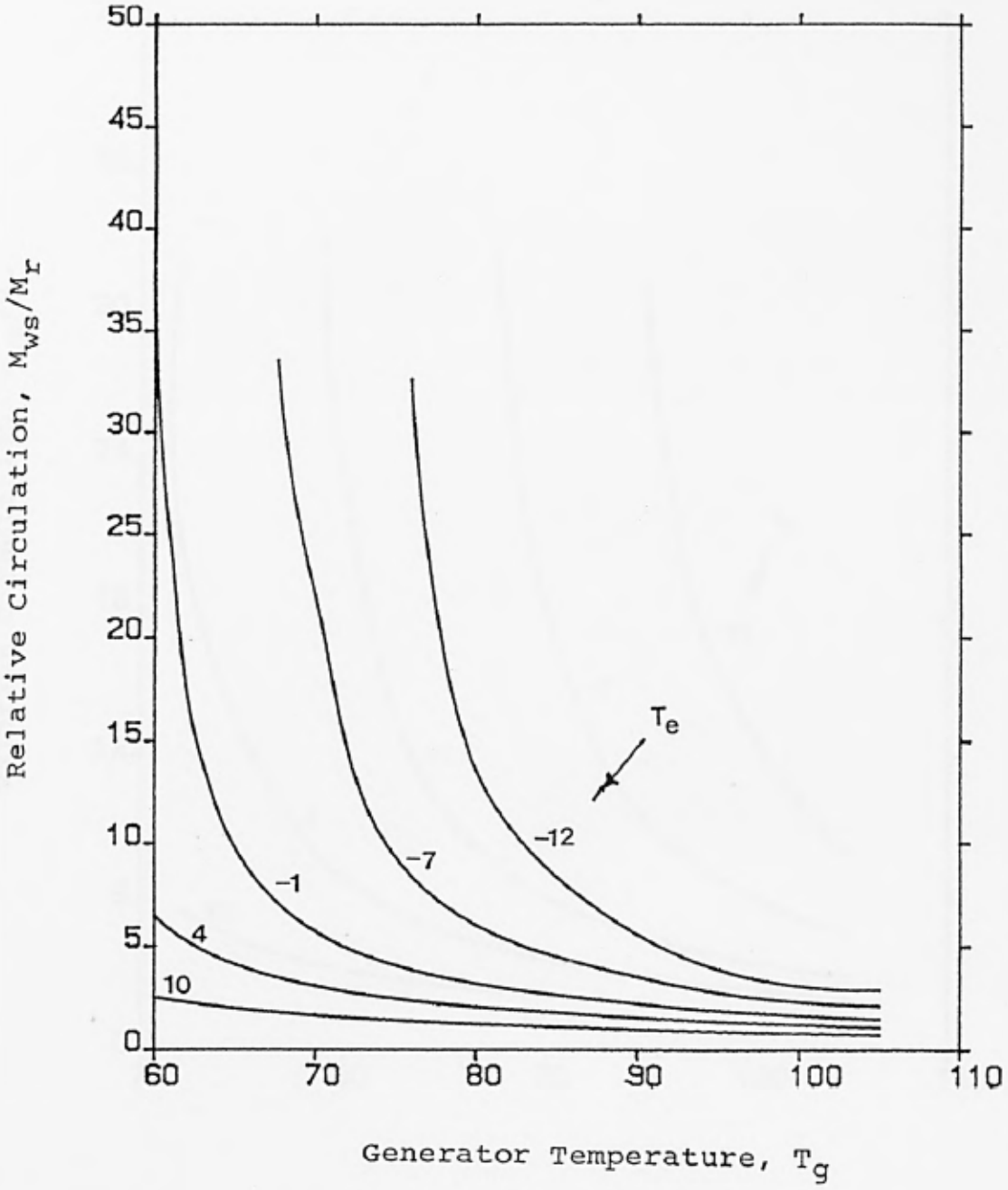


Fig. 5.16 Variation of the Basic cycle M_{ws}/M_r for, $T_c = T_a = 27$

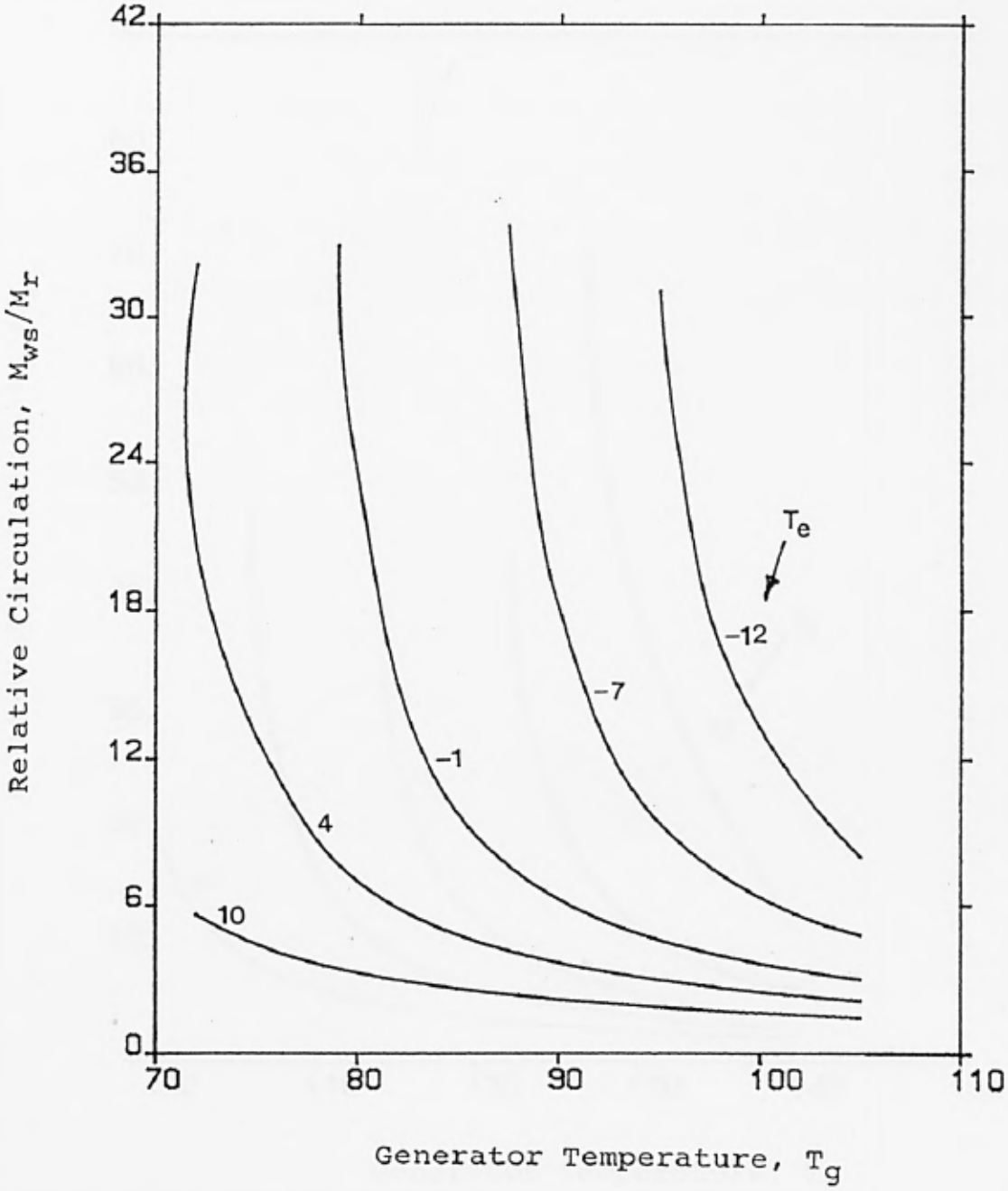


Fig. 5.17 Variation of the Basic cycle M_{ws}/M_r for, $T_c = T_a = 35$

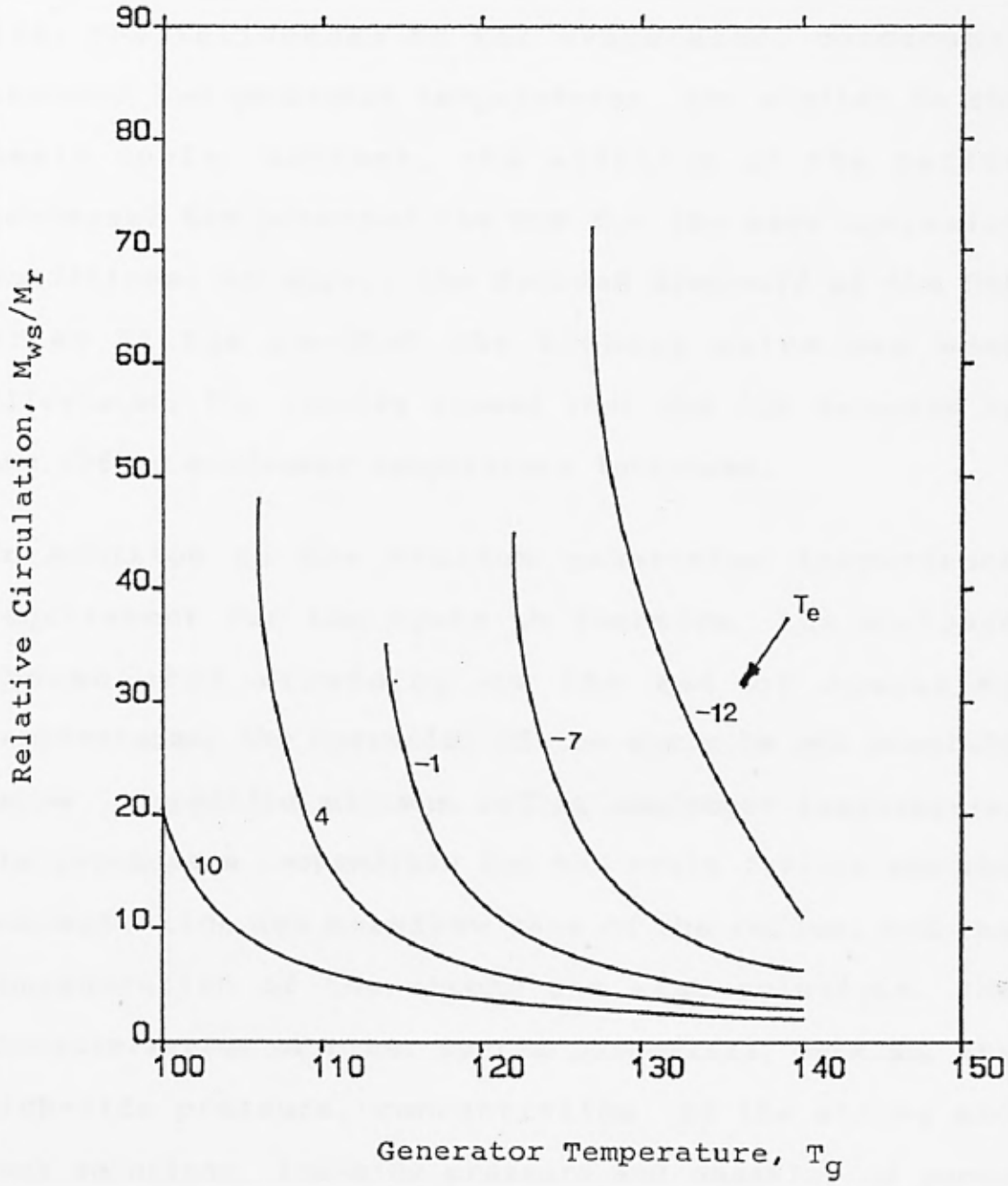


Fig. 5.18 Variation of the Basic cycle M_{ws}/M_r for, $T_c = T_a = 50$

5.8.3 THE BASIC CYCLE WITH A REFLUX CONDENSER

The basic cycle has been refined with a reflux condenser as shown in figure 5.11, page 157. Its performance curves are shown in figures 5.19 to 5.21, pages 172 to 174. The influences of the evaporator, condenser, absorber and generator temperatures are similar to the basic cycle, however, the addition of the reflux condenser has increased the COP for the same operating conditions. Moreover, the decided drop-off of the COP after it has reached the highest value has been alleviated. The results showed that the COP deceases as the reflux condenser temperature increases.

In addition to the minimum generation temperature requirement for the cycle to function, the analyses showed that depending on the set of operating temperatures, the operation of the cycle is not possible below a specific minimum reflux condenser temperature. The parameters responsible for the cycle failure are the concentration and massflow rate of the reflux, and the concentration of the strong and weak solutions. The characteristics of other system parameters, such as, the high-side pressure, concentration of the strong and weak solutions, low-side pressure and massflow of purge liquid are similar to the basic cycle.

Depending on the generator, condenser, absorber and evaporator temperatures; as the reflux condenser temperature increases, the high-side pressure drops, the

concentration of vapour leaving the reflux condenser to the total condenser decreases, the distillation breadth decreases, the purge liquid leaving the evaporator increases causing the refrigerating effect to fall and the COP to drop accordingly.

Variations of the cycle relative circulation with operating temperatures are shown in figures 5.22 to 5.24, pages 175 to 177 . As in the basic cycle, it is dependent on the concentrations of the strong and weak solutions.

5.8.4 ADDITION OF A SOLUTION HEAT EXCHANGER

The effects of adding a solution heat exchanger to the basic cycle, and to the basic cycle refined with a reflux condenser are shown in figure 5.25, page 178. The processes in these cycles are similar to those of the previous cycles figures 5.8 and 5.11, pages 150 and 157, before the heat exchanger was added, except that the COP is higher at the same set of operating conditions. The generator heat requirement and the absorber cooling requirement are found to be lower.

The heat exchanger performance is found to be affected by the reflux condenser temperature. At low reflux condenser temperature, depending on the generator, condenser, absorber and evaporator temperatures, much heat is transferred to the cold strong solution in the reflux condenser, such that the quantity of heat it could

absorb in the heat exchanger is limited. This is due to the limited heat capacity of the strong solution. The above effect was observed at high generator temperature exceeding 150^{o}C, condenser and absorber temperatures above 50^{o}C, coupled with low evaporator temperature below -7^{o}C and reflux condenser temperature below 90^{o}C

5.8.5 THE ADDITION OF A REFRIGERANT PRECOOLER

The effect of adding a refrigerant precooler to a cycle as shown in figure 5.10, page 156, is also presented in figure 5.25 . The refinement of a cycle with a precooler does not affect the system parameters except the COP, which increases due to the subcooling of liquid flowing into the evaporator causing the refrigerating effect to increase.

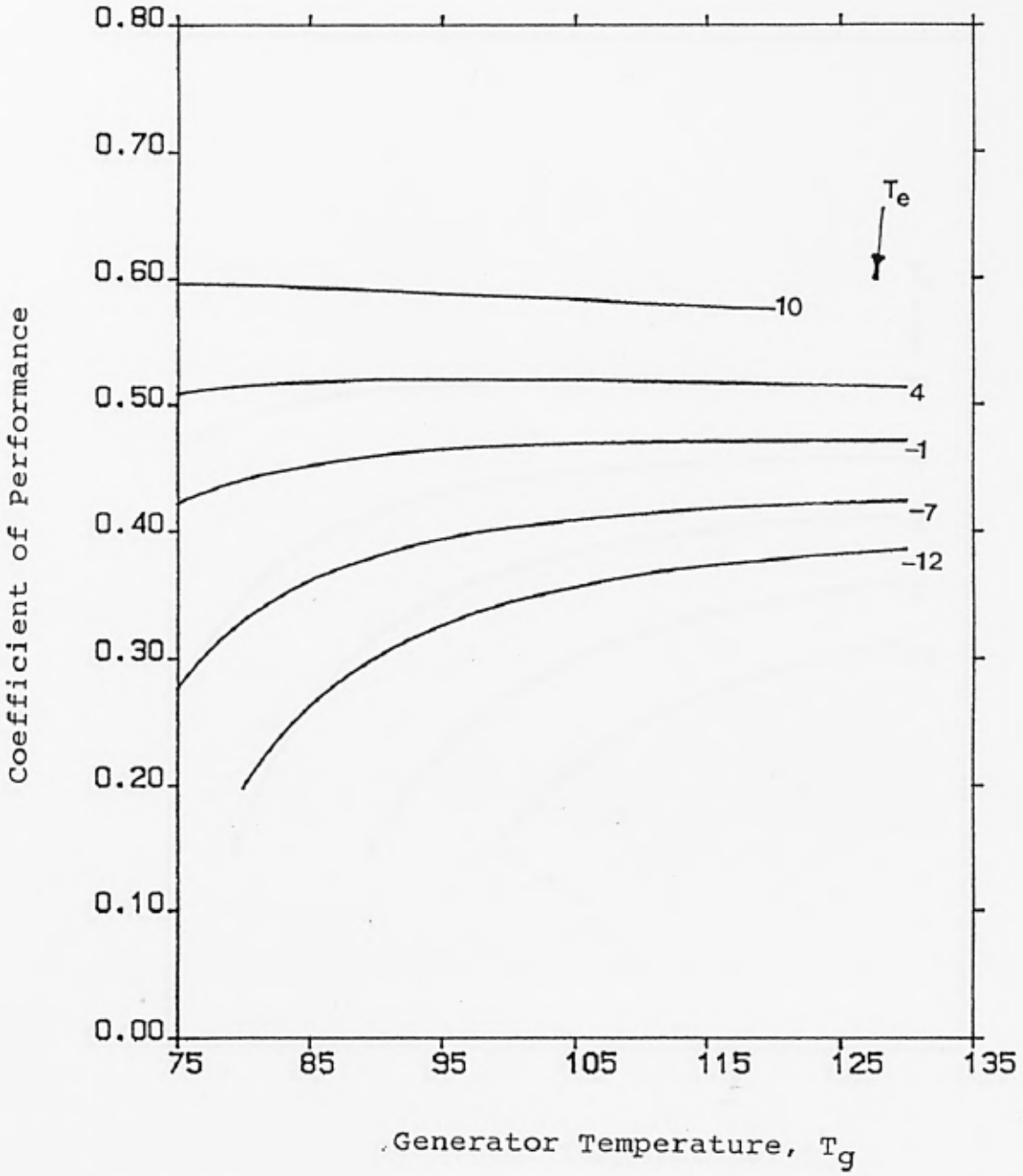


Fig. 5.19 Variation of COP for the basic cycle refined with a Reflux Condenser for, $T_c = T_a = 27$; $T_r = 70$

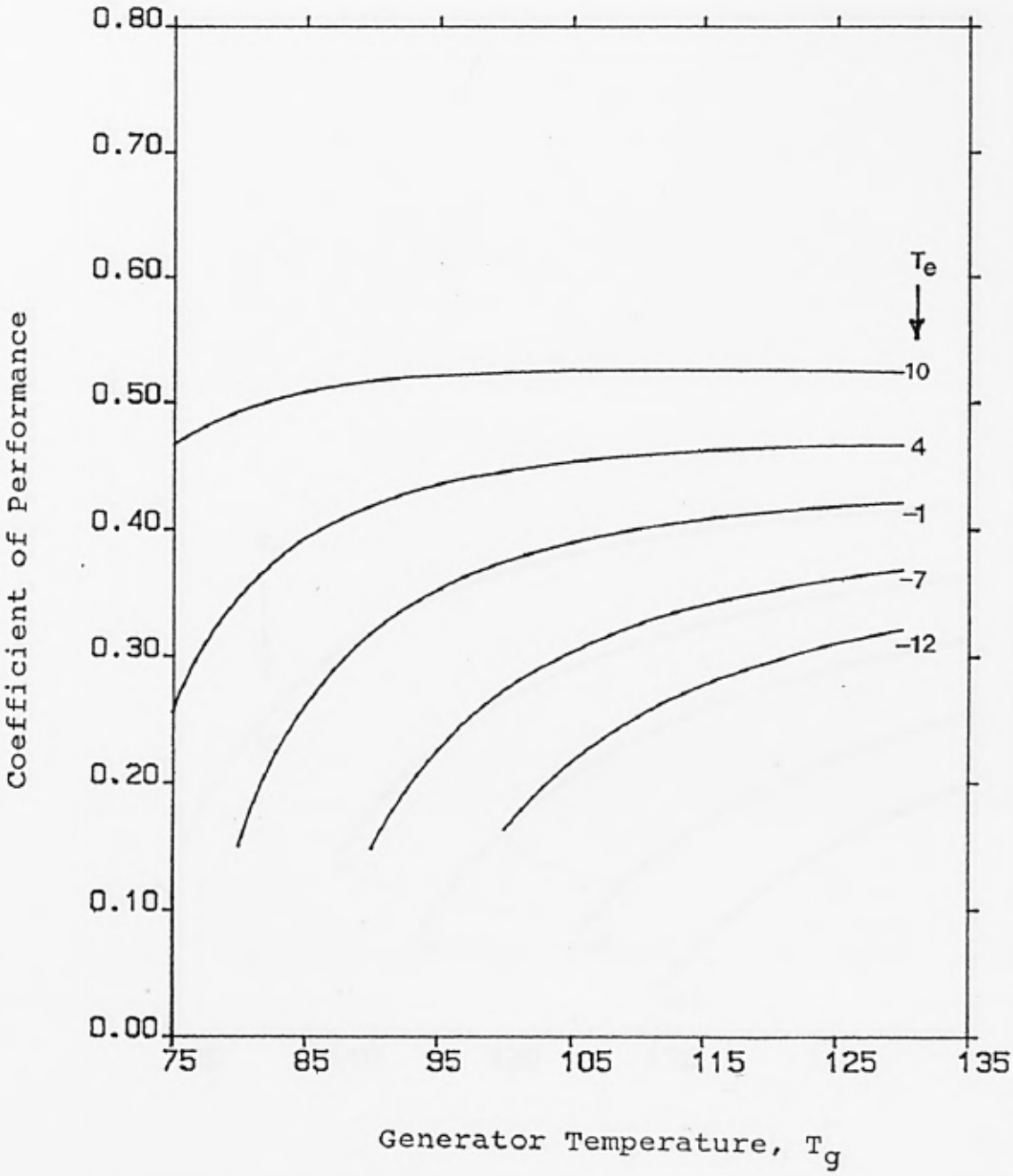


Fig. 5.20 Variation of COP for the basic cycle refined with a Reflux Condenser for, $T_c = T_a = 35$; $T_r = 70$

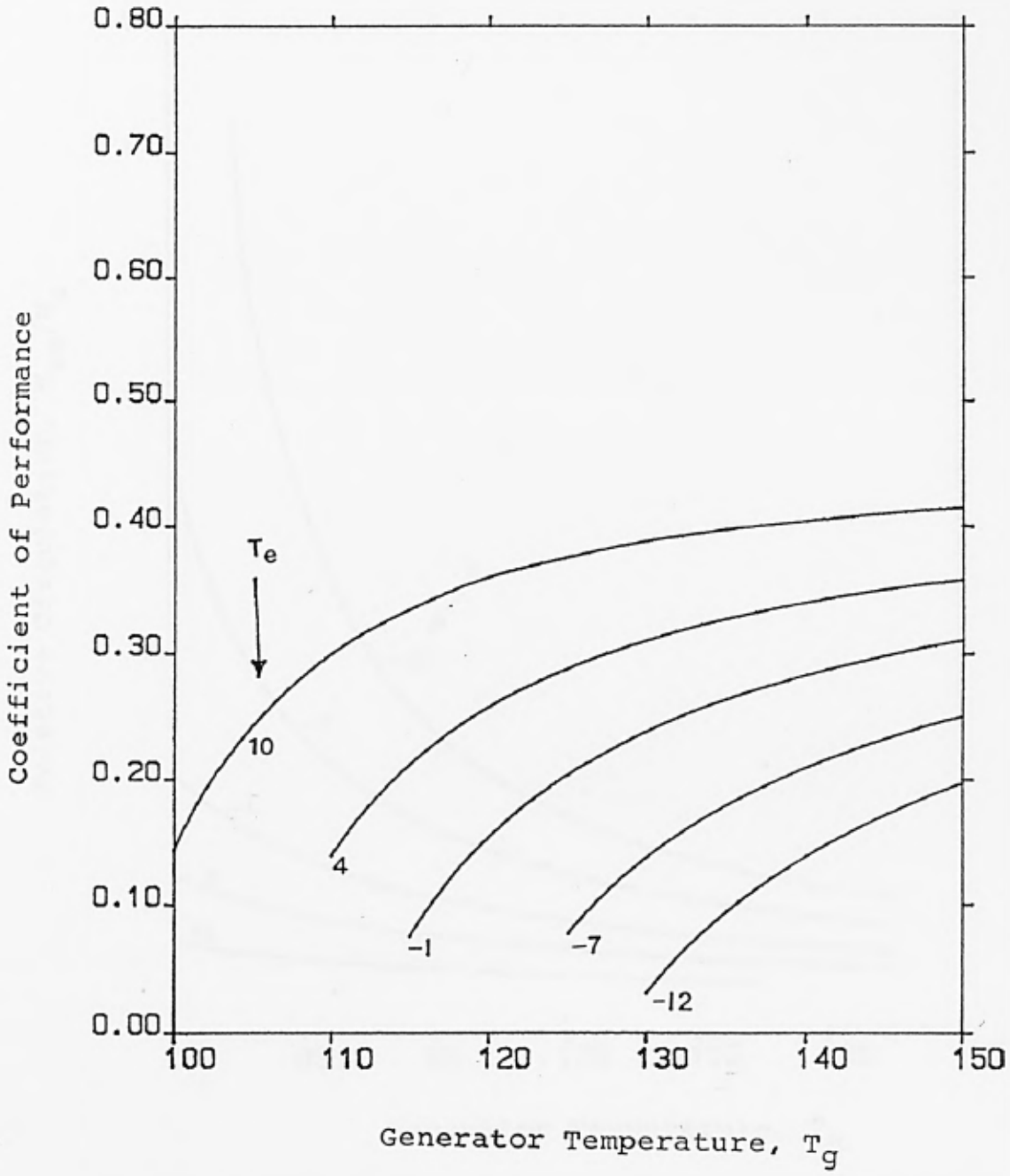


Fig. 5.21 Variation of COP for the basic cycle refined with a Reflux Condenser for, $T_c = T_a = 50$; $T_r = 70$

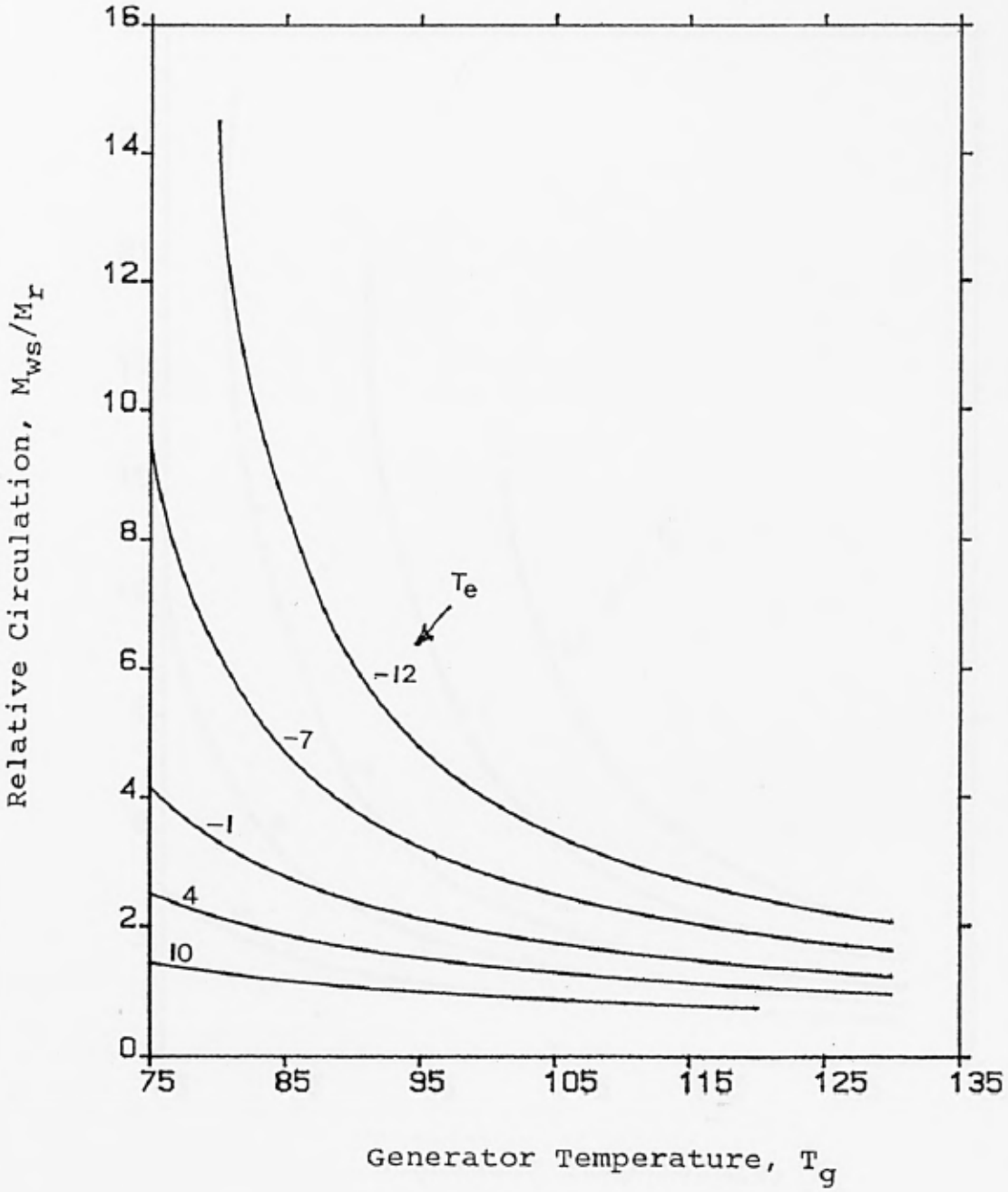


Fig. 5.22 Variation of M_{ws}/M_r for the basic cycle refined with a Reflux Condenser for, $T_c = T_a = 27$; $T_r = 70$

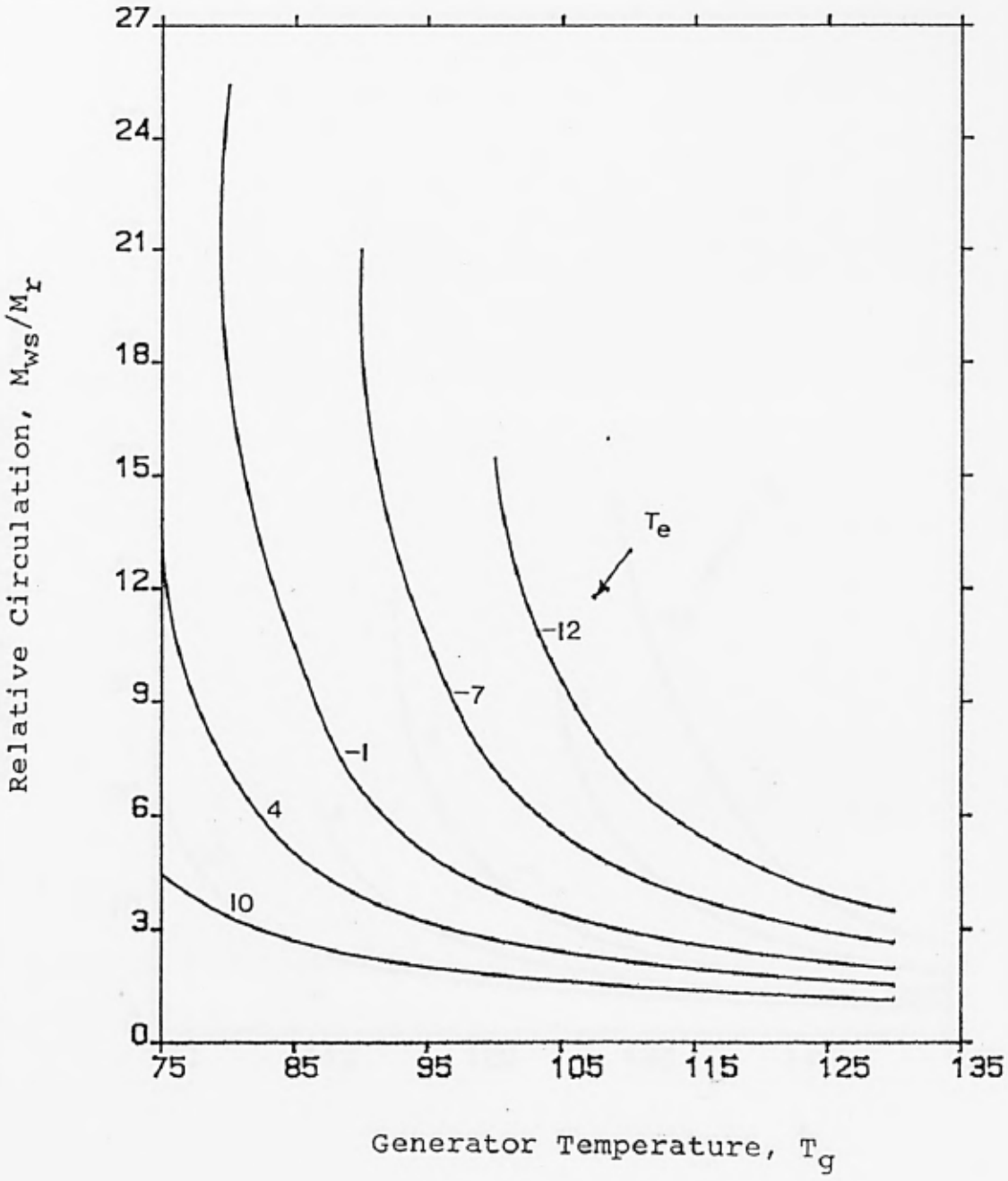


Fig. 5.23 Variation of M_{ws}/M_r for the basic cycle refined with a Reflux Condenser for, $T_c = T_a = 35$; $T_r = 70$

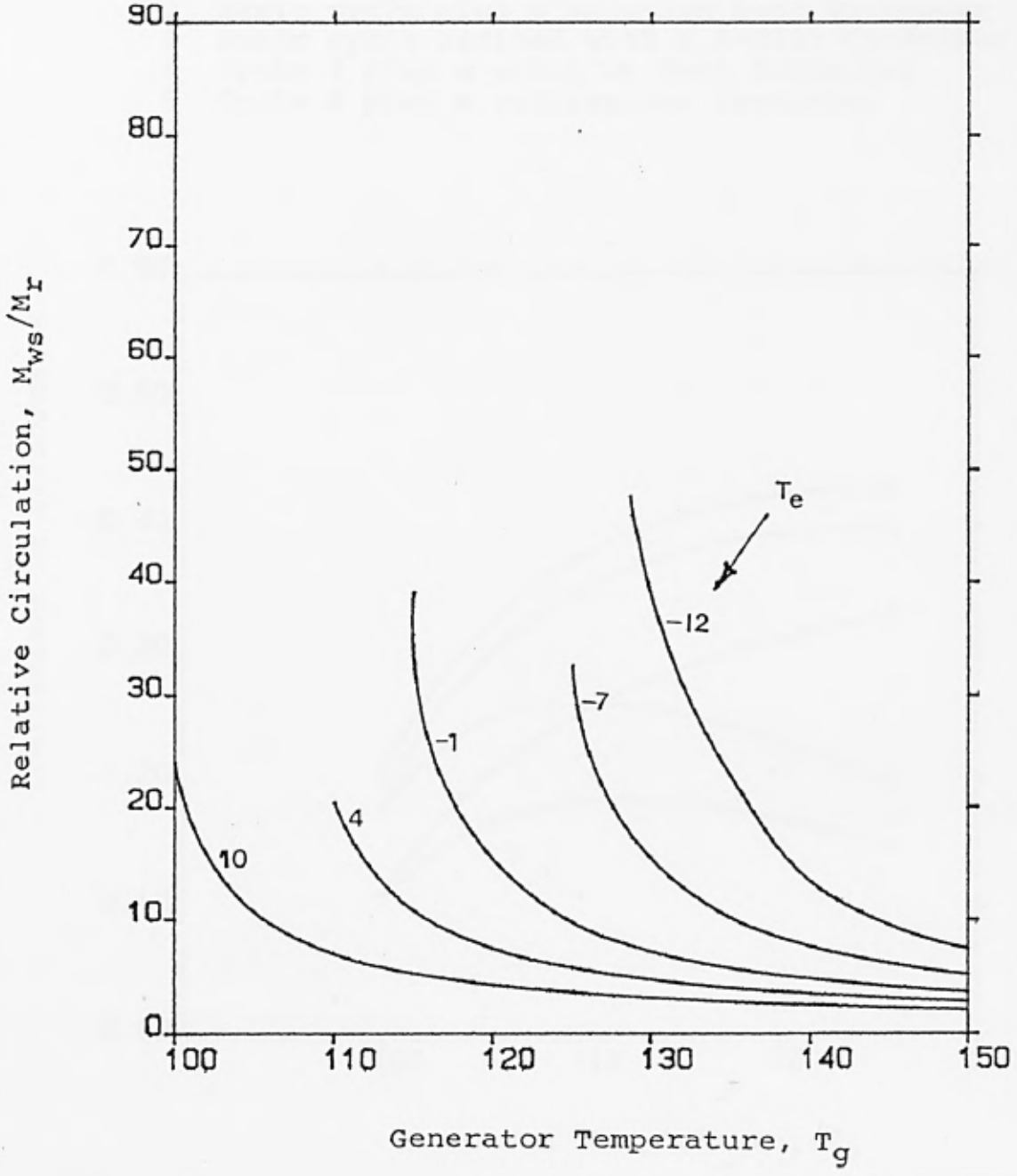


Fig. 5.24 Variation of M_{ws}/M_r for the basic cycle refined with a Reflux Condenser for, $T_c = T_a = 50$; $T_r = 70$

1 Basic cycle
2 Basic cycle plus a solution Heat Exchanger
3 Basic cycle refined with a Reflux Condenser
4 Cycle 3 plus a solution Heat Exchanger
5 Cycle 4 plus a refrigerant Precooler

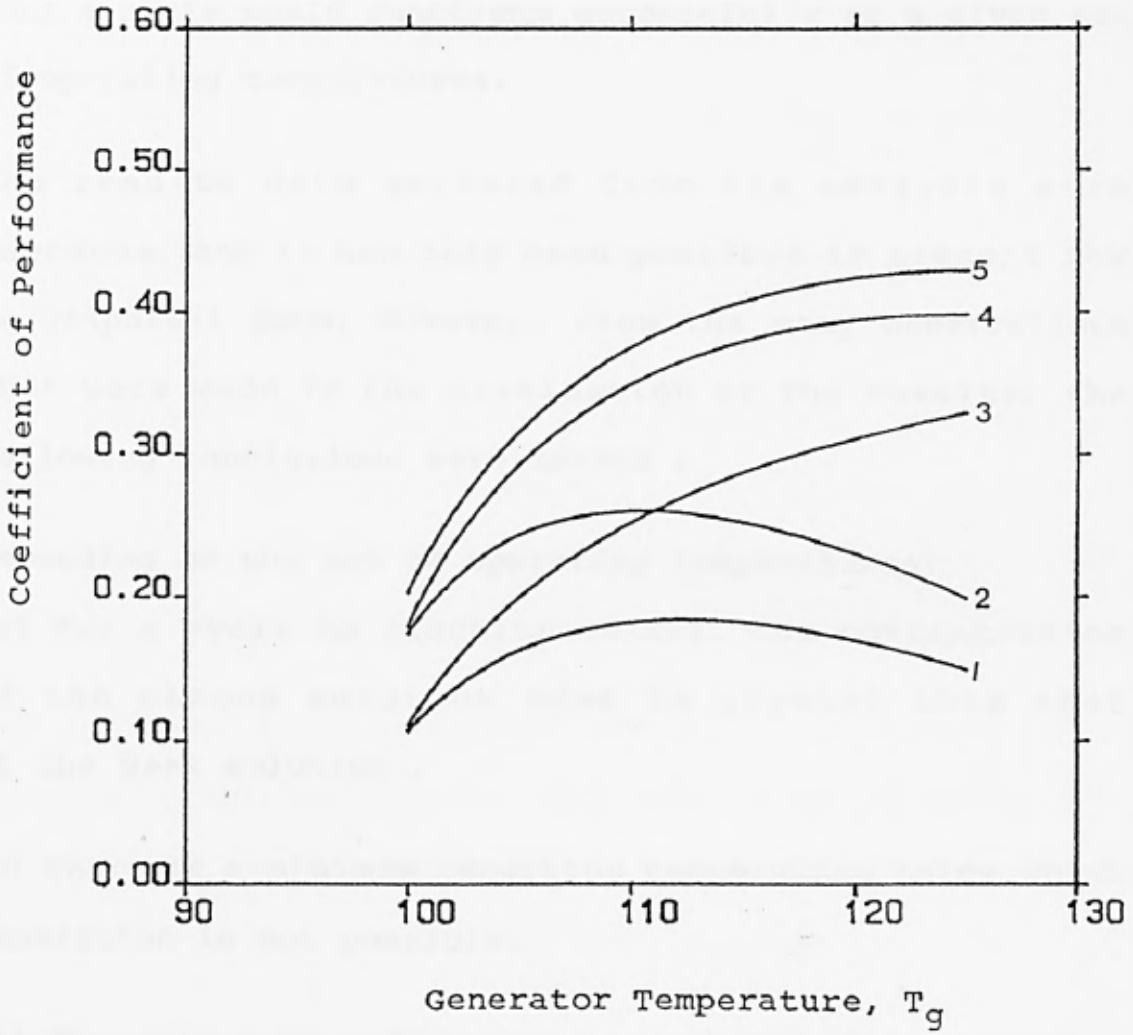


Fig. 5.25 Comparison of the COP for five different cycles for, $T_c = T_a = 43^{\circ}C$; $T_r = 70^{\circ}C$; $T_e = -1^{\circ}C$

5.9 CONCLUSION

Extensive thermodynamic analysis of the various aqua-ammonia absorption refrigeration cycles has been carried out. Important system parameters, limitations and requirements that should be taken into consideration in the design of the system for use through solar energy have been identified. The computer program which has been developed for the analysis provides the indication that a cycle would functionm successfully at a given set of operating temperatures.

The results data gathered from the analysis were enormous, and it has only been possible to present few in graphical form. However, from the many observations that were made in the examination of the results, the following conclusions were formed :

Depending on the set of operating temperatures;

(a) For a cycle to function at all, the concentration of the strong solution must be greater than that of the weak solution .

(b) There is a minimum generator temperature below which generation is not possible.

(c) There is a specific generator temperature at which the highest COP is attainable.

(d) The strong and weak solution concentrations affect the relative circulation and the specific solution circulation. These two circulation ratios indicate the

quantity of solution being circulated between the absorber and the generator, and hence the size requirement of the generator and heat exchanger.

(e) There is a minimum reflux condenser exit temperature below which the system operation is not possible because of large reflux massflow and concentration.

(f) For a cycle consisting of a reflux condenser, the concentration of the reflux must be less than the concentration of vapour entering the reflux condenser from the generator, and the concentration of vapour leaving the reflux condenser to the total condenser. The reflux ratio must be low.

(g) Even when step (e) has been satisfied, it was found that, the reflux concentration and massflow cannot be greater than a certain value which depends on the set of operating temperatures for successful operation.

(h) The cold strong solution from the absorber has a limited heat capacity, and the reflux condenser temperature should not be too low if the strong solution is to absorb any heat in the heat exchanger.

(i) The concentration of the strong solution is greatly influenced by the evaporator and absorber tempeartures, and less by the reflux condenser temperature.

(j) The concentration of the weak solution is greatly affected by the generator temperature and less by the

condenser temperature, and much less by the reflux condenser temperature.

These observations form the basis for determining the set of operating temperatures for the solar-powered NH_3-H_2O refrigeration system simulated in chapter six.

5.10 DISCUSSION

The cycles analyses have shown the desirability of high generator temperature, and low absorber and condenser temperatures. With low absorber and condenser temperatures, it would be possible to operate an aqua-ammonia cycle for low temperature applications at a generator temperature obtainable from a treated flat plate collector. However, to provide the low sink temperature of 15 to 27^{o}C required for the absorber and condenser, would require a cascade system where the high temperature evaporator would serve as the absorber of the low temperature evaporator cycle.

To use a cycle with the condenser and absorber temperatures between 27 and 35^{o}C, would require water-cooling. Cold water from wells, cool water from water mains or cooling tower may be used. However, the water cost and the additional problems of scaling, corrosion and water treatment requirements need to be considered.

For absorber and condenser temperatures above 40^{o}C, air-cooling is possible depending on the location's weather,

but higher generator temperature from about 120°C upwards would be required, and the COP would be low especially at low evaporator temperatures. Such high generator temperature could only be provided by a concentrating solar energy collector.

Knowing the minimum generation temperature for a given set of operating temperatures, and allowing a temperature approach of about 10° between the collector fluid and the design generator temperature, collector temperature and size could be estimated.

CHAPTER 6

COOLING LOAD

6.1 INTRODUCTION

The general procedure for calculating cooling load is presented. Calculation of the transient heat gain into the conditioned space is based on the ASHRAE Transfer Function Method. Transformation of individual heat gain components to respective cooling load components using the room transfer function is also presented. A computer program based on this procedure has been developed, and used to estimate the cooling load for an office building and a cold storage room in chapter seven.

6.1.1 COOLING LOAD CALCULATION METHOD

An accurate calculation of the air-conditioning or refrigeration load is essential to a careful design of a solar cooling system because of the energy requirement and its availability. The cooling load is the rate at which heat energy must be removed from a conditioned space to maintain the temperature and humidity at the design values. To calculate the space heat gain and cooling load, the following steps are determined :

1. outdoor and indoor design conditions
2. characteristics of the building structure
3. building location, orientation, and shading
4. lighting, occupancy, and other internal heat gains
6. instantaneous heat gain

7. cooling load using the result of the heat gain calculations.

6.1.2 SPACE HEAT GAIN BY TRANSFER FUNCTION METHOD

The heat gain is the rate at which heat is transferred to or generated within a conditioned space, and consists of sensible and latent heat. The space instantaneous heat gain is variable with time due to the transient effect created by the hourly variation in solar radiation. There is also an appreciable difference between the heat gain of a building structure, and the heat removed by the cooling system at any particular time due to the energy storage characteristic of the structure. Therefore, to accurately size a cooling system which would operate at optimum efficiency, an extensive design calculations for the cooling load must be performed using transient analysis.

A space heat gain is made up of the following contributing components :

1. Solar radiation
2. Heat conduction through exterior surfaces and interior partitions
3. Heat generated by occupants, products, lights and equipment
4. Ventilation and inflitration
5. Latent heat gains generated within the space

In the present study, calculation of the transient heat gain through the building structure is based on the transfer function method presented in ASHRAE (1977). The transfer function is a set of coefficients that relate an output function at some specific time to the value of one or more driving functions at that time, and to the previous values of both the input and output functions. For example, the calculation of heat gain through the exterior walls and roofs is carried out using sol-air temperature to represent the outside conditions, and a design constant indoor air temperature. Thus, the heat transfer from the inside surface of a wall at a particular time is related through the use of the appropriate transfer function coefficients; to the sol-air temperature at the same time and previous times, to the indoor temperature, and to the heat transfer rate at the previous times. This can be expressed as :

$$Q_{h,t} = A[\sum_{n=0} b_n (T_{sol,t-n\Delta}) - \sum_{n=0} d_n (Q_{h,t-n\Delta}/A) - T_{rm} \sum_{n=0} C_n] \qquad 6.1$$

Where,

A = indoor surface area of a wall or roof, m^2

$Q_{h,t}$ = space heat gain through indoor surface of a wall or roof at time t, W

t = time, hours (1.00 = 1 a.m ; 17.00 = 5 p.m)

Δ = time interval,1 hour

n = summation index for the coefficients

$T_{sol,t-n\Delta}$ = sol-air temperature at time t-nΔ, ^oC

T_{rm} = constant space temperature, ^oC

b_n, d_n, and C_n = transfer function coefficients, tables(39 and 40), ASHRAE(1977).
Unit for C_n and b_n : $W/m^2\ ^oC$
d_n is dimensionless.

The use of equation 6.1, and calculation of the heat gain components are presented in section 6.2 .

6.1.3 SPACE COOLING LOAD BY TRANSFER FUNCTION METHOD

A space cooling load depends on both the magnitude and nature of the sensible heat gain. Each component of the space heat gain gives rise to a distinct cooling load component, and the total cooling load at a particular time is equal to the sum of all the cooling load components at that time. A heat gain component can be related to the corresponding cooling load component by using the room transfer function, which depends on the nature of the heat gain, and on the heat storage characteristic of the space.

Thus, a cooling load at a particular time is related through the use of appropriate room transfer function coefficients; to the heat gain at that and previous times and to the cooling load at previous time by :

$$Q_{c,t} = (v_0 Q_{h,t} + v_1 Q_{h,t-\Delta} + v_2 Q_{h,t-2\Delta} + \text{---------}) - \omega_1 Q_{c,t-\Delta} - \omega_2 Q_{c,t-2\Delta} - \omega_3 Q_{c,t-3\Delta} - \text{----} \qquad 6.2$$

Where,

$Q_{c,t}$ = cooling load at time t, W

$Q_{h,t}$ = heat gain component at time t, W

t = time, hours (1.00 = 1 a.m ; 17.00 = 5 p.m)

Δ = time interval, 1 hour

i = 1 to the number of heat gain components

v_0, v_1, -----, ω_1, ω_2, ------, = coefficient of room transfer functions, Table 44 in ASHRAE(1977). They are dimensionless.

Application of equation 6.2, and calculation of the cooling load components and total cooling load are presented in section 6.3 below .

6.2 THE HEAT GAIN COMPONENTS

6.2.1 HEAT GAIN THROUGH EXTERIOR WALLS AND ROOF

The method for calculating the heat gain through the exterior walls and roof involves the concept of sol-air temperature. The sol-air temperature is a fictitious temperature of the outside air, which in the absence of all radiation exchanges gives the same rate of heat entry into the exterior surface as actually would occur by combination of incident solar radiation, radiant energy exchange with the sky, and convective heat exchange with the outside air.

Calculation of heat transfer through a wall or roof section with a variable outside temperature, and a

variable solar radiation impinging on the outside surface requires that the heat conduction equation be transient. For a given homogeneous slab, the governing differential equation and boundary conditions are given by :

$$\frac{dT}{dt} = \frac{k}{\rho c} \frac{d^2T}{dx^2} \qquad 6.3$$

Where,

T = local temperature at a point in the wall, ^oC

t = time, hour

$k/\rho c$ = thermal diffusity of the wall, m^2/hr

x = thickness, m

Using the sol-air temperature for the outside air, the boundary condition at outside surface, x=0, is given by:

$$-k_w \left[\frac{dT}{dx}\right]_{x=0} = h_o(T_{sol}(t) - T_{wo}) \qquad 6.4$$

and the boundary condition at the inside surface, x=L, is given by :

$$-k_w \left[\frac{dT}{dx}\right]_{x=L} = h_i(T_{wi} - T_{rm}) \qquad 6.5$$

Where,

h = coefficient of heat transfer, $W/m^2\ ^oC$

$T_{sol}(t)$ = sol-air temperature at time t, ^oC

(subscript; i for inside, o for outside, and w for wall)

In the ASHRAE transfer function method, equation 6.3 was solved with the boundary conditions given by equations 6.4 and 6.5 . The results were then matched to equation 6.1 to obtain the transfer function coefficients, b_n, d_n, and C_n.

The sol-air temperature is given by :

$$T_{sol} = T_{o,t} + \alpha I_{s,t}/h_o - \epsilon \, dR/h_o$$

Where,

$T_{o,t}$ = outside air temperature at time t, ^oC

α = absorptance of the surface for solar radiation

$I_{s,t}$ = total solar radiation incident on surface s, at time t, W/m^2

h_o = coefficient of heat transfer by long wave radiation and convection at outside surface, $W/m^2\ ^oC$

ϵ = emmitance of the surface

dR = the difference between the longwave radiation incident on the surface from the sky and surroundings, and the radiation emitted by a black body at the outside air temperature.

The following values have been assumed for the above variables, and used in subroutine SOLARP presented in appendix B to calculate the hourly sol-air temperature:

α/h_o = 0.026 $m^2\ ^oC/W$, for light coloured surface

h_o = 31 $W/m^2\ ^oC$, for 7.5 MPH summer outside air

$\epsilon dR/h_o$ = 3.9°C for horizontal surface, and 0°C for vertical surface

The hourly solar radiation for respective surfaces, $I_{s,t}$, is obtained from the actual observed daily average solar radiation data.

The outside air temperature for every hour is calculated from :

$$T_{o,t} = T_d - DR\ X\% \qquad 6.7$$

Where,

T_d = design day outside dry bulb temperature, °C

DR = daily range of outside temperature, °C

X%= percentage of the daily range, listed in table 6.1, page 194 .

Using the 24 hourly sol-air temperatures for a surface, equation 6.1 is expanded and solved in subroutine HTGAIN presented in appendix B . Initially, the history of heat flow through the structure section is unknown, and at the start of the calculation the unknown heat gain, $Q_{h,t}$, at t =1, is assumed to be zero. Since the calculation is repeated for successive 24-hour cycle until the solution converges to a value, the effect of above assumption is negligible on the final calculated heat gain. This procedure is shown in subroutine HTGAIN in appendix B .

6.2.2 HEAT GAIN THROUGH PARTITION, CEILING AND FLOOR

The heat gain through a separating structural section between the conditioned space and an adjacent space which is at a different temperature has been calculated using equation 6.1, but with transfer function coefficients listed in table 29, ASHRAE(1977). Also, The sol-air temperature in equation 6.1 has been substituted with the hourly air temperature of the adjacent unconditioned space. If this temperature is constant, then the heat gain through the partition, or ceiling or floor is given by :

$$q_{part} = U_p(T_p - T_{rm}) \qquad 6.8$$

Where,

q_{part} = heat gain through the section, W/m^2

U_p = U-value for the seperating section, $W/m^2\ ^oC$

T_p = constant temperature in the unconditioned space, ^oC

6.2.3 HEAT GAIN THROUGH THE GLASS WINDOWS

The total heat admission through a glass window is made up of the solar heat gain due to the incident solar radiation , and the conduction heat gain which occurs whether the sun is shining or not .

The conduction heat gain depends on the overall coefficient of heat transfer, U_{gl}, for the glass material, and the outdoor-indoor temperature difference. It is given by :

$$q_{gl,c} = U_{gl}(T_{o,t} - T_{rm}) \qquad 6.9$$

where,

$q_{gl,c}$ = window glass conduction heat gain, W/m^2

U_{gl} = U-value of glazing system , $W/m^2\ ^oC$

T_{rm} = room temperature, ^oC

The solar heat gain can be calculated for a given location, date and time, and window orientation. The procedure adopted in the present study is based on the ASHRAE (1977) method. However, actual observed radiation data have been used instead of clear day values used in ASHRAE. For any given glazing system, the solar heat gain is given by :

$$q_{gl,sh} = SC\ (SHGF) \qquad 6.10$$

Where,

$q_{gl,sh}$ = solar heat gain, W/m^2

SC = shading coefficient for the type of glazing, or combination of the glazing and shading device. It is unique for each type of system and can be obtained from a manufacturer.

SHGF = solar heat gain factor, W/m^2

The solar heat gain factor, SHGF, is calculated using actual observed solar radiation, and the properties of the glazing material. It is expressed as :

$$SHGF = (\text{Transmitted component}) + N_i(\text{Absorbed component}) \qquad 6.11$$

The transmitted component is given by :

$$T_{shgf} = I_b \quad t_j \cos^j(\theta) + I_d \; 2 \quad t_j/(j+2) \qquad 6.12$$

The absorbed component is given by :

$$A_{shgf} = I_b \quad a_j \cos^j(\theta) + I_d \; 2 \quad a_j/(j+2) \qquad 6.13$$

and,

$$N_i = h_i/h_o \qquad 6.14$$

Where,

I_b and I_d = beam and diffuse radiation incident on the window, W/m^2

θ = beam incidence angle

h_i = heat transfer coefficient for still air at inside surface, 8.3 $W/m^2\ ^oC$

h_o = heat transfer coefficient for 7.5 MPH wind speed at outer surface, 31 $W/m^2\ ^oC$

a_j and t_j = properties of the glass material. The values used in the present study are listed in table 6.2, page 194, for double strength clear sheet glass. They can be obtained from maunfacturers for other type of glass.

Calculation of the solar heat gain factor,SHGF, is performed in subroutine SOLARP presented in appendix B . The total instantaneous heat gain through the glazing is given by :

$$q_{gl} = SC\ SHGF + U_{gl}(T_{o,t} - T_{rm}) \qquad 6.15$$

where,

q_{gl} = the total heat gain through the window, W/m^2

Table 6.1 Percentage of the daily range of the outside temperature

Time,hr	Percent	Time,hr	Percent	Time,hr	Percent
1	87	9	71	17	10
2	92	10	56	18	21
3	96	11	39	19	34
4	99	12	23	20	47
5	100	13	11	21	58
6	98	14	3	22	68
7	93	15	0	23	76
8	84	16	3	24	82

Table 6.2 Coefficients a_j and t_j for regular sheet glass window

j	a_j	t_j
0	0.01154	-0.00885
1	0.77674	2.71235
2	-3.94657	-0.62062
3	8.57881	-7.07329
4	-8.38135	9.75995
5	3.01188	-3.89922

6.2.4 HEAT GAIN THROUGH DOORS

The doors have been assumed to have negligible energy storage capacity, and the heat gain is mainly sensible heat. Using the hourly sol-air temperature on a vertival surface, the heat gain through a door is given by :

$$q_{dr} = U_{dr} (T_{sol,t} - T_{rm}) \qquad 6.16$$

where,

q_{dr} = heat gain through the door, W/m^2

U_{dr} = U-value of the door, $W/m^2\ ^oC$

6.2.5 HEAT GAIN FROM WITHIN THE CONDITIONED SPACE

The sources of heat energy in the conditioned space and their estimation are as follows :

(a) People

The rates at which heat and moisture are given off by occupants of a conditioned space depend on the different activity engaged in. For a given number of people engaged in a specific activity, the sensible and latent heat gain can be estimated using the data given in table 6.3, page 202.

The sensible heat gain is given by :

$$Q_{p,s} = N\ (RSH) \qquad 6.17$$

The latent heat gain is given by :

$$Q_{p,l} = N\ (RLH) \qquad 6.18$$

where,

N = number of occupants

$Q_{p,s}$ = sensible heat gain, W

$Q_{p,l}$ = latent heat gain, W

RSH = rate of sensible heat gain, table 6.3

RLH = rate of latent heat gain, table 6.3

(b) Lights

To use the transfer function method to estimate the cooling load due to heat gain from lights, the heat gain is seperated into two operating schedules :

1. heat gain from lights that are on continuously for 24 hours, and
2. heat gain from lights that are on for part of the day, for example, between 8.00am and 17.00pm

The heat gain is simply the rated wattage of the lights, except for fluorescent lights where a factor of 1.2 has been applied to account for power absorbed by ballast.

(c) Equipment

The rate of heat gain from the equipment depends on the use of the conditioned space, type of equipment , and schedule of operation. In the absence of any information on the rate of heat transfer from many equipment , ASHRAE(1981) has suggested some values for the rate of heat gain for various applications. These rates are listed in table 6.4, page 202 . The heat gain from the equipment is then given by :

$$Q_{equip} = A_f \text{ (REHG)} \qquad 6.19$$

Where,

Q_{equip} = heat gain from equipment, W

A_f = the space floor area, m^2

REHG = rate of heat gain from equipment, table 6.4

6.2.6 HEAT GAIN FROM VENTILATION AIR

The main purpose of the introduction of outside air to a conditioned space is to control odour. The amount of air required is dependent on the rate of odour generation, and the maximum acceptable odourant level. Table 6.5, page 203, gives the recommemded and minimum ventilation rates for various applications. It has been assumed that sufficient outside air is introduced into the conditioned space through the cooling equipment to maintain outward escape of air, and the infiltration gain has been discarded.

The heat gain from the ventilation air is made of sensible and latent heat. The sensible heat gain results from temperature difference between the incoming outside air and the room air. The latent heat gain is due to the difference in humidity ratio between the incoming air and room air. They are given by ASHRAE(1977) as :

$$Q_{v,s} = 1.232\ V\ (T_{o,t} - T_{rm}) \qquad 6.20$$

$$Q_{v,l} = 3012\ V\ (W_o - W_{rm}) \qquad 6.21$$

Where,

$Q_{v,s}$ = sensible heat gain, W

$Q_{v,l}$ = latent heat gain, W

$T_{o,t}$ = outside air temperature at time t, ^{o}C

T_{rm} = room temperature, ^{o}C

W_{o} = outside humidity ratio, kg of water/kg of dry air

W_{rm} = room humidity ratio, kg of water/kg of dry air

V = air flow rate, l/s

6.3 THE SPACE COOLING LOAD

The cooling load for a space is generally different from the space heat gain. For example, the radiant heat transfer inputs to the structure is delayed before it reaches the inside surface of the conditioned space, whereas the convective and the latent heat inputs are not. Consequently, the cooling load resulting from each heat gain component is distinct.

6.3.1 INSTANTANEOUS COOLING LOAD COMPONENTS

The following instantaneous heat gain components would appear immediately as cooling load components :

1. Heat gain due to lights that are on continuously
2. Sensible heat gain due to ventilation
3. 50% of the sensible heat gain from occupants

4. The latent heat gains due to people, ventilation and others.

6.3.2 TRANSFORMED COOLING LOAD COMPONENTS

Using the coefficients of the room transfer function, v's and ω`s, with equation 6.2, the following heat gain components are transformed to cooling load components:

1. Sum of solar heat gain for windows with no interior shading
2. Sum of conduction heat gains through walls, roof, partitions, and solar heat gain for windows with interior shading
3. Sum of heat gain due to lights that are not on for continuous 24 hours
4. Sum of heat gains due to equipment and 50% of sensible heat gain from people.

The transformation of the above heat gain components using equation 6.2 is performed in subroutine CLOAD presented in appendix B.

6.3.3 TOTAL COOLING LOAD

The total space cooling load for each hour is obtained by adding together, the instantaneous cooling load components in section 6.3.1, and the transformed cooling load components in section 6.3.2 .

6.3.4 ADJUSTMENT OF THE ROOM TRANSFER COEFFICIENTS

The room transfer function coefficients listed in table 44 in ASHRAE(1977) are for rooms where all the input heat gain eventually appear as a cooling load. In most cases, a fraction of the input heat gain is lost to the surroundings, and the coefficients are multiplied by the factor, f_c, to account for this loss :

$$f_c = 1 - 0.116\ K_c \qquad 6.22$$

and K_c is given by :

$$K_c = (1/L_f)\ (U_w\ A_w + U_{wd}\ A_{wd} + U_{cr}A_{cr}) \qquad 6.23$$

Where,

K_c = unit length conductance of the enclosure surroundings, $W/m^2\ ^oC$

L_f = length of the enclosure surrounding, m

U = U-value of the space enclosure element (subscript; w for wall, wd for window, cr for corridor)

A = area of space enclosure element, m^2

6.4 REFRIGERATION LOAD

The refrigerated space heat gain calculation procedure is the same as presented in section 6.2 . However, the heat gain due to occupancy is estimated using table 6.6, page 204; The ventilation air heat gain is replaced by infiltration air, using air change rate given in table 6.7, and rate of heat gain from the air in table 6.8, page 204 .

The heat gain in cooling the product from an initial temperature to some lower temperature above the product freezing point is given by :

$$Q_{prod} = M\ C_1\ (T_1 - T_2) \qquad 6.24$$

Where,

Q_{prod} = heat gain from the product, kJ

M = mass of product, kg

C_1 = specific heat of product at temperature T_1, kJ/kg ^{o}C

T_1 = initial temperature of product, ^{o}C

T_2 = the cold store temperature, ^{o}C

The heat from the product is assumed to be removed within a given number of hours, and the cooling load due to the product is given by :

$$Q_{c,p} = Q_{prod}/(3600\ n) \qquad 6.25$$

where,

n = hours

$Q_{c,p}$ = refrigeration load due to the product, kW

Table 6.3 Rates of heat gain per hour from Occupants of a conditioned space

Degree of Activity	Typical Application	Sensible Heat, W	Latent Heat, W
Seated at rest	Theatre-matinee	66	31
	Theatre-evening	72	31
Seated, very light work	Offices, hotels, apartments	72	45
Moderately active office work	Offices, hotels, apartments	73	59
Standing, light work; or walking slowly	Department, retail and dime stores	73	59
Walking; seated	Drug store, bank	73	73
Sedentary work	Restaurant	81	81
Light bench work	Factory	81	139
Moderate dancing	Dance hall	89	160
Walking 3 mph, moderately heavy work	Factory	110	183
Bowling	Bowling alley		
Heavy work	Factory	170	255

Table 6.4 Rate of heat gain from equipment

Space application	heat gain, W/sq m floor area
General office	9.5 - 12.6
Accounting office	19 - 22
Office VDU	47
Digital computer area	237 - 552
Analog computer area	158 - 475
Laboratory	47 - 220
Manufacturing plant	65 - 475

Table 6.5 Ventilation air requirements

Application	Smoking	L/s per Person		L/s per m^2, floor
		Recommended	Minimum	Minimum
Apartment	Some	9.4	4.7	.....
Bank	Some	4.7	3.5	.....
Beauty parlors	Some	4.7	3.5	.....
Board rooms	heavy	23.6	9.4	.....
Department stores	None	3.5	2.4	0.25
Drug stores	some	4.7	3.5	.....
Factory	None	4.7	3.5	0.51
Hospitals,				
Operating rooms	None	.....	.....	10.16
Private rooms	None	14.2	11.8	1.68
Wards	None	9.4	4.7	.....
Hotel rooms	Heavy	14.2	11.8	1.68
Kitchens,				
Restaurant		.....	.....	20.31
Residence		.....	.....	10.16
Laboratories	Some	9.4	7.1	.....
Offices,				
General	Some	7.1	4.7	1.27
Private	None	11.8	7.1	1.27
Private	Some	14.2	11.8	1.27
Schoolrooms	None	4.7	3.5	.....
Theatre	None	3.5	2.4	.....
	Some	7.1	4.7	.....
Toilets (exhaust)	.....	.....	.....	10.16

Table 6.6 Heat equivalent of Occupancy

Refrigerated space temperature, ^{o}C	Heat equivalent/person/hour kW
10	0.211
4.4	0.246
-1.1	0.278
-6.7	0.308
-12.2	0.352

Table 6.7 Average air changes for storage rooms due to door opening and infiltration

Room volume, m^3	Air changes per 24 hour	
	$T_{room} > 0^{o}C$	$T_{room} < 0^{o}C$
5	50.1	38.0
15	25.3	19.6
40	14.3	11.7
75	10.1	8.0
125	7.7	6.0
200	5.9	4.6
500	3.7	2.8

Table 6.8 Rate of heat gain from infiltration air at $32.2^{o}C$ outside temperature, and 50% relative humidity inside the storage room

T_{room} ^{o}C	Heat gain, kJ/m^3	T_{room} ^{o}C	Heat gain kJ/m^3
15.6	33.27	4.4	59.35
10.0	47.46	1.7	64.79
7.2	53.35	-1.1	70.06

CHAPTER 7

COMBINED SYSTEM SIMULATION AND ECONOMIC COMPARISON

7.1 INTRODUCTION

The combined system of the CPC solar collector and the aqua-ammonia absorption cycle has been simulated for two applications, cooling of an office building and a refrigerated cold storage. The system dynamic performance and overall instantaneous efficiency have been determined.

To carry out the simulation, the hourly cooling loads for the office building and the cold store have been estimated. The computer program which has been developed for the load estimation is based on the calculation procedure presented in chapter 6. Also, refrigerant and solution storage for the absorption cycle have been modelled, and results are presented.

7.2 SYSTEM DESCRIPTION AND SIMULATION

7.2.1 DESCRIPTION AND DATABASE

Simulation of the solar powered refrigeration system shown in figure 7.1, page 210, involves interconnecting the CPC solar collector model, the aqua-ammonia absorption cycle model, and the cooling load estimation program result, with the solution of the first order differential equations describing the refrigerant and solution stores.

Simulation of the system for the two applications was carried out using the weather data for the location 6.45^{o}N (Lagos). The design database for these applications are :

For the one-story office building shown in figure 7.2, page 211 :

Indoor condition : 25^{o}C dry bulb , 18.3^{o}C wet bulb

Occupancy : 37 office workers, from 9.00 to 17.00 hour

Lights : 26 W/m^{2}floor area ; Tungsten lights = 1200 W continuously ON, the remaining lighting is Fluorescent(ON between 9.00 and 17.00)

Office appliances : 9.7 W/m^{2}floor area

Window : single glazing with venetian blind , U = 4.6 W/m^{2} ^{o}C , Shading coefficient = 0.55

Door : pine panels ; U = 3.35 W/^{2} ^{o}C

Ventilation air : 7.1 l/s

Evaporator temperature = 7^{o}C

Condenser and Absorber temperature = 44^{o}C

Reflux condenser temperature = 70^{o}C

For the beef cold storage room, the same weather conditions are used. Other data are as follows :

Room temperature : 1.7^{o}C

Room dimension : 8.5 X 4.5 X 3.0m

Internal electrical load : 300 W

Product : 2010 kg lean beef , Enter room at 28^{o}C , Specific heat = 3.23 kJ/kg ^{o}C

Air change rate : 9.5 air changes per 24 hour

Evaporator temperature : $-7^{o}C$

Condenser and Absorber temperature : $44^{o}C$

Reflux condenser temperature : $70^{o}C$

The transfer function coefficients, b_n, d_n, and C_n for the types of construction considered are given in table 7.1, page 212. The Coefficients for the room transfer function for the same construction are listed in table 7.2, page 213 . These values were used in subroutines HTGAIN and CLOAD shown in appendix B .

7.2.2 THE SIMULATION

Using the given set of operating temperatures for the absorption cycle, the steady state minimum generation temperature was determined from program REFRIG developed in chapter five, and shown in appendix B . The hourly cooling loads were estimated using the formulations developed in chapter six in the cooling load computer program.

Next, the total energy collected for a given collector area is determined from :

$$Q_u = A_c\ Fr[q_s - (U_t/C)(T_i - T_b)] \qquad 7.1$$

and the collector outlet water temperature from :

$$T_o = T_i + Q_u/M\ cp \qquad 7.2$$

The collector top loss coefficient, U_t, is determined from equations 4.79 and 4.80, in chapter four, by iteration.

For the absorption cycle, the energy collected, Q_u, is reduced by 10% and then used as the energy input to the generator. The 10% reduction is a safety factor that accounts for sensible heating and heat losses from the generator. Moreover, a constant $10^{o}C$ minimum approach temperature between the collector outlet water temperature and the steady state minimum generation temperature has been used.

Next, the refrigerant, weak and strong solutions mass flows, and the components energy flows were determined for the generator temperature and energy input for any particular time. Based on the assumption that the state points 3, 4, 8, 9, 12, and 14 on figure 7.1, page 210, are saturated, the equations (7.3, 7.4, 7.5, 7.8, and 7.9) below were solved iteratively to determine the massflow rates that correspond to the input generator energy and temperature. From figure 7.1, these equations are :

Mass and NH_3 balance around the reflux condenser :

$$M_6 = M_8 + M_7 \qquad 7.3$$

$$M_6\ XV_6 = M_8\ XV_8 + M_7\ XL_7$$

rearranging to eliminate M_8 :

$$M_7 = M_6\left(\frac{XV_8 - XV_6}{XV_8 - XL_7}\right) \qquad 7.4$$

Generator mass balance :

$$M_{15} = M_6 + M_4 - M_7 \qquad 7.5$$

substituting equation 7.3 into 7.5 :

$$M_{15} = M_6[1 - (\frac{XV_8 - XV_6}{XV_8 - XL_7})] + M_4 \qquad 7.6$$

Generator NH_3 balance :

$$M_{15}\ XL_{15} = M_6\ XV_6 + M_4\ XL_4 - M_7\ XL_7 \qquad 7.7$$

By eliminating M_{15} and M_7 from equations 7.6 and 7.7, and rearranging :

$$M_4 = M_6\{[[(XV_6 - \frac{XV_8 - XV_6}{XV_8 - XL_7}\ XL_7)/XL_{15}] - (1 - \frac{XV_8 - XV_6}{XV_8 - XL_7})]/\ (1 - \frac{XL_4}{XL_{15}})\} \qquad 7.8$$

Energy balance around the generator :

$$Q_g = M_4\ h_4 - M_{15}\ h_{15} + M_8\ h_8 \qquad 7.9$$

Initially, a value of 0.001 kg/s was assumed for M_6 to solve equation 7.8, then equations 7.4, 7.3 and 7.5 are solved respectively; Next, Q_g is calculated from equation 7.9, and then compared with the input energy to the generator. Subsequently, the iteration continues until the difference between Q_g and the input energy is less than $\pm$ 0.001 . The program REFSIM in appendix B shows this procedure.

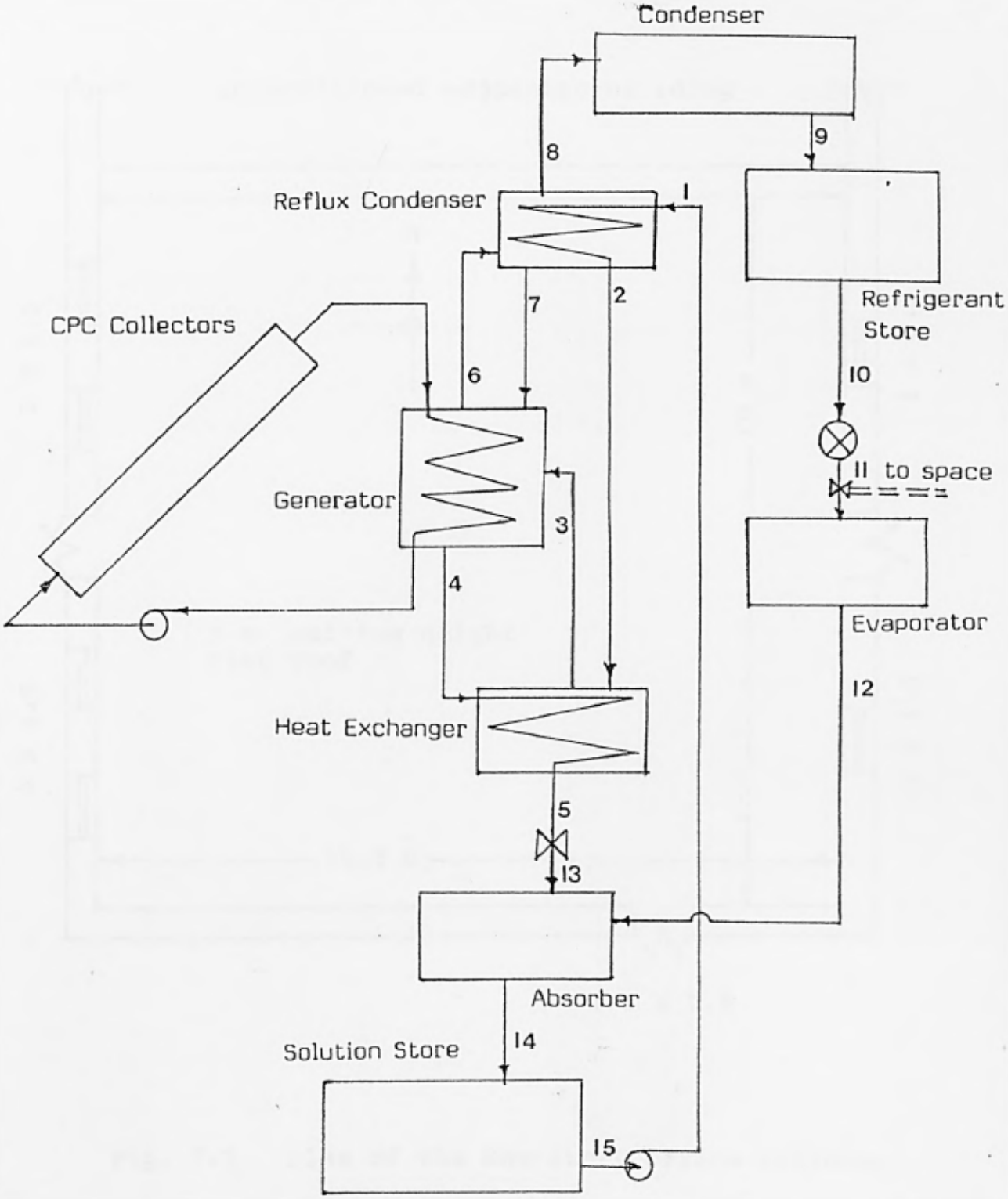


Fig. 7.1 Solar powered NH_3-H_2O absorption system

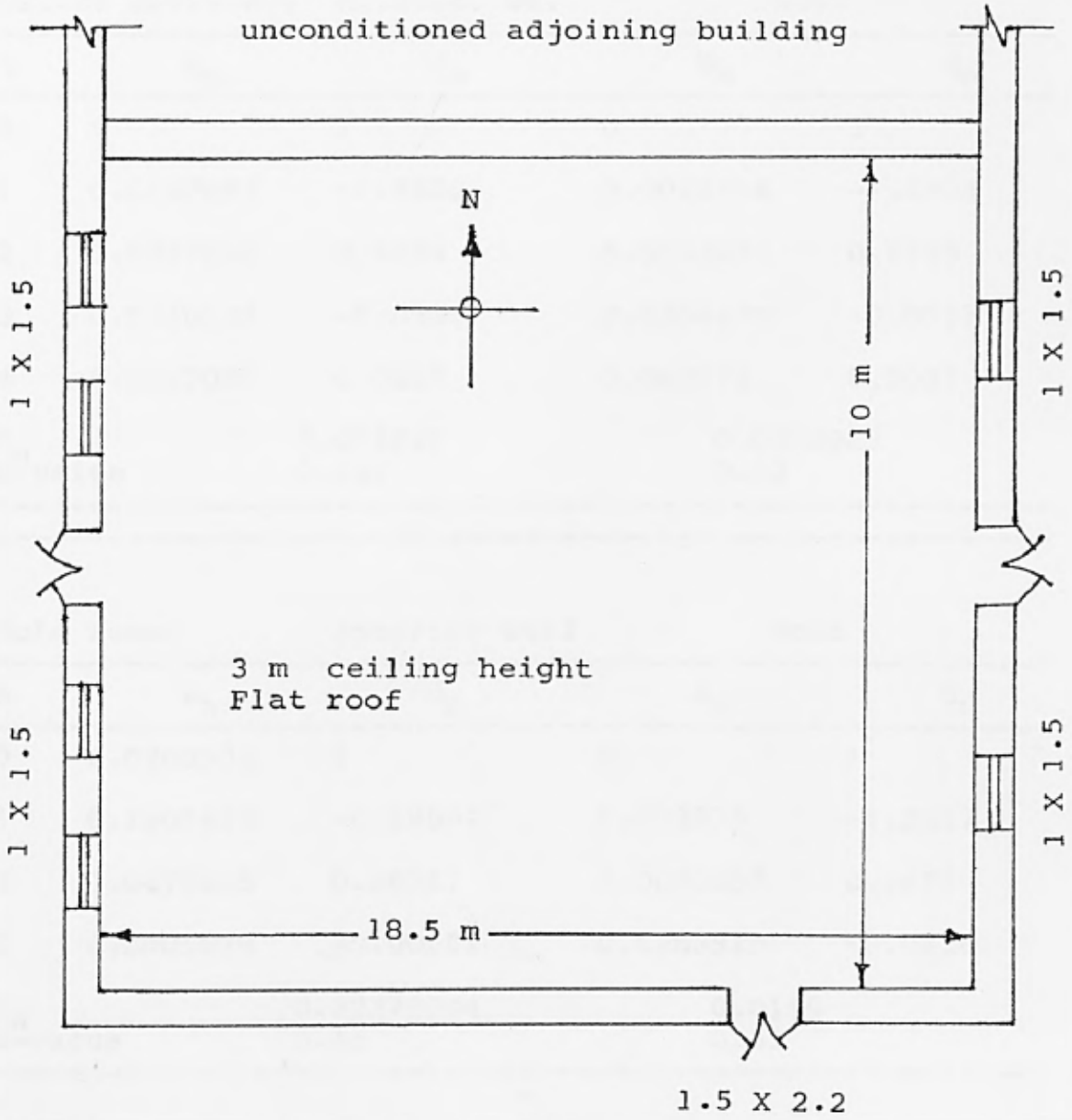


Fig. 7.2 Plan of the One-story office building

Table 7.1 Transfer function coefficients

Office building:	Exterior wall		Roof	
n	b_n	d_n	b_n	d_n
0	0	1	0	1
1	0.0107893	-1.4580	0.0022714	-1.4904
2	0.0397501	0.6409	0.0193072	0.6549
3	0.0210107	-0.0996	0.0204429	-0.0937
4	0.0017035	0.0037	0.003975	0.0037
C_n		0.073822		0.0459965
U-value		0.846		0.62

Cold room:	Exterior wall		Roof	
n	b_n	d_n	b_n	d_n
0	0.0208904	1	0	1
1	0.1501419	-0.59602	0.003975	-1.2437
2	0.0475805	0.08757	0.0090857	0.2877
3	0.0005678	-0.00002	0.0283929	-0.0128
C_n		0.22272004		0.0159
U-value		0.46		0.51

Cold room :	Floor			
n	0	1	2	3
b_n	0.0073821	0.1130039	0.09483	0.0068143
d_n	1	-0.9849	0.1677	-0.0016
C_n =		0.22033		
U -value		1.23		

Table 7.2 Coefficients of room transfer function

coefficients v_n	v_0	v_1	v_2	v_3
Solar heat gain through window with no interior shading	0.2727	-0.3400	0.1169	-0.0064
Conduction through walls, roof, doors, and windows with interior shading	0.6982	-1.2017	0.6617	-0.1150
heat generated by lights	0.3178	-0.4507	0.2089	-0.0328
Heat generated by people and equipment and dissipated by radiation	0.3251	-0.4267	0.1524	-0.0076

coefficients ω_n	ω_0	ω_1	ω_2	ω_3
	1	-1.8260	1.0697	-0.2005

7.3 REFRIGERANT AND SOLUTION STORAGE

Modelling of the refrigerant and solution stores involves mass and energy balances around each store. Based on figure 7.1, page 210, they are as follows :

Refrigerant store :

$$\frac{dM_{rs}}{dt} = M_9 - M_{10} \qquad 7.10$$

$$\frac{dU_{rs}}{dt} = M_9\, h_9 - M_{10}\, h_{10} - Q_{rs} \qquad 7.11$$

Solution store :

$$\frac{dM_{ss}}{dt} = M_{14} - M_{15} \qquad 7.12$$

$$\frac{dU_{ss}}{dt} = M_{14}\, h_{14} - M_{15}\, h_{15} \qquad 7.13$$

Where,

M_{rs} = refrigerant in store, kg

M_{ss} = solution in store, kg

Q_{rs}=heat transfer from the refrigerant to ambient air, kW

U_{rs} = internal energy of refrigerant in store, kJ

U_{ss} = internal energy of solution in store, kJ

The above equations were solved with first order approximation using Euler integration method.

7.4 SYSTEM PERFORMANCE

The hourly cooling loads for each day of the 365 days in the year were estimated for the two applications. The result showed that the cooling loads are a maximum at the month of March. Hence, the results presented here are for 21st of March, which has been taken as the design day for the location considered (6.45^{o}N).

For the given set of operating temperatures, the rates of heat transfer, mass of refrigerant and solution stored, and the performance curves, are shown in figures 7.3 to 7.6, pages 218 to 221, for the office cooling application, and figures 7.7 to 7.10, pages 222 to 225, for the beef cold storage application. The incident solar radiation on the collector surface is shown in figure 7.11, page 226, and the collector and generator temperatures are shown in figure 7.12, page 227 .

Figures 7.3 and 7.4 show that generation starts at about 8.00, and stops just after 16.00 when the collector outlet temperature can not sustain generation.

For the office application, figure 7.4 shows that the refrigerant store level at the start of generation is about 32 kg, and the refrigerant produced between 8.00 and 9.00 is stored until the start of occupancy. The refrigerant generated between 9.00 and 10.00 is just sufficient to meet the cooling load. Then from 10.00 to 14.00, as the generator temperature rises, more

refrigerant is produced than it is required and the refrigerant storage rate increases. At 15.00 when the cooling load exceeds the evaporator load, refrigerant is drawn from the store to meet the cooling demand. When the generation finally ceases at 16.00, the cooling load is met entirely from the store until 17.00 when the system is switched off.

Figure 7.5 shows the solution storage rate. The store is at the lowest level at the time when the refrigerant store level is at the highest. At the start and end of the day, the solution storage level is always at the highest.

Figure 7.6 shows the variations of the collector efficiency η_c , absorption cycle COP, and the overall instantaneous efficiency (η_cCOP). The maximum overall efficiency achieved is about 0.14 .

For the cold store application, the cooling requirement is continuous over the 24 hour period. Therefore, sufficient refrigerant must be in store to satisfy the cooling load both during the day and night. Figure 7.8 shows that at 1.00 the refrigerant in store is about 316 kg. Between this time and the start of generation the store level has been reduced to about 14 kg . The start of generation at 8.00 and continuous rise of the generator temperature increases the store level to the highest level at about 15.00 . When the generation

stops at about 16.00, enough refrigerant has been stored to meet the cooling load from then till the next day. Figure 7.9 shows the solution storage rate. The lowest level occurs at the time of highest refrigerant store level .

The variations of the collector efficiency, absorption cycle COP, and the overall instantaneous efficiency is shown in figure 7.10 . The maximum overall efficiency is about 0.1 .

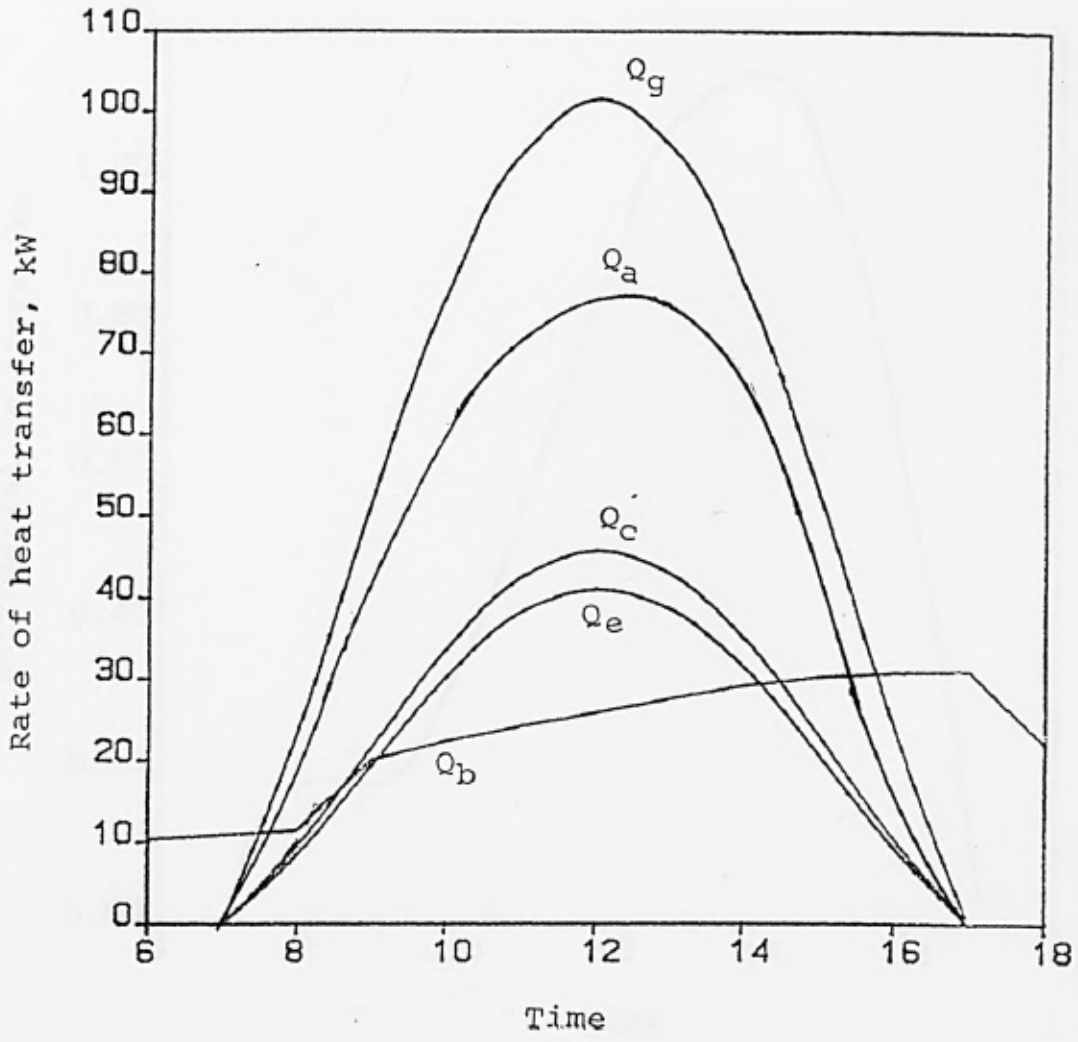


Fig. 7.3 Heat transfer rates for the office building application, $T_{rm} = 25^{o}C$, $T_e = 7^{o}$, $A_c = 410\ m^2$

Q_g = generator energy
Q_a = absorber heat rejection
Q_c = condenser duty
Q_e = evaporator load
Q_b = building cooling load

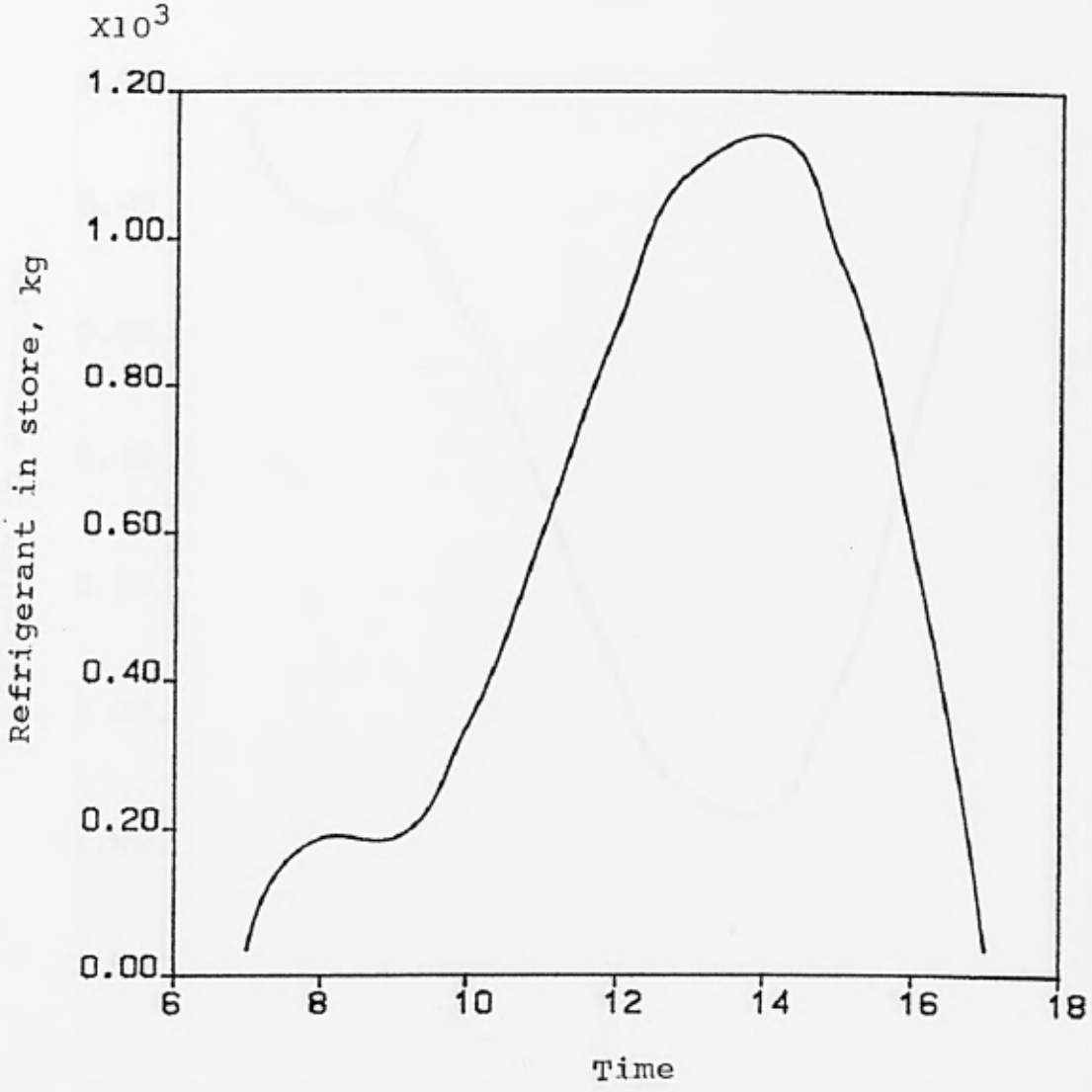


Fig. 7.4 Refrigerant store for the office building application, $T_{rm} = 25^{o}C$, $T_e = 7^{o}C$, $A_c = 410\ m^2$, $XL_{store,i} = 0.4927$

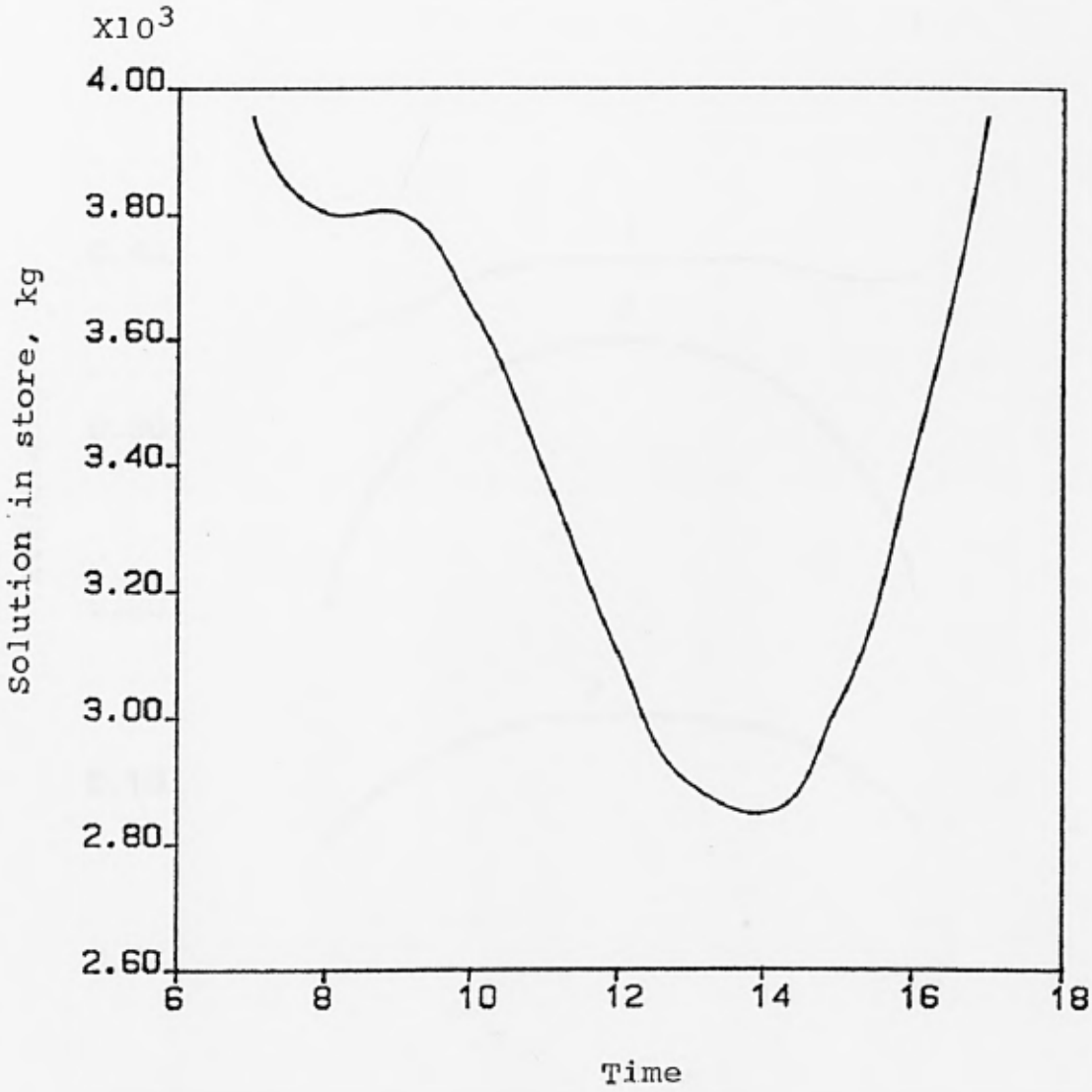


Fig. 7.5 Solution store for the office building application, $T_{rm} = 25^{o}C$, $T_e = 7^{o}C$, $A_c = 410\ m^2$, $XL_{store,i} = 0.4927$

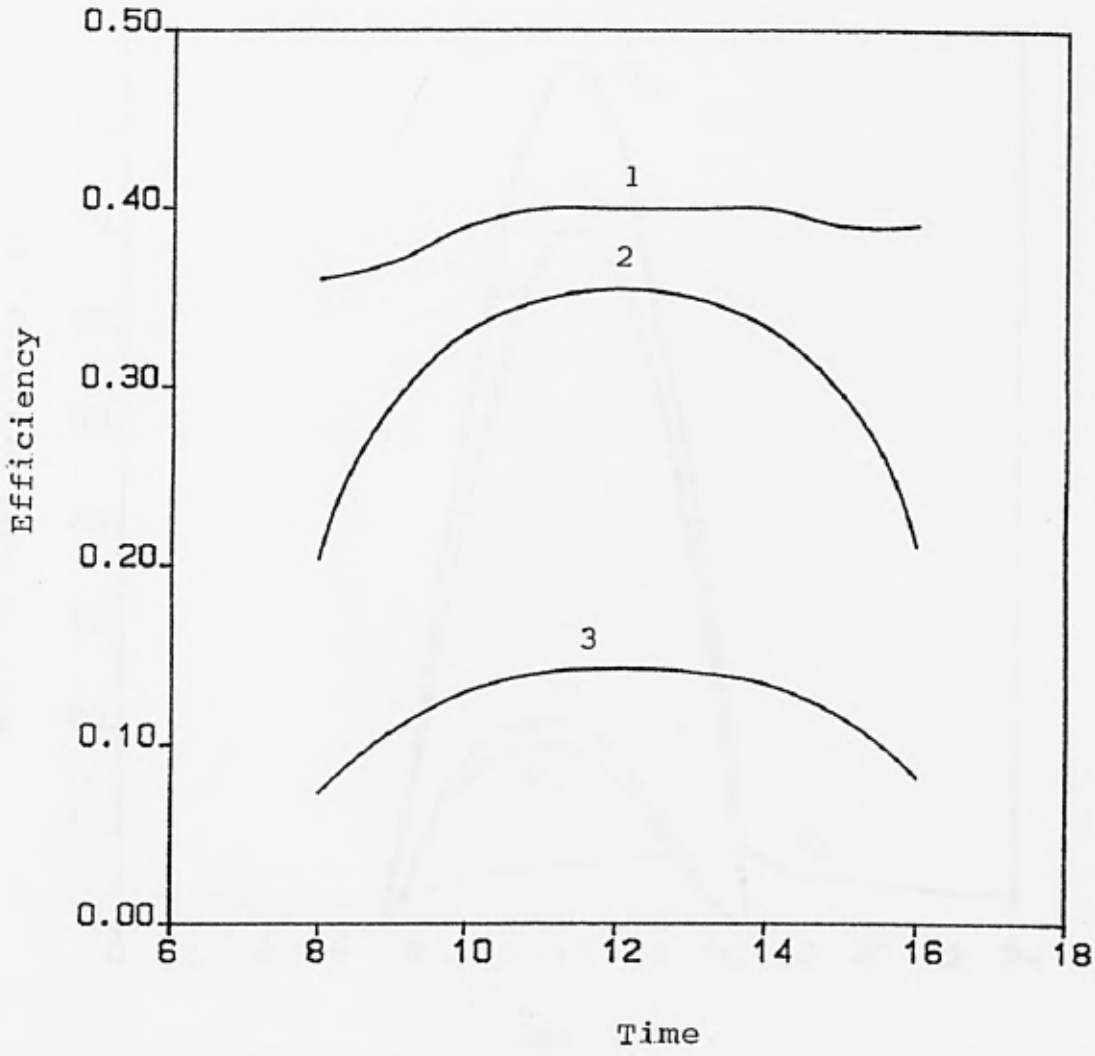


Fig. 7.6 System performance for the office building application.

1, Absorption cycle COP
2, Collector thermal efficiency, η_c
3, Overall instantaneous efficiency, (η_c COP)

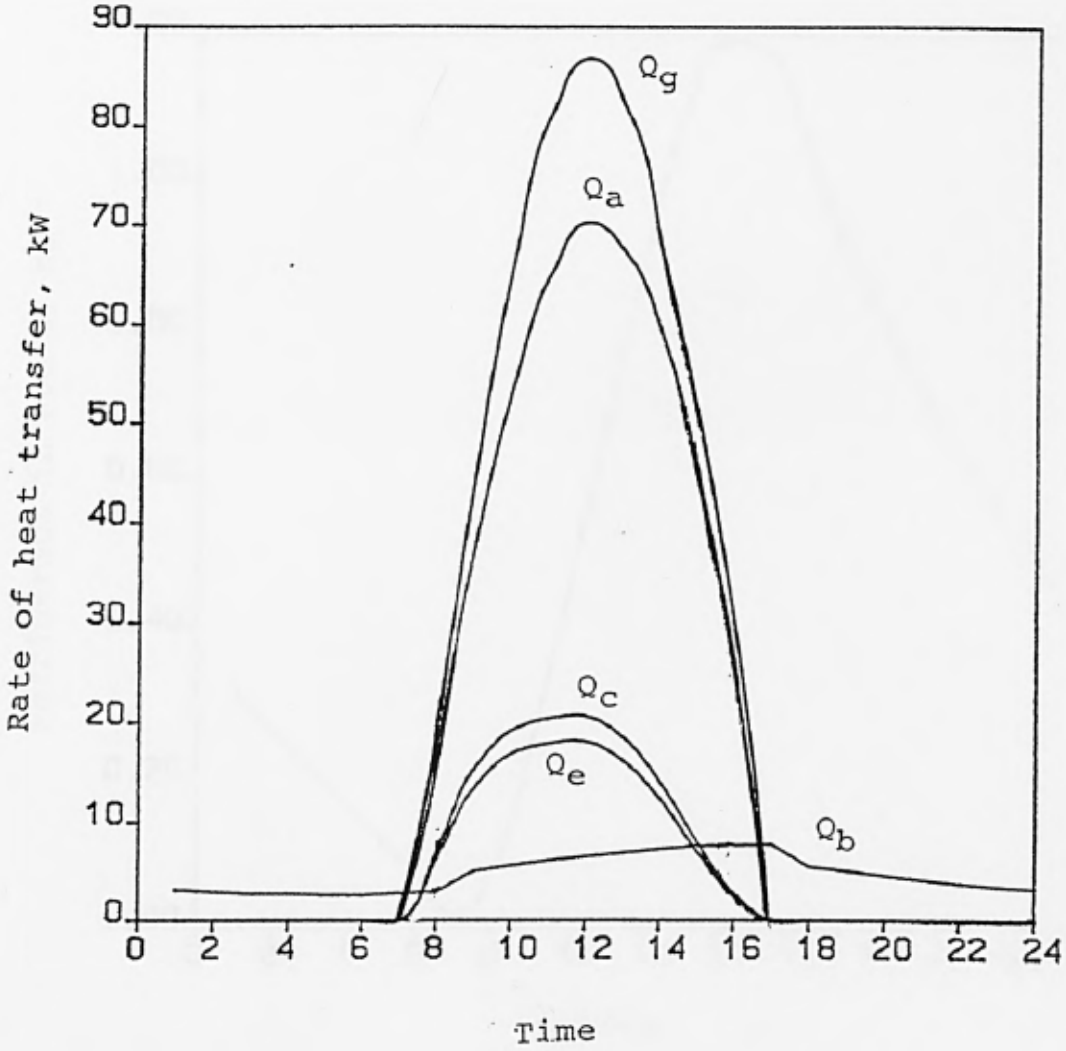


Fig. 7.7 Heat transfer rates for the beef cold storage application, $T_{rm} = 1.7^{o}C$, $T_e = -7^{o}C$, $A_c = 350\ m^2$

Q_g = generator energy
Q_a = absorber heat rejection
Q_c = condenser duty
Q_e = evaporator load
Q_b = cold store cooling load

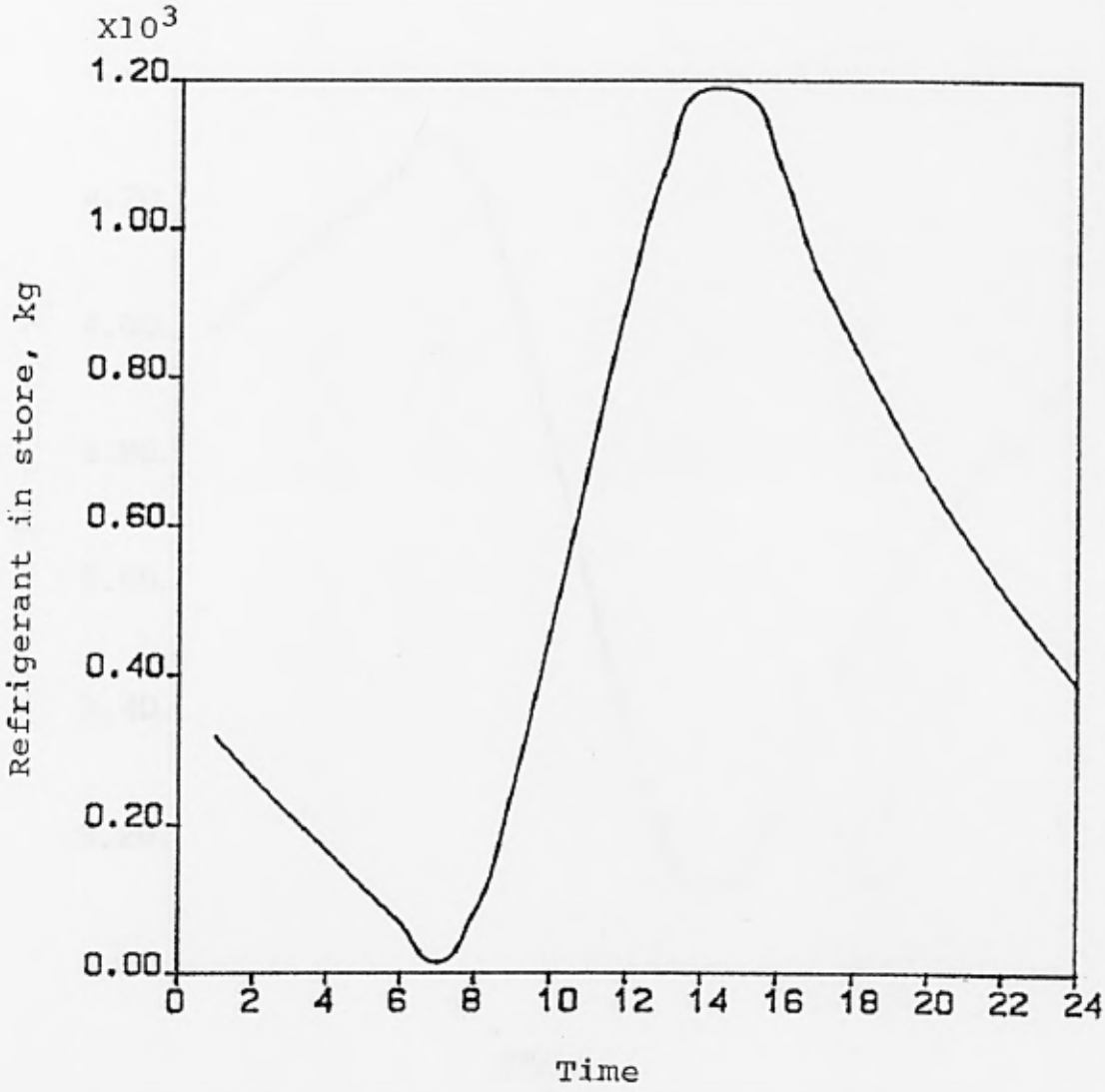


Fig. 7.8 Refrigerant store for the beef cold storage application, $T_{rm} = 1.7^{o}C$, $T_{e} = -7^{o}C$, $A_{c} = 350\ m^{2}$, $XL_{store,i} = 0.385$

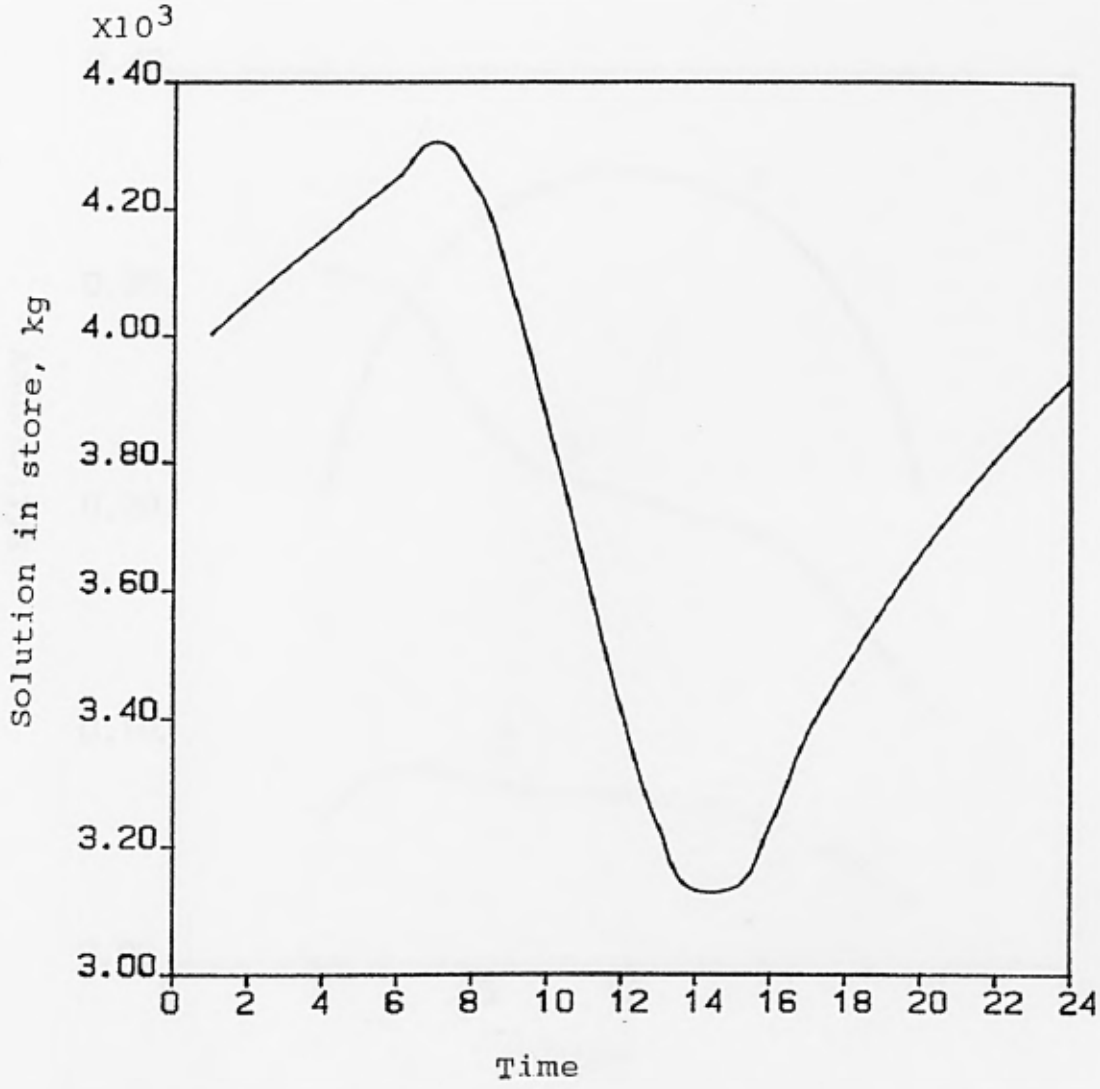


Fig. 7.9 Solution store for the beef cold storage application, $T_{rm} = 1.7^{o}$, $T_{e} = -7^{o}C$, $A_{c} = 350\ m^{2}$, $XL_{store,i} = 0.385$

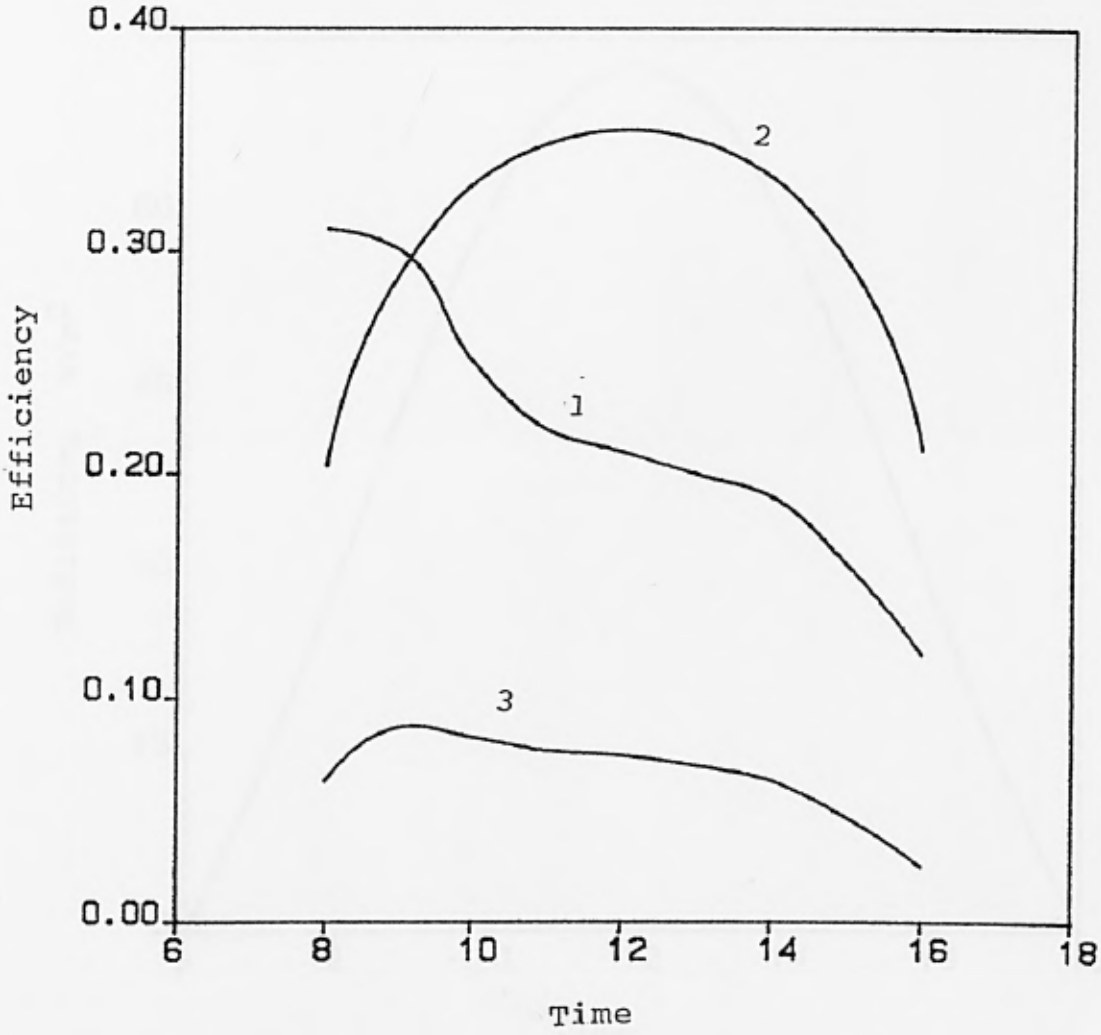


Fig. 7.10 System performance for the beef cold storage application.

1, Absorption cycle COP
2, Collector thermal efficiency, η_c
3, Overall instantaneous efficiency, (η_c COP)

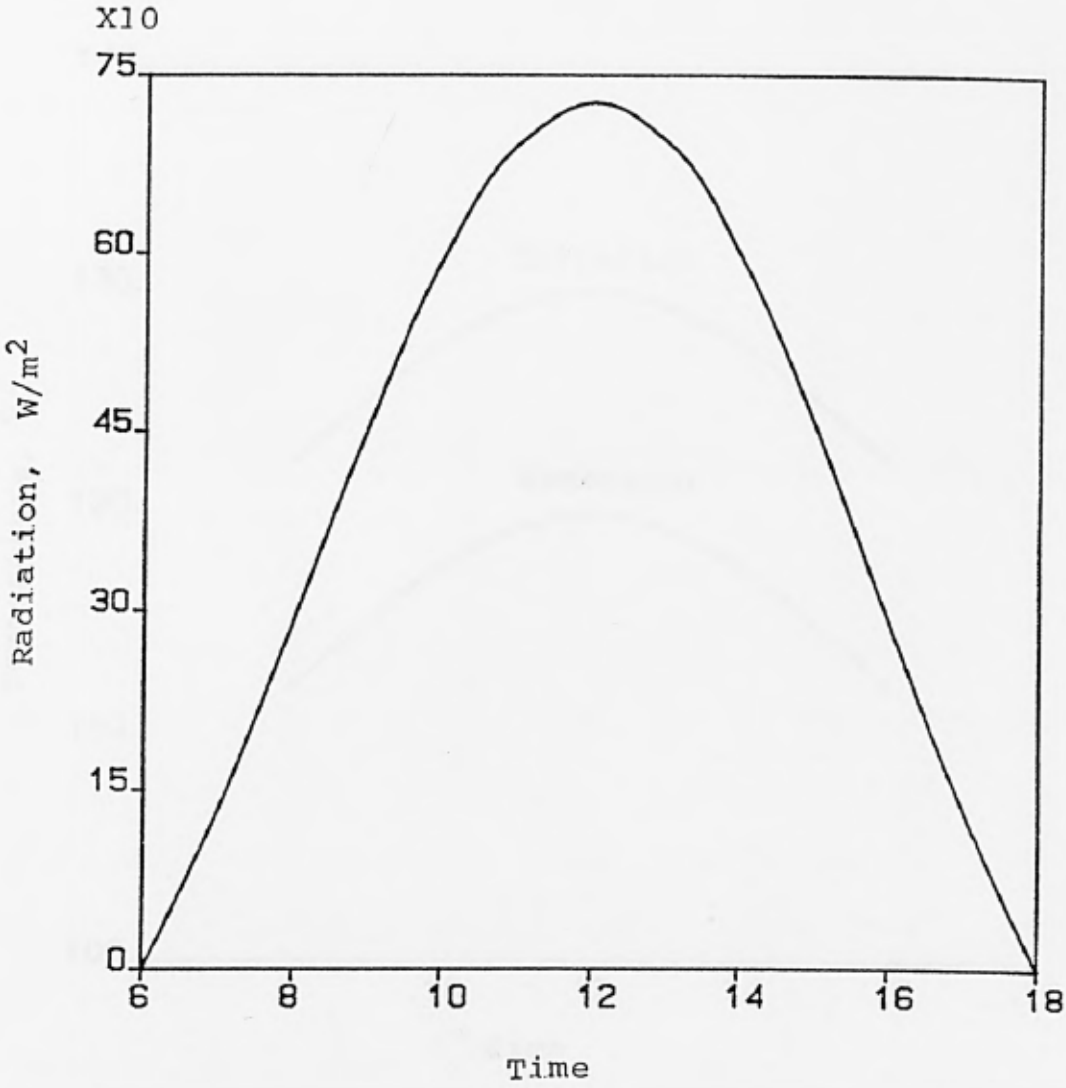


Fig 7.11 Solar radiation incident on the Collector surface on 21st March at latitude 6.45°N for, θ_a = 15°, S = 15°

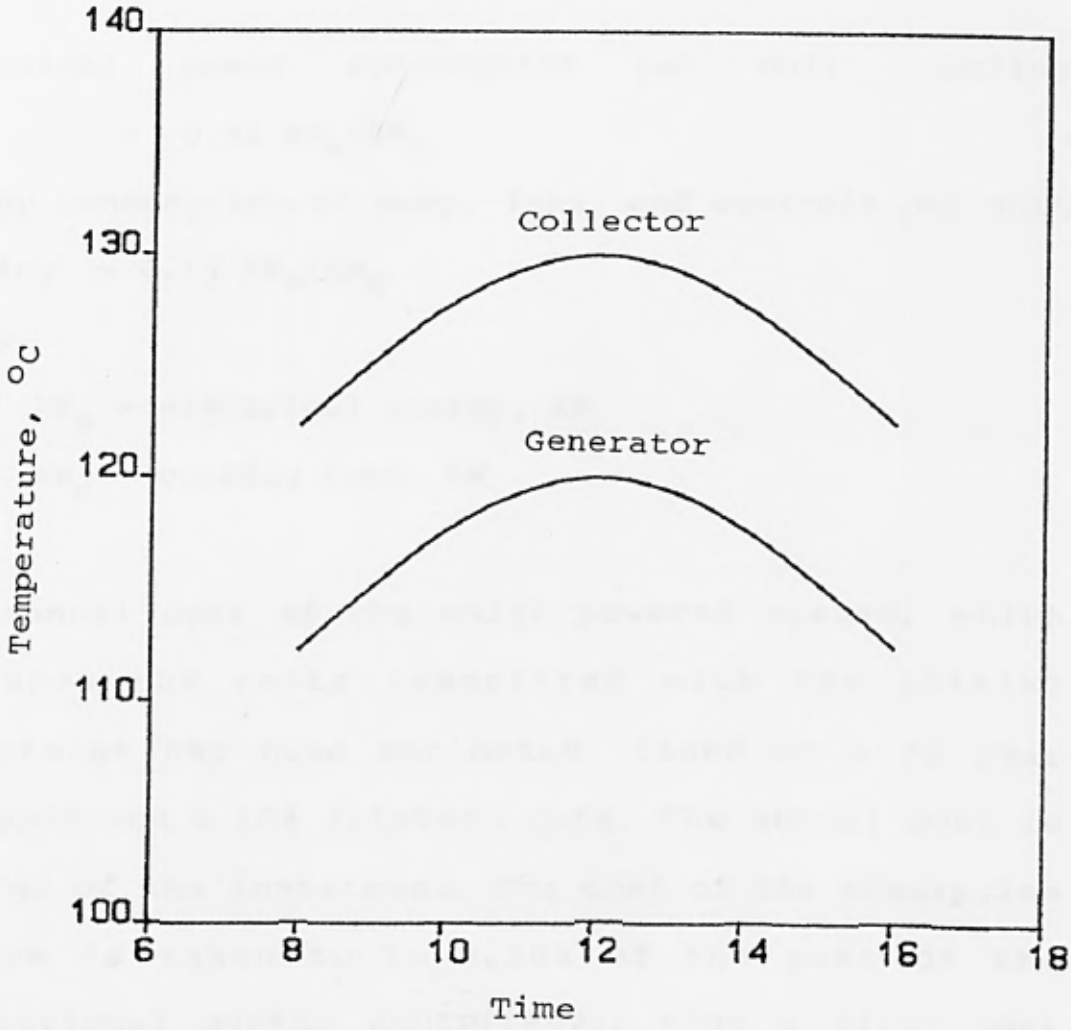


Fig. 7.12 Collector outlet water temperature and Generator temperature, for $\theta_a = 15^{o}$, $S = 15^{o}$, for 21st March at Latitude $6.45^{o}N$

7.5 ECONOMIC COMPARISON

To compare the annual cost of the solar powered system with a conventional vapour compression system, the following factors have been assumed :

Electrical power consumption per unit cooling

$$= 0.41\ kW_e/kW_c$$

Energy consumption of pump, fans, and controls per unit cooling $= 0.14\ kW_e/kW_c$

Where,

kW_e = electrical energy, kW

kW_c = cooling load, kW

The annual cost of the solar powered system, which includes the costs associated with the initial investment has been estimated. Based on a 20 year lifespan and a 10% interest rate, the annual cost is 0.11746 of the investment. The cost of the absorption system is taken to be 1.28% of the cost of the conventional system EQUIP(1982), plus a first cost penalty of $1500 .

The total cost of the solar powered refrigeration system, including the equipment costs, operation and maintenance of the system, in dollars ($) per year is estimated from the equation given by Duffie and Beckman (1974) :

$$C_{a,sy} = [(C_c + C_{st})A_c + C_{a,E} + C_{pp}] I + P\ ce + C_{ml} \quad 7.14$$

Where,

$C_{a,sy}$ = annual cost of the solar powered system, $

C_c = capital cost per unit area of collector, $220/m^2

A_c = total collector area, m^2

C_{st} = capital cost of storage, $16/m^2 collector area

$C_{a,E}$ = capital cost of absorption system

C_{pp} = capital cost of pumps, fans, and controls, $800

I = fraction of investment charged per year, 0.11746

P = annual power requirement of the pumps, fans, and controls, 0.14 kW_e/kW_c

ce = unit cost of electricity, 9 C/kW-hr

C_{ml} = annual cost of maintenance and labour, $300

The electrical energy requirement of the conventional system per year is given by :

$$E_c = (0.41\ kW_e/kW_c)\ (\text{total yearly cooling load})$$

The annual cost of the conventional system is given by :

$$C_{c,sy} = (C_{c,E})\ I + E_c\ ce + C_{ml} \quad 6.15$$

Where,

$C_{c,sy}$ = annual cost of conventional system, $

$C_{c,E}$ = capital cost of conventional sytem, $135/$kW_c$

E_c = electrical energy requirement of the system

C_{ml} = annual cost of maintenance, \$800

Table 7.3, page 232, shows the office building monthly cooling load and the year total which has been used to estimate the annual costs. Based on the above cost assumptions, the annual cost of the solar powered system for the office cooling application is about three times the cost of the conventional system. The annual costs are \$3940 and \$13,220 for the conventional system and the solar powered system respectively. The solar collector area of 410 m^2 used in the above cost estimate would power the solar system without any need for auxilliary power source, for the total daily cooling load of 248 kW .

The cost of electrical power consumed by the conventional system constitutes the major fraction of its annual cost, whereas the capital costs of the collector and the storage system account for a large proportion of the solar system cost.

7.6 CONCLUSION

A cooling load computer program based on the ASHRAE transfer function method has been developed. Actual observed solar radiation data were used instead of clear day and assumed cloud covers values. The values of solar heat gain factors and sol-air temperatures calculated for location 6.45^{o}N have been compared with the ASHRAE

(1981) values. The ASHRAE values were found to be 15 to 25% higher, and would result in oversizing of the cooling system if it were used. Using actual observed solar radiation data to estimate the cooling load thus provide a more accurate design of a cooling system either powered by solar or conventional energy sources.

Storage of refrigerant and solution for the solar powered aqua-ammonia system have been shown to be thermodynamically feasible. Refrigerant stored during the day can be used for night cooling, or to sustain cooling during part of the day.

The diurnal values of the collector thermal efficiency, coefficient of performance of the absorption cycle, and the overall instantaneous efficiency for the office building cooling application are higher than those of the cold storage application. This is due to the higher evaporator temperature of 7°C required for the office application compared to the -7°C for the cold storage. This shows the need of high evaporating temperature if high perfomance values are desirable.

For the solar powered aqua-ammonia system to be economically competitive with the conventional system, the costs of the CPC collector and the equipment must be reduced to about one-third of the assumed values.

Table 7.3 Monthly cooling load for the office building

Month	Cooling load, kW
Jan	6464.9
Feb	6199.7
Mar	6996.0
Apr	6543.6
May	6745.0
Jun	5791.2
Jul	5573.8
Aug	5640.9
Sep	5639.2
Oct	6112.1
Nov	6293.4
Dec	6712.1
Total(year)	747112

CHAPTER 8

CONCLUSION

8.1 GENERAL REMARKS

The collection time for the trough-like CPC solar collector has been described, and can be obtained by testing the conditions :

$(S - \theta_a) \lesssim (\tan^{-1}(\tan\theta_z \cos \gamma_s)) \lesssim (S + \theta_a)$ given by equation 3.41. The simple test shows the effect of orientation and slope on the collection time, and can be used to determine the collector optimal orientation and slope for any given location and period. Using this simple technique, the number of seasonal tilt adjustments required for minimum 7 hour per day collection time for various acceptance angles have been determined as shown in tables 3.2 to 3.6 . The results give good agreement with the work of Rabl(1976a) on tracking requirements of solar concentrators.

The results for the geometric parameters of the CPC solar collector with tubular receiver, obtained from the collector model agreed with the result of McIntire(1979) within $\pm$ 2% . The average number of reflections, $\langle n \rangle_i$, for acceptance angles between 30 and 20^o determined from the model also agreed with the result of Carvalho(1985). In the absence of any data for acceptance angles less than 20^o, the calculated values of $\langle n \rangle_i$ were compared with the result of Rabl(1976a) for CPC solar collector with fin receiver. The average

values for the fin receiver are within ± 5.5% for the same parameters.

To predict the performance of a solar collector, the collector loss coefficient, U_l, must be known. In the absence of any empirical equation for calculating the top loss coefficient for the CPC solar collector with nonevacuated tubular receiver, an analytical solution based on heat transfer formulations has been made. This allows the use of computer modeling to calculate U_t, and to use the calculated U_t to develop correlation equations. The values of U_t calculated were compared with those for a CPC Collector with nonevacuated flat plate receiver by Rabl(1976c). The general trend was found to be in good agreement, however, the values for the flat plate receiver were higher by about 17% for the same concentration ratio and operating parameters.

Accuracy of the correlation equations 4.79 and 4.80 was determined and found to be well correlated with the input data of U_t. The correlation coefficients are 98 and 99%, and the standard deviations are 0.26 and 0.29 . The correlation is restricted to values of receiver temperature between 45 and 300°C, ambient temperature from 10 to 40°C, receiver surface emittance between 0.1 and 0.9, collector slope from 5 to 30°, acceptance angles between 30 and 6°, concentration ratio from 1.5 to 8, and heat transfer coefficient for wind blowing over the collector glazing between 5 and 30 $W/m^2\,°C$.

The average number of reflections in the CPC, <n>, is a function of the concentration ratio, the degree of truncation and the incidence angle. It has been used to estimate the effective emissivity in the collector, which is then used in the calculation of the top loss coefficient, U_t. Hence, it has not been used as one of the independent variables in the correlation.

The developed CPC solar collector model was used to predict its performance, using the weather data for the location 6.45°N. The results have shown that outlet water temperature up to 140°C is obtainable with acceptance angles from 20° and concentration ratio from 2.5 upwards, with two or less than six seasonal tilt adjustments.

The property data equations for the NH_3-H_2O mixtures which have been developed is readily adaptable to a computer program. The equations, obtained from polynomia regression of the mixtures property data, are well correlated with the original data of Macriss (1964). Correlation coefficient between 95 and 98%, and standard deviation between 0.15 and 0.35 were obtained.

To predict the performance of the NH_3-H_2O absorption cycle, the property data equations and the cycle model were programmed. The results have shown the influence of the operating temperatures on the cycle performance. To operate the cycle with a generator temperature below

120°C for low temperature applications below 0°C requires a water-cooled condenser and absorber. For air-cooled condenser and absorber, the delivery energy temperature to the generator must be greater than 120°C. The results also show that for any given set of operating temperatures, there is a minimum generation temperature below which the operation of the cycle is not possible.

The developed cooling load program provides the hourly cooling load required for the accurate design of a cooling system. Actual observed solar radiation data were used to calculate the solar heat gain factors and the sol-air temperatures. Comparison of these values with those of ASHRAE(1981) for the same location of 6.45°N, showed the ASHRAE values to be higher by between 15 and 25% . To the author, the use of long-term averages of actual observed solar radiation is more accurate than the use of clear day and asumed cloud cover values.

Simulation of the combined system of the CPC solar collector and the NH_3-H_2O absorption cycle have shown that, application of the system is possible for cooling of office building and refrigerated products. The storage of refrigerant and solution for the system has been shown to be thermodynamically feasible. If hot water storage is considered for the office building cooling application with 410m^2 collector area, at 50L/m^2

a total storage capacity of 20,500 litre would be needed compared to less than 4500 kg required for both the refrigerant and solution stores. If the heat losses from a hot water store at above 130°C is also considered with the storage of the refrigerant and solution at ambient temperature, then the advantage of the later is validated. Although the refrigerant store would require a thicker container because of the NH_3-H_2O cycle high side pressure.

The collector area has been sized to provide the amount of energy required to generate sufficient refrigerant that would meet the cooling load for the desired period. For the office building cooling application with a total evaporator load of 248 kW between 9.00 and 17.00, the required collector area is 410 m^2 . Whereas a total cooling load of 113 kW between 1.00 and 24.00 for the cold storage application is met by 350 m^2 collector area.

Comparison of the total annual cost of the solar-powered NH_3-H_2O system with a conventional vapour compression system show the cost of the solar system to be about three times higher. The cost of the collector and storage constitutes the major fraction of the solar system total cost, whereas the cost of electrical power accounts for a large proportion of the total cost of the conventional system. The solar system would be more economical if the collector and storage cost is reduced

to about 30% of the assumed costs. The small electrical power demand of the solar system, however makes it suitable for use in many developing countries where electrical power generation and availability is limited.

Finally, while the technical conclusions which demonstrate the feasibility and thermodynamic efficiencies of the solar-powered system are not greatly dependent upon the quality of assumptions made, the economic comparison is critically dependent upon the assumed cost values, and only allow tentative and contigent conclusions.

8.2 FUTURE DEVELOPMENT

The following suggestions are made for further investigation in the future:

(a) The absorption cycle components design calculations for optimal sizing of the components

(b) Construction of a prototype system with refrigerant and solution storage for experimental study.

(c) Economic optimization of the CPC solar collector, the aqua-ammonia system, and the refrigerant and solution storage.

It is hoped that with the above investigations, improvements in the system performance and costs would result.

A P P E N D I X A

Table A1 Collection dates for CPC collector(minimum collection time 7hr/day) tilted at an angle S towards the equator : $\theta_a = 7^{\circ}$, $\phi = 4^{\circ}N$

	COLLECTION DATES			
TILT (S°)	5	7	10	13
JAN	–	–	–	–
FEB	–	–	26 - 28	19 - 28
MAR	7 - 31	3 - 31	1 - 22	1 - 16
APR	1 - 20	1 - 24	8 - 30	16 - 30
MAY	–	–	1	1 - 9
JUN	–	–	–	–
JUL	–	–	–	–
AUG	23 - 31	19 - 31	12 - 31	4 - 27
SEP	1 - 30	1 - 30	1-4,21-30	27 - 30
OCT	1 - 6	1 - 10	1 - 15	1 - 22
NOV	–	–	–	–
DEC	–	–	–	–

Table A1 cont.

	COLLECTION DATES			
TILT (S^{o})	15	16	18	22
JAN	–	–	–	28 - 31
FEB	15 - 28	13 - 28	8 - 28	1 - 21
MAR	1 - 12	1 - 10	1 - 3	–
APR	21 - 30	24 - 30	30	–
MAY	1 - 15	1 - 19	1 - 27	16 - 31
JUN	–	–	–	1 - 30
JUL	29 - 31	25 - 31	17 - 31	1 - 28
AUG	1 - 22	1 - 19	1 - 13	–
SEP	–	–	–	–
OCT	1 - 26	3 - 28	10 - 31	20 - 31
NOV	–	–	1 - 2	1 - 13
DEC	–	–	–	–

Table A1 cont.

COLLECTION DATES				
TILT (S°)	23	25	29	S>35
JAN	25 - 31	17 - 31	1 - 28	_
FEB	1 - 18	1 - 12	_	_
MAR	_	_	_	_
APR	_	_	_	_
MAY	21 - 31	_	_	_
JUN	1 - 30	1 - 30	_	_
JUL	1 - 23	1 - 12	_	_
AUG	_	_	_	_
SEP	_	_	_	_
OCT	23 - 31	29 - 31	_	_
NOV	1 - 16	1 - 24	13 - 30	_
DEC	_	_	1 - 31	_

Table A2 Collection dates for CPC collector(minimum collection time 7hr/day) tilted at an angle S towards the equator : $\theta_a = 7^{\circ}$, $\phi = 6.25^{\circ}N$

C O L L E C T I O N D A T E S				
TILT (S°)	5	7	10	14
JAN	–	–	–	–
FEB	–	–	–	22 - 28
MAR	11 - 31	8 - 31	2 - 26	1 - 19
APR	1 - 24	1 - 29	14 - 30	25 - 30
MAY	–	–	1 - 7	1 - 20
JUN	–	–	–	–
JUL	–	–	–	24 - 31
AUG	19 - 31	14 - 31	6 - 29	1 - 18
SEP	1 - 30	1 - 30	17 - 30	24 - 30
OCT	1 - 2	1 - 5	1 - 11	1 - 19
NOV	–	–	–	–
DEC	–	–	–	–

Table A2 cont.

COLLECTION DATES				
TILT (S^{o})	15	19	20	21
JAN	–	–	–	–
FEB	20 - 28	11 - 28	9 - 28	6 - 28
MAR	1 - 17	1 - 6,8	1 - 4	1
APR	27 - 30	–	–	–
MAY	1 - 24	13 - 31	17 - 31	22 - 31
JUN	–	1 - 30	1 - 30	1 - 30
JUL	20 - 31	1 - 31	1 - 27	1 - 22
AUG	1 - 16	–	–	–
SEP	26 - 30	–	–	–
OCT	1 - 21	5 - 30	9 - 31	12 - 31
NOV	–	–	1	1 - 4
DEC	–	–	–	–

Table A2 cont.

COLLECTION DATES				
TILT (S^{O})	24	31	35	S>37
JAN	29 - 31	1 - 29	1 - 10	_
FEB	1 - 21	_	_	_
MAR	_	_	_	_
APR	_	_	_	_
MAY	_	_	_	_
JUN	14 - 29	_	_	_
JUL	_	_	_	_
AUG	_	_	_	_
SEP	_	_	_	_
OCT	20 - 31	_	_	_
NOV	1 - 12	12 - 30	_	_
DEC	_	1 - 31	1 - 31	_

Table A3 Collection dates for CPC collector(minimum collection time 7hr/day) tilted at an angle S towards the equator : $\theta_a = 7^{\circ}$, $\phi = 14^{\circ}N$

	COLLECTION DATES			
TILT (S°)	5	7	11	15
JAN	–	–	–	–
FEB	–	–	–	–
MAR	26 - 31	22 - 31	14 - 31	7 - 31
APR	1 - 30	1 - 30	1 - 8	–
MAY	1 - 15	1 - 23	12 - 31	–
JUN	–	–	1 - 30	1 - 30
JUL	29 - 31	21 - 31	1 - 31	1 - 12
AUG	1 - 31	1 - 31	1	–
SEP	1 - 17	1 - 21	4 - 29	12 - 30
OCT	–	–	–	1 - 6
NOV	–	–	–	–
DEC	–	–	–	–

Table A3 cont.

COLLECTION DATES				
TILT (S^{O})	20	22	25	30
JAN	–	–	–	–
FEB	26 - 28	22 - 28	15 - 28	3 - 26
MAR	1 - 22	1 - 18	1 - 12	–
APR	–	–	–	–
MAY	–	–	–	–
JUN	–	–	–	–
JUL	–	–	–	–
AUG	–	–	–	–
SEP	21 - 30	25 - 30	–	–
OCT	1 - 15	1 - 19	1 - 26	15 - 31
NOV	–	–	–	1 - 7
DEC	–	–	–	–

Table A3 cont.

COLLECTION DATES				
TILT (S^{o})	32	35	39	40
JAN	29 - 31	17 - 31	1 - 28	1 - 24
FEB	1 - 21	1 - 12	–	–
MAR	–	–	–	–
APR	–	–	–	–
MAY	–	–	–	–
JUN	–	–	–	–
JUL	–	–	–	–
AUG	–	–	–	–
SEP	–	–	–	–
OCT	20 - 31	29 - 31	–	–
NOV	1 - 13	1 - 24	13 - 30	17 - 30
DEC	–	–	1 - 31	1 - 31

Table A4 Collection dates for CPC collector(minimum collection time 7hr/day) tilted at an angle S towards the equator : $\theta_a = 10^{o}$, $\phi = 4^{o}N$

COLLECTION DATES				
TILT (S^{o})	5	10	15	20
JAN	–	–	–	–
FEB	–	19 - 28	8 - 28	1 - 28
MAR	1 - 31	1 - 31	1 - 18	1 - 7
APR	1 - 26	1 - 30	10 - 30	27 - 30
MAY	–	1 - 9	1 - 27	1 - 31
JUN	–	–	–	1 - 30
JUL	–	–	17 - 31	1 - 31
AUG	17 - 31	4 - 31	1 - 30	1 - 16
SEP	1 - 30	1 - 30	2,25-30	–
OCT	1 - 12	1 - 22	1 - 31	6 - 31
NOV	–	–	1 - 2	1 - 16
DEC	–	–	–	–

Table A4 cont.

COLLECTION DATES				
TILT (S^{o})	25	30	35	S>39
JAN	1 - 31	1 - 31	1 - 18	_
FEB	1 - 21	1 - 6	_	_
MAR	_	_	_	_
APR	_	_	_	_
MAY	14 - 31	_	_	_
JUN	1 - 30	15 - 28	_	_
JUL	1 - 30	_	_	_
AUG	_	_	_	_
SEP	_	_	_	_
OCT	20 - 31	_	_	_
NOV	1 - 30	4 - 30	23 - 30	_
DEC	1 - 12	1 - 31	1 - 31	_

Table A5 Collection dates for CPC collector(minimum collection time 7hr/day) tilted at an angle S towards the equator : $\theta_a = 10^{\circ}$, $\phi = 6.25^{\circ}N$

COLLECTION DATES				
TILT (S°)	5	10	15	20
JAN	–	–	–	–
FEB	–	24 - 28	13 - 28	1 - 28
MAR	6 - 31	1 - 31	1 - 23	1 - 12
APR	1 - 30	1 - 30	19 - 30	–
MAY	1 - 2	1 - 16	1 - 31	4 - 31
JUN	–	–	1-13,30	1 - 30
JUL	–	28 - 31	1 - 31	1 - 31
AUG	11 - 31	1 - 31	1 - 24	1 - 9
SEP	1 - 30	1 - 30	20 - 30	–
OCT	1 - 7	1 - 17	1 - 28	1 - 31
NOV	–	–	–	1 - 9
DEC	–	–	–	–

Table A5 cont.

COLLECTION DATES				
TILT (S^{O})	25	30	35	40
JAN	14 - 31	1 - 31	1 - 27	_
FEB	1 - 27	1 - 13	_	_
MAR	1	_	_	_
APR	_	_	_	_
MAY	24 - 31	_	_	_
JUN	1 - 30	_	_	_
JUL	1 - 20	_	_	_
AUG	_	_	_	_
SEP	_	_	_	_
OCT	12 - 31	28 - 31	_	_
NOV	1 - 27	1 - 30	14 - 30	_
DEC	_	1 - 31	1 - 31	13 - 31

Table A6 Collection dates for CPC collector(minimum collection time 7hr/day) tilted at an angle S towards the equator : $\theta_a = 10^{o}$, $\phi = 14^{o}N$

COLLECTION DATES				
TILT (S^{o})	5	10	15	20
JAN	–	–	–	–
FEB	–	–	–	19 - 28
MAR	20 - 31	11 - 31	1 - 31	1 - 28
APR	1 - 30	1 - 30	1 - 6	–
MAY	1 - 27	1 - 31	14 - 31	–
JUN	–	1 - 30	1 - 30	15 - 28
JUL	17 - 31	1 - 31	1 - 30	–
AUG	1 - 31	1 - 31	–	–
SEP	1 - 23	1 - 30	6 - 30	15 - 30
OCT	–	1 - 2	1 - 12	1 - 22
NOV	–	–	–	–
DEC	–	–	–	–

Table A6 cont.

COLLECTION DATES				
TILT (s^{o})	25	30	36	40
JAN	–	25 - 31	1 - 31	1 - 31
FEB	8 - 28	1 - 28	1 - 18	1 - 6
MAR	1 - 18	1 - 7	–	–
APR	–	–	–	–
MAY	–	–	–	–
JUN	–	–	–	–
JUL	–	–	–	–
AUG	–	–	–	–
SEP	25 - 30	–	–	–
OCT	1 - 31	6 - 31	23 - 31	–
NOV	1 - 2	1 - 16	1 - 30	4 - 30
DEC	–	–	1 - 31	1 - 31

Table A7 Collection dates for CPC collector(minimum collection time 7hr/day) tilted at an angle S towards the equator : $\theta_a = 15^{\circ}$, $\phi = 4^{\circ}N$

COLLECTION DATES				
TILT (S°)	5	10	15	20
JAN	–	–	25 - 31	1 - 31
FEB	19 - 28	8 - 28	1 - 28	1 - 28
MAR	1 - 31	1 - 31	1 - 31	1 - 18
APR	1 - 30	1 - 30	1 - 30	10 - 30
MAY	1 - 9	1 - 27	1 - 31	1 - 31
JUN	–	–	1 - 30	1 - 30
JUL	–	17 - 31	1 - 31	1 - 31
AUG	4 - 31	1 - 31	1 - 31	1 - 31
SEP	1 - 30	1 - 30	1 - 30	1-2,25-30
OCT	1 - 22	1 - 31	1 - 31	1 - 31
NOV	–	1 - 2	1 - 16	1 - 30
DEC	–	–	–	1 - 12

Table A7 cont.

COLLECTION DATES				
TILT (S^{O})	25	30	35	40
JAN	1 - 31	1 - 31	1 - 31	1 - 18
FEB	1 - 28	1 - 24	1-6,9-11	_
MAR	1 - 7	_	_	_
APR	23 - 30	_	_	_
MAY	1 - 31	14 - 31	_	_
JUN	1 - 30	1 - 30	15 - 28	_
JUL	1 - 31	1 - 30	_	_
AUG	1 - 20	_	_	_
SEP	_	_	_	_
OCT	6 - 31	17 - 31	30 - 31	_
NOV	1 - 30	1 - 30	1,4 - 30	23 - 30
DEC	1 - 31	1 - 31	1 - 31	1 - 31

Table A8 Collection dates for CPC collector(minimum collection time 7hr/day) tilted at an angle S towards the equator : $\theta_a = 15^o$, $\phi = 6.25^oN$

	COLLECTION DATES			
TILT (S^o)	5	10	15	20
JAN	–	–	–	14 - 31
FEB	24 - 28	13 - 28	1 - 28	1 - 28
MAR	1 - 31	1 - 31	1 - 31	1 - 23
APR	1 - 30	1 - 30	1 - 30	16 - 30
MAY	1 - 16	1 - 31	1 - 31	1 - 31
JUN	–	1 - 13,30	1 - 30	1 - 30
JUL	28 - 31	1 - 31	1 - 31	1 - 31
AUG	1 - 31	1 - 31	1 - 31	1 - 27
SEP	1 - 30	1 - 30	1 - 30	20 - 30
OCT	1 - 17	1 - 28	1 - 31	1 - 31
NOV	–	–	1 - 9	1 - 27
DEC	–	–	–	–

Table A8 cont.

COLLECTION DATES				
TILT (S^{O})	25	30	35	40
JAN	1 - 31	1 - 31	1 - 31	1 - 27
FEB	1 - 28	1 - 28	1 - 17	_
MAR	1 - 12	1	_	_
APR	29 - 30	_	_	_
MAY	1,4 - 31	24 - 31	_	_
JUN	1 - 30	1 - 30	_	_
JUL	1 - 31	1 - 20	_	_
AUG	1 - 9,12 -14	_	_	_
SEP	_	_	_	_
OCT	1 - 31	12 - 31	24 - 31	_
NOV	1 - 30	1 - 30	1 - 30	14 - 30
DEC	1 - 31	1 - 31	1 - 31	1 - 31

Table A9 Collection dates for CPC collector(minimum collection time 7hr/day) tilted at an angle S towards the equator : $\theta_a = 15^{\circ}$, $\phi = 14^{\circ}N$

	COLLECTION DATES			
TILT (S°)	5	10	15	20
JAN	–	–	–	–
FEB	–	–	19 - 28	8 - 28
MAR	11 - 31	1 - 31	1 - 31	1 - 31
APR	1 - 30	1 - 30	1 - 30	1 - 6
MAY	1 - 31	1 - 31	1 - 31	14 - 31
JUN	1 - 30	1 - 30	1 - 30	1 - 30
JUL	1 - 31	1 - 31	1 - 31	1 - 30
AUG	1 - 31	1 - 31	1 - 31	–
SEP	1 - 30	1 - 30	1 - 30	6 - 30
OCT	1 - 2	1 - 12	1 - 22	1 - 31
NOV	–	–	–	1 - 2
DEC	–	–	–	–

Table A9 cont.

COLLECTION DATES				
TILT (S^{o})	25	31	35	40
JAN	25 - 31	1 - 31	1 - 31	1 - 31
FEB	1 - 28	1 - 28	1 - 28	1 - 24
MAR	1 - 28	1 - 16	1 - 7	–
APR	–	–	–	–
MAY	–	–	–	–
JUN	15 - 28	–	–	–
JUL	–	–	–	–
AUG	–	–	–	–
SEP	15 - 30	27 - 30	–	–
OCT	1 - 31	1 - 31	6 - 31	17 - 31
NOV	1 - 16	1 - 30	1 - 30	1 - 30
DEC	–	1 - 31	1 - 31	1 - 31

Table A10 Collection dates for CPC collector(minimum collection time 7hr/day) tilted at an angle S towards the equator : $\theta_a = 20^o$, $\phi = 4^oN$

	COLLECTION DATES			
TILT (S^o)	5	10	15	20
JAN	_	25 - 31	1 - 31	1 - 31
FEB	8 - 28	1 - 28	1 - 28	1 - 28
MAR	1 - 31	1 - 31	1 - 31	1 - 31
APR	1 - 30	1 - 30	1 - 30	1 - 30
MAY	1 - 27	1 - 31	1 - 31	1 - 31
JUN	_	1 - 30	1 - 30	1 - 30
JUL	17 - 31	1 - 31	1 - 31	1 - 31
AUG	1 - 31	1 - 31	1 - 31	1 - 31
SEP	1 - 30	1 - 30	1 - 30	1 - 30
OCT	1 - 31	1 - 31	1 - 31	1 - 31
NOV	1 - 2	1 - 16	1 - 30	1 - 30
DEC	_	_	1 -12	1 - 31

Table A10 cont.

COLLECTION DATES				
TILT (S^{O})	25	30	35	40
JAN	1 - 31	1 - 31	1 - 31	1 - 31
FEB	1 - 28	1 - 28	1 - 24	1 - 11
MAR	1 - 18	1 - 7	–	–
APR	10 - 30	23 - 30	–	–
MAY	1 - 31	1 - 31	7 - 31	26 - 31
JUN	1 - 30	1 - 30	1 - 30	1 - 30
JUL	1 - 31	1 - 31	1 - 31	1 - 18
AUG	1 - 31	1 - 20	1 - 6	–
SEP	1-2,25-30	–	–	–
OCT	1 - 31	6 - 31	17 - 31	30 - 31
NOV	1 - 30	1 - 30	1 - 30	1 - 30
DEC	1 - 31	1 - 31	1 - 31	1 - 31

Table A11 Collection dates for CPC collector(minimum collection time 7hr/day) tilted at an angle S towards the equator : $\theta_a = 20^\circ$, $\phi = 6.25^\circ N$

COLLECTION DATES				
TILT (S°)	5	10	15	20
JAN	–	–	14 - 31	1 - 31
FEB	1 - 28	1 - 28	1 - 28	1 - 28
MAR	1 - 31	1 - 31	1 - 31	1 - 31
APR	1 - 30	1 - 30	1 - 30	1 - 30
MAY	1 - 31	1 - 31	1 - 31	1 - 31
JUN	1 - 13,30	1 - 30	1 - 30	1 - 30
JUL	1 - 31	1 - 31	1 - 31	1 - 31
AUG	1 - 31	1 - 31	1 - 31	1 - 31
SEP	1 - 30	1 - 30	1 - 30	1 - 30
OCT	1 - 28	1 - 31	1 - 31	1 - 31
NOV	–	1 - 9	1 - 27	1 - 30
DEC	–	–	–	1 - 31

Table A11 cont.

COLLECTION DATES				
TILT (S^{o})	25	30	35	40
JAN	1 - 31	1 - 31	1 - 31	1 - 31
FEB	1 - 28	1 - 28	1 - 28	1 - 17
MAR	1 - 23	1 - 12	1	–
APR	16 - 30	29 - 30	–	–
MAY	1 - 31	1 - 31	14 - 31	–
JUN	1 - 30	1 - 30	1 - 30	12 - 30
JUL	1 - 31	1 - 31	1 - 30	1
AUG	1 -27	1 - 14	–	–
SEP	20 - 30	–	–	–
OCT	1 - 31	1 - 31	12 - 31	24 - 31
NOV	1 - 30	1 - 30	1 - 30	1 - 30
DEC	1 - 31	1 - 31	1 - 31	1 - 31

Table A12 Collection dates for CPC collector(minimum collection time 7hr/day) tilted at an angle S towards the equator : $\theta_a = 20^\circ$, $\phi = 14^\circ N$

	COLLECTION DATES			
TILT (S°)	5	10	15	20
JAN	–	–	–	25 - 31
FEB	–	19 - 28	8 - 28	1 - 28
MAR	1 - 31	1 - 31	1 - 31	1 - 31
APR	1 - 30	1 - 30	1 - 30	1 - 30
MAY	1 - 31	1 - 31	1 - 31	1 - 31
JUN	1 - 30	1 - 30	1 - 30	1 - 30
JUL	1 - 31	1 - 31	1 - 31	1 - 31
AUG	1 - 31	1 - 31	1 - 31	1 - 31
SEP	1 - 30	1 - 30	1 - 30	1 - 30
OCT	1 - 12	1 - 22	1 - 31	1 - 31
NOV	–	–	1 - 2	1 - 16
DEC	–	–	–	–

Table A12 cont.

COLLECTION DATES				
TILT (S^{O})	25	30	35	40
JAN	1 - 31	1 - 31	1 - 31	1 - 31
FEB	1 - 28	1 - 28	1 - 28	1 - 28
MAR	1 - 31	1 - 28	1 - 18	1 - 7
APR	1 - 6	_	_	_
MAY	7 - 31	26 - 31	_	_
JUN	1 - 30	1 - 30	_	_
JUL	1 - 31	1 - 18	_	_
AUG	1 - 6	_	_	_
SEP	6 - 30	15 - 30	25 - 30	_
OCT	1 - 31	1 - 31	1 - 31	6 - 31
NOV	1 - 30	1 - 30	1 - 30	1 - 30
DEC	1 - 12	1 - 31	1 - 31	1 - 30

Table A13 Collection dates for CPC collector(minimum collection time 7hr/day) tilted at an angle S towards the equator : $\theta_a = 30^o$, $\phi = 4^oN$

C O L L E C T I O N	D A T E S			
TILT (S^o)	5	6<S<30	35	40
JAN	1 - 31	1 - 31	1 - 31	1 - 31
FEB	1 - 28	1 - 28	1 - 28	1 - 28
MAR	1 - 31	1 - 31	1 - 18	1 - 7
APR	1 - 30	1 - 30	10 - 30	23 - 30
MAY	1 - 31	1 - 31	1 - 31	1 - 31
JUN	1 - 30	1 - 30	1 - 30	1 - 30
JUL	1 - 31	1 - 31	1 - 31	1 - 31
AUG	1 - 31	1 - 31	1 - 31	1 - 20
SEP	1 - 30	1 - 30	1-2,25-30	_
OCT	1 - 31	1 - 31	1 - 31	6 - 31
NOV	1 - 30	1 - 30	1 - 30	1 - 30
DEC	1 - 12	1 - 31	1 - 31	1 - 31

Table A14 Collection dates for CPC collector(minimum collection time 7hr/day) tilted at an angle S towards the equator : $\theta_a = 30^{\circ}$, $\phi = 6.25^{\circ}N$

C O L L E C T I O N D A T E S				
TILT (S°)	5	8<S<30	35	40
JAN	14 - 31	1 - 31	1 - 31	1 - 31
FEB	1 - 28	1 - 28	1 - 28	1 - 28
MAR	1 - 31	1 - 31	1 - 23	1 - 12
APR	1 - 30	1 - 30	16 - 30	29 - 30
MAY	1 - 31	1 - 31	1 - 31	1 - 31
JUN	1 - 30	1 - 30	1 - 30	1 - 30
JUL	1 - 31	1 - 31	1 - 31	1 - 31
AUG	1 - 31	1 - 31	1 - 27	1 - 14
SEP	1 - 30	1 - 30	20 - 30	_
OCT	1 - 31	1 - 31	1 - 31	1 - 31
NOV	1 - 27	1 - 30	1 - 30	1 - 30
DEC	_	1 - 31	1 - 31	1 - 31

Table A15 Collection dates for CPC collector(minimum collection time 7hr/day) tilted at an angle S towards the equator : $\theta_a = 30^\circ$, $\phi = 14^\circ N$

	COLLECTION DATES			
TILT (S°)	5	15	20<S<30	40
JAN	_	1 - 31	1 - 31	1 - 31
FEB	8 - 28	1 - 28	1 - 28	1 - 28
MAR	1 - 31	1 - 31	1 - 31	1 - 28
APR	1 - 30	1 - 30	1 - 30	_
MAY	1 - 31	1 - 31	1 - 31	26 - 31
JUN	1 - 30	1 - 30	1 - 30	1 - 30
JUL	1 - 31	1 - 31	1 - 31	1 - 18
AUG	1 - 31	1 - 31	1 - 31	_
SEP	1 - 30	1 - 30	1 - 30	15 - 30
OCT	1 - 31	1 - 31	1 - 31	1 - 31
NOV	1 - 2	1 - 30	1 - 30	1 - 30
DEC	_	1 - 12	1 - 31	1 - 31

Table A16 THE CPC COLLECTOR SIMULATION INPUT DATA

Collector specification :

D_o = 0.015

D_i = 0.01275

θ_a = 30, 20, 15 and 10°

C = 1.5, 2.4, 3.3, and 4.7

g = 0.005

L_C = 1.0

Radiation data :

Daily radiation data for Lagos (6.45°N)

Ambient condition :

Daily ambient temperature for Lagos (6.45°)

Wind velocity = 5 m/s

Heat transfer medium (Water) :

V_w = 0.0088 m/s or M = 0.0112 Kg/m^2,s

Thermophysical properties of water from property data equations in appendix D.

Material properties :

Glass refractive index = 1.526

ϵ_c = 0.88 ; ρ_c = 0.1

$\alpha_{b,s} = \alpha_{d,s}$ = (0.9 for black paint; 0.89 for Cu black)

$\epsilon_{b,s} = \epsilon_{d,s}$ = (0.9 for black paint; 0.17 for Cu black)

ρ_r = 0.85 ; ϵ_r = 0.15

ρ_s = 0.1

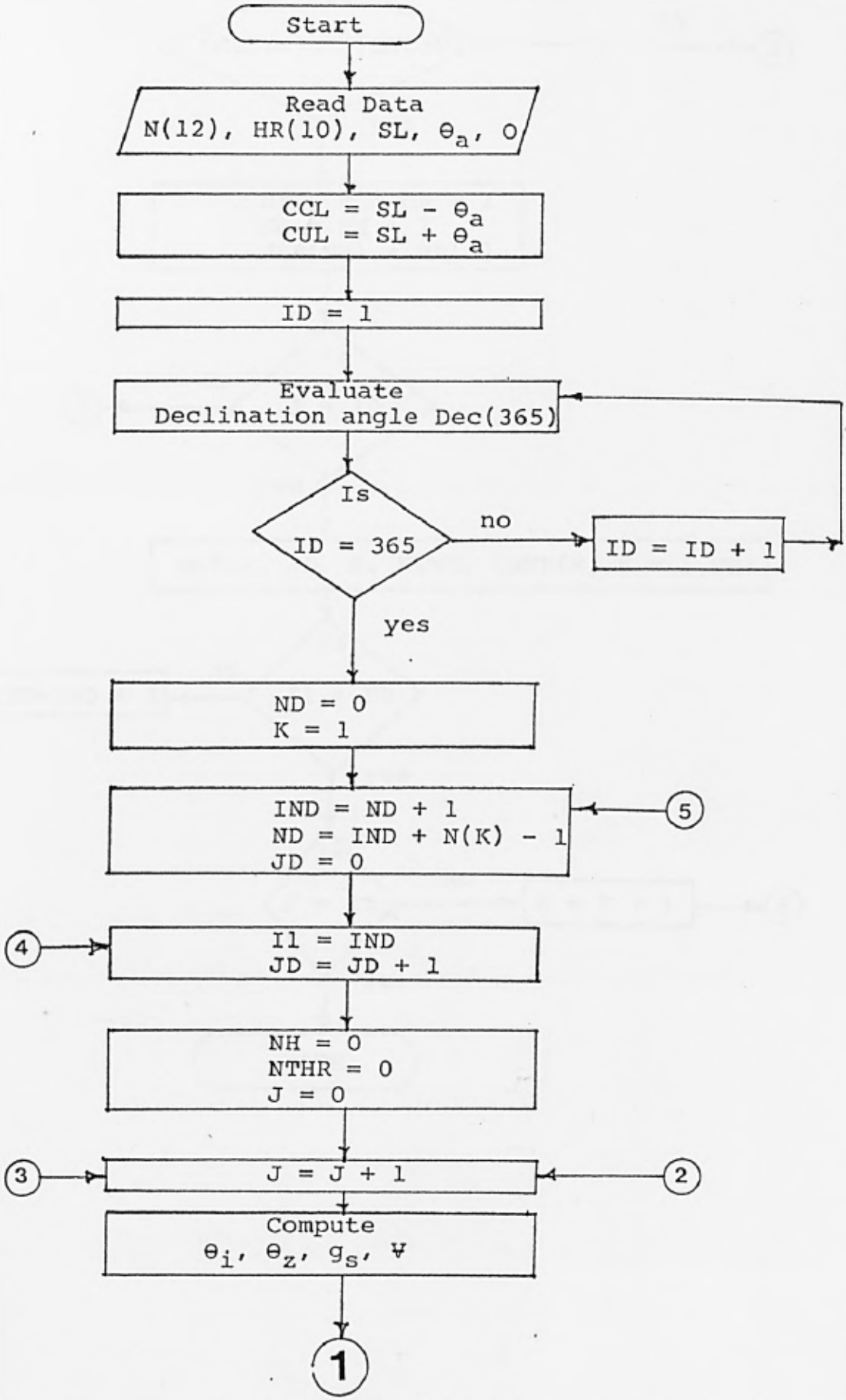
A P P E N D I X B

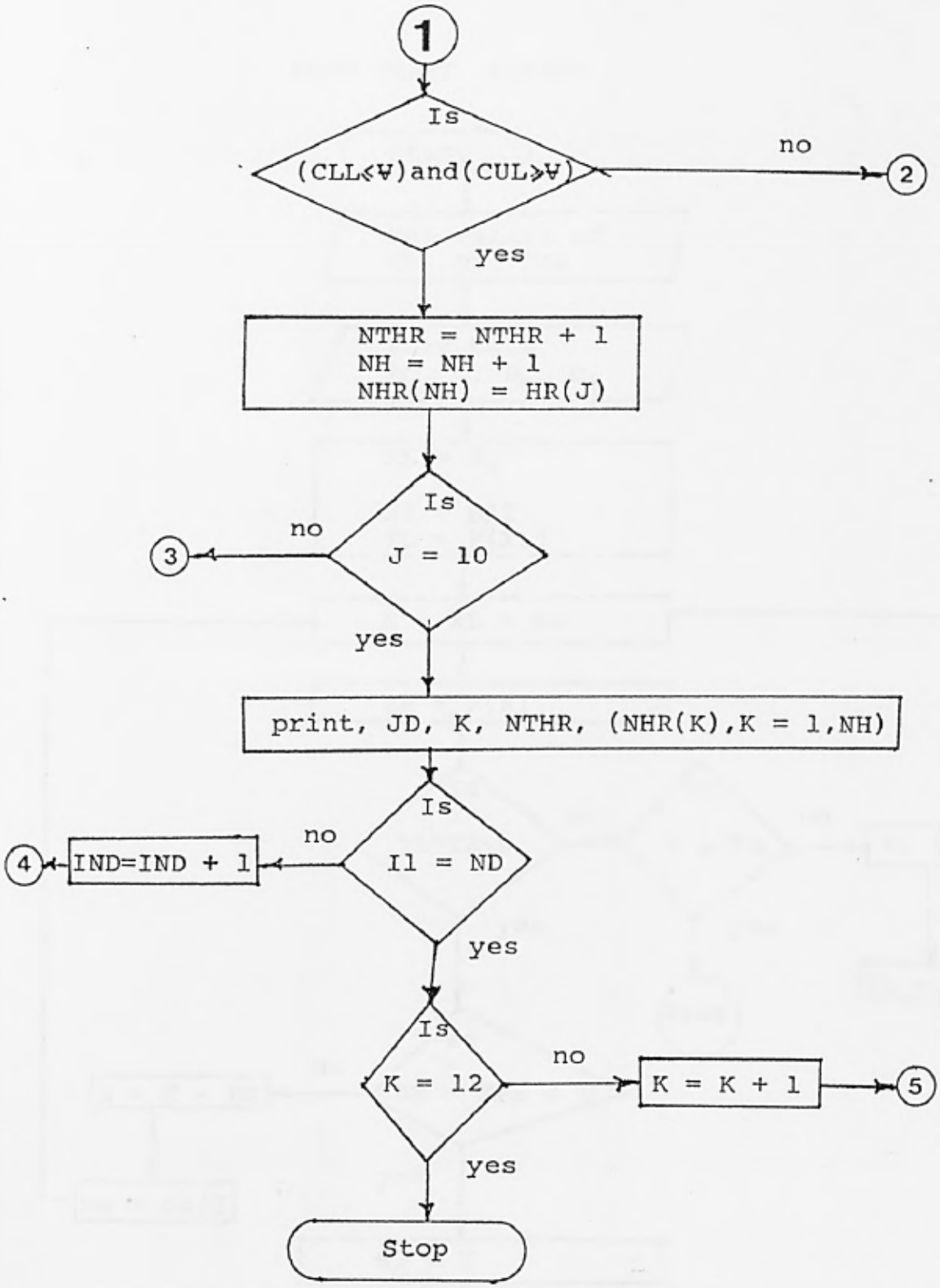
Computer programs (pages 270-304) removed for copyright reasons

APPENDIX C

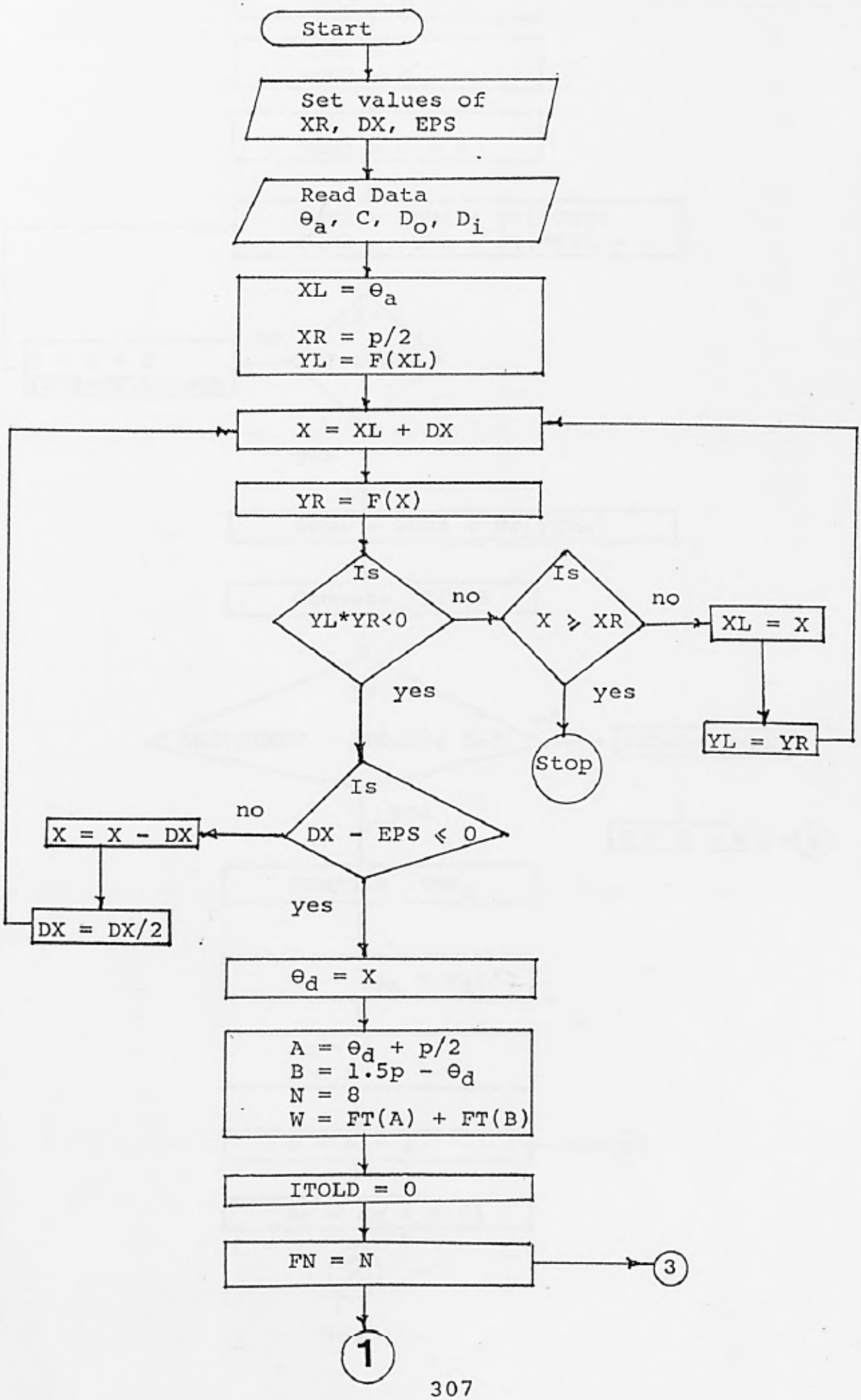


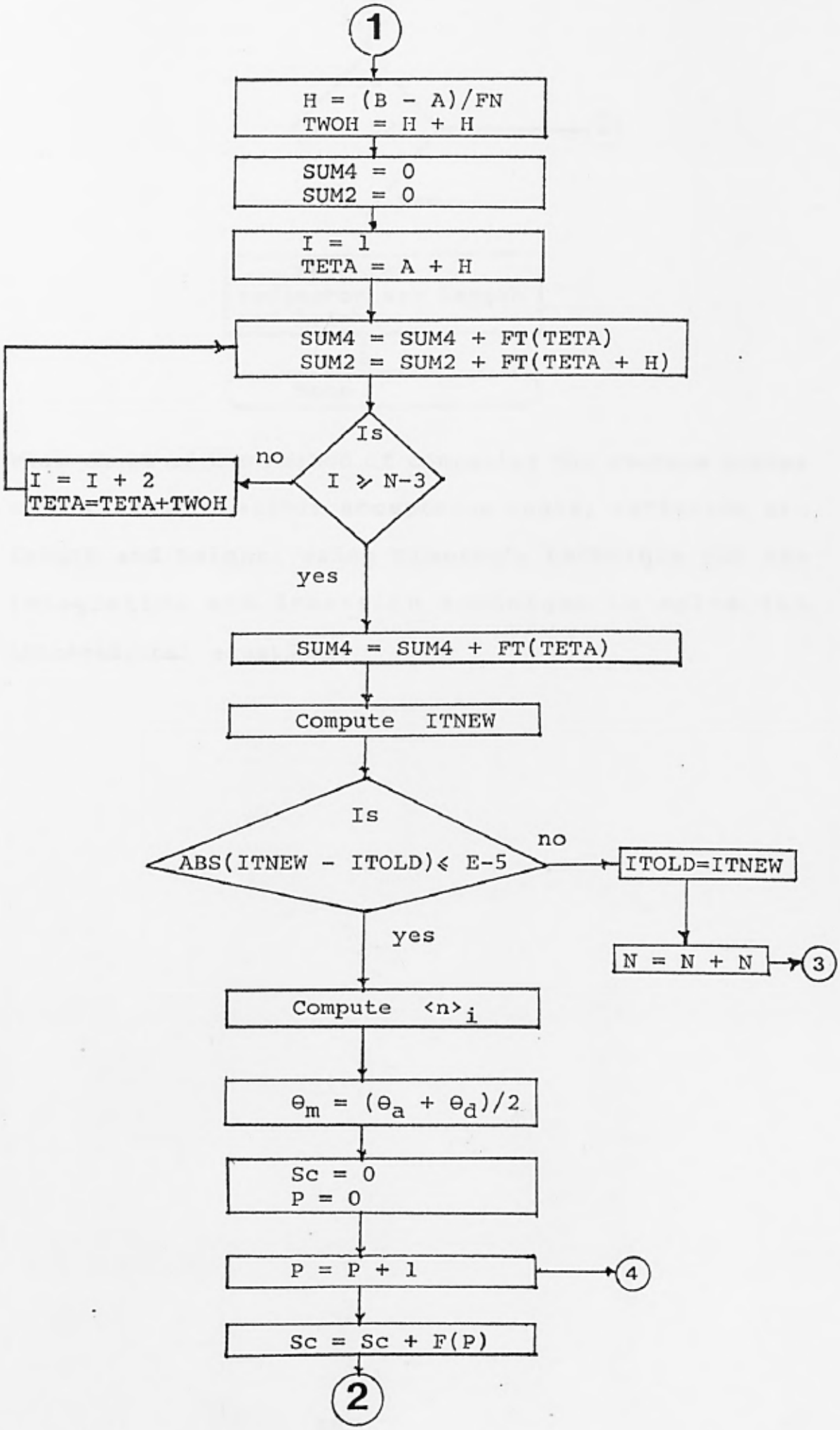
FLOW CHART FLACCP

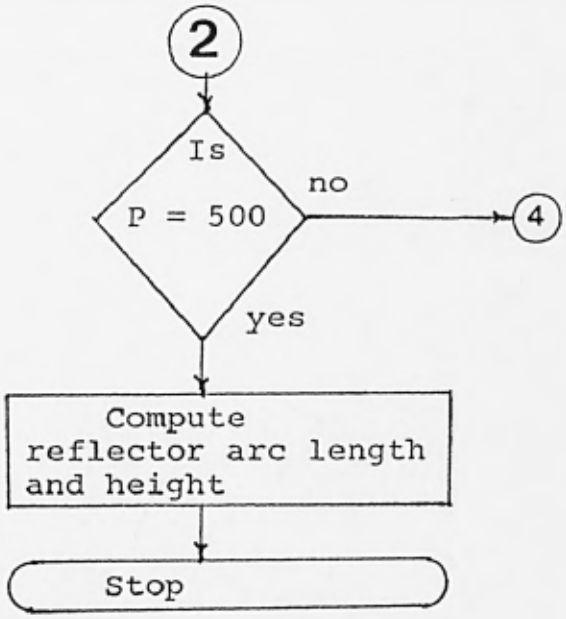



1
Is
(CLL≤W)and(CUL≥W)
no
2
yes
NTHR = NTHR + 1
NH = NH + 1
NHR(NH) = HR(J)
Is
J = 10
no
3
yes
print, JD, K, NTHR, (NHR(K),K = 1,NH)
Is
I1 = ND
no
4
IND=IND + 1
yes
Is
K = 12
no
K = K + 1
5
yes
Stop

FLOW CHART FLPROP

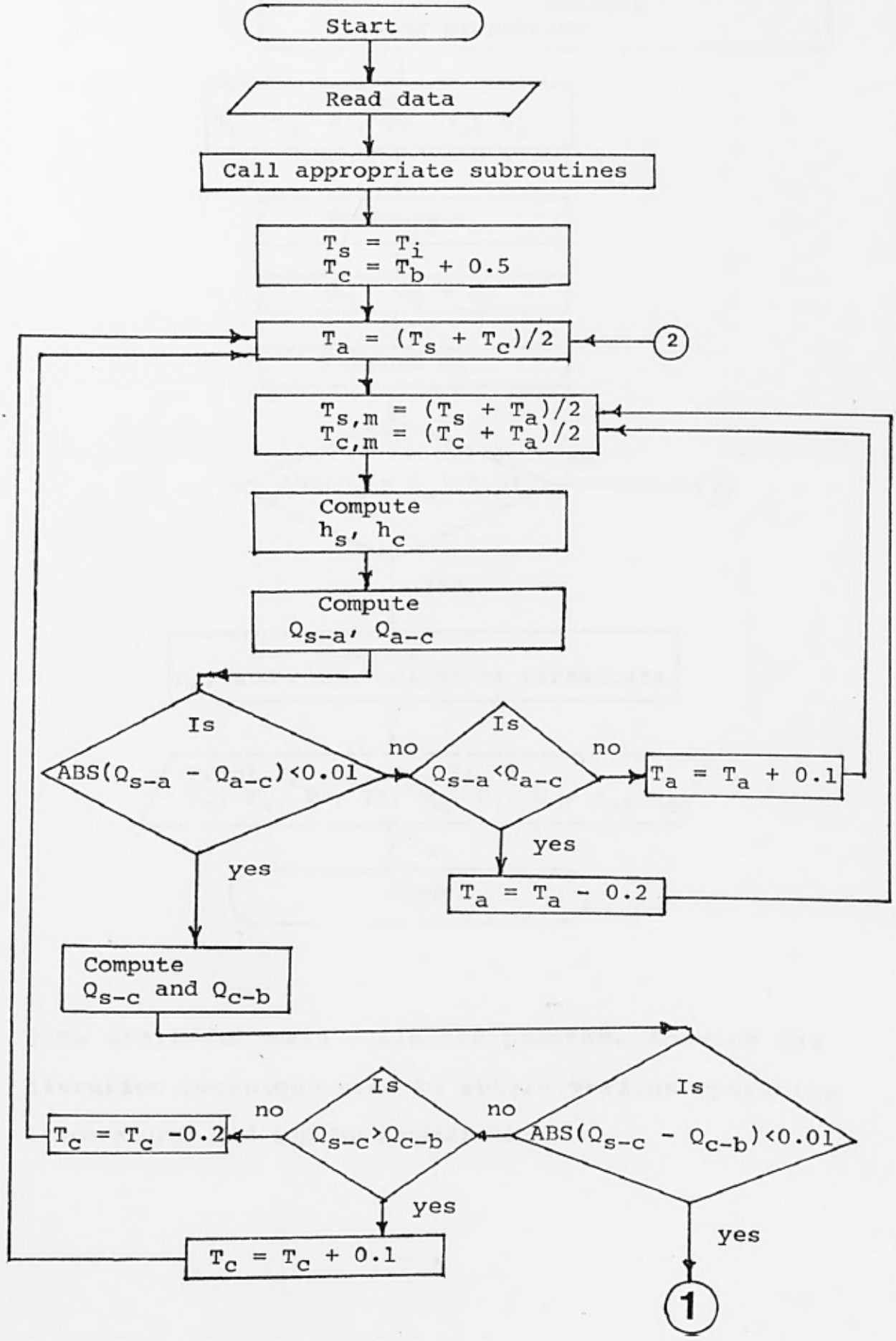


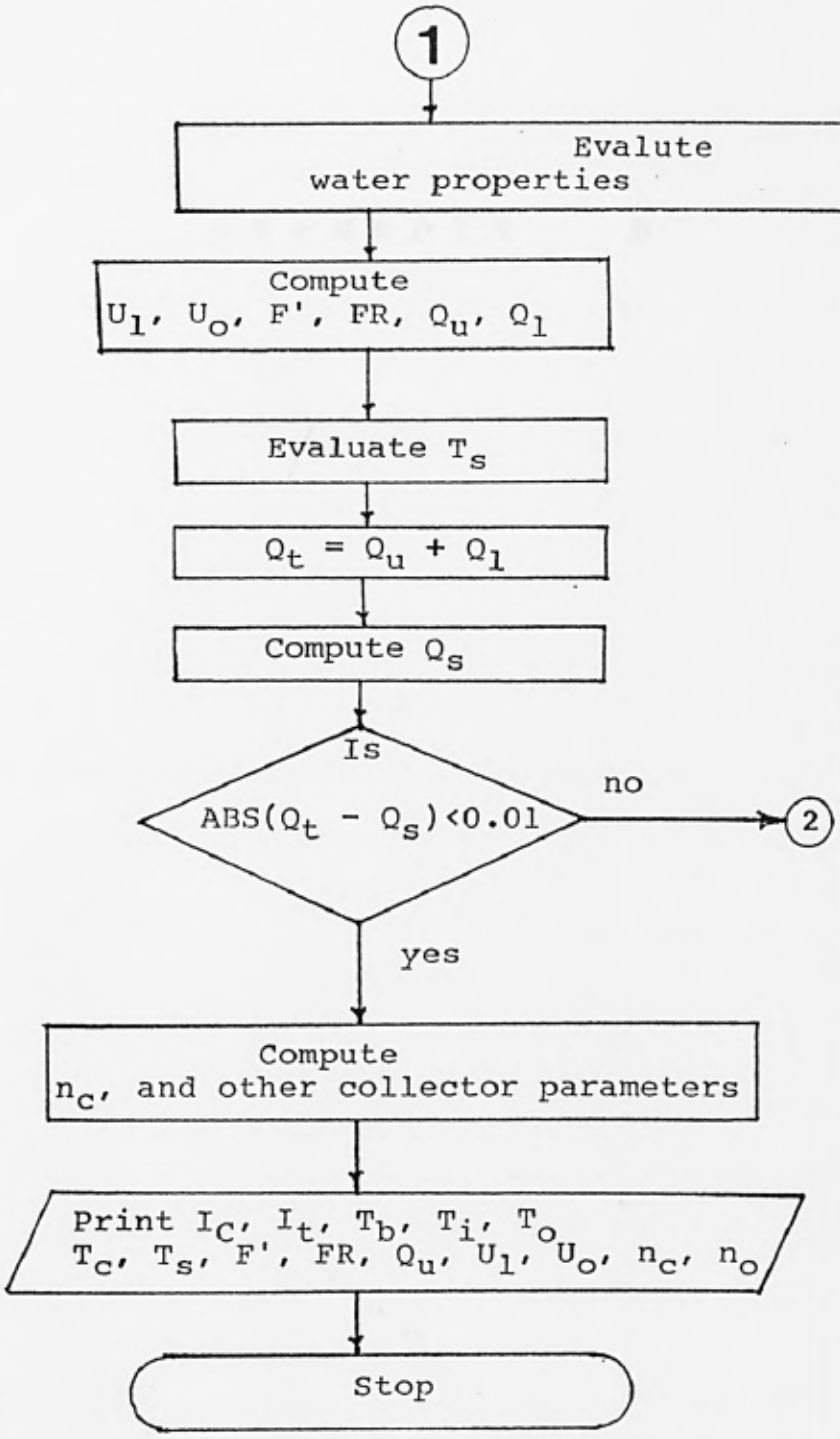

1
H = (B - A)/FN
TWOH = H + H
SUM4 = 0
SUM2 = 0
I = 1
TETA = A + H
SUM4 = SUM4 + FT(TETA)
SUM2 = SUM2 + FT(TETA + H)
Is
I ⩾ N-3
no
I = I + 2
TETA=TETA+TWOH
yes
SUM4 = SUM4 + FT(TETA)
Compute ITNEW
Is
ABS(ITNEW - ITOLD)⩽ E-5
no
ITOLD=ITNEW
N = N + N
3
yes
Compute <n>i
θm = (θa + θd)/2
Sc = 0
P = 0
P = P + 1
4
Sc = Sc + F(P)
2



Flow chart of the method of computing the average number of reflections within acceptance angle, reflector arc length and height, using Simpson's technique for the integration and iteration technique to solve the transcedental equations.

FLOW CHART FLHEAT





Flow chart for main collector program, showing the iteration technique used to obtain various operating temperatures and top loss coefficient.

APPENDIX D

PROPERTY DATA EQUATIONS FOR WATER

$$Pr = EXP(81.2063 + 0.0302035\ T - 15.5223\ Log_e\ T)$$

$$Cp = (7.3053 - 0.017945\ T + 2.5679E\text{-}05\ T^2)$$

$$k = (-2.876E\text{-}04 + 4.7390E\text{-}06\ T - 5.755E\text{-}09\ T^2)$$

$$u = 0.0045374 - 1.820E\text{-}05\ T + 1.8503E\text{-}08\ T^2)$$

Where,

T = temperature of water, K

Pr = Prantl number

Cp = specific heat, kJ/kg K

k = thermal conductivity, kW/m K

u = dynamic viscosity, kg/m s

TOP LOSS COEFFICIENT REGRESSION ANALYSIS: $45 \leq T_s \leq 215^{\circ}C$

Predictor	Coef	Stdev	t-ratio
Constant	1.0535	0.2776	3.80
C2	0.002567	0.003755	0.68
C5	-0.009460	0.006886	-1.37
C10	0.00005141	0.00004481	1.15
C16	0.00000406	0.00001356	0.30
C12	0.000855	0.003901	0.22
C13	-0.24112	0.04283	-5.63
C14	-0.00001113	0.00004722	-0.24
C17	0.00003209	0.00001425	2.25
C15	0.0050406	0.0009050	5.57
C18	-0.0003397	0.0006349	-0.54
C19	0.002046	0.005238	0.39
C20	-0.00000350	0.00000770	-0.46
C21	-0.00000271	0.00000231	-1.17
C22	-0.0000390	0.0001156	-0.34
C7	0.015557	0.003700	4.20
C8	0.002607	0.005313	0.49
C23	-0.0041131	0.0006328	-6.50
C24	-0.0011235	0.0006317	-1.78
C25	0.168214	0.007272	23.13
C26	-0.002906	0.003843	-0.76
C27	0.024225	0.003864	6.27
C28	0.10190	0.03126	3.26
C30	0.0000050	0.0001030	0.05
C31	0.00011244	0.00002267	4.96

s = 0.2662 R-sq = 97.8% R-sq(adj) = 97.5%

Analysis of Variance

SOURCE	DF	SS	MS
Regression	24	534.450	22.269
Error	167	11.838	0.071
Total	191	546.289	

SOURCE	DF	SEQ SS
C2	1	42.233
C5	1	0.021
C10	1	0.739
C16	1	0.057
C12	1	181.243
C13	1	6.024
C14	1	2.909
C17	1	0.122
C15	1	1.963
C18	1	192.063
C19	1	6.373
C20	1	4.754
C21	1	1.728
C22	1	3.506
C7	1	2.533
C8	1	4.103

C23	1	3.072
C24	1	0.224
C25	1	75.235
C26	1	0.041
C27	1	3.006
C28	1	0.753
C30	1	0.006
C31	1	1.744

Unusual Observations

Obs.	C2	C1	Fit	Stdev.Fit	Residual	St.Resid
9	45	4.4131	4.9054	0.1091	-0.4923	-2.03R
129	215	8.3742	7.5789	0.1098	0.7953	3.28R
133	215	8.7329	7.8314	0.1077	0.9015	3.70R
137	215	7.9995	7.2975	0.1098	0.7020	2.89R
141	215	8.3835	7.5500	0.1077	0.8335	3.42R

R denotes an obs. with a large st. resid.

SYMBOL :

$C1 = U_t$; $C2 = T_s$; $C3 = \theta_a$; $C4 = C$; $C5 = T_b$;

$C6 = E$; $C7 = S$; $C8 = h_b$; $C10 = T_s\ T_b$; $C16 = T_s^2$;

$C12 = E\ T_s$; $C13 = E\ T_b$; $C14 = E\ T_s\ T_b$;

$C15 = E\ T_b^2$; $C17 = E\ T_s^2$; $C18 = C\ T_s$; $C19 = C\ T_b$

$C20 = C\ T_s\ T_b$; $C21 = C\ T_s^2$; $C22 = C\ T_b^2$;

$C23 = C\ h_b$; $C24 = C\ S$; $C25 = E\ \theta_a$; $C26 = E\ S$;

$C27 = E\ h_b$ $C28 = E\ C$; $C30 = T_b\ h_b$; $C31 = T_s\ h_b$;

s = Standard deviation of equation 4.79;

R-sq = (Correlation coefficient)^2

DF = Degree of Freedom

SS = Sum of Squared deviation

t-ratio = Coef/Stdev

MS = SS/DF

TOP LOSS COEFFICIENT REGRESSION ANALYSIS: $215 \leq T_s \leq 300^{o}C$

Predictor	Coef	Stdev	t-ratio
Constant	-1.9848	0.8597	-2.31
C2	0.006895	0.003054	2.26
C5	0.00289	0.02640	0.11
C10	0.0000019	0.0001010	0.02
C12	-0.009211	0.005277	-1.75
C13	0.00386	0.02804	0.14
C14	0.0000231	0.0001069	0.22
C17	0.00004733	0.00001462	3.24
C18	0.0026509	0.0006486	4.09
C19	-0.001178	0.004545	-0.26
C20	0.00000128	0.00001736	0.07
C21	-0.00000838	0.00000212	-3.94
C3	0.05185	0.01024	5.06
C7	0.016657	0.005086	3.27
C8	0.02015	0.01223	1.65
C23	-0.0069126	0.0008676	-7.97
C24	-0.0011126	0.0008682	-1.28
C25	0.18275	0.01599	11.43
C26	-0.004088	0.005282	-0.77
C27	0.038188	0.005276	7.24
C28	-0.12954	0.05981	-2.17
C46	0.00006021	0.00004784	1.26

s = 0.2988 R-sq = 98.8% R-sq(adj) = 98.5%

Analysis of Variance

SOURCE	DF	SS	MS
Regression	21	756.945	36.045
Error	106	9.464	0.089
Total	127	766.409	

SOURCE	DF	SEQ SS
C2	1	18.418
C5	1	0.403
C10	1	0.069
C12	1	323.619
C13	1	0.399
C14	1	0.028
C17	1	0.047
C18	1	267.939
C19	1	0.239
C20	1	0.185
C21	1	0.245
C3	1	44.420
C7	1	1.899
C8	1	10.659
C23	1	5.646
C24	1	0.138
C25	1	77.312
C26	1	0.052
C27	1	4.657
C28	1	0.429
C46	1	0.141

Unusual Observations

Obs.	C2	C1	Fit	Stdev.Fit	Residual	St.Resid
33	215	6.2836	6.9952	0.1329	-0.7116	-2.66R
37	225	6.8438	7.4539	0.1316	-0.6101	-2.27R
41	215	6.1118	6.7124	0.1329	-0.6006	-2.24R
65	300	10.8772	10.1170	0.1360	0.7602	2.86R
69	300	11.3270	10.4225	0.1331	0.9045	3.38R
73	300	10.5382	9.8343	0.1360	0.7039	2.65R
77	300	11.0052	10.1397	0.1330	0.8655	3.23R
79	300	4.1287	4.6991	0.0994	-0.5704	-2.02R

R denotes an obs. with a large st. resid.

SYMBOL :

$C1 = U_t$; $C2 = T_s$; $C3 = \theta_a$; $C4 = C$; $C5 = T_b$;

$C6 = E$; $C7 = S$; $C8 = h_b$; $C10 = T_s\ T_b$; $C12 = E\ T_s$;

$C13 = E\ T_b$; $C14 = E\ T_s\ T_b$; $C17 = E\ T_s^2$;

$C18 = C\ T_s$; $C19 = C\ T_b$; $C20 = C\ T_s\ T_b$;

$C21 = C\ T_s^2$; $C23 = C\ h_b$; $C24 = C\ S$;

$C25 = E\ \theta_a$; $C26 = E\ S$; $C27 = E\ h_b$;

$C28 = E\ C$; $C46 = (T_s - T_b)\ h_b$;

s = Standard deviation of equation 4.79;

R-sq = (Correlation coefficient)^2

DF = Degree of Freedom

SS = Sum of Squared deviation

t-ratio = Coef/Stdev

MS = SS/DF

NH_3-H_2O ABSORPTION CYCLE SAMPLE CALCULATION

The sample calculation below has been performed with the following assumptions for the refined cycle shown in figure 5.10, page 156.

Strong solution massflow rate through the pump = 1 kg/s

Condenser temperature = 45°C

Absorber temperature = 45°C

Evaporator temperature = -1.0°C

Generator temperature = 120°C

Reflux condenser exit temperature = 80°C

Heat exchanger and Precooler Effectiveness = 0.40

To establish the thermodynamic state of the mixture requires the knowledge of the pressure (P), temperature (T), and the concentration of ammonia in the mixture (X). As shown in this sample calculation and the computer program that has been developed subsequently, only the operating temperatures are known, the pressures and concentrations are determined by iteration process. The property chart shown on page 326 has been used to obtain the properties for this sample calculation; In the computer program the properties are obtained by solving the property data equations numerically.

1. Determination of the high-side pressure (HSP) :

Iteration technique : the iteration process continues

until the pressure and vapour concentration in the reflux condenser equals the pressure and liquid concentration in the condenser respectively, as follows:

Initialization of HSP; assume HSP = 7 bar, then from the property chart :

At P_8 = 7 bar and T_8 = 80°C, XV_8 = 0.951

Since, $XL_9 = XV_8$ = 0.951 then from the chart :

At XL_9 = 0.951 and T_9 = 45°C, P_9 = 17.08

Begin a new iteration with P_8 = 17.08

At P_8 = 17.08 and T_8 = 80 , XV_8 = 0.986

$XL_9 = XV_8$ = 0.986

At XL_9 = 0.986 and T_9 = 45, P_9 = 17.79

Begin a new iteration with P_8 = 17.79

At P_8 = 17.79 and T_8 = 80, XV_8 = 0.987

$XL_9 = XV_8$ = 0.987

At XL_9 = 0.987 and T_9 = 45 , P_9 = 17.81

Begin a new iteration with P_8 = 19.81

At P_8 = 19.81 and T_8 = 80 , XV_8 = 0.987

Since $XL_9 = XV_8$ at the same value of pressure and respective operating temperature, then that pressure corresponds to the high-side pressure of the cycle.

2. Determination of state points 8 and 9 :

P_8 = 17.81 , T_8 = 80 , XV_8 = 0.987 , HV_8 = 260.2 kJ/kg

P_9 = 17.81 , T_9 = 45 , XL_9 = 0.987 , HL_9 = 38.6 kJ/kg

3. Determination of state point 10 :

$T_{11} = -1$, $T_{12} = T_{11} + 6 = 5^{o}C$, $cp_{12} = 0.258$ kJ/kg ^{o}C

$T_9 = 45$, $cp_9 = 0.282$ kJ/kg ^{o}C

assuming the massflow through the evaporator = 1 kg/s

then, $M_8 = M_9 = M_{10} = M_{11} = M_{12} = M_{13} = 1$ kg/s

The hot fluid heat capacity :

$$M_8\ cp_8 = 1*0.282 = 0.282\ kJ/^{o}C$$

The cold fluid heat capacity :

$$M_8\ cp_{12} = 1*0.257 = 0.257\ kJ/^{o}C$$

Thus, $cp_{min} = 0.257$

The precooler effectiveness is given by :

$$E = (T_{13} - T_{12})/(T_9 - T_{12})$$

re-arranging and with E = 0.40 :

$$T_{13} = 5 + 0.4(45 - 5)$$

$$= 21\ ^{o}C$$

Precooler heat transfer balance :

$$M_9\ cp_9(T_9 - T_{10}) = M_{12}\ cp_{12}(T_{13} - T_{12})$$

$$T_{10} = 30.4^{o}C$$

At $T_{10} = 30.4$ and $XL_{10} = 0.987$, $HL_{10} = 25.2$ kJ/kg

4. Determination of the low-side pressure (LSP) :

Iteration technique ; iteration process continues until the pressure converges to a value, as follows :

Initialisation of LSP , assume $P_{11} = 0.56$ bar, then from the property chart :

At $P_{11} = 0.56$ and $T_{11} = -1^{o}C$;

$XL_{11} = 0.40$, $HL_{11} = -45.2$ kJ/kg,

$XV_{11} = 0.996$, $HV_{11} = 237.3$ kJ/kg

The throttling process at the expansion valve gives :

$H_{11} = HL_{10} = 25.2$ kJ/kg

The total enthalpy at point 11, H_{11}, is made up of enthalpy of the liquid and that of the flashed vapour and is given by :

$$H_{11} = MFL_{11}\ HL_{11} + (1 - MFL_{11})HV_{11}$$

rearranging :

$$MFL_{11} = (H_{11} - HV_{11})/(HL_{11} - HV_{11})$$
$$= (25.2 - 237.3)/(-45.3 - 237.3)$$
$$= 0.751$$

H_2O mass balance around the expansion valve gives :

fraction of water at (11) = fraction of water at (10)

$$MFL_{11}(1 - XL_{11}) = (1 - XL_{10})$$

rearranging :

$$XL_{11} = [(XL_{10} - 1)/MFL_{11}] + 1$$
$$= 0.983$$

At $XL_{11} = 0.983$ and $T_{11} = -1$, $P_{11} = 3.9$bar .

Begin a new iteration with $P_{11} = 3.9$ bar :

At $P_{11} = 3.9$, $T_{11} = -1$, $XL_{11} = 0.983$, $HL_{11} = -2.8$ kJ/kg

$XV_{11} = 0.999$ and $HV_{11} = 236.2$ kJ/kg

$MFL_{11} = 0.882$

$XL_{11} = 0.986$

At $XL_{11} = 0.986$ and $T_{11} = -1$, $P_{11} = 3.91$

Further iteration did not change the value of P_{11} from 3.91 bar, thus the pressure has conveged to 3.91 and

that is the low-side pressure.

5. Determination of state points 6, 7, 4 and 15 :

point 6 : $P_6 = 17.81$ $T_6 = 120$

$XV_6 = 0.911$ $HV_6 = 287.9$

point 7 : $P_7 = 17.81$ $T_7 = 80$

$XL_7 = 0.54$ $HL_7 = 23.3$

point 4 : $P_4 = 17.81$ $T_4 = 120$

$XL_4 = 0.326$ $HL_4 = 62.1$

point 15 : $P_{15} = 3.91$ $T_{15} = 45$

$XL_{15} = 0.422$ $HL_{15} = -7.8$

6. Determination of total enthalpy at state point 12 :

$P_{12} = 3.91$, $T_{12} = 5$, $X_{12} = XV_8 = 0.987$

$XL_{12} = 0.80$, $HL_{12} = -21.5$

$XV_{12} = 0.999$, $HV_{12} = 239.5$

NH_3 balance at point 12 :

$$M_{12}\, X_{12} = MFL_{12}\, XL_{12} + (M_{12} - MFL_{12})XV_{12}$$

assuming, massflow rate through the evaporator = 1 kg/s:

$$1\, X_{12} = MFL_{12}\, XL_{12} + (1 - MFL_{12})XV_{12}$$

Mass of purge liquid to remove water from the evaporator is given by :

$$MFL_{12} = (X_{12} - XV_{12})/(XL_{12} - XV_{12})$$

$$= 0.061 \text{ kg/s}$$

Total enthalpy at point 12 :

$$1\, H_{12} = MFL_{12}\, HL_{12} + (1 - MFL_{12})HV_{12}$$

$$H_{12} = 222.7$$

7. Determination of state point 13 :

$P_{13} = 3.91$, $T_{13} = 21$, $X_{13} = 0.987$

Energy balance around the precooler :

$$M_{13}\ H_{13} = M_9\ HL_9 + M_{12}\ H_{12} - M_{10}\ HL_{10}$$

$$H_{13} = 236.1$$

8. Determination of massflow rates :

Assuming the massflow through the evaporator is 1 kg/s ;

Reflux condenser mass and NH_3 balance :

$$M_6 = M_7 + M_8$$

$$M_6\ XV_6 = M_7\ XL_7 + M_8\ XV_8$$

rearranging :

$$M_7 = M_8(XV_8 - XV_6)/(XV_6 - XL_7)$$

$$= 0.2034$$

$$M_6 = 0.2034 + 1$$

$$= 1.2034$$

Generator mass and NH_3 balance :

$$M_3 = M_4 + M_6 - M_7$$

$$M_3\ X_3 = M_4\ XL_4 + M_6\ XV_6 - M_7\ XL_7$$

$$X_3 = XL_2 = XL_1 = XL_{15}$$

substituting for M_4 and rearranging :

$$M_3 = [(M_7 - M_6)XL_4 + M_6\ XV_6 - M_7\ XL_7]/(XL_1 - XL_4)$$

$$= 6.8325$$

$$M_4 = M_3 - M_6 + M_7$$

$$= 5.8325$$

since the above massflow rates are based on assumed 1 kg/s flow rate through the evaporator, it has to be converted to the initial assumption of 1 kg/s flow rate through the Pump. Thus :

$M_{15} = M_1 = M_2 = M_3 = 1$ kg/s

$M_8 = M_9 = M_{10} = M_{12} = M_{13} = 1/6.8325$

$= 0.1463$

$M_7 = 0.2034/6.8325$

$= 0.02978$

$M_6 = 1.2034/6.8325$

$= 0.1761$

$M_4 = 5.8324/6.8325$

$= 0.8536$

9. Determination of Temperature at state point 2 :

Reflux condenser energy balance :

$M_2 H_2 = M_1 HL_1 + M_6 HV_6 - M_7 HL_7 - M_8 HV_8$

(Pump work is negligible, and $HL_1 = HL_{15}$)

$H_2 = 4.1$

assuming the solution is completely liquid at point 2 :

$XL_2 = XL_1 = XL_{15}$

at XL_2 and $H_2 = 4.1$, $T_2 = 57.3$

10. Determination of Temperatures and Enthalpies at state points 3 and 5 :

$T_2 = 57.3$, $cp_2 = 0.29$

$T_4 = 120$, $cp_4 = 0.381$

fluid heat capacity :

$M_2\ cp_2 = 1*0.29$

$= 0.29\ kJ/^oC$

$M_4\ cp_4 = 0.8536*0.381$

$= 0.325\ kJ/^oC$

$(M\ cp)_{min} = 0.29$

heat exchanger effectiveness is given by :

$E = (T_3 - T_2)/(T_4 - T_2)$

rearranging :

$T_3 = T_2 + (T_4 - T_2)E$

$= 82.4$

heat exchanger heat transfer balance :

$M_4\ cp_4\ (T_4 - T_5) = M_2\ cp_2\ (T_3 - T_2)$

rearranging :

$T_5 = 97.6$

assuming the solution at point 5 is completely liquid :

$XL_5 = XL_4$

at $XL_5 = 0.326$ and $T_5 = 97.6$, $HL_5 = 35.8$

heat exchanger energy balance :

$M_3\ H_3 = M_2\ H_2 + M_4\ HL_4 - M_4\ HL_5$

$H_3 = 25.7\ kJ/kg$

11. Determination of Q_g , Q_c , Q_a , Q_e

Generator heating load :

$Q_g = M_4\ HL_4 + M_6\ HV_6 - M_3\ H_3 - M_7\ HL_7$

$= 77.4\ kW$

Condenser duty :

$Q_c = M_8\ (HV_8 - HL_9)$

$= 32.4\ kW$

Absorber cooling load :

$$Q_a = M_4\ HL_4 + M_8\ H_{13} - M_{15}\ HL_{15}$$

$$= 73.9 \text{ kW}$$

Evaporator load :

$$Q_e = M_8\ (H_{12} - H_{11})$$

$$= 28.9 \text{ kW}$$

12. Determination of Circulation ratios and COP

Relative Circulation :

$$RC = M_4/M_8$$

$$= 5.8325$$

Specific Circulation :

$$SC = M_{15}/M_8$$

$$= 6.8324$$

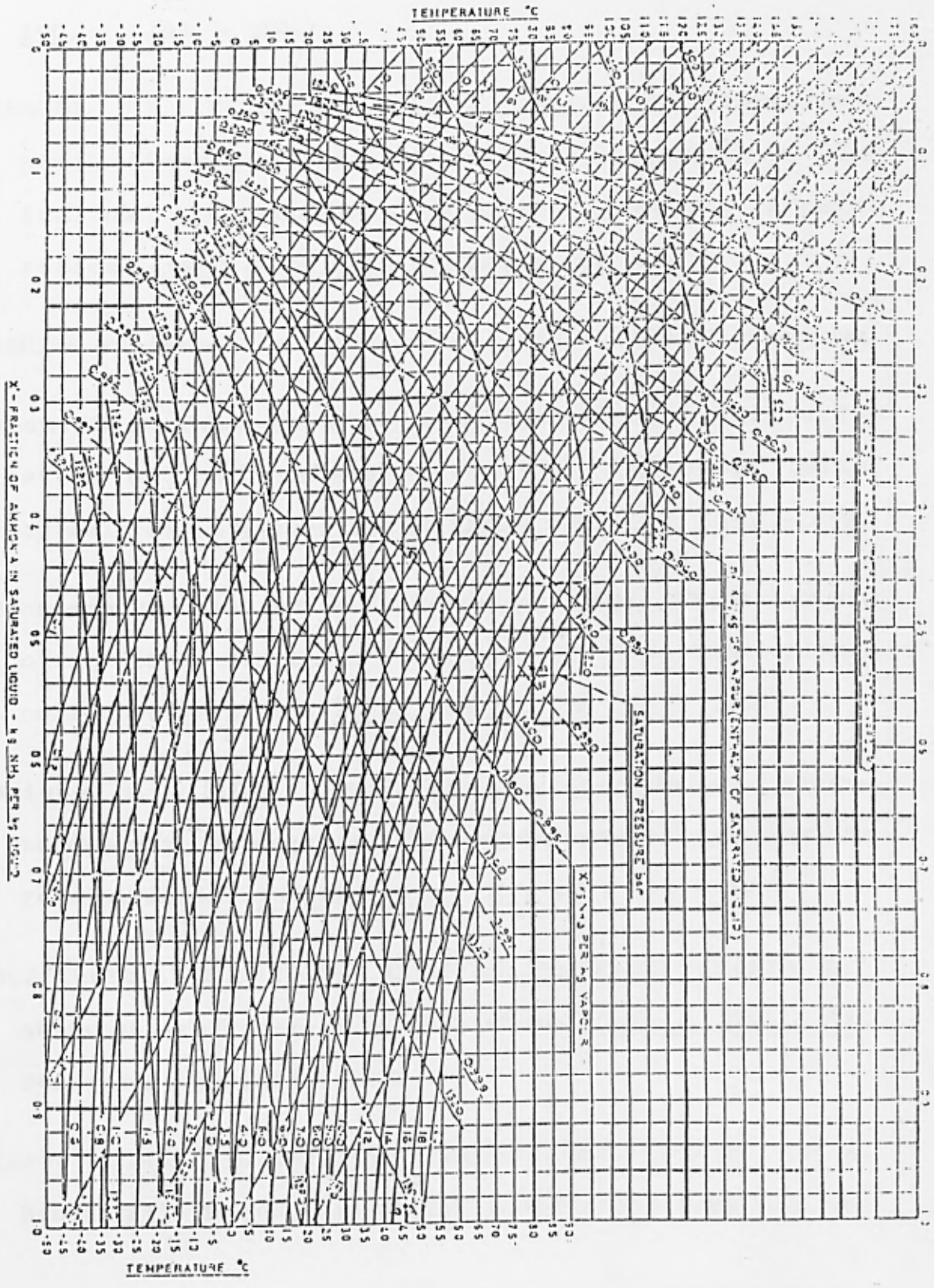
The Coefficient of Performance :

$$COP = Q_e/Q_g$$

$$= 0.374$$

The above calculation steps have been incorporated into the program REFRIG in appendix B .

PROPERTIES OF AQUA-AMMONIA



REFERENCES

Abdel-Khalik, S.I., H.W. Li, and K.R. Randall (1978). Natural convection in Compound Parabolic Concentrators - A finite element solution. J. of Heat Transfer, 100, 199 - 204.

Arnold, J.N., I. Catton and D.K. Edwards(1976).Experimental investigation of natural convection in inclined rectangular regions of differing aspect ratios. ASME J. of Heat Transfer, 19, 67.

ASHRAE Fundamentals (1972, 1977, 1981). ASHRAE, New York

Baum, H.P. and J.M. Gordon (1984). Geometric characteristics of ideal nonimaging CPC solar collector with cylindrical absorber. Solar Energy, 33, (5), 455 - 458.

Brandemuehl, M.J. and W.A. Beckman (1980). Transmission of diffuse radiation through CPC and flat plate collector glazings. Solar Energy, 24, 511 - 513.

Briggs, S.W. (1971).Concurrent,crosscurrent,and countercurrent absorption in ammonia-water absorption refrigeration. ASHRAE Trans., 77, (1), 171 - 175.

Buffington, R.M.(1949). Qualitative requirements for absorbent-refrigerant combinations. Refrig. Eng., 57, 343 - 345, 384, 386, 388 .

Carvalho,M.J., M. Collares-Pereira, J.M. Gordon and A. Rabl(1985). Truncation of CPC solar collectors and its

effect on energy collection. Solar Energy, 35, 393 - 399 .

Carvalho, M.J., M.Collares-Pereira and J.M. Gordon Gordon (1987). Economic optimization of stationary nonevacuated CPC solar collectors. Trans. ASME, 109, 40 - 45 .

Chinnappa, J.C.V(1961). Experimental study of the intermittent vapour absorption refrigeration cycle employing the refrigerant-absorbent systems of ammonia water and ammonia lithium nitrate. Solar Energy, 5, 1.

Chinnappa, J.C.V.(1962). Performance of an intermittent refrigerator operated by a flat plate collector. Solar Energy, 6, 143 .

Collares-Pereira, M. and A. Rabl(1979). The average distribution of solar radiation-correlations between diffuse and hemispherical and between daily and hourly insolation values. Solar Energy, 22, 155 - 164 .

Collares-Pereira, M.(1985). Description and testing of a nonevacuated 1.5X CPC collector thermal performance comparison with other collector types. J. of Solar Energy Engineering, 107, 227 - 280 .

Dao, K., M. Simmons, R. Wolgast and M. Whalig(1976). Performance of an air-cooled ammonia-water absorption air conditioner at low generator temperatures. Proc. Inter. Solar Energy Conf., 3. Winnipeg, U S A.

Davis, J.A.(1966). Solar radiation estimates for Nigeria. Nigerian Geographical J., 9, 85 - 100.

Dodge, B.F.(1944). Chemical Engineering Thermodynamics, McGraw-Hill Book Co., New York.

Duffie, J.A. and W.A. Beckman(1980). Solar Engineering of Thermal Processes, Wiley Interscience, New York.

Equip-IARD(1982). Air conditioning Price List, 5, Agbara industrial estate, Ikeja-Lagos.

Faber, E.A., F.M. Flanigan, L. Lopez and R.W. Polifka(1966). University of Florida solar air conditioning system. Solar Energy, 10, (2), 91 -95

Gervais, R.L. and P.B. Box(1975). Astronautics and Aeronautics, 13, 38.

Gordon, J.M.(1986). Low-concentration CPC's for low-temperature solar energy applications. J. of Solar Energy Engineering, 108, 49 - 55 .

Hsieh, C.K.(1981). Thermal analysis of CPC collectors. Solar Energy, 27, 19 - 29 .

Hsieh, C.K.(1983). Empirical equations for calculation of CPC collector coefficients. Solar Energy, 30, 487 - 489.

Huang, B.J. and T.Y. Chang(1978). Design analysis of ammonia-water absorption refrigeration systems. Society of Automotive Eng., SAE/P-78/75/$02.50, 798 - 804 .

Jacob, X., L.F. Albright and W.H. Turker(1969). Factors affecting the coefficient of performance for absorption air conditioning systems. ASHRAE Trans., 75, 103 - 110 .

Kreith, F.(1973). Principles of Heat Transfer, Intext, New York.

Krochta, J.M. and T.R. Rumsey(March,1977). Solar energy cooling and freezing of food: a computer analysis. Food Technology, 61 -66 .

Laszlo, T.S.(1965). Image Furnace Techniques. Wiley Interscience, New York.

Liu, B.Y. and R.C. Jordan(1962). Daily insolation on surfaces tilted towards the equator. ASHRAE Trans., 526 - 541 .

Macriss, R.A., B.E. Eakin, R.T. Ellington and J. Huebler(1964). Physical and thermodynamic properties of ammonia-water mixtures. IGT Research Bulletin, 34.

Mansoori, G.A. and V. Patel(1979). Thermodynamic basis for the choice of working fluids. Solar Energy, 22, 483 - 491 .

Mayhew, Y.R. and G.F.C. Rogers(1974). Thermodynamic and Transport Properties of Fluids. 10, Basil Blackwell, Oxford.

McAdams, W.H.(1954). Heat Transmission, 3rd edition. McGraw-Hill, New York .

McIntire, W.R.(1979). Truncation of nonimaging cusp concentrators. Solar Energy, 23, 351 -355 .

Mills, D.R. and J.E. Guitronich(1978). Asymmetrical nonimaging cylindrical solar collectors. Solar Energy, 20, 45 .

Nelson, D.T., D.L. Evans and R.R. Bansal(1975). Linear Fresnel lens concentrators. Solar Energy, 17, 285 .

Ojo, O.(1972). Distribution of net radiation in Nigeria. Nigerian Geographical Journal, 15, 115 - 125 .

Page, J.K.(1966). The estimation of monthly mean values of daily shortwave radiation on vertical and inclined surfaces from sunshine records for latitudes 40°N-40°S. Proc. U.N. Conf. New Sources of Energy, 4,378 .

Perman, E.P.(1901,1903). Vapour pressure of aqueous ammonia solution, part I and II. Chemical Society Trans., 79 & 83, 718 - 725, 1168 - 1184 .

Prapas, D.E., B. Norton and S.D. Probert(1987). Optics of parabolic-trough solar energy collectors, possessing small concentration ratios. Solar Energy, 39, (6), 541 - 550

Rabl, A.(1976a). Comparison of solar concentrators. Solar Energy, 18, 93 - 111 .

Rabl, A.(1976b). Solar concentrators with maximal concentration for cylindrical absorbers. Apllied Optics, 15, (7), 1871 - 1873 .

Rabl, A.(1976c). Optical and thermal properties of Compound Parabolic Concentrators. Solar Energy, 18, 497- 511 .

Rabl, A. and R. Winston(1976). Ideal concentrators for finite sources and restricted exit angles. Appl. Opt., 15, 2880

Rabl, A.(1977). Radiation transfer through specular passages- A simple approximation. Int. J. Heat Mass Transfer, 20, 323 - 330 .

Rabl, A., N.B. Goodman and R. Winston(1979). Practical design consideration for CPC solar collectors. Solar Energy, 22, 373 - 381 .

Rigmore, D. and R. Barber(1975). Cooling with the Sun's heat; design consideration and test data for a Rankine cycle prototype. Solar Energy, 17, 185 - 192 .

Sarofim, A.F. and H.C. Hottel(1966). Radiative exchange among non-lambert surfaces. J. Heat Transfer, 88, 37 .

Sayigh, A.A.M (1977). Solar Energy Engineering. Academic Press, New York.

Scatchard, G., L.F. Epstein, J. Warburton and P.J. Cody.(1947). Thermodynamic properties- saturated liquid and vapour of ammonia-water mixtures. Refrig. Eng., 53, 413 - 419 .

Shiran, Y., A. Smitzer and D. Degari(1982). Computerized design and economic evaluation of aqua-ammonia solar operated absorption system. Solar Energy, 29, (1), 43 - 54 .

Simmons, M. and M, Whalig(1975). Ammonia-water absorption air conditioner. Proc. 2nd Wkshop on the use of solar energy for the cooling of buildings. Los angeles, U S A .

Simonson, J.R.(1984). Computing Methods in Solar Heating Design. Mcmillan Press, London.

Sparrow, E.M. and R.D. Cess (1970). Radiation Heat Transfer. Brooks/Cole Publishing Co. Belmont.

Stoecker, W.F. and L.D. Reed(1971). Effect of operating temperatures on the coefficient of performance of aqua-ammonia refrigeration systems. ASHRAE Trans., 77, (1), 163 - 170 .

Swinbank, W.C. (1963). Longwave radiation from clear skies. Quart. J. Roy. Soc., 89 .

Tabour, H.(1958). Stationary mirror systems for solar collectors. Solar Energy, 2, 27 .

Threlkeld,J.L.(1970).Thermal Environmental Engineering. 2nd edition, Prentice-Hall, Inc. , New york .

Vankatesh,V., V. Sriramulu and M.C. Gupta(1979). Theoretical and experimental investigations of an intermittent solar refrigerator. Sun II, 1, 749 - 753.

Welford, W.T. and R. Winston(1978). The Optics of Nonimaging Concentrators, Academic Press, New York .

Whitlow, E.P.(December, 1966). Trends of efficiencies in the absorption refrigeration machine. ASHRAE Journal, 44 - 48 .

Whitlow, E.P.(1976). Relationship between heat source temperature, heat sink temperature and coefficient of performance for solar-powered absorption air conditioners. ASHRAE Trans., 82, 950 - 958 .

Wilbur, P.J. and C.E. Mitchell(1975). Solar absorption air conditioning alternatives. Solar Energy, 17, 193 - 199 .

Winston, R.(1970). Light collection within the framework of geometrical optics. J. Opt. Soc. Am., 60, 245 .

Winston, R.(1974). Principles of solar concentrators of a novel design. Solar Energy, 16, 89 - 95 .

Winston, R. and H. Hinterberger(1975). Principles of cylindrical concentrators for solar energy. Solar Energy, 17, 255 - 258 .